Rock alteration at high pH relevant to the geological disposal of radioactive waste

Elizabeth Bernice Annwen Moyce

Submitted in accordance with the requirements for the degree of
Doctor of Philosophy

The University of Leeds
School of Earth and Environment

December 2014

The candidate confirms that the work submitted is her own, except where work which has formed part of jointly-authored publications has been included. The contribution of the candidate and the other authors to this work has been explicitly indicated below. The candidate confirms that appropriate credit has been given within the thesis where reference has been made to the work of others.

Paper status and collaborator contributions

The work included in the thesis as Chapter 4 is intended to be redrafted and published in a jointly authored publication:

> The contribution of each of the co-authors to this publication was:
>
> Moyce, E. B. A. – set up and sampled the experiments, conducted the analysis of the samples, carried out the computer modelling, interpreted the experimental and modelling data and prepared the manuscript; Shaw, S. - aided development of the experimental design, supported interpretation of the experimental data and assisted manuscript preparation; Morris, K. - aided interpretation of experimental data and supported manuscript preparation

The work included in the thesis as Chapter 5 has been published in the jointly authored publication:

> Moyce, E. B. A., Rochelle, C., Morris, K., Milodowski, A. E., Chen, X., Thornton, S., Small, J. S. & Shaw, S. 2014. Rock alteration in alkaline cement waters over 15 years and its relevance to the geological disposal of nuclear waste. Applied Geochemistry. 50. 91-105.
>
> The contribution of each of the co-authors to this publication was:
>
> Moyce, E. B. A. – sampled the experiments, conducted the analysis of the samples, developed the conceptual model of the system for the computer modelling, interpreted the experimental and modelling data and prepared the manuscript; Rochelle, C. - set up the experiments in 1995 and advised on experiment sampling; Morris, K. - aided

interpretation of experimental data and supported manuscript preparation; Milodowski, A. E. - aided interpretation of experimental data and supported manuscript preparation; Chen, X. – created the computer model; Thornton, S. – aided creation of the computer model; Small, J. S. - aided creation of the computer model and supported interpretation of the modelling data; Shaw, S. - aided development of conceptual model of the system for computer modelling, supported interpretation of the experimental data and assisted manuscript preparation

The work included in the thesis as Chapter 6 has been submitted for publication in the jointly authored publication:

MOYCE, E. B. A., MILODOWSKI, A. E., MORRIS, K., & SHAW, S. In submission. Herbert's Quarry, South Wales - an analogue for host rock alteration at a cementitious radioactive waste repository? *Mineralogical Magazine.*

The contribution of each of the co-authors to this publication was:

Moyce, E. B. A. – conducted the desk study and field work, conducted the analysis of the samples, interpreted the results of analysis and prepared the manuscript; Milodowski, A. E. - aided fieldwork and supported manuscript preparation; Morris, K. - supported manuscript preparation; Shaw, S. - aided interpretation of the analytical results and assisted manuscript preparation

Acknowledgements

The author would like to thank:

Dr Sam Shaw, Tony Milodowski and Professor Kath Morris for their supervision and support throughout the PhD.

EPSRC for funding the PhD studentship through the Nuclear FiRST Doctoral Training Centre (DTC) NERC for providing support through the BIGRAD research consortium.

The British Geological Survey for providing use of their analytical facilities.

Natural Resources Wales and the Brecon Beacons National Park Authority for permission to collect samples from the Mynydd Du Site of Special Scientific Interest (which includes Herbert's Quarry).

Dr Chris Rochelle for allowing access to the experiments he tended for 15 years and generously giving his help and advice.

The students and researchers of the BIGRAD research consortium for providing lively discussion on the subject of geodisposal.

The Nuclear FiRST DTC for making nuclear science fun, and particularly the other Cohort 1 students for their comradeship and an education on the rise and fall of empires.

Janice, Tim, Amy and Cindy for making entrapment at the anaerobic chamber more bearable.

Tom for understanding.

Abstract

Dissolution of the cement used in radioactive waste repositories will produce a high pH leachate (pH 10.5-13.1) that will evolve in pH and composition over time, remaining hyperalkaline for 10^6 years. This will migrate into the repository host rock potentially altering the rock's physical and chemical properties, and its function as a barrier to radionuclide migration. To investigate the possible alteration over timescales relevant for geological disposal (10^4 to 10^5 years), previous studies included short term (< 2 years) laboratory experiments, natural analogue studies (100s to 10^5 years) and predictive modelling. However, the geochemical and mineralogical processes which may occur as such systems evolve remain poorly constrained.

Here, rock alteration in high pH solutions, analogous to cement leachates, has been investigated on short (1 year), medium (15 years) and long (100s years) timescales. The short term investigation agreed with previous studies finding that silicate mineral dissolution and C-S-H precipitation were the predominant alteration processes. In the medium term study, although initially silicate mineral dissolution and C-S-H precipitation occurred, by 15 years of reaction neo-formed Mg-silicates replaced the C-S-H. To investigate rock alteration on a longer timescale Herbert's Quarry, where high pH fluids have existed for 100s years, was characterised and assessed as a potential analogue site. However, the site was found to have limited applicability in the context of the high pH rock alteration expected at a radioactive waste repository.

The impact of rock alteration on U(VI) behaviour was also investigated in the short and medium term. In the short term, U(VI) behaviour during rock alteration varied between solutions representative of different periods of cement leachate evolution, with potential impacts for radionuclide transport. The sorption of U(VI) to unaltered rock and rock altered for 15 years was also investigated. This suggested alteration may increase a rock's sorption capacity for U(VI).

Table of Contents

List of Tables

List of Figures

Abbreviations

BET	Brunauer-Emmet-Teller
BGS	British Geological Survey
BVG	Borrowdale Volcanic Group
C-(A)-(K)-S-H	Aluminium and Potassium Bearing Calcium Silicate
C-(A)-S-H	Aluminium Bearing Calcium Silicate Hydrate
CCD	Charge Couple Device
CDZ	Chemically Disturbed Zone
CoRWM	Committee on Radioactive Waste Management
C-S-H	Calcium Silicate Hydrate
DECC	Department of Energy and Climate Change
DEFRA	Department for Environment, Food and Rural Affairs
EBS	Engineered Barrier System
EDX(A)	Energy Dispersive X-ray Analysis
ENFG	Evolved Near Field Groundwater
ESEM	Environmental Scanning Electron Microscope
EXAFS	Extended X-ray Absorption Fine Structure
FEG	Field Emission Gun
FIB	Focused Ion Beam
GDF	Geological Disposal Facility
HLW	High Level Waste
IAEA	International Atomic Energy Association
IC	Ion Chromatography
ICDD	International Centre for Diffraction Data
ICL	Intermediate Cement Leachate
ICP-AES	Inductively Coupled Plasma Atomic Emission Spectroscopy
ICP-MS	Inductively Coupled Plasma Mass Spectroscopy
ILW	Intermediate Level Waste
LLNL	Lawrence Livermore National Laboratory
LLW	Low Level Waste
MRWS	Managing Radioactive Waste Safely
NDA	Nuclear Decommissioning Authority
NMR	Nuclear Magnetic Resonance

NRVB	Nirex Reference Vault Backfill
NSARP	Nirex Safety Assessment Research Programme
OCL	Old Cement Leachate
OECD-NEA	Organisation for Economic Co-operation and Development – Nuclear Energy Agency
OPC	Ordinary Portland Cement
PPB	Parts Per Billion
RWM	Radioactive Waste Management
SAED	Selected Area Electron Diffraction
SEM	Scanning Electron Microscope
SDD	Silicon Drift Detector
SI	Saturation Index
SIT	Specific Ionic Theory
SSSI	Site of Special Scientific Interest
TDS	Total Dissolved Solids
TEM	Transmission Electron Microscope
THMC	Thermo-Hydro-Mechanical-Chemical
YCL	Young Cement Leachate
YNFP	Young Near Field Pore fluid
XANES	X-ray Absorption Near Edge Spectroscopy
XAS	X-ray Absorption Spectroscopy
XRD	X-ray Diffraction

1 Introduction

1.1 Project context and relevance

Worldwide many countries have accumulated significant volumes of nuclear waste from the defence, civil and medical sectors (World Nuclear Association, 2014). Geological disposal is internationally accepted as the best practicable option for long-term waste management and is being pursued by countries including the UK, France, Canada, Switzerland, Sweden and Finland (OECD-NEA, 2008). This method of management is intended to isolate waste from the biosphere and involves containment of nuclear waste in several engineered barriers emplaced in rock at 500-1000m depth in a host rock in a Geological Disposal Facility (GDF - Miller et al., 2000; Umeki, 2007). In these systems the host rock is intended to act as a geological barrier to contaminant migration after the breakdown of the engineered barriers after thousands of years of waste containment (IAEA, 1999). However, in currently proposed GDF designs, for example those of the UK, France, Canada and Switzerland (NDA, 2010a; Andra, 2012; Nuclear Waste Management Organisation, 2010; NAGRA, 2014) cement is a prevalent construction material / wasteform / backfill material. As groundwater interacts with this cement, high pH leachates will be produced as components of the cement dissolve (Atkinson, 1985; Berner, 1992; Butcher et al., 2012). The leachates produced will evolve in composition and pH over time from an initially NaOH and KOH dominated leachate at pH 13.1 to a $Ca(OH)_2$ dominated leachate at pH 12.5 and finally to a leachate in equilibrium with C-S-H at pH 10.5 with hyperalkaline pH estimated to persist for over 4 million years (Atkinson, 1985). These high pH leachates will migrate into the geosphere and form a Chemically Disturbed Zone (CDZ) when groundwater chemistry and pH are perturbed from natural levels. In the CDZ the elevated pH will cause the dissolution of primary minerals and formation of secondary phases and thereby alter the host rock's physical (e.g. porosity and permeability) and chemical (e.g. sorption capacity) properties. This may affect the rock's ability to perform as a geological barrier

to radionuclide migration. Therefore, understanding mineral alteration at high pH is directly relevant to the safety assessment of a GDF.

However, there has been no detailed investigation of the implications of rock alteration for radionuclide transport and the availability of pertinent data is limited. For example, U in the waste will remain hazardous for hundreds of thousands of years after the closure of a GDF (NDA, 2010b), and so will be of concern over the potential timescale of CDZ development. Therefore if U(VI) migrates into the geosphere it is possible that its mobility may be affected by the high pH leachate and any subsequent rock alteration. Understanding these effects will be integral to a GDF safety case and performance assessment. This study aims to improve understanding of the impact of high pH rock alteration on U(VI) mobility through investigation of the behaviour of U(VI) when present during the high pH alteration of a sandstone.

Due to the probable longevity of high pH in the CDZ and the long-lived hazard posed by the radionuclides, such as U(VI), in a GDF, any safety case will also need to consider the impact and potential evolution of high pH rock alteration reactions over millions of years (Atkinson, 1985; NDA, 2010b). However, previous long-term experimental studies are rare, therefore research has focused on natural and anthropogenic analogue sites and computer modelling studies. While laboratory experiments will not be able to provide insight on the same timescales as analogue sites, it is possible to extend the timescales of laboratory studies and provide well constrained experimental evidence of high pH reaction processes over longer periods than has currently been achieved. This thesis presents a study of rock alteration after 15 years of reaction at high pH, significantly beyond the timescales of previous studies. The effect of this longer term alteration on the sorption behaviour of U(VI) is also examined.

As mentioned, analogue studies are an important tool for understanding potential high rock reactions at much longer timescales than it is possible to recreate in a laboratory. However, analogue sites can be limited by site specificity and the ability to constrain site history. Therefore increasing the number of analogue sites studied will provide a greater base of knowledge for

mineral alteration at longer timescales. This study investigates the potential of a former lime working site in South Wales as a potential industrial analogue for high pH alteration over hundreds of years.

1.2 Hypothesis and aims

The central hypothesis behind this thesis is that mineral alteration in the CDZ of a GDF will change the chemical and physical properties of a rock, affecting U(VI) mobility as a result, and that the alteration processes which occur may evolve over time. The aims of this research are to:

- Investigate the impact of high pH rock alteration on the behaviour of U(VI)
- Improve knowledge of the evolution of rock alteration processes at high pH at longer-timescales than previously examined in laboratory studies
- Assess the potential of a previously unstudied site as an analogue for rock alteration at a cementitious GDF

To achieve these aims the following objectives have been defined:

- Study the effect of alkaline alteration on rock samples reacted in synthetic cement leachates via batch reaction after 1-1.5 years and 15 years
- Determine how the high pH alteration of rock over 1-1.5 years affects the fate and speciation of U(VI) when present during batch reaction of rock in synthetic cement leachates
- Assess the effect of 15 years of rock reaction in high pH solution on U(VI) adsorption to the rock
- Characterise the alteration of rock in high pH solutions at a disused lime working site in South Wales and assess the site's potential as an anthropogenic analogue of rock alteration at high pH

1.3 Thesis structure

Initially this thesis provides an introduction to the context of nuclear waste disposal in cementitious systems with particular focus on the UK disposal

concept. This is followed by a review of the current research in the field of high pH mineral / rock alteration and the behaviour of uranium at high pH. An overview of the experimental and analytical methods used in the work presented is then given in chapter 3 and the results of this study are presented in the following three chapters. Chapter 4 describes the behaviour of U(VI) during the alteration of a sandstone in cement leachates of 3 different compositions. In chapter 5 the alteration of a volcanic rock fracture wall-rock and infill in cement leachates of two different compositions after 15 years of reaction is presented. Chapter 6 describes a field study of a disused lime working site to characterise the applicability of the site as an anthropogenic analogue for high pH rock alteration. The findings of this work are then summarised in chapter 7 with a discussion of their implications and suggestions for further work to extend this study.

References

ANDRA. 2012. Low and intermediate level short-lived waste [online]. Available at: <www.andra.fr/international/pages/en/menu21/waste-management/waste-classification/short-lived-low--and-intermediate-level-waste-1609.html> [accessed 19/01/2014].

ATKINSON, A. 1985. The time dependence of pH within a repository for radioactive waste Disposal. *UKAEA,* AERE-R 11777.

BERNER, U. R. 1992. Evolution of pore water chemistry during degradation of cement in a radioactive waste repository environment. *Waste Management,* 12**,** 201-219.

BUTCHER, E. J., BORWICK, J., COLLIER, N. & WILLIAMS, S. J. 2012. Long term leachate evolution during flow-through leaching of a vault backfill (NRVB). *Mineralogical Magazine*. 76(8). 3023-3031.

IAEA 1999. Hydrogeological investigation of sites for the geological disposal of radioactive waste. *Technical report series No. 391.* Vienna: IAEA

MILLER, W., ALEXANDER, R., CHAPMAN, N., MCKINLEY, I. & SMELLIE, J. 2000. Geological disposal of radioactive wastes and natural

analogues. Waste Management series vol. 2. Elsevier Science Ltd. Kidlington, Oxford.

NAGRA. 2014. Geological repository for low- and intermediate-level waste [online]. Available at: <www.nagra.ch/en/tlsmae.htm> [accessed 19/01/2014].

NDA. 2010a. Geological Disposal: Generic disposal system technical specification. NDA/RWMD/044.

NDA. 2010b. Geological Disposal: Radionuclide behaviour status report. NDA/RWMD/034.

NUCLEAR WASTE MANAGEMENT ORGANISATION. 2010. DGR key features [online]. Available at: < www.nwmo.ca/dgr_keyfeatures> [accessed 19/01/2014].

WORLD NUCLEAR ASSOCIATION. 2014. International nuclear waste disposal concepts [online]. Available at: <http://www.world-nuclear.org/info/Nuclear-Fuel-Cycle/Nuclear-Wastes/International-Nuclear-Waste-Disposal-Concepts/> [Accessed 29/01/2014]

UMEKI, H. 2007. Repository Design. *In:* ALEXANDER, W. R. & MCKINLEY, L. E. (eds.) *Deep geological disposal of radioactive waste.* Amsterdam: Elsevier Science.

2 Literature Review

2.1 Geological Disposal of Radioactive Waste

2.1.1 Radioactive Waste and Geological Disposal

Worldwide over 50 countries have accumulated large inventories of radioactive waste from civil, defence and medical uses of radioactive material (World Nuclear Association, 2014). Nations generally classify their waste by volume into categories based on radioactivity and heat generation, though the category definitions vary between countries (IAEA, 2014). For example, UK radioactive waste is divided into three categories, Low, Intermediate and High Level Waste (LLW, ILW and HLW respectively) differentiated both by activity and the capacity to generate heat (Table 2.1; NDA, 2010a). However, different nations use different classifications making inter-comparison between wastes challenging (Stockdale and Bryan, 2013).

Table 2.1: UK nuclear waste classification scheme and UK radioactive waste inventory reproduced from NDA (2010a)

Waste Classification	Definition	Volume in UK nuclear waste inventory (m^3)*
Low Level Waste (LLW)	Wastes with radioactive content < 4 GBq per tonne of alpha or 12 GBq per tonne of beta / gamma activity	69,100
Intermediate Level Waste (ILW)	Wastes which exceed the upper radioactive content for LLW but which do not generate heat that needs to be accounted for in the design of storage / disposal facilities	103,000
High Level Waste (HLW)	Wastes in which the temperature may rise significantly due to their radioactivity needing to be accounted for in the design of storage / disposal facilities	1,850

* total packaged and unpackaged waste volumes destined for geological disposal correct as of 01/04/2010 (NDA, 2010a)

Worldwide lower activity wastes are currently disposed of in near surface disposal sites such as the LLW repository at Drigg, Cumbria or the sites in South Carolina, Washington, Utah and Texas in the USA (LLWR, 2014;

USNRC, 2013). However, higher level wastes require additional containment and the internationally accepted method for their disposal is geological disposal. This has been adopted as the preferred method for the long-term management of higher activity, long-lived nuclear wastes by many countries including the UK, France, Canada, Switzerland, Sweden and Finland (OECD-NEA, 2008). Geological disposal is founded on the principle of containing the waste until such a time as radioactive decay has minimised the hazard it poses (IAEA, 2003, Umeki, 2007). For example, it has been calculated that UK nuclear waste would require 100,000 to 100,000,000 years to decay to a hazard resembling that of a natural uranium ore body (Figure 2.1; NDA, 2010b).

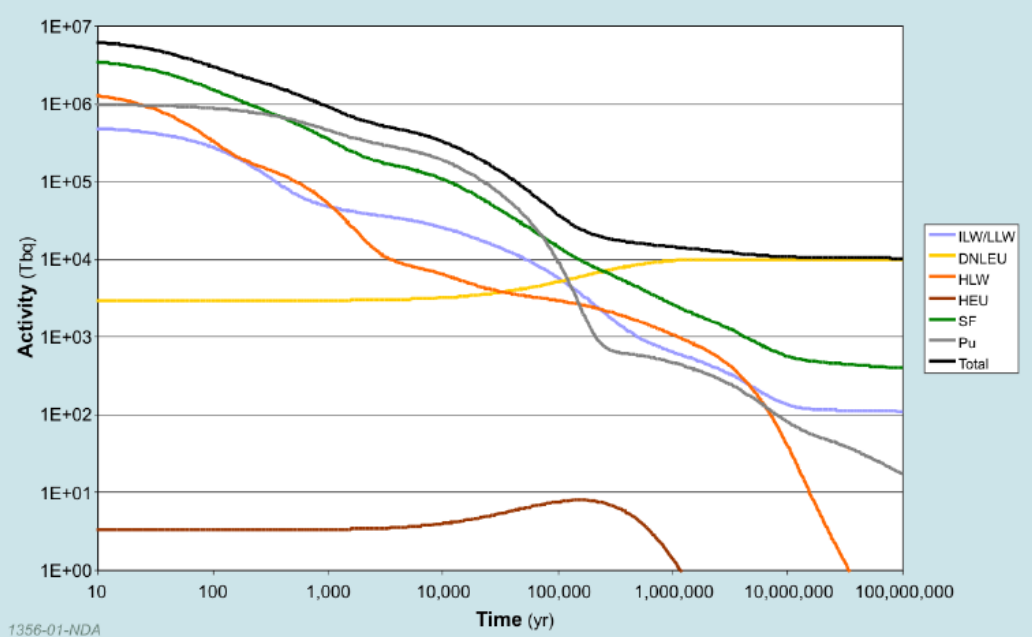

Figure 2.1: The decrease in radioactivity with time from closure of the GDF per cubic meter of conditioned waste for the different types of UK waste (LLW – Low Level Waste; ILW – Intermediate Level Waste; DNLEU – Depleted; Natural and Low Enriched Uranium; HLW – High Level Waste; HEU – High Enriched Uranium; SF – Spent Fuel; Pu – Plutonium) in the UK radioactive waste inventory (NDA, 2010b)

2.1.2 Geological Disposal in the UK

The geological disposal of HLW has been supported in the UK since the mid-1950s when significant volumes of radioactive waste started to accumulate (Flowers, 1976). As a result, the Atomic Energy Association (AEA) commissioned the preparation of a programme of research and development to underpin the geological disposal of HLW by the Institute of Geological Sciences (IGS) in 1975 (Flowers, 1976). At this point solid LLW and ILW was

generally disposed of in surface sites or dumped in the North Atlantic Ocean (Flowers, 1976). The study recommended that the UK adopt a policy of geological disposal either on land or under the ocean for the long-term management of all radioactive waste types and that research should be directed in both these areas (Flowers, 1976). Following this, the government set up the Radioactive waste management Advisory committee in 1978 which founded the organisation that became UK NIREX Ltd in 1982 (Select Committee on Science and Technology, 1999). NIREX pursued site evaluation for a potential repository in the Borrowdale Volcanic Group (BVG) at the Longlands Farm site, Sellafield as the preferred site for a Geological Disposal Facility (GDF). However, after much public controversy all site characterisation ceased in 1997 (Select Committee on Science and Technology, 1999). In reaction to this, the 1999 House of Lords Science and Technology Select Committee report on the management of nuclear waste was commissioned and found geological disposal of radioactive waste to be both a feasible and desirable approach to the management of both ILW and HLW (Select Committee on Science and Technology, 1999). As a result, the government initiated the Managing Radioactive Waste Safely (MRWS) programme (DEFRA, 2008) and established the Committee for Radioactive Waste Management (CoRWM) to review the options for higher activity radioactive waste management (CoRWM, 2006). In 2006 CoRWM reported that geological disposal with interim storage would be the best available long-term approach to the management of radioactive waste (CoRWM, 2006) and in 2008 the Government set out its plans and policy for implementing geodisposal in the 'Managing Radioactive Waste Safely' publication (DEFRA, 2008). This outlined a staged process for site selection based on volunteerism by potential site communities. However, the withdrawal of Cumbria, the only potential volunteer community, from the MRWS process in 2012 has led to the process has been reassessed and national geological screening being undertaken by Radioactive Waste Management (RWM) Ltd, the developer responsible for the delivery of the UK GDF (DECC 2014). This national screening will inform a future volunteerism approach to site selection (DECC

2014). At present, UK ILW and HLW are in interim storage pending the availability of a geological disposal facility (NDA, 2014).

2.1.3 Geological Disposal Facility Design

The design of geological disposal facilities involves the emplacement of nuclear waste in underground vaults and is based on the concept of multi-barrier containment (Umeki, 2007). At the heart of this method of containment is an Engineered Barrier System (EBS) in which ILW / HLW is conditioned in a wasteform, packaged in a container, and surrounded by a buffer / backfill material (Fig. 2.2). Each component of the EBS has a role in limiting radionuclide release. The wasteform increases the waste's resistance to leaching; the container acts to ease waste handling, emplacement and retrievability; and the backfill component is used to retard radionuclide transport, reduce repository permeability (in the case of bentonite) and stabilise GDF Thermo-Hydro-Mechanical-Chemical (THMC)-coupled conditions (IAEA, 2003; Umeki, 2007). The EBS is generally considered the most important part of the barrier system for the initial hundreds to thousands of years of waste containment but components may begin to degrade after this time (IAEA, 1999).

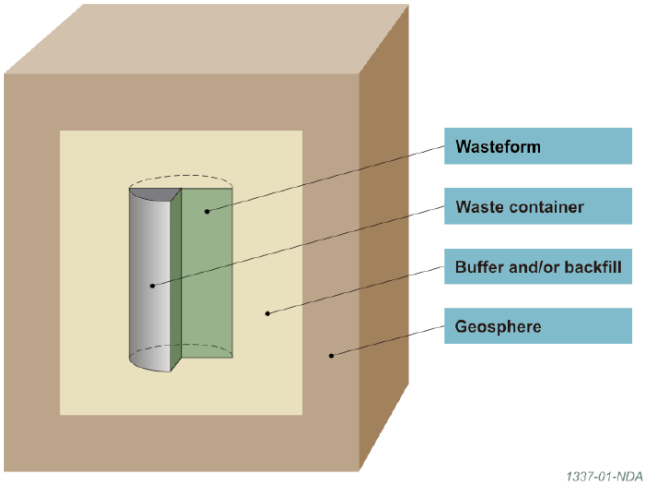

Figure 2.2: Schematic of the components which make up the multi-barrier approach (NDA, 2010c)

Further isolation of the EBS is achieved by constructing the facility in rock (termed 'host rock') at 500-1000m depth (Miller et al., 2000). The role of the rock in the waste containment is manifold. Firstly, the host rock acts as a geological barrier to isolate waste from the surface environment. This not only

protects the EBS from dynamic human and natural (e.g. glaciation) processes which occur at ground surface, but also, in an ideal situation, provides a chemically, mechanically and hydrogeologically stable environment in which any changes can be predicted with confidence (Norris, 2012). The geological barrier will also allow conduction of heat away from heat generating waste and allow diffusion of gases produced in a GDF to prevent mechanical disruption of the EBS (Norris, 2012). In addition, the geological barrier also has the potential to actively retard the transport of radionuclides in groundwater through sorption of radionuclides to mineral surfaces and can aid the dispersion, and therefore dilution, of radionuclides through promotion of hydraulic dispersion (Norris, 2012). The geological barrier is deemed to be the most significant barrier to radionuclide transport from a GDF beyond thousands of years of waste containment (IAEA, 1999). Generally, suitable environments may be described as extremely low permeability rocks, deep groundwater systems with extremely low advective fluxes or groundwater systems which have low fluxes and long transport paths, minimising the risk of biosphere interaction (IAEA, 2003; Falck and Nilsson, 2009). Specifically, three rock types have been suggested as of interest as GDF host rocks; evaporites (salt formations), clay and hard crystalline rocks (Flowers, 1976; NDA, 2010d). For example, the Waste Isolation Pilot Plant (WIPP) site in New Mexico is located in natural rock salt and has been open since 1999 for the disposal of transuranic wastes from US defence operations (National Research Council, 2004). France and Belgium propose GDF sites in clay formations and Sweden and Finland propose GDF sites in hard crystalline rock (IAEA, 2009).

The nature of the host rock is fundamental for determination of the disposal concept to be used and the design of the GDF (NDA, 2010e). However, the final design of the repository and EBS will also be dictated to some extent by the nature of the waste and the wasteform (NDA, 2010e). In the UK, as no host rock has been chosen, generic GDF design concepts have been developed. However, the different disposal requirements of ILW and HLW will necessitate different GDF designs. In the UK, glass / ceramic wasteforms will

be used to condition HLW and vaults will be backfilled with bentonite clay (NDA, 2010e). Bentonite will be used as it provides a low permeability barrier which will attenuate radionuclide migration, filter GDF derived colloids, and limit the transport of dissolved species which could cause corrosion into the GDF (NDA, 2010e). Bentonite will also provide stability during canister emplacement and over long term disposal, create a chemical environment which maintains canister integrity, provides an environment that minimises microbial activity and will protect the host rock from the thermal effect of the waste (NDA, 2010e). In the case of ILW the waste is immobilised in cement based grouting material in stainless steel containers (DEFRA, 2008). The containers will then be placed in engineered vaults in the GDF and backfilled with cement based material (Fig. 2.3; NDA, 2010e). Bentonite cannot be used in an ILW GDF as cement and bentonite are incompatible (Bach et al., 2013). However, cement has manifold advantages as a backfill material. It will raise pH of groundwater and raise Ca levels which will preserve the integrity of cementitious wasteform, limit radionuclide solubility, provide a large surface area for radionuclide sorption, provide mechanical support for the GDF, allows migration of gas from waste, of low strength to allow retrievability of waste if required and is a well-established and economical material to use (NDA, 2010e). It is also likely that cement will be used as a repository construction material (NDA, 2010e). GDF designs containing cementitious materials are also currently proposed by France, Canada and Switzerland (Andra, 2012; Nuclear Waste Management Organisation, 2010; NAGRA, 2014).

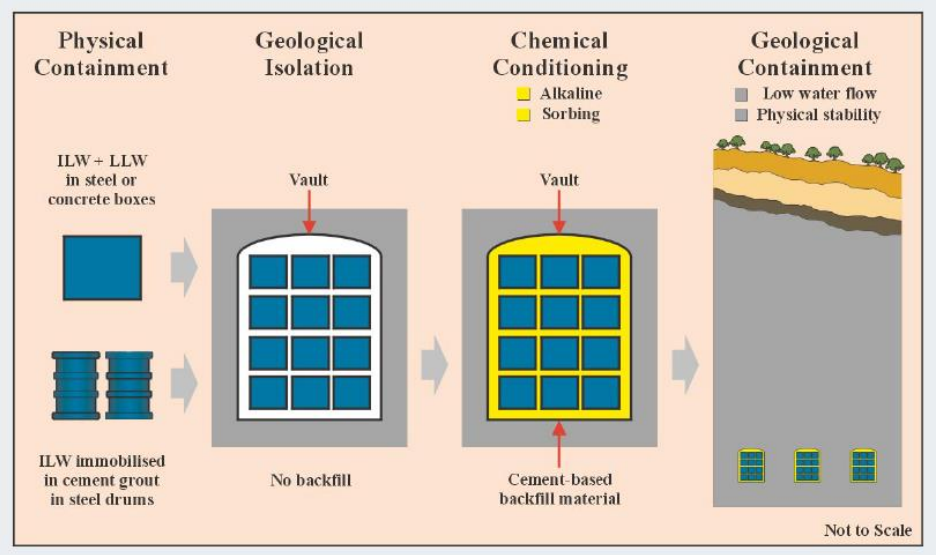

Figure 2.3: Schematic design of a GDF for the long-term management of ILW (NIREX, 2002).

2.2 The Chemically Disturbed Zone (CDZ)

The most common variety of cement, Ordinary Portland Cement (OPC), is generally composed of alite, belite, aluminate and ferrite (Taylor, 1997). Conceptual UK ILW GDF designs include the use of Nirex Reference Vault Backfill (NRVB) which is composed of Portland cement, hydrated lime and limestone flour (Butcher et al., 2012). When mixed with water the cement rapidly hydrates forming predominantly (approximately 2/3 of the hydrated mineralogy) Calcium Silicate Hydrate (C-S-H) phases (Taylor, 1997). C-S-H phases are part of a complex group of silicate phases of varying Ca:Si ratio (Fig. 2.4) and varying crystallinity (Shaw et al., 2000). The remainder of hydrated cement is composed of portlandite (approximately 25% of the hydrated mineralogy) with minor calcite, hydrogarnet, ettringite and non-hydrated primary phases (Taylor, 1997). Hydration also results in the formation of an alkali rich pore solution, containing predominantly K^+ and Na^+ (Glasser, 2003).

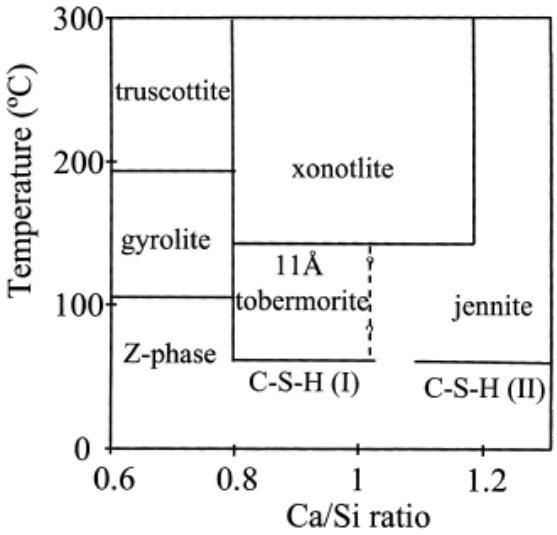

Figure 2.4: Schematic C-S-H stability diagram displaying the different stable C-S-H phases and related minerals (Shaw et al., 2000)

The emplacement of a cementitious GDF for ILW will affect the chemical properties geosphere (Umeki, 2007). Once emplacement and backfilling of waste into a GDF is complete, the facility will re-saturate with groundwater (NDA, 2010f). As groundwater interacts with the cement in a GDF components of the cement will begin to dissolve. This will raise the pH of the groundwater and form a hyperalkaline leachate plume (Fig. 2.5; Atkinson, 1985; Berner, 1992; Butcher et al., 2012).

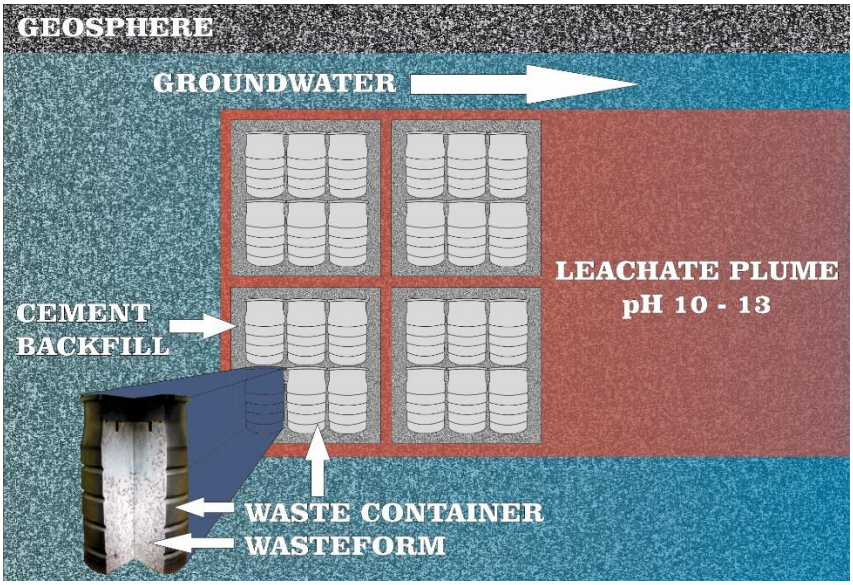

Figure 2.5: Schematic diagram illustrating the Engineered Barrier System (EBS) concept and developing high pH leachate plume in a cementitious GDF.

The chemical composition and pH of this leachate will evolve over time as different components of the cement dissolve (Fig. 2.6; Atkinson, 1985; Berner, 1992). In general initial mobilisation of KOH and NaOH from the cement pore fluid will form a leachate of pH ~ 13. This will also be saturated with respect to the portlandite ($Ca(OH)_2$) but, due to the low solubility of $Ca(OH)_2$ at high pH, the concentration of Ca in solution will be low (~ 80-100 mg l^{-1} (Mäder et al., 2006)). Once the KOH and NaOH are consumed, the leachate pH will fall to ~ 12.5 where it will be buffered by equilibration with portlandite ($Ca(OH)_2$). The leachate will remain at this pH until all the $Ca(OH)_2$ in the cement has dissolved. Latterly, the leachate composition and pH will be controlled by equilibrium with C-S-H phases in the cement buffering pH at ~ 10.5 before returning to the unperturbed groundwater pH. The timescale for each phase of leachate evolution will depend on many factors, including cement type and groundwater flow rate. For an OPC in groundwater free from components which affect cement dissolution (e.g. Ca, Si, CO_3) with a representative sub-surface flow rate of 10^{-10} m s^{-1}, the initial pH ~ 13 period (NaOH / KOH buffered) was modelled to last for ~ 8.5×10^3 years (Atkinson, 1985). The second period ($Ca(OH)_2$ buffered pH ~ 12.5) was modelled to persist for ~ 2.3×10^5 years, and the final phase (C-S-H gel buffer, pH ~10.5) for ~ 2.8×10^6 years (Atkinson, 1985). The exact chemical composition of cement leachate formed will depend on local groundwater chemistry and the particular cement paste used and any additives contained within it (Andersson et al., 1989). However, generally it is estimated that cement dissolution would raise pH above 10.5 until 10^4 – 4×10^6 years post repository closure (Atkinson, 1985).

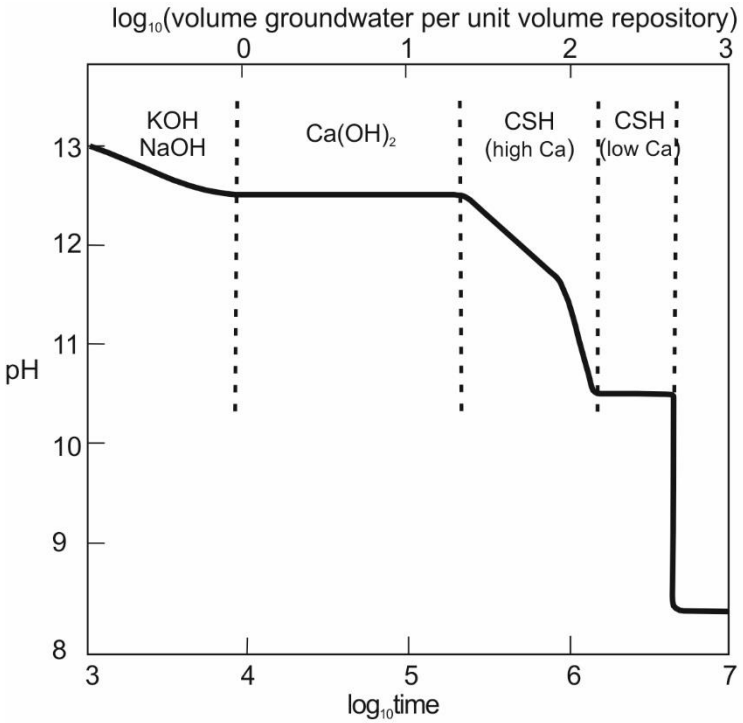

Figure 2.6: Graph of the modelled evolution of cement pore fluid pH around a GDF over time for a repository with 185 kg m^{-3} average cement content and 10^{-10} ms^{-1} water flux density (Atkinson, 1985).

The leachate will form a temporally and spatially heterogeneous Chemically Disturbed Zone (CDZ) in the geosphere surrounding the repository where groundwater composition is altered and pH is elevated (NDA, 2010d). In addition to evolving over time due to the dissolution of different cement components reaction with the host rock will also cause the composition and pH of the plume to evolve (Savage, 2010).

2.3 High pH rock alteration in the CDZ

2.3.1 Dissolution and precipitation reactions and ion exchange

The high pH leachate in the CDZ will react with the host rock and change its physical (e.g. porosity and permeability) and chemical (e.g. sorption capacity) properties potentially affecting its ability to act as a geological barrier. For example, mineral dissolution could increase rock permeability and promote radionuclide transport, or the formation of secondary phases could block flow paths and have the converse effect (NDA, 2010d). The formation of secondary phases on the surfaces of primary minerals will also change the nature of the surfaces onto which radionuclides could adsorb e.g. if secondary

phases have a greater reactive surface area or sorption capacity for radionuclides this could retard contaminant transport (Nirex, 2002).

In a solution, the breakdown of mineral surfaces at the solution interface occurs through interactions between charged mineral surfaces and ions in solution. For example, OH^- bind to exposed surface cations and H^+ bind to surface anions (Loughnan, 1969). The formation of these bonds then polarises and weakens the structural bonds of the surface species in the mineral structure and the progressive sorption of 1 or more ions may cause structural bonds to break and the surface species to enter solution (Schott et al., 2009). pH will affect the ionic properties of the solution and the stoichiometry and concentration of charged surface species (Schott et al., 2009). For example high solution pH will result in a greater abundance of uncharged and negatively charged surface sites. Dissolution will also vary depending on the solution's ionic strength, as if there are more ions available to sorb to the mineral surface the mineral's structural bonds are more likely to be broken, and the aqueous species in solution, foreign to the mineral structure, will promote dissolution by creating defects in the mineral structure (Schott et al., 2009). As cement leachates can be expected to have high ionic strength, due to dissolved cement components and the high salinity groundwaters presence at depth, they are therefore likely to promote mineral dissolution in the CDZ. The effect of elevated pH on dissolution can be understood by looking at specific minerals in detail. For example, the dissolution of quartz requires only the breaking of Si-O bonds and dissolution as a function of pH is interpreted as a function of $>SiOH_2^+$, >SiOH and $>SiO^-$ (Schott et al., 2009). At high pH $>SiO^-$ will be the dominant surface species and it has been shown that the dissolution rate constant of this deprotonated species is several orders of magnitude greater than the neutral species (Fig. 2.7; Nangia and Garrison, 2008).

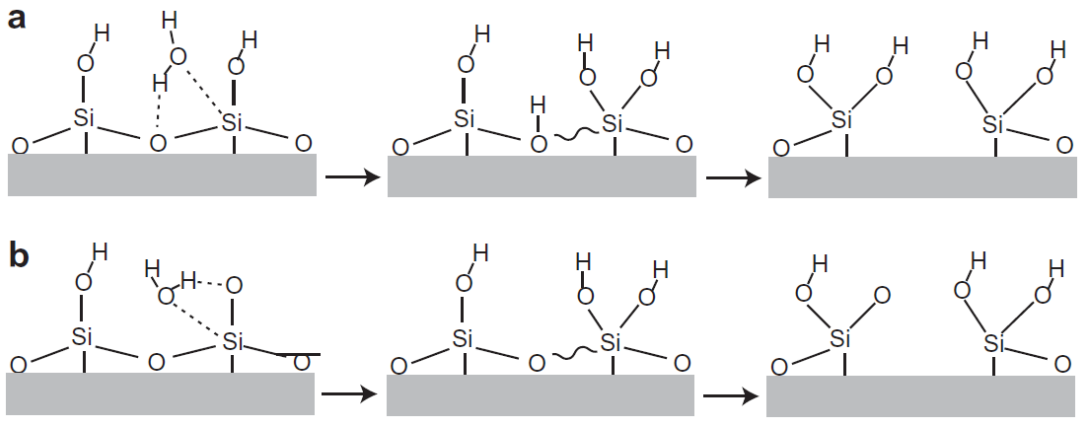

Figure 2.7: schematic diagram of the hydrolysis of a quartz surface in which a) H_2O hydrolyses a Si center and weakens the adjacent bridging bond (low pH) b) H_2O hydrolyses a Si center and weakens the adjacent bridging bond catalysed by the presence of an $>SiO^-$ group (high pH), (adapted from Bickmore et al., 2008).

The variation of quartz solubility as a function of pH is shown in Fig. 2.8, highlighting the increased stability of aqueous species above pH 10.

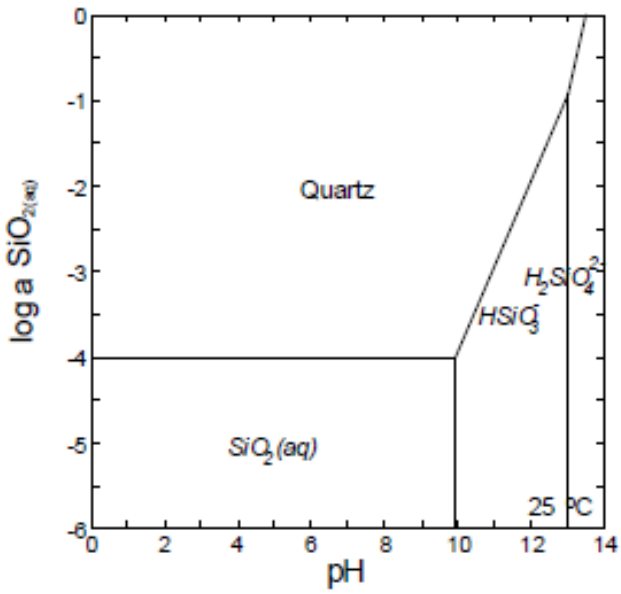

Figure 2.8: Variation in quartz and silica stability with pH at 25°C (Savage, 2010)

The dissolution of mixed oxide minerals, such as feldspars, requires the breaking of more than one type of bond (Schott et al., 2009). These bonds will have differing strengths and the relative rate of breaking metal-oxygen bonds appears to be dependent on pH to some extent e.g. breaking Al-O and Mg-O bonds is slower than breaking Si-O bonds at alkaline pH (Schott et al., 2009). The rate of dissolution of mixed oxides is governed by the rate limiting step for dissolution, i.e. the breaking of the slowest breaking metal-oxygen

bond that is essential for maintaining the mineral structure (Schott et al., 2009). Mixed oxide dissolution can also involve the exchange of protons for metals not essential to maintain mineral structure (Schott et al., 2009). For example, during the dissolution of feldspars metal depleted surface layers are formed leaving residual alumina-silicate gels or insoluble silica (Schott et al., 2009; Loughnan, 1969; Oelkers et al., 1994).

After the breakdown of the parent mineral structure with the release of the more soluble cations and silica to solution, the residue is reconstituted with components from solution to create more stable phases or secondary phases may precipitate directly from solution via nucleation and growth (Loughnan, 1969; Fritz and Noguera, 2009). In natural systems clay minerals are the most common secondary phases formed (Oelkers et al., 1994). However, the secondary phases that form in the CDZ will be affected by solution composition and the difference in species' solubility at elevated pH. For example, the precipitation of brucite ($MgOH_2$) above pH 10 (Pokrovsky and Schott, 2004) would limit the concentration of Mg in the highest pH zones at the site whereas gibbsite ($Al(OH)_3$) solubility increases with increasing pH above pH 6 (May et al., 1979).

Minerals in solution may also undergo ion exchange in which ions in the mineral structure are replaced by ions from the solution (Appelo and Postma, 2005). This alteration process is common in clay minerals where metal cations in the octahedral layers are exchanged (Appelo and Postma, 2005). The ion exchange properties of a mineral are dependent on both its permanent and pH dependent surface charge (Chichester et al., 1970). In general, the cation exchange capacity of a mineral, the extent to which a mineral can adsorb and exchange cations, increases with increased pH due to the reduced availability of competing H^+ ions in solution.

Reaction kinetics will have an important role in dissolution and precipitation reactions as these are heterogeneous reactions affected by many different processes (Langmuir, 1997). The reaction kinetics of many minerals are poorly constrained at hyperalkaline pH (Fig. 2.9; Brantley, 2008). However, most of the more soluble mineral phases, for example carbonates, react

rapidly and will reach equilibrium with the solution in a short period compared with groundwater residence times (Appelo and Postma, 2005).

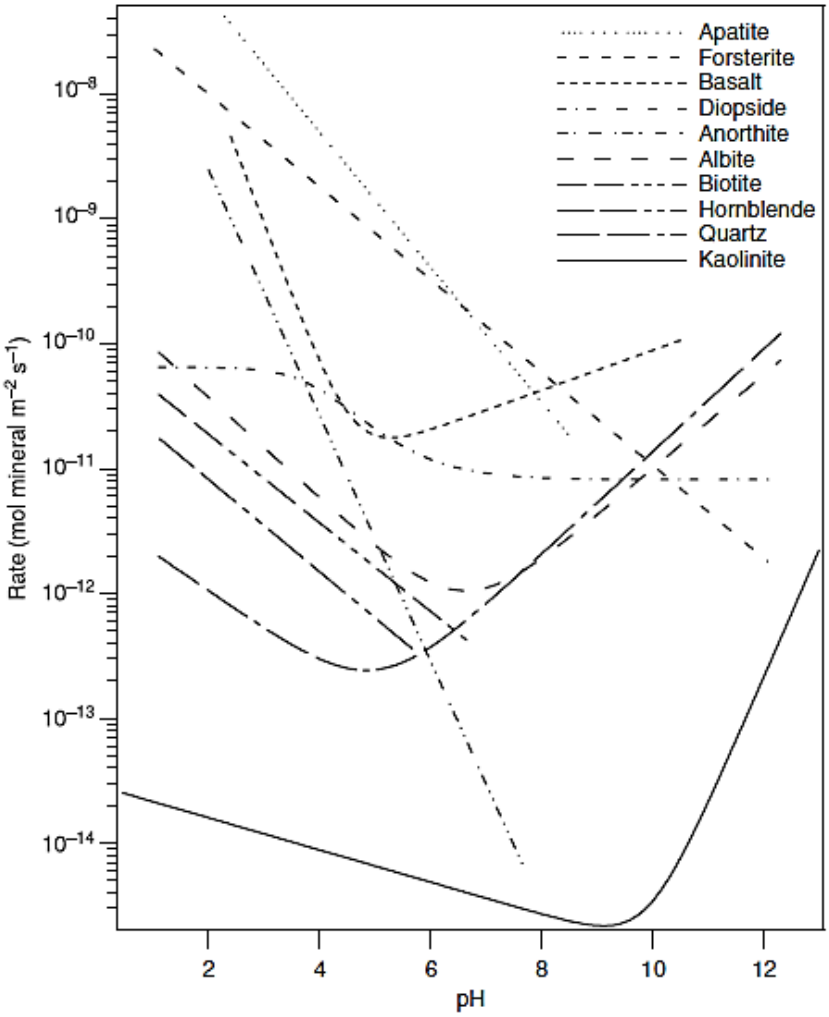

Figure 2.9: predicted dissolution rates for various silicate minerals as a function of pH at 25°C (Brantley, 2008).

The precipitation of minerals from solution in deviation from thermodynamic equilibrium is a common occurrence (Fritz and Noguera, 2009). For example, the formation of secondary metastable minerals (e.g. Calcium Silicate Hydrates (C-S-H) which have rapid growth rates occur preferentially over the formation of thermodynamically stable phases with slow growth rates (Santen, 1984). In the CDZ the very low solution flow rates (e.g. 10^{-10} ms^{-1} (Atkinson, 1985)) and the long timescale relevant to geodisposal may mean that relatively slow reactions may occur and equilibrium / near equilibrium conditions may be attained. Therefore, it is possible that the dominant reaction processes observed on the timescale of laboratory experiments may

be succeeded by reaction processes with slower reaction rates over timescales relevant to geodisposal.

2.3.2 Previous experimental studies

Cement leachates have the potential to alter the fundamental properties of the host rock in the CDZ. Therefore, understanding the potential chemical and mineralogical changes is fundamental to developing a long term safety case for any cementitious repository. As a result, much research has been conducted into rock and mineral alteration in high pH cement leachates (e.g. Gaucher and Blanc, 2006; Rochelle et al., 1998; Mader et al., 2006; Savage, 2011; Hodgkinson and Hughes, 1999; Braney et al., 1993; Savage et al., 1992; Bateman et al., 1999; Ramirez, 2005; Fernandez et al., 2010; Fernández et al., 2009; Ramirez et al., 2002). In order to understand the processes which may occur at high pH in the CDZ, alteration needs to be considered at the timescales over which the geological barrier will be required to maintain its integrity and over which leachate development will occur. To date, much work has focused on short term laboratory and in-situ experiments in Underground Rock Laboratories (URLs) to assess the processes which may occur in the first years of reaction (e.g. Gaucher and Blanc, 2006; Mader et al., 2006). Laboratory experiments provide well-constrained data under controlled conditions providing insight into processes predicted to occur in the geosphere. Experiments conducted in URLs extend this knowledge and play an important role in increasing our understanding of alkaline rock alteration reactions as they allow experiments to be conducted in complex, natural environments. URLs have been constructed at many sites including former mines (e.g. Tono (sedimentary rock) and Kamaishi (granite), Japan and Stripa Mine (granite), Sweden), existing tunnel excavations (e.g. Grimsel (granite) and Mont Terri (clay), Switzerland) and purpose built facilities (e.g. Mol/Dessel (clay), Belgium and Äspö Hard Rock Laboratory (granite), Sweden; IAEA, 2001). The examples given above are generic URLs at sites not intended for waste disposal. However, worldwide a number of site-specific URLs have also been constructed as precursors to repository development to provide experimental evidence of geosphere reactions in proposed rock types. These

include ONKALO (granite), Finland, Haute Marne (shale / argillite), France, Gorleben (salt dome), Germany (IAEA, 2001). Work at these sites has included experimental programmes focussed on cement-rock interactions such as the high pH plume experiment at Grimsel (European Commission, 2005), the high-pH cement water experiment at Mont Terri (European Commission, 2005; Adler et al, 1999) and a cement study at Haute Marne (Claret et al., 2010).

Experimental studies have been complimented by investigation of industrial / anthropogenic and natural analogues at sites where cement leachates or similar solutions have undergone reactions with rock over hundreds – hundreds of thousands of years (Fig. 2.10; e.g. Savage, 2011). To better understand the reaction processes occurring, computer modelling has also been used to aid interpretation of experimental and analogue studies and to predict how high pH systems might evolve over time (e.g. Soler and Mäder, 2007; Fernandez et al., 2010; Alexander et al., 1992).

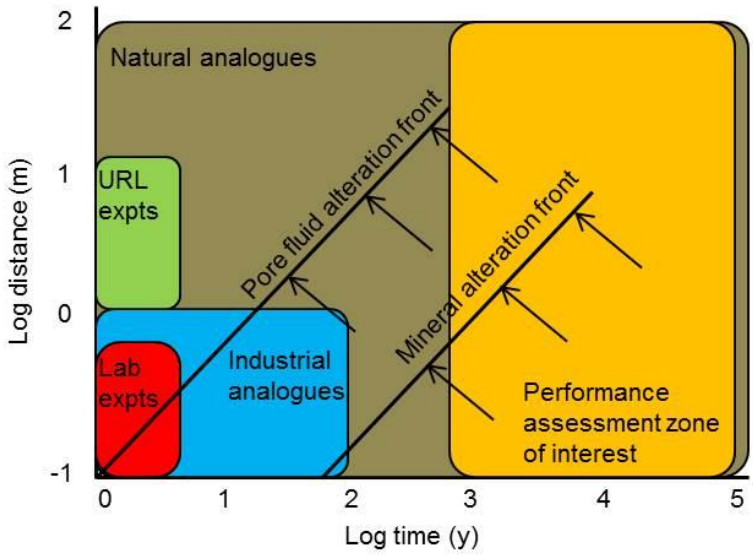

Figure 2.10: Schematic illustration of how different investigative techniques relate to the temporal and spatial scales of interest for the Performance Assessment (PA) of a GDF (adapted from Savage, 2011)

Overall is has been suggested that CDZ alteration can usefully be divided into two regions (Fig. 2.11; Savage, 2011). Firstly, in the zone closest to the cement/rock interface (zone 1) where extensive mineral alteration occurs, including dissolution of the primary silicate minerals and precipitation of

secondary phases, which can be crystalline or amorphous. Secondly, there is a zone further from the cement rock interface (zone 2) where the pH and composition of the groundwater are also perturbed and ion exchange reactions between the minerals and fluid are important, but where rock alteration is significantly diminished. Previous research has predominantly focused on the potential rock alteration in zone 1 due to predicted greater reactivity in this zone.

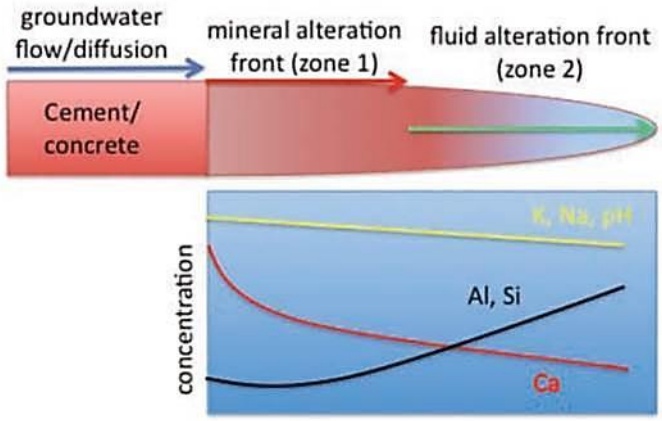

Figure 2.11: Variation in high pH plume chemistry with time / distance due to interactions with groundwater and host lithology (Savage, 2011).

Many short term experimental studies have investigated rock alteration in high pH cement leachates (zone 1), using a variety of solution compositions (e.g. early and late stage leachates), single minerals and rock types (Gaucher and Blanc, 2006 and references therein). Generally, these studies have found that reaction in high pH, Ca-bearing cement-type leachates results in the dissolution of silicate minerals (Eq. 2.1; e.g. Rochelle et al., 1998; Honty et al., 2010) followed predominantly by the precipitation of secondary C-S-H phases (Eq. 2.2) of varying Ca:Si ratio (e.g. 0.5-1.5 (Gaucher and Blanc, 2006)), morphology and crystallinity e.g. C-S-H gel (Savage and Rochelle, 1993; Hodgkinson and Hughes, 1999) and fibrous C-S-H phases thought to be related to the chain structured C-S-H minerals jennite and tobermorite (Braney et al., 1993).

$$KAlSi_3O_8 + 3OH^- + 2H_2O \rightarrow Al(OH)_4^- + 3HSiO_{3\,(aq)}^- + K^+_{(aq)} \qquad \text{Eq. 2.1}$$

$$SiO_{2(aq)} + Ca^{2+}_{(aq)} + H_2O \rightarrow C\text{-}S\text{-}H_{gel} \qquad \text{Eq. 2.2}$$

In situations where aluminium (e.g., from primary mineral dissolution) and potassium (e.g. dissolved in cement leachate) are present, secondary aluminium and potassium bearing C-S-H (C-(A)-(K)-S-H) phases have also been identified (e.g. Fig. 2.12; Braney et al., 1993; Savage et al., 1992). The incorporation of aluminium and potassium has been found to vary and to be dependent on the primary minerals present. For example, Bateman et al. (1999) identified C-(A)-S-H phases containing up to 1% aluminium formed as secondary phases during the high pH reaction of albite and muscovite while Hodgkinson and Hughes (1999) found C-(A)-S-H phases containing 8-24 mol% following the alteration of anorthite, chlorite and muscovite. It has also been found that secondary C-(A)-(K)-S-H formation is rapid compared to the dissolution of aluminosilicate minerals at high pH, and dependent on the availability of dissolved silica, which suggests the dissolution of the primary minerals is the rate limiting step in the formation of secondary C-(A)-(K)-S-H (Savage et al., 1992; Savage et al., 1998).

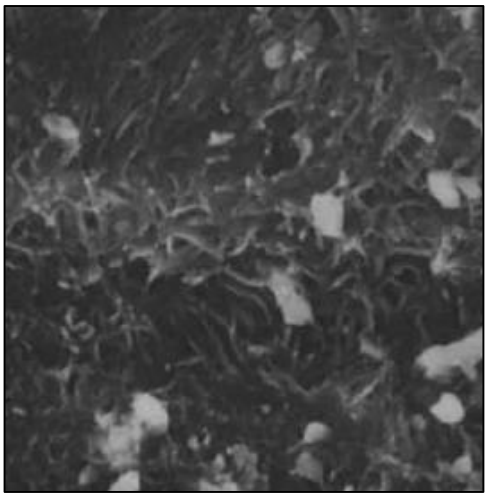

Figure 2.12: Secondary 'sheet-like' C-S-H formed on mineral grain surfaces during the alteration of silicate minerals in synthetic cement leachate (from Savage et al., 1992).

In addition to secondary C-(A)-(K)-S-H phase formation, studies of clay alteration (e.g. bentonite) in cement leachates containing Na and K have also noted the formation of a number of Na/K/Ca bearing silicate phases including zeolites (e.g. phillipsite $(K,Na,Ca)_{1\text{-}2}(Si,Al)_8O_{16}\cdot 6H_2O$ and analcime $NaAlSi_2O_6\cdot H_2O$) and apophyllite ($KCa_4Si_8O_{20}(OH).8H_2O$) (Gaucher and Blanc, 2006; Ramirez, 2005; Fernandez et al., 2010; Fernandez et al., 2009; Ramirez et al., 2002). Secondary analcime and phillipsite formation was also

identified in experiments investigating the alteration of the Opalinus shale in NaOH and KOH dominated cement porewaters formed at the expense of kaolinite, quartz and chlorite, though these experiments were conducted at 150-200 °C (Chermak, 1992; Chermak, 1993). The formation of zeolitic phases at high pH is known to be affected by several factors. For example a lower Si:Al ratio results in accelerated zeolite growth (Mariner and Surdam, 1970). However, the formation of these phases is also affected by pH as zeolites form at lower pH (pH 7.5-10.5) than C-(A)-S-H phases (Savage et al., 2007).

Though dissolution-precipitation processes have been found to be the principle reaction mechanisms at high pH in zone 1 in the CDZ, ion exchange has been found to be important in the alteration of clay minerals in zone 1 (Gaucher and Blanc, 2006; Savage et al., 1998; Haworth et al., 1988). However, it is thought that at longer timescales relevant to geodisposal (greater than years) ion exchange will have little effect in zone 1 as smectite will eventually dissolve and be replaced (Hodgkinson and Hughes, 1999). When dissolved carbonate is present within the high pH system, it will react with the dissolved Ca^{2+} in these solutions and form calcium carbonate minerals e.g. calcite (Hodgkinson and Hughes, 1999). Carbonate may also be released into solution during high pH rock alteration. For example, cement pore water has been shown to promote the breakdown of dolomite ($CaMg(CO_3)_2$) according to the reaction shown in Eq. 2.3 (Bérubé et al., 1990; Braithwaite and Heath, 2013 and references therein) releasing carbonate and Mg^{2+} to solution which would then form calcium carbonate and brucite. Brucite and the subsequent formation of Mg-silicates have also been identified as secondary phases produced during the high pH alteration of Mg-smectite and during high pH experimentation at the Mont Terri and Bure clay URLs (Lentz et al., 1985 in Hodgkinson and Hughes, 1999; Adler et al, 1999; Read et al., 2001).

$$MgCa(CO_3)_2 + 2OH^- \rightarrow Mg(OH)_2 + CaCO_3 + CO_3^{2-}{}_{(aq)} \qquad \text{Eq. 2.3}$$

It has been identified that high pH rock dissolution is affected by several parameters including primary mineralogy (Hodgkinson and Hughes, 1999), fluid composition (Bateman et al., 1999, Fernández et al., 2009, Savage et al., 1992) and temperature (Ramirez et al., 2002, Fernandez et al., 2010). $Ca(OH)_2$ dominated solutions have been found to be significantly less reactive than KOH and NaOH dominated fluids, attributed to their lower, less aggressive pH (Bateman et al., 1999, Fernández et al., 2009, Savage et al., 1992). In other studies it has been found that pH, affected by the dominant cation in solution, has a significant impact on mineral dissolution with the dissolution of silicates found to be 2-3 orders of magnitude greater at pH 12-13 than at neutral pH (Honty et al., 2010; Savage et al., 1992). For example, the volume of precipitates has been found to be greater in KOH and NaOH dominated fluids than $Ca(OH)_2$ dominated solutions as would be expected due to the increased dissolution at higher pH in KOH and NaOH dominated fluids releasing more components to solution for the formation of secondary phases (Rochelle et al., 1997). Increased temperature has been found to increase the dissolution of primary phases (Fernandez et al., 2010, Ramirez et al., 2002). The formation of secondary minerals has been found to be affected by the same factors i.e. primary mineral type (Hodgkinson and Hughes, 1999), fluid composition (Bateman et al., 1999, Fernández et al., 2009, Savage et al., 1992) and temperature (Ramirez et al., 2002, Fernandez et al., 2010). However, generally the same reaction processes have been found to occur and the same assemblage of secondary phases form in leachates of different composition when all other factors are the same (Bateman et al., 1999; Rochelle et al., 1997). Increased temperature has been found to increase the amount of secondary phase produced and favour the formation of crystalline secondary phases, as would be expected due to the increased energy in the system (Fernandez et al., 2010, Ramirez et al., 2002).

The dissolution and precipitation of minerals in the CDZ will be further complicated by the alteration processes themselves changing the fluid chemistry and pH of the migrating leachate plume. For example, as secondary minerals form they may take in / release H+ or OH- which may alter pH (Savage et al., 2007; Savage, 2010). This may affect alteration processes

such as silicate mineral dissolution. However, generally, experimental studies have been limited in timescale, with few lasting longer than 1-2 years (e.g. a 540 day experiment is the longest study reviewed by Gaucher and Blanc, 2006; Fernandez et al. (2010) conducted a 600 day experiment) and no longer-term (>10 years) experimental studies examine the stability of these secondary phases over extended timescales. However, even at this temporal scale the potential for metastable phases to form and be succeeded by more stable phases. For example, secondary chabazite can be succeeded by the formation of merlinoite (Fernandez et al., 2010). C-(A)-S-H phases have also been shown to evolve in composition and crystallinity over time with poorly ordered C-S-H gel of variable composition evolving to a more ordered structure with a narrower range of compositions (Savage et al., 2007). For example, (Hodgkinson and Hughes, 1999) found that after 200 hours reaction of anorthite with a $Ca(OH)_2$ saturated fluid, products included a poorly ordered fibrous C-A-S-H phase which has evolved to a well ordered fibrous C-A-S-H phase by 800 hours.

2.3.3 Analogue studies

As GDFs will evolve over hundreds of thousands of years, in order to investigate potential mineral alteration and evolution at loner timescales investigators have turned to natural analogue studies. Analogue studies of CDZ-type alteration provide useful indications of the long-term of effect alteration (hundreds – hundreds of thousands of years). A review of many such sites representing timescales of alteration from ~ 30 years to > 1 million years is provided by Savage (2011). These include natural analogues such as Maqarin, Jordan (Milodowski et al., 1998) where naturally produced alkaline groundwaters of similar composition to cement pore fluids have interacted with surrounding rocks at timescales extending beyond 1 million years. At the Maqarin site natural cements, analogous to OPC, formed from the metamorphosis of clayey limestones and interaction of groundwater with them has produced high pH plumes (Savage, 2010). Two alkaline systems have been identified: Eastern Springs calcium hydroxide saturated, pH 12-12.7; Western Springs calcium hydroxide saturated with high K and Na

concentrations, pH 12.9 (Savage, 2010). Generally in the hyperalkaline groundwater quartz, chert, K-feldspar, glass and plagioclase had undergone significant dissolution while dolomite was moderately reactive (Milodowski et al., 1998). C-S-H was the predominant secondary phase formed, with minor additional phases such as zeolites and ettringite, and the distribution of these phases was broadly similar across the site irrespective of primary rock type (Milodowski et al., 1998). Alteration at Maqarin indicates that a sequence of alteration products may form over time from CSH-type phases (with varying Ca:Si ratio) to zeolite-type phases (Milodowski et al., 1998). In addition, where the hyperalkaline waters discharge at springs travertine ($CaCO_3$) deposits have formed where $Ca(OH)_2$ saturated groundwater has interacted with atmospheric CO_2 (Savage, 2010).

Studies of cements used in the construction of historic structures allow the interaction of cement leachates with rock to be studied up to 1800 years of reaction. For example the Tournemire tunnel, France (Tinseau, 2006; Techer et al., 2012) provides evidence of high pH mineral alteration over ~ 15-125 years of reaction. The tunnel was constructed from breeze blocks in limestone and bedded with lime in the 1880s within the Tournemire argillite (Tinseau et al., 2006). Analysis of samples gathered at the tunnel–argillite interface showed that in the absence of water there was no significant modification of the argillite over 125 years (Tinseau et al., 2006). However, under wet conditions, which would lead to the formation of cement leachate type fluids, dissolution of primary minerals including dolomite is observed and the formation of mixed-layer illite / smectite, zeolites, K-feldspar, calcite and minor occurrences of C-S-H (Tinseau et al., 2006). A shorter term 15 year study of a borehole at the same site identified the secondary formation of predominantly C-S-H and calcite and the limited formation of a Mg-rich mineral phase (Techer et al., 2012). At Hadrian's Wall, UK cement pastes exist which are over 1700 years old (Hodgkinson and Hughes (1999). Study of the interaction of aggregates within this cement found that after 1700 years some quartz, K-feldspar, chert and calcareous material have undergone dissolution and have been replaced by C-(A)-S-H phases of varying composition (Hodgkinson and Hughes, 1999). Dissolution and replacement by C-(A)-S-H

was also observed at the interface of the mortar with blocks of quartz dolerite, in which feldspar was found to be the most reactive primary phase (Hodgkinson and Hughes, 1999).

Saline lakes are also cited as analogue sites for high pH mineral alteration with secondary mineralisation at these sites dominated by the formation of zeolites, analcime, K-feldspar (Surdam and Sheppard, 1978) and Mg-clays (Furquim et al., 2008, Aydogan and Kadir, 2003). These lakes, for example Searles Lake, California, occur in arid areas where extensive evaporation can concentrate lake waters. Despite being of generally lower pH than cement pore fluids (pH 7.5 – 10.5 (Surdam, 1977 and Taylor and Surdam, 1981 in Savage 2010)), these lakes are studied analogues to GDF sites as their waters are similar in composition to the low pH cement leachates formed during equilibrium with C-S-H phases, and to cement leachates which have undergone reaction with rock (Chermak 1992; Chermak 1993). A marked feature of alteration in saline lakes is a distinct zonation of secondary minerals (Surdam and Sheppard, 1978) (Surdam, 1977, Hay 1977 and Hay 1986 in Savage 2010). For example, lateral zonation basinward from predominantly unaltered material to secondary zeolites to analcime to K-feldspar related to basinward increase in pH and evolving solution chemistry (Surdam and Sheppard, 1978). The zeolites commonly found in saline alkaline-lake deposits are analcime, clinoptilolite, phillipsite, erionite, chabazite and mordenite (Surdam and Sheppard, 1978). In higher alkalinity and higher pH lake systems with correspondingly higher K^+:H^+ the crystallisation of K-feldspar from analcime and zeolites is favoured (Surdam and Sheppard, 1978).

In general, analogue studies indicate that over time the dissolution of primary minerals can result in the formation of a variety of secondary phases, predominantly alkali-silica gels (e.g. C-S-H gel), which can crystallise with time to zeolites, C-S-H minerals, and feldspars. However, evidence from Hadrian's Wall show that C-(A)-S-H phases within an hydrated cement can persist for 1700 years, and naturally formed C-S-H phases can persist for tens of millions of years remaining stable without significant crystallisation to an ordered

phase (Hodgkinson and Hughes, 1999). Although, as the condition at many analogue sites vary from those of a repository, or cannot be well constrained, they only provide an indication of the potential processes which may occur and cannot necessarily be viewed as directly comparable systems.

2.3.4 Computer modelling

Experimental and analogue research of high pH rock/mineral alteration have been complimented by many computer modelling studies (e.g. De Windt et al., 2004; De Windt et al., 2008; Watson et al., 2013; Savage et al., 1992; Savage and Rochelle, 1993; Braney et al., 1993; Bateman et al., 1999; Pfingsten et al., 2006; Soler and Mäder, 2007; Fernandez et al., 2010; Alexander et al., 1992; Steefel and Lichtner, 1994). Many of these have been undertaken to aid understanding of the processes which occur during high pH mineral dissolution and precipitation reactions. For example, modelling of the Maqarin analogue site has found zeolite distribution to be linked to the availability of Al in the primary mineral assemblage (Smellie, 1998). Modelling has also shown that ion exchange is an important process in the formation of C-S-H minerals during the high pH alteration of clay (De Windt et al., 2004; Watson et al., 2013).

Computer modelling has also been used to extend experimental and analogue studies and as a predictive tool to forecast the chemical and physical evolution within the CDZ (e.g. Savage et al., 1992; Savage and Rochelle, 1993; Braney et al., 1993; Bateman et al., 1999; Pfingsten et al., 2006; Soler and Mäder, 2007; Fernandez et al., 2010; Alexander et al., 1992). These studies generally support the experimental findings that initially silicate mineral dissolution is followed by secondary phase (e.g. C-S-H) formation (e.g. Steefel and Lichtner, 1994), but at longer timescales there is subsequent transformation of C-S-H to feldspar and zeolite phases, as found at analogue sites (Savage et al., 1992; Eikenberg and Lichtner, 1992; Savage and Rochelle, 1993). However, modelling predictions are limited by their ability to constrain which solid phases will form due to slow reaction rates, and a lack of reliable thermodynamic data for some phases (Hodgkinson and Hughes, 1999; Bateman et al., 1999; Savage and Rochelle, 1993; Savage et al., 2007;

Gaucher and Blanc, 2006). For example, models may over-predict zeolite precipitation as they cannot account for the precipitation of C-(A)-(K)-S-H gel phases, and so model Al precipitates as other phases, mainly zeolite (Hodgkinson and Hughes, 1999). Also, due to the variable composition and crystallinity of C-S-H phases, some models use thermodynamic data for more well constrained crystalline minerals to represent C-S-H in models. For example, tobermorite was used as representative of CSH phases in the modelling of the Maqarin analogue site (Steefel and Lichtner, 1998). This places limitations on the understanding of high pH rock alteration which can be gained from them.

2.3.5 Spatial distribution of alteration

In addition to investigating the reactions which might occur at high pH in the CDZ and the potential effect of this on the host rock, studies have also examined how these processes may vary spatially. Column experiments and associated reactive transport modelling of high pH systems have shown that distinct zonation of secondary phase formation occurs along flow paths (Soler and Mäder, 2007). For example, where C-S-H / C-A-S-H phases form their composition and crystallinity have been found to vary spatially, with composition reflecting the evolving fluid composition with distance (Savage et al., 2007). Bateman et al., also (1999) noted the morphology of secondary C-S-H phases in column studies varied with distance from inlet and included C-S-H crust, flaky, fluffy and fibrous morphologies. Comparison of experimental, analogue and computer modelling studies have allowed development of a conceptual model of the evolution of mineral alteration in the CDZ in which the secondary phases formed changes with distance from the cement barrier from C-(A)-S-H through zeolites and feldspars to a region where ion exchange is the predominant alteration process occurring (Fig. 2.13; Savage, 1998).

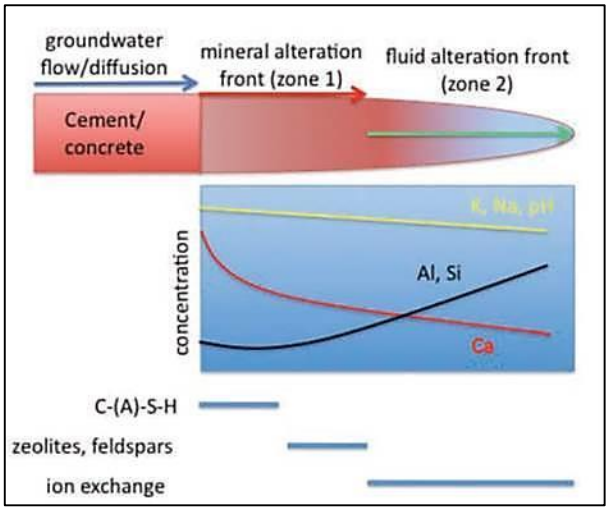

Figure 2.13: Schematic diagram of hyperalkaline plume migration, with theoretical fluid chemistry and dominant secondary mineral type (Savage, 1998).

2.3.6 Porosity and permeability

In addition to changing the chemical nature of mineral surfaces and the assemblage of mineral phases present, dissolution and precipitation in the CDZ could have a significant impact on the porosity and permeability of a host rock. This may affect the advective transport of contaminants from a GDF. However, the importance of the thermodynamic stability and kinetics of mineral dissolution, and their coupling to changing porosity and permeability are poorly understood (Savage, 2010). Variation in mineral/rock alteration spatially may also result in zones of differing porosity and permeability. Studies have found that permeability decreases during the reaction of rock in high pH cement leachates, and reduced porosity has been noted in many studies (e.g. Braney et al., 1993; Rochelle et al., 2001; Fernández et al., 2009; Mäder et al., 2006; Pfingsten et al., 2006). In several of these studies C-(A)-(K)-S-H formation has been found to be responsible for the porosity decrease. For example, core infiltration experiments with fault gouge taken from the Grimsel test site, Switzerland showed a gradual decrease in transmissivity over 9 months attributed to primary mineral dissolution followed by the sealing of flow paths by secondary C-S-Hs/C-(K)-SHs (Mäder et al., 2006; Pfingsten et al., 2006). Secondary C-S-H phases formed during high pH alteration of quartz, muscovite and albite have also been found to coat mineral grains and cement them together leading to reduced sample porosity (Bateman et al., 1999). In-situ tests at the Grimsel test site, Switzerland of a KOH and NaOH

dominated fluid in granite / granodiorite over 2.5 years have also indicated a decrease in the overall transmissivity of the shear zone tested but this was accompanied by a focussing of flow (Mäder et al., 2006). However, modelling of the reaction of a quartz-albite rock in both a $Ca(OH)_2$ solution and a NaOH and KOH dominated solution has suggested that, despite the precipitation of C-S-H phases and zeolites, the reaction would lead to an overall increase in porosity around a repository (Savage and Rochelle, 1993). Some researchers have also noted increased porosity, but in association with reduced permeability. For example, a column experiment flowing sodium hydroxide solution through silica sand found that despite feldspar dissolution the sand permeability decreased, which was attributed to either the rearrangement of grains following dissolution or the precipitation of secondary phases despite no evidence for the presence of secondary phases (Usui et al., 2007). Therefore it is possible that either even small volumes of precipitates greatly affect permeability in these systems or that particle rearrangement along flow paths dominates the change in permeability (Soler and Mäder, 2007, Usui et al., 2007).

Analogue sites have provided evidence of porosity and permeability changes at larger temporal and spatial scales. For example, modelling and field observations of the Maqarin analogue site suggest that the evolution of the flow system at Maqarin is thought to have occurred via cementation of the rock matrix and sealing of fractures due to secondary mineral precipitation (Steefel and Lichtner, 1998). Mineral precipitation in the vicinity of the Tournemire tunnel is also thought to reduce permeability and limit the percolation of water into the argillite (Tinseau et al., 2006). However, analysis of the reaction rims present on aggregates in the historical cements of Hadrian's wall have been found to have increased porosity in outer regions due to dissolution while the inner region exhibited unchanged macro porosity due to the precipitation of secondary minerals (Hodgkinson and Hughes, 1999).

2.4 Uranium behaviour at high pH

2.4.1 Uranium geochemistry

Uranium-238 and uranium-235 are the main components by mass of nuclear fuel. It has been estimated that the UK's civil radioactive waste and materials inventory in 2007 included 80,000 tonnes (once packaged) of uranium (DEFRA, 2008). Uranium-238 is a long lived (half-life of 4.5 billion years) radionuclide expected to be hazardous over hundreds of thousands of years post GDF closure, once components of the EBS have begun to degrade (NDA, 2010b). At this point the geosphere will be of most importance for radionuclide containment and therefore it is likely that U(VI) sorption will be affected by alteration in the CDZ (NDA, 2010b). As high pH rock alteration has been shown to affect both the mineralogy and porosity and permeability of rock, it has the potential to affect the transport of contaminants from a GDF to the biosphere.

Uranium is a redox active element and exists in 5 different oxidation states. However, only U(IV) and U(VI) are stable under natural conditions (Bourdon et al., 2003). Under reducing conditions U(IV) is stable, and is sparingly soluble, readily forming oxides such as uraninite (UO_2; Bourdon et al., 2003; Langmuir, 1997). U(VI) is stable under oxic conditions and is readily soluble, reacting with water through hydrolysis to form the very stable uranyl cation, UO_2^{2+} (Fig. 2.14; Bourdon et al., 2003; Langmuir, 1997). As pH increases the form of this ion changes to $U(OH)^+$ or $UO_2(OH)_3^-$ (Fig. 2.14a). However, uranium readily forms complexes with organic and inorganic (e.g. F^-, Cl^-, PO_4^{3-}, CO_3^{2-} and potentially silicate) ligands as exemplified with carbonate in Fig. 2.14b (Bourdon et al., 2003; Guillaumont et al., 2003). Therefore in natural systems the dominant species present may be variable (Bourdon et al., 2003). For example, at higher pH values (above pH 7.5) carbonate complexes are important and the di- and tri-carbonate complexes of U(VI) dominate and can largely replace U(VI) hydroxyl complexes above pH 6-7 (Langmuir, 1997).

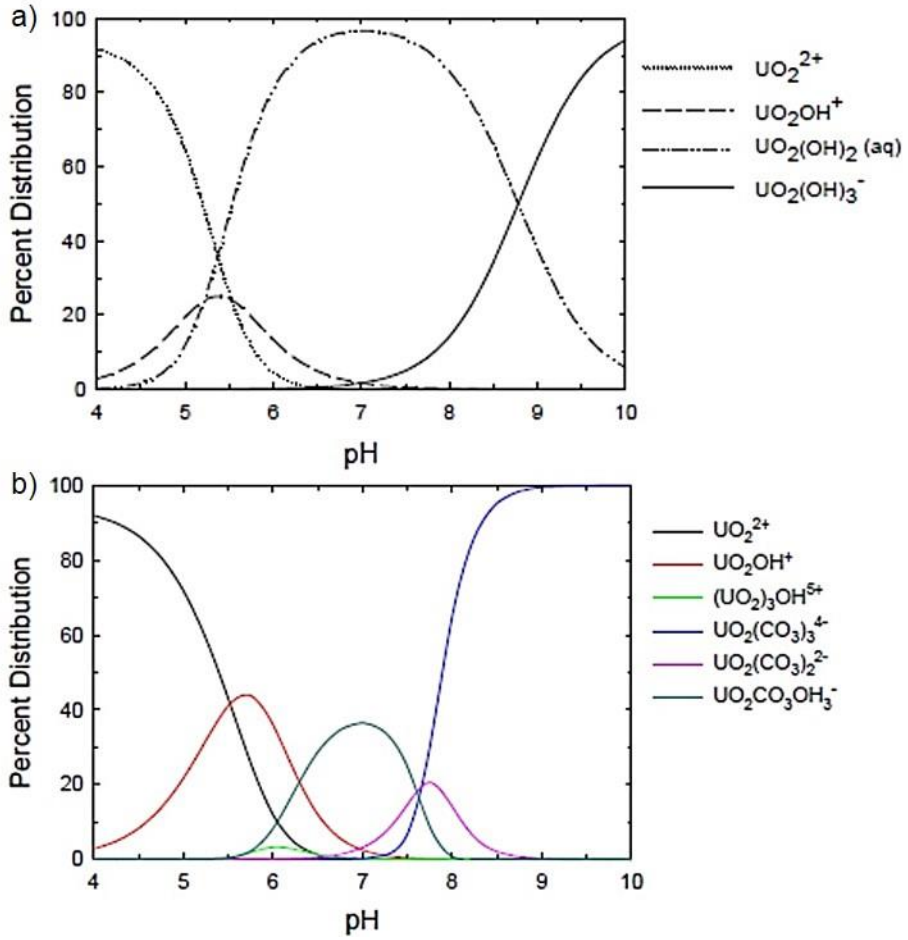

Figure 2.14: Percentage distribution of U(VI) species at 25 °C for a) ΣU = 10-6 M in the absence of complexing ligands other than hydroxide and b) ΣU = 10-6 M at a CO2 pressure of $10^{-3.5}$ bar (reproduced from Golovich et al., 2005).

In non-complexing media the solubility of U(VI) is limited by the hydroxide form ($UO_2(OH)_2$) (Bourdon et al., 2003). However, there is significant uncertainty associated with the thermodynamic constants for soluble and solid U(VI) species (Jang et al., 2006; Guillaumont, 2003) and the presence of complexing media, resulting in the formation of complexes such as those of carbonate, can increase the solubility of uranium by an order of magnitude (Langmuir, 1997; Kramer–Schnabel et al., 1992). Generally where solutions are oversaturated with respect to U(VI), carnotite ($K_2(UO_2)_2(VO_4)_2 \cdot 3(H_2O)$), tyuyamunite ($Ca(UO_2)2V_2O_8 \cdot (5\text{-}8)H_2O$), the autunite group ($Ca(UO_2)_2(PO_4)_2 \cdot 12(H_2O)$) and uranophane ($Ca(UO_2)_2(HSiO_4)2 \cdot 5H_2O$) are the most commonly formed uranyl minerals under natural conditions (Guillaumont et al., 2003; Langmuir, 1997). Schoepite ($\beta\text{-}UO_3 \cdot 2H_2O$) can also form but is relatively soluble and so is rare (Langmuir, 1997). At high pH, in

cement leachates additional phases such as calcium uranate ($CaUO_4$; Harfouche et al., 2006; Mace et al., 2013) could also limit U(VI) solubility, these are summarised in Table 2.2 (Golovich et al., 2005).

Table 2.2: U(VI) minerals with potential to form in cement equilibrated solutions (from Golovich et al., 2005)

Minerals	Chemical Formula
Hydrates:	
Schoepite	$UO_3 \cdot 2H_2O$
Becquerelite	$Ca(UO_2)_6O_4(OH)_6 \cdot 8H_2O$
Compreignacite	$K_2(UO_2)_6O_4(OH)_6 \cdot 8H_2O$
Calcium uranate	$CaUO_4$, CaU_2O_7
Sodium uranate	Na_2UO_4, $Na_2U_2O_7$, $Na_6U_7O_{24}$, or $Na_2U_6O_{19} \cdot 11H_2O$
Silicates:	
Soddyite	$(UO_2)_2(SiO_4) \cdot 2H_2O$
Weeksite	$K_2(UO_2)(Si_2O_5)_3 \cdot 4H_2O$
Boltwoodite	$K(H_3O)(UO_2)(SiO_4)$
Uranophane	$Ca(UO_2)_2(SiO_3OH)_2 \cdot 5H_2O$
Haiweeite	$CaO \cdot 2UO_3 \cdot 6SiO_2 \cdot 5H_2O$
Kasolite	$Pb(UO_2)(SiO_4) \cdot H_2O$
Sklodowskite	$Mg(H_3O)_2(UO_2)(SiO_4)_2 \cdot 4H_2O$

At lower U(VI) solution concentrations, in the geosphere the sorption of uranyl species to mineral surfaces may also occur. The minimum solubility of uranyl minerals and maximum U(VI) sorption to most natural sorbents (e.g. Fe(III)/Mn/Ti-oxyhydroxides, zeolites and clays) occur in the same pH range (pH 5-8.5; Langmuir, 1997). However, carbonate complexation can increase U(VI) solubility at higher pH and so limit U(VI) adsorption to mineral surfaces (Langmuir, 1997). Sorption is controlled by the nature of the adsorbent's surface and the aqueous speciation of U(VI) which can both be affected by pH. For example, the adsorption behaviour of U(VI) with various minerals suggests that at low pH the dominance of positively charged surface sites can repulse UO_2^{2+} reducing sorption but that the increasing availability of neutral / negatively charged surface sites at higher pH values promotes UO_2^{2+} sorption (Langmuir, 1997). However, if carbonate is present (as carbonate complexes dominate at high pH), at higher pH neutral / negatively charged carbonate complexes tend to be repulsed by neutral / negatively charged surface sites, though even in the absence of carbonate U(VI) adsorption has been found to decrease above pH 10 (Barnett et al., 2002). Due to their common occurrence in natural environments and their high sorption capacity for U(VI), Fe-(oxy)hydroxides are cited as the most important sorbents for U, and have been

widely studied in this context (Langmuir, 1997; Waite et al., 1994). These phases are also redox active, due to the stability of Fe^{2+} and Fe^{3+}, and so have the ability to facilitate change in the oxidation state of the sorbed U. However, U(VI) sorption to silicate minerals is also important and research has illustrated significant U(VI) adsorption to many phases such as clay minerals (e.g. smectite (Morris et al., 1994; Ames et al., 1982) and montmorillonite (Chisholm-Brause et al., 1994)), gibbsite and silica (Fig. 2.15; McKinley et al., 1995). It has also been found that during radionuclide sorption most activity is held <10 nm from the mineral surface so even a thin layer of altered rock or coating of secondary precipitates could have a dramatic effect on sorption (Berry et al., 1999).

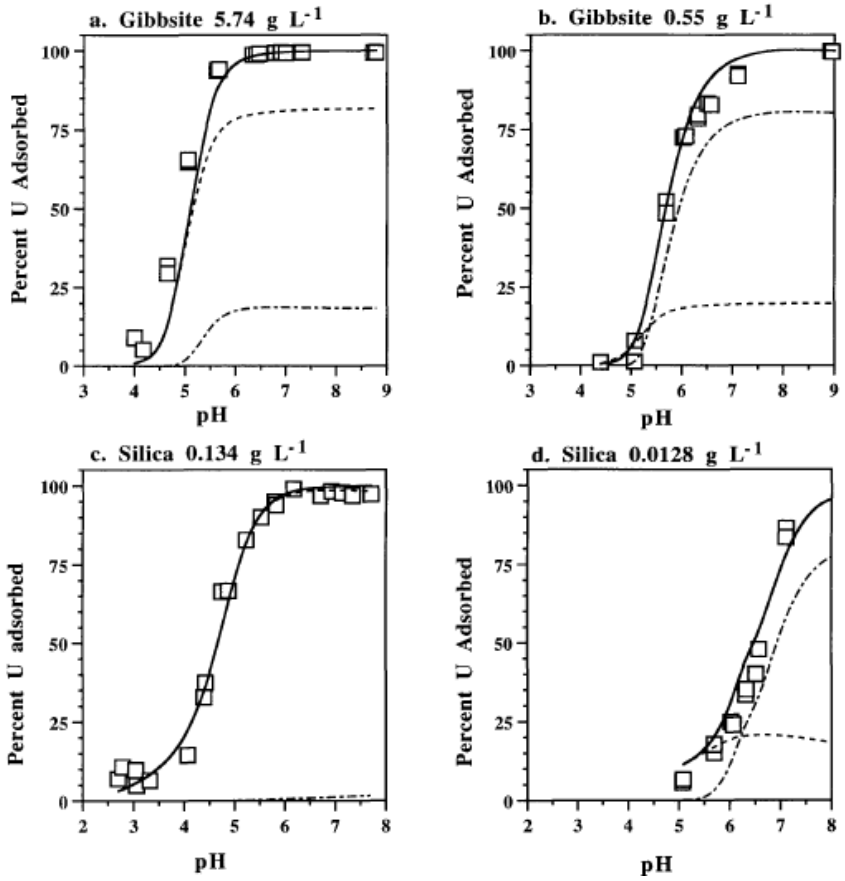

Figure 2.15: Experimental (squares) and modelled uranyl interactions with gibbsite and silica with a U solution concentration of 0.2 mg L^{-1} (adsorption = solid line, UO_2^{2+} surface complexs = dashed line, $(UO_2)_3(OH)_5^+$ surface complex = dot-dashed line; from McKinley et al., 1995).

The availability of competing ions in solution may also affect the sorption of U(VI). Research in this area has been limited, however, the presence of Ca^{2+} in solution has been observed to affect U(VI) sorption. For example, in

systems containing carbonate the formation of calcium uranyl carbonate complexes has been found to decrease U(VI) sorption to surfaces while in carbonate free systems has been found to have no effect or to decrease U(VI) sorption through competitive sorption where positively charged U(VI) species sorb to negatively charged surface sites (Fox et al., 2006).

2.4.2 Uranium interaction with C-S-H

In addition to its potential interactions with existing mineral surfaces, as U(VI) moves into the geosphere surrounding a GDF, it may encounter secondary minerals formed during high pH rock alteration. For example, C-S-H, the predominant secondary phase predicted to form in the geosphere surrounding a cementitious GDF (Gaucher and Blanc, 2006; Savage and Rochelle, 1993; Hodgkinson and Hughes, 1999, Braney et al., 1993; Savage et al., 1992). The interactions of U(VI) with C-S-H have been studied in detail (Pointeau et al., 2004; Harfouche et al., 2006; Tits et al., 2011; Mace et al., 2013). Not only because C-S-H phases are predicted to form in the CDZ, but also because they are abundant in hardened cement paste (Taylor, 1990), a common wasteform for nuclear waste and potential GDF building material. C-S-H phases also have large surface areas and are known sorb other ions such as Zn(II), K^+, Na^+ and Eu^{3+} (Ziegler et al., 2001; Hong and Glasser, 2002; Pointeau et al., 2001).

It has been identified that U(VI) is retained by C-S-H phases through both adsorption and incorporation processes (Pointeau et al., 2004; Harfouche et al., 2006; Tits et al., 2011; Mace et al., 2013) with U(VI) distribution ratios (Rd values) of 10^3 L kg^{-1} to 10^6 L kg^{-1} (Pointeau et al., 2004; Tits et al., 2008). However, the occurrence of U(VI) adsorption versus incorporation was dependent on pH, the Ca:Si ratio of the C-S-H and U(VI) loading (Tits et al., 2011; Harfouche et al., 2006). At pH 13.3 Tits et al. (2011) inferred that up to 50% of U(VI) remained in solution as $UO_2(OH)_4^{2-}$. Whereas at pH 9-12 U(VI), as uranyl (UO_2^{2+}), has been inferred to substitute for Ca^{2+} in the interlayer of the C-S-H and bonded in a uranophane-like ($Ca(UO_2)_2(SiO_3OH)_2 \cdot 5H_2O$) coordination environment (Fig. 2.16; Ca:Si ratio 0.75-1.07, Tits et al. (2011); Ca:Si ratio 0.65-1.1, Harfouche et al. (2006)). Substitution of uranyl into the

C-S-H interlayer has also been suggested in thermodynamic modelling of U(VI) uptake into C-S-H (Gaona et al., 2012). However, Tits et al. (2011) also found that at pH 10.1-12.1, at low Ca:Si ratio (0.75-1.07) U(VI) was adsorbed to C-S-H surfaces, potentially as inner-sphere surface silanol (Si-OH) complexes. As a result of sorption to C-S-H, U(VI) solubility is significantly limited to 10^{-6}-10^{-7} M (Atkins and Glasser, 1992).

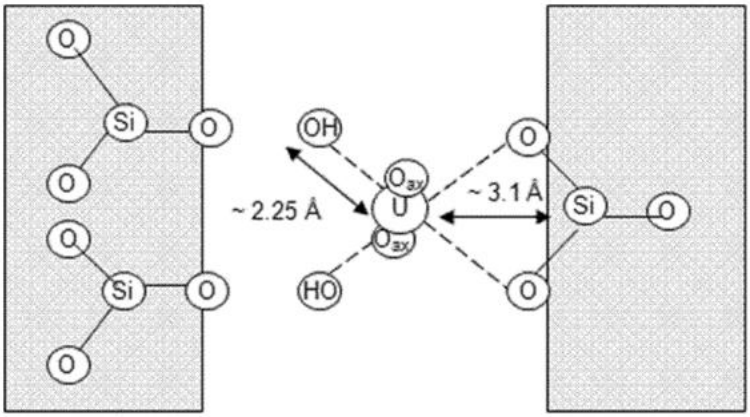

Figure 2.16: Proposed structural model for the immobilisation of U(VI) in C-S-H in the interlayer of C-S-H (from Macé et al., 2013).

U(VI) may also be immobilised through co-precipitation with C-S-H (Harfouche et al., 2006; Gougar et al., 1996; Evans, 2008). However, this has been found to be influenced by U(VI) concentration. For example, at U(VI) surface loadings of 1100 ppm, Harfouche et al. (2006) identified the formation of co-precipitated uranyl-silicate-like structures while in systems with 3400 ppm U(VI) surface loadings a U(VI) solid phase was inferred to precipitate independently of C-S-H formation. The precipitation of a U(VI) solid phase was also identified during sorption experiments at pH 12.1 and high U(VI) loading (1 mol kg^{-1}), believed to be a Ca-uranate precipitate (Tits et al., 2011; Macé et al., 2013). However, the uptake mechanisms of U(VI) by C-S-H are not understood (Harfouche et al., 2006).

References

ADLER, M., MÄDER, U.K. & WABER, H.N. 1999. High-pH alteration of argillaceous rocks: an experimental study. Swiss Bull. Mineral. Petrol. 79, 445-454.

ALEXANDER, W.R., DAYAL, R., EAGLESON, K., EIKENBERG, J., HAMILTON, E., LINKLATER, C.M, MCKINLEY, I.G. AND TWEED, C.J. 1992. A natural analogue of high pH cement pore waters from the Maqarin area of northern Jordan II: results of predictive geochemical calculations. *Journal of Geochemical Exploration,* 46, pp l33-146.

AMES, L. L., MCGARRAH, J. E. WALKER, B. A. & SALTER, P. F. 1982. Sorption of uranium and cesium by Hanford basalts and associated secondary smectite. *Chemical Geology*. 35. 205-225.

ANDERSSON, K., ALLARD, B., BENGTSSON, M. & MAGNUSSON, B. 1989. Chemical composition of cement pore fluids. *Cement and Concrete Research,* 19**,** 327-332.

ANDRA. 2012. Low and intermediate level short-lived waste [online]. Available at: <www.andra.fr/international/pages/en/menu21/waste-management/waste-classification/short-lived-low--and-intermediate-level-waste-1609.html> [accessed 19/01/2014].

APPELO, C. A. J. & POSTMA, D. 2005. *Geochemistry, groundwater and pollution.* A. A. Balkema Publishers, London.

ATKINSON, A. 1985. The time dependence of pH within a repository for radioactive waste Disposal. *UKAEA,* AERE-R 11777.

AYDOGAN, A. & KADIR, S. 2003. The geology and origin of sepiolite, palygorskite and saponite in neogene lacustrine sediments of the Serinhisar-Acipayam Basin, Denizli, SW Turkey. *Clays and Clay Minerals,* 51**,** 279-292.

BACH, T., POCHARD, I., CAU-DIT-COUMES, C., MERCIÉR, C. & NONAT, A. 2013. Prediction of the long-term chemical evolution of a low-pH cement designed for underground radioactive waste repositories. *In*: BART, F., CAU-DIT-COUMES, C., FRIZON, F. & LORENTE, S. 2013. Cement-based materials for nuclear waste storage. Springer, London.

BARNETT, M. O., JARDINE, P. M. & BROOKS, S. C. 2002. U(VI) adsorption to heterogeneous subsurface media: application of a surface complexation model. *Environmental Science and Technology*. 36(5). 937-942.

BATEMAN, K., COOMBS, P., NOY, D. J., PEARCE, J. M., WETTON, P., HAWORTH, A. & LINKLATER, C. 1999. Experimental simulation of the alkaline disturbed zone around a cementitious radioactive waste repository: numerical modelling and column experiments. *Geological Society, London, Special Publications,* 157**,** 183-194.

BERNER, U. R. 1992. Evolution of pore water chemistry during degradation of cement in a radioactive waste repository environment. *Waste Management,* 12**,** 201-219.

BERRY, J. A., BAKER, A. J., BOND, K. A., COWPER, M. M., JEFFERIES, N. L. & LINKLATER, C. M. 1999. The role of sorption onto rocks of the Borrowdale Volcanic Group in providing chemical containment for a potential repository at Sellafield. *Geological Society, London, Special Publications,* 157**,** 101-116.

BICKMORE, B. R., WHEELER, J. C., BATES, B., NAGY, K. L. & EGGETT, D. L. 2008. Reaction pathways for quartz dissolution determined by statistical and graphical analysis of macroscopic experimental data. *Geochimica et Cosmochimica Acta.* 72. 4521-4536.

BOURDON, B., TURNER, S., HENDERSON, G. M. & LUNDSTROM, C. C. 2003. Introduction to U-series geochemistry. In: Bourdon, B., Henderson, G. M., Lundstrom, C. C. & Turner, S. eds. 2003. Uranium-

series geochemistry. Reviews in mineralogy and geochemistry vol. 52. Mineralogical Society of America, Washington DC, USA.

BRANEY, M. C., HAWORTH, A., JEFFERIES, N. L. & SMITH, A. C. 1993. A study of the Effects of an Alkaline Plume From a Cementitious Repository on Geological Materials. *Journal of Contaminant Hydrology,* 13**,** 379-402.

BRANTLEY, S. L. 2008. Kinetics of mineral dissolution. In: Brantley, S. L., Kubicki, J. D. & White, A. F. eds. 2008. Kinetics of water-rock interaction. Springer Science and Business Media. New York.

BUTCHER, E. J., BORWICK, J., COLLIER, N. & WILLIAMS, S. J. 2012. Long term leachate evolution during flow-through leaching of a vault backfill (NRVB). *Mineralogical Magazine*. 76(8). 3023-3031.

CHERMAK. 1992. Low temperature experimental investigation of the effect of high pH NaOH solutions on the Opalinus shale, Switzerland. *Clays and Clay Minerals*. 40. 6. 650-658.

CHERMAK. 1993. Low temperature experimental investigation of the effect of high pH KOH solutions on the Opalinus shale, Switzerland. *Clays and Clay Minerals*. 41. 3. 365-372.

CHICHESTER, F. W., HARWARD, M. E. & YOUNGBERG, C. T. 1970. pH dependent ion exchange properties of soils and clays from Mazama Pumice. *Clays and Clay Minerals*. 18. 81-90.

CHISHOLM-BRAUSE, C., CONRADSON, S. D., BUSCHER, C. T., ELLER, P. G. & MORRIS, D. E. 1994. Speciation of uranyal sorbed at multiple binding sites on montmorillonite. *Geochimica et Cosmochimica Acta.* 58. 17. 3625-3631.

CLARET, F., GABOREAU, S., LEROUGE, C., GAUCHER, E. C., LINARD, Y., DEWONCK, S., BOURBON, X., MAZURIER, A., PARNEIX, J. C., PRET, D. & BORSCHNECK, D. 2010. Concreter/clay reactivity in the Bure underground research laboratory. *In*: BIRKLE, P., & TORRES-

ALVARADO, I. S. (*eds*) 2010. Water Rock Interaction XIII. CRC Press. Florida.

CORWM. 2006. Managing our radioactive waste safely: CoRWM's recommendations to Government. CoRWM Doc 700.

DECC. 2014. Implementing geological disposal: a framework for the long-term management of higher activity radioactive waste. HMSO. London. URN 14D/235.

DE WINDT, L., MARSAL, F., TINSEAU, E. & PELLEGRINI, D. 2008. Reactive transport modelling of geochemical interactions at a concrete/argillite interface, Tournemire site (France). *Physics and Chemistry of the Earth.* 33. S295-S305.

DE WINDT, L., PELLEGRINI, D. & VAN DER LEE, J. 2004. Coupled modelling of cement/claystone interactions and radionuclide migration. *Journal of Contaminant Hydrology*. 68. 165-182.

DEFRA. 2008. Managing radioactive waste safely: A framework for implementing geological disposal. Department of the environment, food and rural affairs. UK.

EIKENBERG, J. & LICHTNER, P. C. 1992. Propagation of hyperalkaline cement pore waters into the geologic barrier surrounding a radioactive waste repository. *In:* KHARAKA, Y. K. & MAEST, A. S. (eds) *Water-Rock Interaction.* Balkema, Rotterdam.

EUROPEAN COMMISSION. 2005. Nuclear science and technology, Ecoclay II. Effects of cement on clay barrier performance – Phase II. EUR 21921.

EVANS, N. D. M. 2008. Binding mechanisms of radionuclides to cement. *Cement and Concrete Research.* 38. 543–553.

FALCK, W. E. & NILSSON, K. –F. 2009. Geological disposal of radioactive waste: moving towards implementation. JRC reference reports. JRC-IE. Report EUR 23925 EN.

FERNÁNDEZ, R., MÄDER, U., RODRÍGUEZ, M., VIRGIL DE LA VILLA, R. & CUEVAS, J. 2009. Alteration of compacted bentonite by diffusion of highly alkaline solutions. *European Journal of Mineralogy,* 21**,** 725-735.

FERNANDEZ, R., RODRÍGUEZ, M., VIGIL DE LA VILLA, R. & CUEVAS, J. 2010. Geochemical constraints on the stability of zeolites and C-S-H in the high pH reaction of bentonite. *Geochimica et Cosmochimica Acta,* 74**,** 890-906.

FLOWERS, B. 1976. Royal commission on environmental pollution, Sixth Report, Nuclear power and the environment.

FOX, P. M., DAVIES, J. A. & ZACHARA, J. M. 2006. The effect of calcium on aqueous uranium(VI) speciation and adsorption to ferrihydrite and quartz. *Geochimica et Cosmochimica Acta.* 70. 1379-1387.

FRITZ, B. & NOGUERA, C. 2009. Mineral precipitation kinetics. *In:* OELKERS, E. H. & SCHOTT, J. (eds.) *Thermodynamics and kinetics of water-rock interaction.* Chantilly, Virginia, USA: The Mineralogical Society of America.

FURQUIM, S. A. C., GRAHAM, R. C., BARBIERO, L., QUEIROZ NETO, J. P. & VALLES, V. 2008. Mineralogy and genesis of smectites in an alkaline-saline environment of Pantanal Wetland, Brazil. *Clays and Clay Minerals,* 56**,** 579-595.

GAONA, X., KULIK, D. A., MACÉ, N & WIELAND, E. 2012. Aqueous-solid solution thermodynamic model of U(VI) uptake in C-S-H phases. *Applied Geochemistry*. 27. 81-95.

GAUCHER, E. & BLANC, P. 2006. Cement/clay interactions – A review: Experiments, natural analogues, and modeling. *Waste Management,* 26**,** 776-788.

GLASSER, F. P. 2003. The pore fluid in Portland cement: its composition and role, Proc. 11th ICCC, Durban South Africa. 341-352.

GOLOVICH, E. C., WELLMAN, D. M., SERNE, R. J. & BOVAIRD, C. C. 2011. Summary of uranium solubility studies in concrete waste forms and vadose zone environments. *U.S. Department of Energy.* PNNL-20726.

GOUGAR, M. L. D., SCHEETZ, B. E. & ROY, D. M. 1996. Ettringite and C-S-H Portland cement phases for waste ion immobilization: a review. *Waste Management*. 16. 295-303.

GUILLAUMONT, R., FANGHÄNEL, J., NECK, V., FUGER, J., PALMER, D.A., GRENTHE, I. & RAND, M.H. 2003. Chemical Thermodynamics 5. Update on the Chemical Thermodynamics of Uranium, Neptunium, Plutonium, Americium and Technetium. NEA OECD, Elsevier.

HARFOUCHE, M., WIELAND, E., DÄHN, R., FUJITA, T., TITS, J., KUNZ, D. AND TSUKAMOTO. 2006. EXAFS study of U(VI) uptake by calcium silicate hydrates. *Journal of Colloid and Interface Science*. 303. 195-204.

HAWORTH, A., SHARLAND, S. M., TASKER, P. W. & TWEED, C. J. 1988. Evolution of the groundwater chemistry around a nuclear waste repository. *Materials Research Society Symposium Proceedings,* 112, 645-651 / 425-434.

HODGKINSON, E. S. & HUGHES, C. R. 1999. The mineralogy and geochemistry of cement/rock reactions: high-resolution studies of experimental and analogue materials. *Geological Society, London, Special Publications,* 157**,** 195-211.

HONG, S. & GLASSER, F. P. 2002. Alkali sorption by C-S-H and C-A-S-H gels: part II. Role of alumina. *Cement and concrete research*. 32. 7. 1101-1111.

HONTY, M., DE CRAEN, M., WANG, L., MADEJOVÁ, J., CZÍMEROVÁ, A., PENTRÁK, M., STRÍČEK, I. & VAN GEET, M. 2010. The effect of high

pH alkaline solutions on the mineral stability of the Boom Clay – Batch experiments at 60°C. *Applied Geochemistry,* 25**,** 825-840.

IAEA. 1999. Hydrogeological investigation of sites for the geological disposal of radioactive waste. *Technical report series No. 391.* Vienna: IAEA

IAEA. 2001. The use of scientific and technical results from underground research laboratory investigations for the geological disposal of radioactive waste. IAEA-TECDOC-1243.

IAEA. 2003. Scientific and technical basis for geological disposal of radioactive wastes. *Technical report series No. 413.* Vienna: IAEA.

IAEA. 2009. Geological disposal of radioactive waste: Technological implications for retrieveability. *IAEA Nuclear Energy Series No. NW-T-1.19.* Vienna: IAEA.

IAEA. 2014. The IAEA online information resource for radioactive waste management [online]. Available at: http://newmdb.iaea.org/default.aspx [Accessed 29/11/2014].

JANG, J., DEMPSEY, B. A. & BURGOS, W.D. 2006. Solubility of schoepite: comparison and selection of complexation constants for U(VI). *Water Research.* 40. 14. 2738-2746.

KRAMER-SCHNABEL, U., BISCHOFF, H., XI, R. H. & MARX, G. 1992. Solubility products and complex formation equilibria in the systems uranyl hydroxide and uranyl carbonate at 25oC and I = 0.1 M, Radiochimica Acta, 56. 183-188.

LANGMUIR, D. 1997. Aqueous environmental geochemistry. Prentice Hall, New Jersey.

LLWR. 2014. National repository [online]. Available at: http://llwrsite.com/national-repository/ [Accessed 29/11/2014].

LOUGHNAN, F. C. 1969. *Chemical weathering of the silicate minerals,* London, Elsevier.

MACE, N., WIELAND, E., DÄHN, R., TITS, J. & SCHEINOST, A. C. 2013. EXAFS investigation on U(VI) immobilization in hardened cement paste: influence of experimental conditions on speciation. *Radiochimica Acta.* 101. 379-389.

MÄDER, U., FIERZ, T., FRIEG, B., EIKENBERG, J., RUTHI, M., ALBINSSON, Y., MORI, A., EKBERG, S. & STILLE, P. 2006. Interaction of hyperalkaline fluid with fractured rock: Field and laboratory experiments of the HPF project (Grimsel Test Site, Switzerland). *Journal of Geochemical Exploration,* 90**,** 68-94.

MARINER, R. H. & SURDAM, R. C. 1970. Alkalinity and formation of zeolites in saline alkaline lakes. *Science*. 170. 3961. 977-980.

MAY, H. M., HELMKE, P. A. & JACKSON, M. L. 1979. Gibbsite solubility and thermodynamic properties of hydroxy-aluminium ions in aqueous solution at 25°C. *Geochimica et Cosmochimica Acta*. 43. 861-868.

MCKINLEY, J. P., ZACHARA, J. M., SMITH, S. C. & TURNER, G. D. 1995. The influence of uranyl hydrolysis and multiple site-binding reactions on adsorption of U(VI) to montmorillonite. *Clay and Clay Minerals.* 43. 5. 586-598.

MILLER, W., ALEXANDER, R., CHAPMAN, N., MCKINLEY, I. & SMELLIE, J. 2000. Geological disposal of radioactive wastes and natural analogues. Waste Management series vol. 2. Elsevier Science Ltd. Kidlington, Oxford.

MILODOWSKI, A. E., HYSSLOP, E. K., PEARCE, J. M., WETTON, P. D., KEMP, S. J., LONGWORTH, G., HODGKINSON, E. S. & HUGHES, C. R. 1998. Mineralogy, Petrology and Geochemistry. *In:* SMELLIE, J. (ed.) *Maqarin Natural Analogue Study: Phase III.* Stockholm: Swedish Nuclear Fuel and Waste Management Company.

MORRIS, D. E., CHISHOLM-BRAUSE, C. J., BARR, M. E., CONRADSON, S. D. & ELLER, P. G. 1994. Optical spectroscopic studies of the sorption of UO_2^{2+} species on a reference smectite. *Geochimica et Cosmochimica Acta*. 58. 17. 3613-3623.

NAGRA. 2014. Geological repository for low- and intermediate-level waste [online]. Available at: <www.nagra.ch/en/tlsmae.htm> [accessed 19/01/2014].

NANGIA, S. & GARRISON, B. J. 2008. Reaction rates and dissolution mechanisms of quartz as a function of pH. *Journal of Physical Chemistry,* 112**,** 2027- 2033.

NATIONAL RESEARCH COUNCIL. 2004. Improving the characterization program for contact-handled transuranic waste bound for the waste isolation pilot plant. The National Academy of Sciences. The National Academies Press, Washington D. C.

NDA. 2009. NDA's Radioactive Waste Management Directorate (RWMD) [online]. Available at: <http://www.nda.gov.uk/aboutus/geological-disposal/index.cfm> [Accessed 19/01/2014].

NDA. 2010a. The 2010 UK radioactive waste inventory: main report. NDA/ST/STY(11)0004.

NDA. 2010b. Geological Disposal: Radionuclide behaviour status report. NDA/RWMD/034.

NDA. 2010c. Geological Disposal: Generic disposal facility designs. NDA/RWMD/048.

NDA. 2010d. Geological Disposal: Geosphere status report. NDA/RWMD/035.

NDA. 2010e. Geological Disposal: Generic disposal system technical specification. NDA/RWMD/044.

NDA. 2010f. Geological Disposal: Near-field evolution status report. NDA/RWMD/033.

NDA. 2014. What is the long-term waste management solution – higher activity wastes [online]. Available at:

<http://www.nda.gov.uk/ukinventory/waste/long-term-waste-higher.cfm> [Accessed 29/01/2014].

NIREX. 2002. Research on the alkaline disturbed zone resulting from cement-water-rock reactions around a cementitious GDF. Nirex Report N/054.

NORRIS, S. 2012. An introduction to geosphere research studies for the UK geological disposal programme. *Mineralogical Magazine*. 76(8). 3105-3114.

NUCLEAR WASTE MANAGEMENT ORGANISATION. 2010. DGR key features [online]. Available at: < www.nwmo.ca/dgr_keyfeatures> [accessed 19/01/2014].

OECD-NEA. 2008. Moving forward with geological disposal of radioactive waste: a collective statement by the NEA radioactive waste management committee (RWMC). NEA no. 6433.

OELKERS, E. H., SCHOTT, J. & DEVIDAL, J. –L. 1994. The effect of aluminium, pH and chemical affinity on the rates of aluminosilicate dissolution reactions. *Geochimica et Cosmochimica Acta.* 58. 9. 2011-2024.

PFINGSTEN, W., PARIS, B., SOLER, J. & MADER, U. 2006. Tracer and reactive transport modelling of the interaction between high-pH fluid and fractured rock: Field and laboratory experiments. *Journal of Geochemical Exploration.* 90. 95-113.

POINTEAU, I., LANDESMAN, C., GIFFAUT, E. & REILLER, P. 2004. Reproducibility of the uptake of U(VI) onto degraded cement pastes and calcium silicate hydrate phases. *Radiochimica Acta*. 92. 645-650.

POINTEAU, I., PIRIOU, B., FEDOROFF, M., BARTHES, M. G., MARMIER, N. FROMAGE, F. 2001. Sorption mechanisms of Eu(3+) on CSH phases of hydrated cements. *Journal of colloid interface science*. 236. 2. 252-259.

POKROVSKY, O. S. & SCHOTT, J. 2004. Experimental study of brucite and precipitation in aqueous solutions: surface speciation and chemical affinity control. *Geochimica et cosmochimica acta.* 68. 1, 31-45.

RAMIREZ, S. 2005. Alteration of the Callovo-Oxfordian clay from Meuse-Haute Marne underground laboratory (France) by alkaline solution. I. A XRD and CEC study. *Applied Geochemistry,* 20**,** 89-99.

RAMIREZ, S., CUEVAS, J., VIGIL, R. & LEGUEY, S. 2002. Hydrothermal Alteration of "La Serrata" bentonite (Almeria, Spain) by Alkaline Solutions. *Applied Clay Science,* 21**,** 257-269.

READ, D., F. P., GLASSER, C., AYORA, M. T., GUARDIOLA, AND A. SNEYERS, 2001. Mineralogical and microstructural changes accompanying the interaction of Boom Clay with ordinary Portland cement. Advances in Cement Research 13, 175-183.

ROCHELLE, C., BATEMAN, K., MACGREGOR, R. A., PEARCE, J. M., SAVAGE, D. & WETTON, P. D. 1998. The evaluation of chemical mass transfer in the disturbed zone of a deep geological disposal facility for radioactive waste: v. reaction of powdered Borrowdale Volcanic Group lithologies with synthetic evolved near-field groundwater. NIREX.

ROCHELLE, C., PEARCE, J., BATEMAN, K., COOMBS, P. & WETTON, P. 1997. The evaluation of chemical mass transfer in the disturbed zone of a deep geological disposal facility for radioactive waste: X. Interaction between synthetic cement pore fluids and BVG: Observations from experiments of 4, 9 and 15 months duration. *BGS technical report* WE/97/16.

SANTEN, V. 1984. The Ostwald Step Rule. *Journal of Physical Chemistry,* 88**,** 5768-5769.

SAVAGE, D. 1998. Zeolite Occurrence, Stability and Behaviour. *In:* SMELLIE, J. (ed.) *Maqarin natural analogue study: Phase III.* Stockholm: Swedish Nuclear Fuel and Waste Management Company.

SAVAGE, D. 2010. A review of PA-relevant data from analogues of alkaline alteration. Wettingen: NAGRA.

SAVAGE, D. 2011. A review of analogues of alkaline alteration with regard to long-term barrier performance. *Mineralogical Magazine*, 75, 2401-2418

SAVAGE, D., BATEMAN, K., HILL, P., HUGHES, C., MILOWDOWSKI, A., PEARCE, J., RAE, M. & ROCHELLE, C. 1992. Rate and mechanism of the reaction of silicates with cement pore fluids. *Applied Clay Science,* 7**,** 33-45.

SAVAGE, D., BATEMAN, K., HILL, P., HUGHES, C. & MILOWDOWSKI, A. 1998. The evaluation of chemical mass transfer in the distrubed zone of a deep geological disposal facility for radioactive waste. II. reaction of silicates with Na-K-Ca hydroxide fluids. *NIREX,* NSS_R283.

SAVAGE, D. & ROCHELLE, C. 1993. Modelling reactions between cement pore fluids and rock: implications for porosity change. *Journal of Contaminant Hydrology,* 13**,** 365-378.

SAVAGE, D., WALKER, C., ARTHUR, R., ROCHELLE, C., ODA, C. & TAKASE, H. 2007. Alteration of bentonite by hyperalkaline fluids: A review of the role of secondary minerals. *Physics and Chemistry of the Earth, Parts A/B/C,* 32**,** 287-297.

SCHOTT, J., POKROVSKY, O. S. & OELKERS, E. H. 2009. The link between mineral dissolution/precipitation kinetics and solution chemistry. *In:* OELKERS, E. H. & SCHOTT, J. (eds.) *Thermodynamics and kinetics of water-rock interaction.* Chantilly, Virginia, USA: The Mineralogical Society of America.

SELECT COMMITTEE ON SCIENCE AND TECHNOLOGY. 1999. Select committee on science and technology, Third Report: Management of nuclear waste.

SHAW, S., CLARK, S. M. & HENDERSON, C. M. B. 2000. Hydrothermal formation of the calcium silicate hydrates, tobermorite

(Ca5Si6O16(OH)2·4H2O) and xonotlite (Ca6Si6O17(OH)1): an in situ synchrotron study. *Chemical Geology*. 167. 129-140.

SMELLIE, J. (ed.) 1998. *Maqarin Natural Analogue Study: Phase III,* Stockholm: Swedish Nuclear Fuel and Waste Management Company.

SOLER, J. M. & MÄDER, U. K. 2007. Mineralogical alteration and associated permeability changes induced by a high-pH plume: Modeling of a granite core infiltration experiment. *Applied Geochemistry,* 22**,** 17-29.

STEEFEL, C. I. & LICHTNER, P. C. 1994. Diffusion and reaction in rock matrix bordering a hyperalkaline fluid-filled fracture. Geochimica et Cosmochimica Acta. 58. 17. 3595-3612.

STOCKDALE, A. & BRYAN, N. D. 2013. The influence of natural organic matter on radionuclide mobility under conditions relevant to cementitious disposal of radioactive wastes: a review of direct evidence. *Earth-Science Reviews*. 121. 1-17.

SURDAM, R. C. & SHEPPARD, R. A. 1978. Zeolites in saline, alkaline-lake deposits. *In:* SAND, L. B. & MUMPTON, F. A. (eds.) *Natural zeolites: occurrence, properties, use.* Oxford: Pergamon Press.

TAYLOR, H. F. W. 1997. *Cement Chemistry,* London, Thomas Telford.

TECHER, I., BARTIER, D., BOULVAIS, PH., TINSEAU, E., SUCHORSKI, K., CABRERA, J. & DAUZÈRES, A. 2012. Tracing interaction between natural argillites and hyper-alkaline fluids from engineered cement paste and concrete: Chemical and isotopic monitoring of a 15-years old deep-disposal analogue. *Applied Geochemistry*, 27, 1384-1402.

TINSEAU, E., BARTIER, D., HASSOUTA, L., DEVOL-BROWN, I. & STAMMOSE, D. 2006. Mineralogical characterization of the Tournemire Argillite after in situ interaction with concretes. *Waste Management,* 26**,** 789-800.

TITS, J., FUJITA, T., TSUKAMOTO, M. & WIELAND, E. 2008. Uranium(VI) uptake by synthetic calcium silicate hydrates. *Materials Research Society Proceedings*. 1107. 467.

TITS, J., GEIPEL, G., MACÉ, N. EILZER, M. & WIELAND, E. 2011. Determination of uranium(VI) sorbed species in calcium silicate hydrate phases: A laser-induced luminescence spectroscopy and batch sorption study. *Journal of Colloid and Interface Science*. 359. 248-256.

USNRC. 2013. Locations of low-level waste disposal facilities [online]. Available at: http://www.nrc.gov/waste/llw-disposal/licensing/locations.html [Accessed 29/11/2014].

WAITE, T. D., DAVIS, J. A., PAYNE, T. E., WAYCHUNAS, G. A. & XU, N. 1994. Uranium (VI) adsorption to ferrihydrite: Application of a surface complexation model. *Geochimica et Cosmochimica Acta.* 58. 24. 5465-5478.

WATSON, C., SAVAGE, D., WILSON, J., BENBOW, S., WALKER, C. & NORRIS, S. 2013. The Tournemire industrial analogue: reactive-transport modelling of a cement-clay interface. Clay Minerals. 48. 167-184.

WORLD NUCLEAR ASSOCIATION. 2014. International nuclear waste disposal concepts [online]. Available at: <http://www.world-nuclear.org/info/Nuclear-Fuel-Cycle/Nuclear-Wastes/International-Nuclear-Waste-Disposal-Concepts/> [Accessed 29/01/2014]

UMEKI, H. 2007. Repository Design. *In:* ALEXANDER, W. R. & MCKINLEY, L. E. (eds.) *Deep geological disposal of radioactive waste.* Amsterdam: Elsevier Science.

USUI, H., NIINORI, Y., TOCHIYAMA, O. & MIMURA, H. 2007. Permeability change of crystalline silicate mineral-packed bed column by highly alkaline plume. *Materials Research Society Symposium Proceedings,* 985.

ZIEGLER, F., SCHEIDEGGER, A M., JOHNSON, C. A., DÄHN, R. & WIELAND, E. 2001. Sorption mechanisms of zinc to calcium silicate hydrate: x-ray absorption fine structure (XAFS) investigation. *Environmental Science and Technology*. 35. 7. 1550-1555.

3 Methods

3.1 Geochemical Analyses

3.1.1 Inductively Coupled Plasma (ICP) spectroscopy

Inductively Coupled Plasma Atomic Emission spectroscopy (ICP-AES) and Inductively Coupled Plasma Mass Spectroscopy (ICP-MS) are techniques used to determine the concentration of elements in a sample in which samples are introduced into a plasma prior to analysis. The plasma is produced by an inductively coupled plasma source at a temperature of approximately 7000-15000 K (Mendham et al., 2000). Generally samples are introduced as solutions and, to avoid cooling of the plasma, they are added via a nebuliser system and spray chamber which produces aerosols of 10µm (Mendham et al., 2000).

In ICP-AES, the plasma evaporates the sample causing it to dissociate to free atoms and ions, which are then excited to higher energy states (Lajunen and Peramaki, 2004). These excited states are unstable and the atoms / ions lose the excess energy through collision with other particles or the emission of radiation. The energy of the emitted radiation is characteristic of the element which produces it and the intensity of the radiation is proportional to the element's concentration (Mendham et al., 2000, Lajunen and Peramaki, 2004). This radiation is detected by a spectrometer within the ICP-AES and the elements present and their concentrations in the sample are determined by comparison of the data to standards and internal standardisation (Lajunen and Peramaki, 2004). Spectrometers for this technique are adapted for either sequential or simultaneous multi-element analysis using either a monochromator or polychromator to select the wavelength(s) of interest for the sample (Lajunen and Peramaki, 2004). The radiation is detected using a photomultiplier tube(s) and the method has detection limits at the ppm level (Lajunen and Peramaki, 2004).

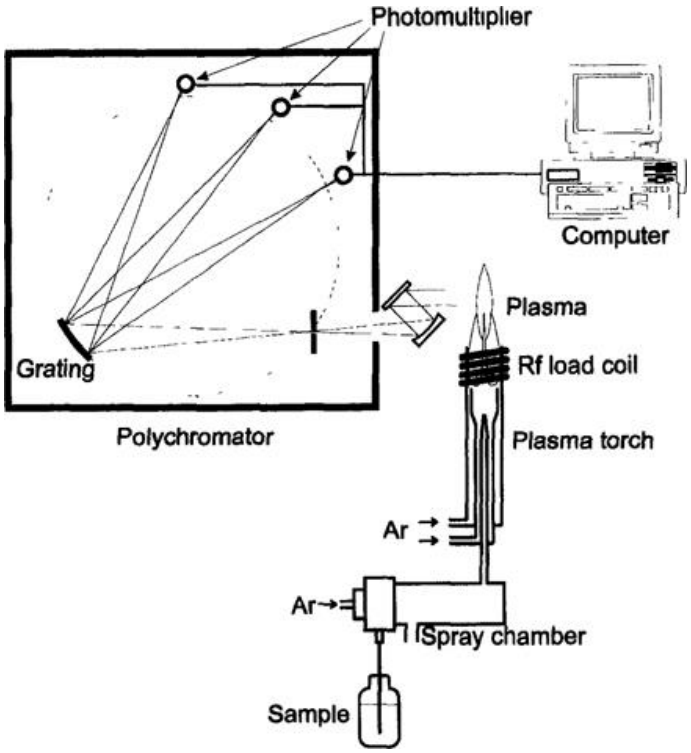

Figure 3.1: Schematic diagram of a multichannel ICP-AES instrument (image from Haraguchi et al., 1998).

In ICP-MS the solution aerosol is ionised by the plasma (Lajunen and Peramaki, 2004). As the ions are generally positively charged they tend to repel each other so an ion lens is used to focus them and analysis is conducted under vacuum to avoid interference due to collisions with gas molecules (Lajunen and Peramaki, 2004). The ions are then separated by mass, generally by using a quadrupole magnet. This separates ions based on their mass to charge ratio (m/z) by selecting and appropriate combination of voltages and frequencies to guide ions of a selected mass to charge ratio through the quadrupole region (Lajunen and Peramaki, 2004). Settings for different m/z can be scanned rapidly allowing for multi element analysis (Lajunen and Peramaki, 2004). The detector then counts the ions passing through the quadrupole and quantitative analysis is conducted by comparison to standards and internal standardisation (Mendham et al., 2000). This method has lower detection limits than ICP-AES, in the order of ppb, and has a wide range, 7-8 orders of magnitude, of detectable concentrations (Lajunen and Peramaki, 2004).

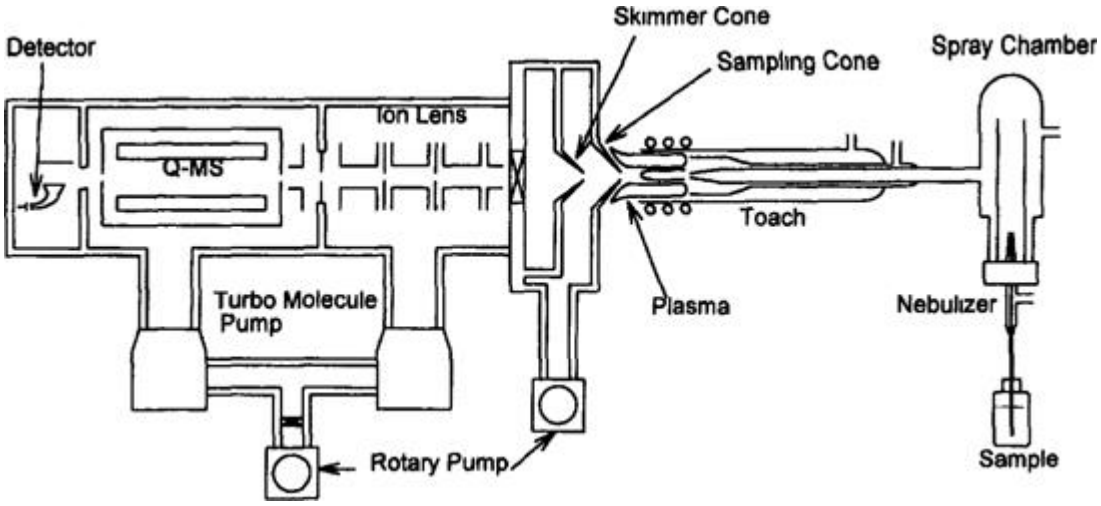

Figure 3.2: Schematic diagram of an ICP-MS instrument (image from Haraguchi et al., 1998).

In this work ICP-AES has been used to measure the concentrations of major cations in solution (e.g. Ca, Fe, S, Al, Si, Mg, K, Na, Sr) using a Perkin-Elmer Optima 5300 dual view system. ICP-MS has been used to determine the concentration of uranium in solution using an Agilent 7500cx. Prior to analysis the solutions were filtered through 0.45 µm syringe filters and acidified with 4N nitric acid. They were then diluted with 2% nitric acid to a 1 in 10 dilution for ICP-AES and a 1 in 100 dilution for ICP-MS.

3.1.2 Ion Chromatography

Ion chromatography is a technique which allows complex mixtures of cations or anions to be separated, based on their charge, and measured quantitatively relatively rapidly (Fritz & Gjerde, 2009). In this method a column containing a stationary ion exchange resin is exposed to a precise volume of a sample solution and the analyte ions are retained by the resin (Mendham et al., 2000). A solution containing a competing ion is then used to flush the resin under pressure causing analyte ions to move down the column (Fritz & Gjerde, 2009). As different ions have different affinities for the resin, the ions will exchange at different times and be separated sequentially (Mendham et al., 2000). Over time the eluent is analysed by an integrated detector (e.g. conductivity or UV-Vis spectrometer) and the different ions present will create peaks at different times and ion concentrations can be quantified relative to standards (Fritz & Gjerde, 2009). Concentrations of ions down to the ppb level can be determined (Fritz & Gjerde, 2009).

Ion Chromatography (IC) was carried out in this work to quantify inorganic anion concentrations (i.e. CO_3^{2-}, Cl^-, NO_3^-, SO_4^{2-}) using a Dionex DX120 ion exclusion system with a Dionex ICE AS1 column for carbonate analysis and a Dionex AS9-HC column for all other anions. Prior to analysis solutions were filtered through a 0.45 µm syringe filter and frozen at -20°C. Stock solutions were created as appropriate for the different solutions analysed and a standard check solution was run approximately every 10 samples.

3.2 Characterisation of Solids

3.2.1 X-ray Diffraction

Atoms cause X-ray waves to scatter due to interactions with electrons (Putnis, 2005). As the wavelength of X-rays is less than the distance between atoms in crystals but of the same order of magnitude (Battey, 1975), a regular array of atoms will cause X-rays to scatter in such a way that the scattered waves will interfere constructively in certain directions related to the arrangement of planes of atoms (Snyder, 1999). This is X-ray Diffraction (XRD). For a given wavelength, the angle of this diffraction is dependent on the distance between planes and the intensity of the reflection is related to the type of reflecting atom (Battey, 1975). Therefore, by directing a monochromatic X-ray beam at a crystalline material and recording the pattern of diffracted X-rays, the crystallographic structure of the material can be elucidated. Generally, XRD makes use of laboratory based diffractometers which contain X-ray generators where a high energy beam of electrons strikes a metal target and a filter is used to isolate the K_α wavelength produced (Battey, 1975). In order to fully assess the 3D arrangement of planes in a sample the sample is rotated in the X-ray beam to vary the angle of incident X-rays and samples can be crushed (powder XRD) to maximise the orientations of crystal present in the sample (Battey, 1975). Diffraction patterns are unique for different crystal structures and so can be indexed to databases of patterns collected / derived for known materials (Putnis, 2005). This distinctiveness also allows the bulk mineralogy of samples containing several crystalline phases to be determined as each phase will produce its signature diffraction pattern independently.

In this study, XRD has been used to determine the bulk mineralogy of rock samples. Prior to analysis, the rock samples were rinsed in isopropanol and dried at room temperature inside a desiccator containing carbosorb to minimise CO_2 interaction. The samples were then microionised under acetone with 10% corundum internal standard and back-loaded into stainless steel sample holders. Analysis was conducted using a PANalytical X'Pert Pro series diffractometer with a cobalt-target tube, X'Celerator detector operated at 45kV and 40mA. The samples were scanned at 4.5-85°2θ at 2.76°2θ/minute. Minerals were identified using PANalytical X'Pert Highscore Plus version 2.2e software coupled to the International Centre for Diffraction Data (ICDD) database and quantification was conducted using Rietveld refinement e.g. (Snyder and Bish, 1989). To characterise the clay phases present, the rock was ground, dispersed in deionised water and allowed to stand with a few drops of sodium hexametaphosphate to prevent clay crystal flocculation. After a time period determined from Stokes' Law, the <2 μm size fraction was isolated and dried at 55 °C. 15 mg of this material was re-suspended in deionised water, Ca-saturated with 0.1M $CaCl_2.6H_2O$ solution, washed, pipetted onto a 'zero-background' silicon crystal substrate and air-dried. The samples were then scanned from 2-40°2θ at 1.02°2θ/minute after ethylene glycol solvation and heating at 550°C for 2 hours. Clay species were identified using their characteristic peak positions and their reaction to the diagnostic testing program, and quantification was conducted through Rietveld refinement using PANalytical Highscore Plus software. To gain further information about the nature of the clay minerals present and assess their relative proportions, modelling of the XRD profiles was conducted using Newmod-for-Windows™ (Reynolds and Reynolds, 1996) software.

3.2.2 X-ray absorption spectroscopy

X-ray absorption spectroscopy (XAS) is used to investigate the chemical state of an element of interest and the local structure surrounding that element. As crystallinity is not a requirement, XAS is useful for characterising non-crystalline materials (Newville, 2004; Bunker, 2010). The technique makes use of X-ray radiation (approx. 500 eV to 500 keV) which can be absorbed by

all elements. When bombarded with X-rays of energy equal to or greater than the binding energy of a tightly bound inner shell electron, an X-ray photon is absorbed and the electron is promoted to an excited state or ejected through the photoelectric effect (Newville, 2004). If the energy of the X-ray is lower than the binding energy of any bound electron the X-ray will not be absorbed. Therefore, when an element is bombarded with X-rays over a range of energies, when an energy equal to the binding energy of a core electron is reached there will be a sharp rise in the absorption of X-rays, termed the absorption edge (Newville, 2004). The binding energies of the electrons of different elements are known and well defined so X-ray energies can be tuned to scan through a range encompassing an absorption edge for a particular element. Therefore XAS is an element specific technique. It also requires an intense and tuneable source of X-rays and so synchrotron radiation is used. The absorption coefficient (μ), which gives the probability of X-ray absorption according to Beer's Law, is the quantity of interest in X-ray absorption (Newville, 2004). While scanning through the specified X-ray energy range, μ is plotted versus X-ray energy in an XAS spectrum. This spectrum can be divided into two regions, the near-edge, typically within 30-40 eV of the absorption edge, and the extended fine structure at energies well beyond the absorption edge (Newville, 2004).

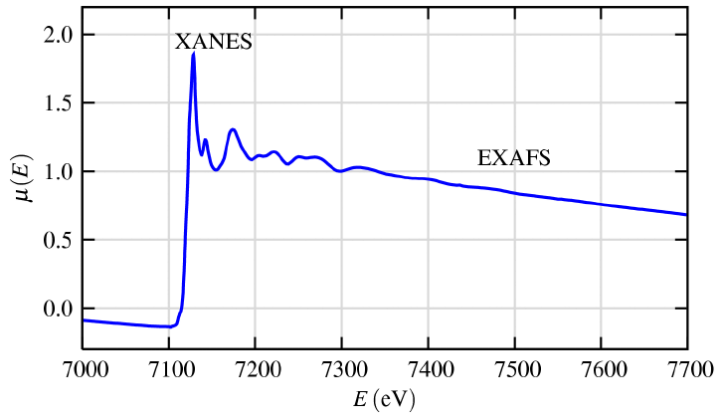

Figure 3.3: Example XAS spectrum (for FeO) indicating the XANES and EXAFS regions (from Newville, 2004).

The studies of these regions are termed X-ray Absorption Near Edge Structure (XANES) spectroscopy and Extended X-ray Fine Structure (EXAFS) spectroscopy respectively (Bunker, 2010). The oscillations in the XANES

region are the product of multiple scattering due to the geometrical arrangement of atoms in a local cluster (Gerson et al., 1999). The oscillations in the EXAFS region arise from interference between the photoelectron wave ejected in the absorption process and the wave backscattered from atoms neighbouring the absorbing atom (Gerson et al., 1999). However, certain approximations and limitations mean that while EXAFS can be interpreted quantitatively, XANES can only be interpreted qualitatively in most circumstances (Newville, 2004). A variety of computer programmes are available for the analysis of XAS spectra including EXCURVE, FEFF, GNXAS, MXAN and FDMNES.

The region of the spectrum used for XANES spectroscopy is highly sensitive to the oxidation state and coordination chemistry of the atom of interest (Newville, 2004). This region can be used to fingerprint samples by comparison of the absorption edge position and edge features with those of spectra from samples of known materials. Linear combinations of spectra from known standards can also be used to determine the approximate proportions (dependent on data quality and how well the reference species chosen match the sample of interest) of two known phases in a sample (Newville, 2004).

The EXAFS region of the XAS spectrum is understood by considering ejected photoelectrons as waves rather than as particles and so X-ray energy is commonly converted to wave number, k, and EXAFS is considered as $\chi(k)$, the sum of oscillations in the data as a function of photoelectron wave number (Newville, 2004). The oscillations in the absorption coefficient are caused by the interaction of ejected photoelectron waves with atoms surrounding the element of interest and are affected by both their distribution and type (Bunker, 2010). As a result, the nature of the oscillations can characterise the number of and atomic species of surrounding atoms and their bond lengths to the element of interest. Analysis is carried out by fitting the oscillations in a hypothetical model created from the EXAFS equation (Eq. 3.1) for a known / ideal structure to the EXAFS from the sample (Bunker, 2010). Analysis can be conducted in k-space or a Fourier transform can be applied to allow for analysis in R-space which gives a representation of groups of atoms at different distances from the central scattering atom (Bunker, 2010).

$$\chi(k) = \Sigma_j \frac{N_j f_j(k) e^{-2k^2\sigma_j^2}}{kR_j^2} \sin[2kR_j + \delta_j(k)]$$ Eq. 3.1*

where:

j represents an individual coordination shell

f(k) and δ(k) are photo-electron scattering properties of the neighbouring atom, scattering amplitude and phase shift respectively

R is distance to neighbouring atom

N is coordination number of neighbouring atom

σ^2 is mean-square disorder of neighbour distance

* *from Newville, 2004*

In this study uranium speciation has been investigated using its L3 edge via XANES and EXAFS spectroscopy. Rock sampled from experiments was frozen at - 80 ºC as a slurry in a minimal amount of experimental solution. Prior to analysis, samples were loaded into Perspex sample holders, covered with Kapton™ tape, and sealed in sample bags inside an anaerobic chamber containing carbosorb to minimize CO_2 ingress. Data collection was conducted at beamline B18 at the Diamond Light Source, Harwell. The electron beam operates at an energy of 3 GeV with a current of 300 mA with a water-cooled, vertically collimating Si mirror, a water-cooled Si(111) and Si(311) double crystal monochromator, a double toroidal mirror and a pair of plane mirrors. The beam size at the sample was approximately 200 x 250 µm and data were collected in fluorescence mode using a 9 element Ge solid state detector. Scans were conducted at room temperature and multiple scans were averaged to improve the signal to noise ratio of the data. Background subtraction was conducted using Athena and the background subtracted EXAFS data were modelled in Artemis (Ravel and Newville, 2005).

3.2.3 Electron microscopy

Electron microscopes use beams of electrons to image samples. Due to the much smaller wavelength of electrons (0.001-0.01 nm) relative to visible light (400-700 nm), these microscopes are able to provide images of much greater magnification and resolution than light microscopes (Goodhew et al., 2001). The electron beam used in an electron microscope is produced by an electron

gun commonly fitted with a tungsten filament (Watt, 1985). The most widely used systems are the thermionic emission gun and Field Emission Gun (FEG) (Goodhew et al., 2001). The FEG system produces a much brighter electron beam with electrons of well-defined energies but requires an extremely high electric field (Goodhew et al., 2001). Once produced, the electrons travel through electromagnetic lenses to focus the beam before interaction with the sample (Goodhew et al., 2001). All electron microscopes also contain a detector(s), though in differing configurations, and as electrons are strongly scattered by gases, microscopy is generally conducted under vacuum (Goodhew et al., 2001). On interaction with the specimen, electrons can be scattered either elastically, whereby they undergo a change in direction without significant energy loss (i.e. backscattered electrons), or inelastically, whereby they transfer energy to the sample (Goldstein et al., 1981). Inelastic scattering can lead to the production of secondary electrons through the excitation of atoms in the sample and ejection of loosely bound electrons (Goldstein et al., 1981). Electron microscopes can be divided into Transmission Electron Microscopes (TEM) and Scanning Electron Microscopes (SEM).

In TEM electrons illuminate a very thin sample with uniform intensity. The image is produced by electrons which pass through and are detected on the other side of the sample necessitating the use of objective and projector lenses either side of the sample (Fig. 4; Goodhew et al., 2001). When electrons pass through a very thin sample they tend to undergo no/minimal scattering deviating little from their original path (Williams and Carter, 1996). However, scattering results in a non-uniform distribution of electrons emerging from the specimen determined by the sample's structural and chemical properties (Williams and Carter, 1996). The spatial distribution of scattering is viewed as the contrast in an electron image and gives information on sample density, while the angular distribution of scattering produces electron diffraction patterns providing information on sample structure (Williams and Carter, 1996). These patterns can be indexed in the same way as XRD patterns.

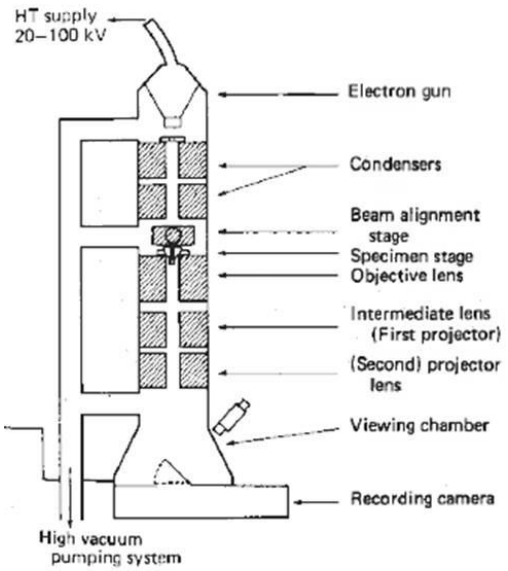

Figure 3.4: Simplified schematic diagram of a TEM (after Watt, 1985)

In SEM, images are produced by raster scanning the electron beam across the surface of the specimen and detecting secondary and backscattered electrons (Watt, 1985). Secondary electrons are abundant as one high energy electron from the beam can excite more than one secondary electron therefore they are the signal most commonly used for imaging in SEM (Goodhew et al., 2001). Backscattered electrons are less abundant but carry high energies and provide additional information about the specimen so are also used for imaging (Goodhew et al., 2001). Only secondary electrons formed near the surface of the sample are detected due to their low kinetic energy and as a result provide information on sample surface features (Goldstein et al., 1981). Backscattered electrons are also sensitive to sample topography but penetrate deeper into the sample though their interaction volume is dependent on the electron beam energy (Goldstein et al., 1981). As the likelihood of an electron being involved in a backscattering event increases with the atomic number of the element involved, backscattered electron images provide qualitative information about the distribution of the elements in the sample, i.e. brighter areas in the image contain elements of higher atomic number (Goldstein et al., 1981).

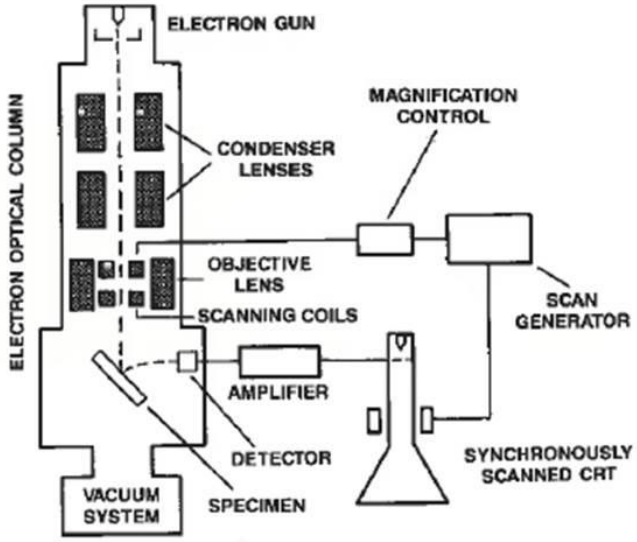

Figure 3.5: Simplified schematic diagram of an SEM (Yacobi et al., 1994).

In both TEM and SEM, inelastic scattering of electrons excites atoms which produce X-rays as they undergo de-excitation (Goldstein et al., 1981). These X-rays are characteristic of different elements and can be used to ascertain the chemical composition of the sample via Energy Dispersive X-ray (EDX) analysis using detectors integrated into the microscopes (Goldstein et al., 1981).

TEM imaging with EDX analysis and selected area electron diffraction (SAED) was conducted for the bulk samples in this work using an FEI Tecnai TF20 FEGTEM fitted with an Oxford Instruments INCA 350 EDX system with 80 mm X-Max (silicon drift detector) SDD and a Gatan Orius SC600A CCD camera. Bulk samples were prepared for TEM by ultrasonicating samples of rock in ethanol to produce suspensions of fine particles from grain surfaces. A few drops of the suspension were then deposited onto copper TEM grids with carbon films.

SEM imaging of bulk samples was conducted in this study using an FEI QUANTA 600 environmental scanning electron microscope (ESEM) and an FEI QUANTA 650 field emission gun ESEM (FEG-ESEM). Both were equipped with Oxford Instruments INCA 450 energy dispersive X-ray (EDX) microanalysis systems with 50 mm X-Max SDDs for semi quantitative chemical analyses. Samples were prepared by either mounting on Al stubs using carbon pads, or by embedding in resin and polishing under ethane-2-

diol. They were imaged either coated with carbon (to improve sample conductivity) using high-vacuum SEM or uncoated (to minimise potential damage to hydrated phases) using low vacuum SEM.

Focused Ion Beam (FIB) milling, using a FEI Nova 200 NanoLab dual beam FIB/SEM fitted with a Kleindiek micromanipulator for in situ lift-out, was also undertaken to produce a section through a single rock particle for TEM analysis. For this a bulk sample of material was first prepared on an Al stub and analysed using SEM as outlined above to locate the area of interest for sectioning. The sample was then transferred to the FIB/SEM, the relevant area re-located and a section cut using the 'lift-out' technique (Giannuzzi and Stevie, 1999; Heaney et al., 2001; Langford and Petford-Long, 2001). The section was then transferred to a Philips CM200 FEGTEM fitted with a Gatan SC200 CCD camera and an Oxford Instruments X-max 80 mm SDD for imaging and analysis.

3.2.4 Characterisation of poorly-crystalline solids

Existing research has shown that alkaline rock alteration can result in alteration products such as C-S-H phases which are poorly-crystalline solids lacking long range order in their structure (see section 2.3). In this study, electron microscopy (methods described in section 3.2.3) has been used to characterise poorly-crystalline solids and are commonly used techniques in this context, with SEM and TEM providing successively finer resolution for characterisation (Richardson and Groves, 1993). As noted, these techniques allow assessment of phase chemical composition and microcrystallinity through analysis of x-ray and electron interactions with a sample respectively (Richardson et al., 2010). However, other analytical techniques could also be used to characterise poorly-crystalline solids including solid-state nuclear magnetic resonance (NMR) spectroscopy and Raman spectroscopy (Richardson et al., 2010).

The basis of solid state NMR spectroscopy is that when placed in a magnetic field and subjected to radiofrequency radiation of an appropriate frequency nuclei with an odd atomic number will absorb energy (Bakhmutov, 2012). Nuclei are positively charged and behave as though they spin, therefore they

have a magnetic moment and produce a magnetic field (James, 1998). As a result, if nuclei are placed in a larger magnetic field they will align to the most favourable, i.e. lowest energy, orientation but may spontaneously flip 180° from one energy state (orientation) to another (James, 1998). If radiofrequency radiation equal to the difference in energies of the two nuclear spin orientation is applied, more frequent flipping between energy levels is induced (James, 1998). The energy absorbed by this process induces a voltage e which is then detected, an NMR spectrum is a plot of the radio frequency applied versus absorption and a signal in the spectrum is referred to as a resonance (James, 1998). The frequency of radiation required for nuclei to flip is characteristic of a particular isotope of a particular element and the chemical environment that the nucleus is present in (James, 1998). However, in NMR analysis a large number of nuclei are analysed which may exist in either energy state, the distribution of which is given by the Boltzmann equation, resulting in some cancellation of the signal produced resulting in the inherently low sensitivity of NMR as an analytical technique (James, 1998). The frequency of the signal, termed its chemical shift, is related to the chemical environment of the nucleus influenced by atoms 1-3 bond lengths from the nucleus of interest (Bakhmutov, 2012). As NMR is sensitive to a nucleus' local environment, it is an effective technique for analysing local structure in poorly crystalline materials and can be used to distinguish between poorly crystalline and amorphous materials (Bakhmutov, 2012). Solid state NMR is a widely used analytical technique in organic chemistry, most commonly focussed on 1H analysis. However, it has been increasingly used to characterise poorly-crystalline solids in cement-based systems focusing on 29Si and 27Al nuclei (Colombet et al., 1998; Skibsted et al., 2002; Skibsted and Hall, 2008). For example, the chemical shift of 29Si primarily affects the condensation of SiO_4 tetrahedra and can allow the identification of C-S-H phases in mixtures of cement phases and has also allowed identification of characteristics of the silicate chain structure of C-S-H phases (Richardson et al, 2010; Bell et al., 1990).

Raman spectroscopy is a vibrational spectroscopy technique which provides a unique chemical fingerprint of molecules not limited to crystalline materials

(Robinson, 1991; Richardson et al., 2010). The technique makes use of the inelastic (Raman) scattering of monochromatic light in the visible, near infrared or near ultraviolet light, usually from a laser source (Robinson, 1991). Photons are absorbed by a sample and then reemitted with the frequency of the photon shifted relative to the original monochromatic light (Richardson et al., 2010). The extent of the Raman shift is dependent on molecular structure including bond strengths, atomic mass of the atoms involved and the chemical state of the material (Richardson et al., 2010). As Rayleigh (elastic) scattering can greatly exceed the intensity of useful Raman scattering in close proximity to the laser wavelength, the spectral range is generally cut off close to the laser line (Robinson, 1991). The remaining Raman signal will usually be relatively weak and a variety of signal enhancements can be used (Robinson, 1991). Raman spectroscopy has been used to quantify the amorphous and crystalline content of materials (Taylor and Zografi, 1998). In addition, spectrometers are commonly coupled to optical microscopes enabling resolution on the scale of microns and rapid analysis times and low sensitivity towards water enable in-situ analysis of hydrating phases (Richardson et al., 2010). This scale of interest, rapid analysis and ability to analyse hydrated phases (e.g. C-S-H) make the technique particularly applicable to characterisation of alkaline alteration products and has also been applied to the examination phases such as C-S-H during their formation in reactions (Ibañéz et al., 2007; Tarridaet al., 1995; Gabrev et al., 2007).

3.2.5 Brunauer-Emmet-Teller surface area analysis

Brunauer-Emmet-Teller (BET) surface area analysis is based on a generalisation of the Langmuir theory (Brunauer et al., 1938). This extends the theory of monolayer molecular adsorption to multilayer adsorption and is known as the BET model (Hudson, 1998). The analytical technique is based on measuring the quantity of a gas adsorbed to a material at different levels of gas pressure (Ościk, 1982). Once these data are plotted the slope of the line and the intersection can be used in the BET equation to derive a value of specific surface area for the material (Ościk, 1982). The measurement encompasses external surface area and pore surface area to give total specific surface area (Ościk, 1982). Prior to measurement the surfaces of the material must be degassed to remove any surface contaminants and during

analysis the sample is cooled and kept at a steady temperature by being placed in liquid nitrogen (Sing, 1992). The low temperature is required for measurable levels of adsorption to occur (Ościk, 1982). The adsorbate gas is then injected into the sample cell and the level of adsorption measured either volumetrically or gravimetrically with calibration of the system before and after each measurement using helium gas which does not adsorb (Sing, 1992). In this study BET surface area analysis has been conducted using a Micromeritics Gemini V Surface Area Analyser.

3.3 Geochemical modelling

The geochemical modelling of experiments in this study has been conducted using the PHREEQC modelling software. The name PHREEQC stems from the model's capability to represent pH-Redox-Equilibrium and its use of the C programming language (Parkhurst and Appelo, 2013). PHREEQC is based on equilibrium chemistry and can simulate the interaction of aqueous solutions with minerals, and calculate the distribution of aqueous species and mineral saturation indices (Parkhurst and Appelo, 2013). In this study, the Lawrence Livermore National Laboratory (LLNL) and the specific ionic theory (SIT) databases of thermodynamic data, which is distributed with PHREEQC, have been used.

References

BAKHMUTOV, V. I. 2012. Solid-state NMR in materials science: principles and applications. CRC Press, Florida.

BATTEY, M. H. 1975. Mineralogy for students. 2nd edition. Longman Group Ltd, London.

BELL, G. M. M., BENSTED, J., GLASSER, F. P., & LACHOWSKI, E. E. 1990. Study of calcium silicate hydrates by solid-state high-resolution 29Si nuclear magnetic resonance. Advances in Cement Research 3(2): 23–37. BUNKER, G. 2010. Introduction to XAFS: a practical guide to X-ray absorption fine structure spectroscopy. Cambridge University Press.

BRUNAUER, S., EMMETT, P. H. & TELLER, E. 1938. Adsorption of gases in multimolecular layers. Journal of the American Chemical Society. 60. 2. 309-319

COLOMBET, P., GRIMMER, A. R., ZANNI H & SOZZANI, P. 1998. Nuclear Magnetic Resonance Spectroscopy of Cement-based Materials. Springer Verlag, Berlin.

FRITZ, J. S. & GJERDE, D. T. 2009. Ion Chromatography. 4th revised edition. Wiley-VCH, Weinham.

GARBEV, K., STEMMERMANN, P., BLACK, L., BREEN, C., YARWOOD, J. & GASHAROVA, B. 2007. Structural features of C–S–H(I) and its carbonation in air – A Raman spectroscopic study. Part I: Fresh phases. Journal of the American Ceramic Society 90(3): 900–907.

GERSON, A. R., HALFPENNY, P. J., PIZZINI, S., RISTIC, R., ROBERTS, K. J., SHEEN, D. B. & SHERWOOD, J. N. 1999. Application of synchrotron X-radiation to problems in materials science. pp. 105-169. In: LIFSHIN, E., ed. 1999. X-ray characterization of materials. Wiley-VCH, Weinham.

GIANNUZZI, L. A. & STEVIE, F. A. 1999. A review of focused ion beam milling techniques for TEM specimen preparation. Micron. 30, 197-204.

GOODHEW, P. J., HUMPHREYS, J. & BEANLAND, R. 2001. Electron microscopy and analysis. 3rd edition. Taylor and Francis, London.

GOLDSTEIN, J. I., NEWBURY, D. E., ECHLIN, P., JOY, D. C., FIORI, C. & LIFSHIN, E. 1981. Scanning electron microscopy and X-ray microanalysis a text for biologists, materials scientists and geologists. Plenum Press. London.

HARAGUCHI, H., FUJIMORI, E. & INAGAKI, K. 1998. Trace element analysis of biological samples by analytical atomic spectroscopy. In: Armstrong, D., ed. 1998. Free radical and antioxidant protocols (methods in molecular biology). Humana Press Inc. Totowa, New Jersey.

HEANEY, P. J., VICENZI, E. P., GIANNUZZI, L. A. & LIVI, K. J. T. 2001. Focused ion beam milling: a method of site-specific sample extraction for microanalysis of Earth and planetary materials. American Mineralogist. 86. 9. 1094-1099.

HUDSON, J. B. 1998. Surface science an introduction. John Wiley & Sons, Inc. United States of America.

IBAÑÉZ, J., ARTÚS, L., CUSCÓ, R., LÓPEZ, A., MENÉNDEZ, E. & ANDRADE, M. C. 2007. Hydration and carbonation of monoclinic C2S and C3S studied by Raman spectroscopy. Journal of Raman Spectroscopy 38. 1. 61–67.

JAMES, T. L. 1998. Fundamentals of NMR. University of California, San Francisco.

LANGFORD, R. M. & PETFORD-LONG, A. K. 2001. Preparation of transmission electron microscopy cross-section specimens using focused ion beam milling. Journal of Vacuum Science and Technology. 19. 5. 2186-2193.

LAJUNEN, L. H. J. & PERAMAKI, P. 2004. Spectrochemical analysis by atomic absorption and emission. 2nd revised edition. The Royal Society of Chemistry, Cambridge.

NEWVILLE M. 2004. Fundamentals of XAFS. Consortium for Advanced Radiation Sources, University of Chicago, Chicago.

MENDHAM, J., DENNEY, R. C., BARNES, J. D. & THOMAS, M. 2000. Vogel's textbook of quantitative chemical analysis. 6th edition. Pearson Eductation Limited, Harlow.

OŚCIK, J. 1982. Adsorption. Ellis Horwood Limited, Chichester.

PARKHURST, D.L. & APPELO, C.A.J. 2013. Description of input and examples for PHREEQC version 3—A computer program for speciation, batch-reaction, one-dimensional transport, and inverse geochemical calculations. In: U.S. Geological Survey Techniques and Methods, book 6, chap. A43. U.S. Geological Survey, Colorado.

PUTNIS, A. 2005. Introduction to mineral sciences. Cambridge University Press, Cambridge.

RAVEL, B. & NEWVILLE, M., 2005. ATHENA, ARTEMIS, HEPHAESTUS: data analysis for Xray absorption spectroscopy using IFEFFIT. J. Synchrotron Radiation. 12, 537–541.

RICHARDSON, I. G. & GROVES, G. W. 1993. The microstructure and microanalysis of hardened ordinary Portland cement pastes. Journal of Materials Science 27. 1. 265–277.

RICHARDSON, I. G., SKIBSTED, J., BLACK, L. & KIRKPATRICK, R. J. 2010. Characterisation of cement hydrate phases by TEM, NMR and Raman spectroscopy. Advances in Cement Research. 22. 233-248.

REYNOLDS, R C & REYNOLDS, R C. 1996. Description of Newmod-for-Windows™. The calculation of one-dimensional X-ray diffraction patterns of mixed layered clay minerals. R C Reynolds Jr., 8 Brook Road, Hanover, NH.

ROBINSON, J. W. 1991. Practical handbook of spectroscopy. CRC Press, Florida.

SING, K. S. W. 1992. Adsorption methods for surface area determination. pp. 13-32. In: STANLEY-WOOD, N. G. & LINES, R. W., ed. 1992. Particle size analysis. Royal Society of Chemistry, Cambridge.

SKIBSTED, J. & HALL, C. 2008. Characterization of cement minerals, cements and their reaction products at the atomic and nano scale. Cement and Concrete Research 38(2): 205–225.

SKIBSTED, J., HALL, C., & JAKOBSEN, H. J. 2002. Nuclear magnetic resonance spectroscopy and magnetic resonance imaging of cements and cement-based materials. In Structure and Performance of Cements. (Bensted J and Barnes P (eds)). Spon Press, London, pp. 457–476.

SNYDER, R. L. 1999. X-ray diffraction. pp. 1-103. In: LIFSHIN, E., ed. 1999. X-ray characterization of materials. Wiley-VCH, Weinham.

TARRIDA, M., MADON, M., LEROLLAND, B., & COLOMBET, P. 1995. An in-situ Raman-spectroscopy study of the hydration of tricalcium silicate. Advanced Cement Based Materials 2. 1. 15–20.

TAYLOR, L. S. & ZOGRAFI, G. 1998. The quantitative analysis of crystallinity using FT-Raman spectroscopy. Pharmaceutical Research. 15. 5. 755-761.

WATT, I. M. 1985. The principles and practice of electron microscopy. Cambridge University Press, Cambridge.

WILLIAMS, D. B. & CARTER, C. B. 1996. Transmission electron microscopy a textbook for materials science. Plenum Press, London.

YACOBI, B. G., HOLT, D. B. 1994. Scanning electron microscopy In: YACOBI, B. G., HOLT, D. B. & KAZMERSKI, L. L. Eds. 1994. Microanalysis of solids. Plenum Press, New York.

4 Uranium Speciation During Sandstone Alteration in High pH Cement Leachate

4.1 Introduction

The disposal of radioactive waste within a Geological Disposal Facility (GDF), is an internationally accepted disposal method (OECD-NEA, 2008). A GDF is comprised of several engineered barriers to aid waste containment and is constructed in rock at 300-1000m depth to provide robust, long term isolation and containment (Miller et al., 2000). Typically, GDF designs for intermediate level waste (ILW) include the use of cement. For example, in the UK, the generic case for ILW disposal involves waste conditioning in a cementitious wasteform inside steel containers (DEFRA, 2008). The containers will be placed in sub-surface GDF vaults, likely to be constructed with cementitious materials, and may be backfilled with cement (NDA, 2010a). Other designs that include the use of cement are proposed by Switzerland, France and Canada (NAGRA, 2014; Andra, 2012; Nuclear Waste Management Organisation, 2010). Once groundwater penetrates cement, the soluble components including hydroxide phases will dissolve raising the pH of the porewater. The composition and pH of the leachate will evolve over time as different constituents of the cement dissolve (Atkinson, 1985; Berner, 1992; Butcher et al., 2012). Dissolution of KOH and NaOH will initially buffer the leachate at pH > 13.1, then $Ca(OH)_2$ will buffer pH at approximately 12.4 (Atkinson, 1985). Once this too has been consumed the solution will equilibrate with Calcium Silicate Hydrate (C-S-H) phases in the cement and pH will buffer at approximately 10.5. Following dissolution of the C-S-H phases pH will return to the unperturbed groundwater level. The formation of hyperalkaline cement leachates has been cited as beneficial for waste containment as high pH can decrease the rate of corrosion of metal wasteform containers and reduce the mobility of radionuclides by decreasing their solubility (Chapman and Flowers, 1986; Glasser, 1997; Sugiyama et al., 2007). However, the leachate will migrate into the geosphere around the repository creating a Chemically Disturbed Zone (CDZ). Here the leachate will react with the rock causing mineral dissolution and recrystallisation to

secondary phases e.g. Calcium Silicate Hydrate (C-S-H) gel. This has the potential to change the physical (e.g. porosity) and chemical (e.g. sorption capacity) properties of the host rock, and significantly alter its ability to act as a barrier to radionuclide migration. The effect the alteration reactions on the speciation and mobility of key radionuclide, including uranium, within the CDZ are poorly constrained.

Generally, rock alteration at high pH results in the dissolution of primary silicate minerals, followed by the precipitation of C-S-H phases (e.g. Gaucher and Blanc, 2006; Savage and Rochelle, 1993; Hodgkinson and Hughes, 1999). Where Al and K are present, due to the dissolution of aluminosilicates, Al and K substituted C-S-H known as C-(A)-(K)-S-H phases may also form (Braney et al., 1993; Savage et al., 1992). Based on studies of natural analogue sites, long-term experiments and geochemical modelling it has been proposed that C-S-H / C-(A)-(K)-S-H may, at longer timescales, recrystallise to feldspars / zeolites (Savage, 2011), or evolve to Mg-silicate clays if Mg^{2+} is present (e.g. dolomite rich rock, Moyce et al., 2014). As the geosphere is intended to act as a barrier to radionuclide migration, understanding the interaction of radionuclides with secondary minerals is key to understanding their fate within the CDZ. For example, C-S-H phases are known to have high retention capacity for certain cations (e.g. U(VI); Gougar et al., 1996; Johnson, 2004) and so could potentially enhance radionuclide retention.

As the engineered barriers of a GDF degrade, radionuclides may mobilise into the geosphere. A key radionuclide of concern is uranium as the U(VI) species is highly mobile and due to its long half-life (e.g. half-life of ^{238}U is 4.51×10^9 years) remains hazardous over long timescales (NDA, 2010b). At high pH, as in the CDZ, dissolved U(VI) commonly forms complexes with carbonate or hydroxide (Qafoku and Icenhower, 2008; Maher et al., 2013). However, in a cementitious GDF CO_2 concentration is expected to be very low due to reaction with Ca in cement to form $CaCO_3$ (Vines and Lever, 2013; Auroy et al., 2013; NDA, 2010; Smith et al., in press). Therefore in the cementitious CDZ the dominant U(VI) species present in solution would be expected to be U(VI) hydroxide species such as $UO_2(OH)^{3-}$ and $UO_2(OH)_4^{2-}$ with solubility

limited by the uranyl hydroxide form, $UO_2(OH)_2$ in a pure solution (Bourdon et al., 2003; Tits et al., 2011). Between pH 9 and 13 U(VI) solubility has been found to vary significantly, in the absence of carbonate (Baston et al., 1993). For example, U(VI) solubility has been determined as ~ 10^{-5} – 10^{-6} M at pH 9-10 (Brownsword et al., 1990), 10^{-7} M at pH 10.5, and 3 x 10^{-5} M at pH 13 (Baston et al., 1993). This increase in solubility with increasing pH is attributed to the formation of the aqueous anionic hydroxide species (Baston et al., 1993). However, the solid phase which limits U(VI) solubility is also affected by the cation composition of the solution (Qafoku and Icenhower, 2008 and references therein). For example, at high pH in KOH (pH 11-12) and NaOH (pH 9-10) dominated solutions (similar to early formed cement leachates) Sutton et al. (1999) found U(VI) precipitated as as K_2UO_4 / $K_2U_2O_7$ or sodium diuranate ($Na_2U_2O_7$) respectively. In high pH solutions (pH 10-13.1, analogous to cement leachates), $CaUO_4$ / CaU_2O_7 precipitates have been found to limit U(VI) solubility (Bots et al., 2014; Sutton et al., 1999; Glasser, 2001). The dissolution of silicate minerals during high pH rock alteration can also release a significant amount of silica into solution. Experimental and modelling studies have also found that in the presence silica the precipitation or various U(VI)-bearing phases may occur at high pH (Evans, 2008). For example, Moroni and Glasser (1995) suggest that at high pH (up to pH 13.3) in the CaO-UO_3-SiO_2-H_2O system the solubility of U(VI) is limited by the precipitation of minerals with weeksite- and becquerelite-like structures and fall to 10^{-8} – 10^{-9} M. In the same system becquerelite and uranophane and synthetic 'phase x' ($Ca_2UO_5 \cdot 1.3\text{-}1.7H_2O$) are also highlighted as important (Atkins and Glasser, 1992). In experiments investigating U(VI)-bearing, high pH (pH 13) tank wastes infiltrating sediments (predominantly quartz, feldspar, mica and clay) at the Hanford site, uranyl-silicate minerals (e.g. Na-boltwoodite) precipitate between pH 9.5-13, due to the dissolution of silicate minerals and presence of aqueous silica (Szecsody et al., 2013).

The mobility of U(VI) migrating into the geosphere would be further affected by mineral surfaces via adsorption and surface mediated (co-)precipitation processes. U(VI) interactions with various silicate mineral (e.g. clay / mica /

quartz) surfaces, have been investigated at mildly alkaline pH (Prikryl et al., 2001; Greathouse et al., 2002; Sylwester et al., 2000; Moyes et al., 2000; Reich et al, 1998), though few studies have examined these processes in hyperalkaline conditions (above pH 9.5). However, it is known that hyperalkaline pH can promote UO_2^{2+} sorption due to the increasing availability of neutral / negatively charged surface sites at higher pH (Langmuir, 1997). For example, U(VI) adsorption onto the Opalinus clay has been shown to increase above pH 9 due to the formation of U(VI) tertiary hydroxo surface complexes (Hartmann et al., 2008).

U(VI) migration may also be affected by the formation of secondary minerals such as C-S-H. The interactions of U(VI) with C-S-H have been studied in detail (Pointeau et al., 2004; Harfouche et al., 2006; Tits et al., 2011; Mace et al., 2013). This is not only because C-S-H phase are predicted to be the predominant secondary phase produced in the geosphere surrounding a cementitious GDF (Gaucher and Blanc, 2006; Savage and Rochelle, 1993; Hodgkinson and Hughes, 1999, Braney et al., 1993; Savage et al., 1992), but they are also abundant in hardened cement paste (Taylor, 1990), a common wasteform for nuclear waste and potential GDF building material, and so are likely to be ubiquitous in a repository. It has been identified that U(VI) is retained by C-S-H phases through both adsorption and incorporation processes (Pointeau et al., 2004; Harfouche et al., 2006; Tits et al., 2011; Mace et al., 2013) with U(VI) distribution ratios (Rd values) of 10^3 L kg^{-1} to 10^6 L kg^{-1} (Pointeau et al., 2004; Tits et al., 2008). However, the occurrence of U(VI) adsorption versus incorporation to be dependent on pH, the Ca:Si ratio of the C-S-H and U(VI) loading (Tits et al., 2011; Harfouche et al., 2006). At pH 13.3 Tits et al. (2011) inferred that up to 50% of U(VI) remained in solution as $UO_2(OH)_4^{2-}$. Whereas at pH 9-12 U(VI), as uranyl (UO_2^{2+}), has been inferred to substitute for Ca^{2+} in the interlayer of the C-S-H and bonded in a uranophane-like ($Ca(UO_2)_2(SiO_3OH)_2 \cdot 5H_2O$) coordination environment (Ca:Si ratio 0.75-1.07, Tits et al. (2011); Ca:Si ratio 0.65-1.1, Harfouche et al. (2006)). Substitution of uranyl into the C-S-H interlayer has also been suggested in thermodynamic modelling of U(VI) uptake into C-S-H (Gaona et al., 2012).

However, Tits et al. (2011) also found that at pH 10.1-12.1, at low Ca:Si ratio (0.75-1.07) U(VI) was adsorbed to C-S-H surfaces, potentially as inner-sphere surface silanol complexes. As a result of sorption to C-S-H, U(VI) solubility is significantly limited to 10^{-6}-10^{-7} M (Atkins and Glasser, 1992).

U(VI) may also be immobilised through co-precipitation with C-S-H (Harfouche et al., 2006; Gougar et al., 1996; Evans, 2008). However, this has been found to be influenced by U(VI) concentration. For example, at U(VI) surface loadings of 1100 ppm, Harfouche et al. (2006) identified the formation of co-precipitated uranyl-silicate-like structures while in systems with 3400 ppm U(VI) surface loadings a U(VI) solid phase was inferred to precipitate independently of C-S-H formation. The precipitation of a U(VI) solid phase was also identified during sorption experiments at pH 12.1 and high U(VI) loading (1 mol kg^{-1}), believed to be a Ca-uranate precipitate (Tits et al., 2011; Macé et al., 2013).

As high pH may alter GDF host rock mineralogy, and its ability to retard U(VI) migration, it is important to study the interaction of U(VI) during high pH rock alteration. This investigation examined the alteration of Hollington Red Sandstone in batch reaction with a range of high pH cement leachates, representative of the different periods of leachate evolution. Alteration was characterised using geochemical solution chemistry analysis and electron microscopy to characterise solid samples. The behaviour of U(VI) was characterised using geochemical and X-ray absorption spectroscopy (XAS) techniques. Overall this approach provides new information on the fate of U(VI) in high pH rock systems relevant to geological disposal.

4.2 Materials and methods

4.2.1 Experiment Set-up

To investigate rock alteration in the presence of U(VI) batch alteration experiments containing disaggregated Red Hollington Sandstone and a synthetic cement leachate were established. The Red Hollington Sandstone, part of the Lower Triassic Sherwood Sandstone Group, was used here as it

represents a naturally occurring assemblage of the common rock forming silicate minerals relevant to many deep disposal scenarios (see Table A1). In addition, it provided natural rather than pristine mineral surfaces for the investigation of mineral-fluid reactions. The sandstone was disaggregated and the 125-250 µm size fraction used in the experiment (Fig. 4.1).

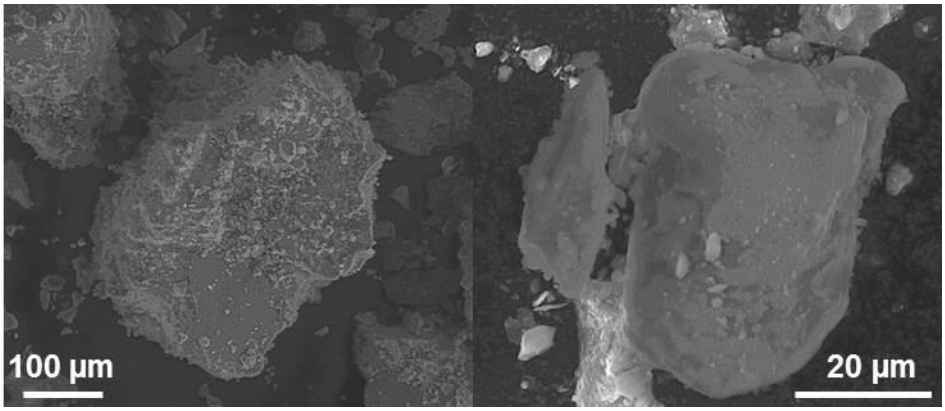

Figure 4.1: Electron micrographs of unaltered, disaggregated Red Hollington Sandstone grains.

Synthetic cement leachates of three different compositions were used (see Table 4.1), 'Young Cement Leachate' (YCL; KOH and NaOH dominated, pH 13.1), 'Intermediate Cement Leachate' (ICL; $Ca(OH)_2$ saturated, 12.3-12.4) and 'Old Cement Leachate' (OCL; $Ca(OH)_2$ dominated, pH 10.4-10.5). The experiments were handled under N_2 to minimise CO_2 interactions. In the case of the YCL and OCL, the reagents were added to deoxygenated deionised water whilst stirring and held at 40°C for 1 week. For the ICL, fresh CaO (produced to the method of Rochelle et al., 1997) was added to deoxygenated deionised water in excess with additional salts also added (Table 4.1). This solution was then held at 40°C for 4 weeks to form a saturated $Ca(OH)_2$ solution. Before use all solutions were filtered through 0.45 µm nylon filters.

Table 4.1: Chemical compositions and pH values of the 3 synthetic cement leachates YCL, ICL and OCL.

	YCL	ICL	OCL
KOH (gl^{-1})	5.2	-	-
KCl (gl^{-1})	-	0.296	-
NaOH (gl^{-1})	3.8	-	-

NaCl (gl^{-1})	-	0.01	-
$Ca(OH)_2$ (gl^{-1})	0.01	1.2	0.015
pH	13.1	12.3 – 12.4	10.4 – 10.5

For the YCL and OCL systems four experimental cells were created as blanks containing no U(VI). These were comprised of 2.5 litre HDPE bottles each containing 2 litres of cement leachate with 20 g of disaggregated sandstone. Two no rock controls for each fluid were also created containing 2 litres of leachate. For each leachate cells were run under N_2 (anoxic conditions) and half under CO_2 free air (oxic conditions). However, the difference in atmosphere did not affect the experiment results, indicating that the reactions occurring were not redox sensitive. In light of this, the ICL experiments were conducted solely under N_2 and the data from the oxic YCL and OCL systems are included in Figure A1 but not discussed. Nitrogen flushed, controlled and low CO_2 conditions were maintained during the experiment. The cells were held at 40°C, regularly shaken and pH monitored. The pH of the OCL experiments dropped during the first few weeks of the experiment. Therefore pH in this leachate was adjusted using 1 M KOH to maintain pH at 10.3-10.4.

To investigate the behaviour of U(VI) at high pH during rock alteration, parallel U(VI)-bearing batch experiments were also established. These were conducted for each leachate, under anoxic and oxic conditions in triplicate with a solution blank (data from the oxic system are included in Fig. A1 but not discussed further). Each YCL experimental cell contained 500 ml YCL with 5 g disaggregated sandstone and was spiked with 10 ppm U(VI) (from a 600 ppm depleted uranium stock solution) and a solution blank was also prepared. Due to the lower solubility of U(VI) in Ca^{2+} rich solutions, the ICL and OCL solutions were spiked with only 1 ppm U(VI) and a lower solid to solution ratio (500ml of leachate with 0.5g of sandstone) was used. A 500 ml solution blank containing 1 ppm U(VI) was also established. After addition of the reactants to the experimental cells their headspaces were purged with CO_2 free N_2 and stored in air-tight N_2 filled containers at 40 °C. The containers were purged with CO_2 free N_2 at each sample point.

Each cell was sampled at approximately 3 days, 1 week, 3 weeks, 6 weeks, 12 weeks and 52 weeks of reaction. The YCL and OCL systems were also sampled after 18 months. For the U(VI)-free experiments, at each sample point 50 ml of solution was taken from the blank and 200 ml of slurry was taken from one experimental cell to provide solid and solution samples. An additional 5 ml of solution was taken from the remaining experimental cell at each sample point to provide a replicate experimental solution sample. The experimental cells used for extracting the slurry / solution check samples were alternated after 4 sampling points to minimise the impact of removing a solution only sample from an experimental cell on the solid:solution ratio of the remaining material. For the U(VI)-bearing experiments 50 ml of slurry was sampled from each cell at each time point. Sampling was conducted inside a CO_2 controlled anaerobic chamber (N_2:H_2 atmosphere). The concentration of carbonate in solution was monitored throughout the experiment and was generally ~ 100 mg l^{-1}, below detection limit and < 40mg l^{-1} in the YCL, ICL and OCL respectively at all sample points.

4.2.2 Solution analyses

The solution samples were filtered through 0.45 µm nylon syringe filters. One aliquot was then frozen for ion chromatography (IC) analysis and another aliquot acidified for Inductively Coupled Plasma Atomic Emission Spectroscopy (ICP-AES) and Inductively Coupled Plasma Mass Spectroscopy (ICP-MS) analysis. Ion Chromatography (IC) was carried out to analyse anion concentrations in solution (CO_3^{2-}, Cl^-, NO_3^-, SO_4^{2-}) using a Dionex DX120 ion exclusion system with a Dionex ICE AS1 column for carbonate analysis and a Dionex AS9-HC column for all other anions. Cation (Ca, Fe, S, Al, Si, Mg, K, Na, Sr) concentrations in solution were analysed at a 1 in 10 dilution in 2% nitric acid with ICP-AES using a Perkin-Elmer Optima 5300 dual view ICP-AES. Uranium concentration was analysed at a 1 in 100 dilution in 2% analar nitric acid by ICP-MS using an Agilent 7500cx.

4.2.3 Characterisation of solids

The solid material from the U(VI)-free experiments was rinsed in isopropanol and dried in a CO_2 free dessicator inside an anaerobic chamber. For the U(VI)-bearing experiments, in order to investigate radionuclide sorption / incorporation during the experiment, the solid material was stored frozen at -80°C as concentrated slurry and characterised using Scanning Electron Microscopy (SEM) and X-ray Absorption Spectroscopy (XAS). High resolution imaging and semi-quantitative EDX analysis of the solid samples was conducted using an FEI QUANTA 650 field emission gun environmental SEM (FEG-ESEM) equipped with Oxford Instruments INCA 450 energy dispersive X-ray (EDX) microanalysis systems with 50 mm X-Max silicon drift detector (SDD). Samples were prepared for SEM by rinsing in isopropanol to remove any remaining leachate then mounted on Al stubs using carbon pads. Polished blocks were also made by embedding grains from the washed samples in resin and polishing under ethane-2-diol. These samples were viewed coated with 1.6 nm of carbon using high-vacuum SEM. The particles suspended in the sample filtrate (which had passed through 0.45 µm filters) were isolated for transmission electron microscopy (TEM) by adding the suspension drop-wise to charged TEM grids while wicking away the solution with filter paper. TEM analysis was conducted using an FEI Tecnai TF20 FEGTEM fitted with an Oxford Instruments INCA 350 EDX system with 80 mm X-Max SDD. A section through the Intermediate Cement Leachate (ICL) reacted sandstone was prepared for TEM analysis using a FEI Nova 200 NanoLab dual beam FIB/SEM fitted with Kleindiek micromanipulator vis the ‘lift-out’ technique technique (Giannuzzi and Stevie, 1999; Heaney et al., 2001; Langford and Petford-Long, 2001), and imaged using a Philips CM200 FEGTEM fitted with a Gatan SC200 CCD camera and an Oxford Instruments INCA 350 X-max 80 mm SDD running Aztec software. The reacted rock from the uranium experiments was prepared for XAS analysis by loading sub-samples of defrosted, damp reacted material into perspex holders and covering with Kapton™ tape. Uranium L_{III} edge XAS data were collected at beamline B18 at the Diamond Light Source. The electron energy of the beam was 3 GeV with a current of 300 mA with a water-cooled, vertically collimating

Si mirror, a water-cooled Si(111) double crystal monochromator, a double toroidal mirror and a pair of plane mirrors (Dent et al., 2009). The beam size at the sample was approximately 200 x 250 µm and data were collected in fluorescence mode using a 9 element Ge solid state detector. To improve the signal to noise ratio multiple scans of each sample were averaged. Data were background subtracted in Athena and EXAFS data analysed using Artemis (Ravel and Newville, 2005).

4.2.4 Geochemical modelling

The experimental systems have been modelled using the code PHREEQC (PHREEQCI version 3.0.6-7757; Parkhurst and Appelo, 2013), to aid the interpretation of the observed results. Calculations were performed using the specific ionic theory (SIT) database (ThermoChimie v.7.b) with thermodynamic equilibrium constants for uranyl hydroxide complexes (Zanonato et al., 2014) added.

The solution compositions at each time point, as found through ICP-AES and ICP-MS, were modelled and the saturation indices of the different U(VI)-bearing minerals noted. The phases identified as oversaturated in the model were then allowed to precipitate to predict which U(VI)-bearing phase would form.

4.3 Results

4.3.1 Young cement leachate experiment

Over 18 months of reaction an appreciable increase in the concentrations of Al and Si occurred in both the U(VI)-free (from 0.5 mg l^{-1} to 40.9 ± 2.2 mg l^{-1} and 12.2 mg l^{-1} to 144.5 ± 15.0 mg l^{-1} respectively) and U(VI)-bearing experiments (from 0.64 mg l^{-1} to 40.6 ± 1.0 mg l^{-1} and 14.8 mg l^{-1} to 162.4 ± 4.9 mg l^{-1} respectively; Fig. 4.3a-b). In both experiments the concentrations of these ions initially rose rapidly in the first week of reaction with a more gradual increase thereafter. In both the U(VI)-free and U(VI)-bearing experiments Ca concentration in solution decreased during the experiment

from ~ 5 mg l^{-1} respectively to <1 mg l^{-1} by 26 weeks of reaction (Fig. 4.3c). No trend in K and Na were observed. The fluid data for Al, Si and Ca in both the U(VI)-free and U(VI)-bearing systems (Fig. 4.3) are similar over time. This gives confidence that the same reaction processes occurred in both systems. The concentrations of phosphate, sulfate and nitrate were < 1 mg l^{-1} (generally below detection limits) throughout the experiment and chloride concentration in solution was predominantly < 10 mg l^{-1} (Tables A2 and A3).

U(VI) solution concentration fell from 9.8 mg l^{-1} to 6.7 ± 0.1 mg l^{-1} in the U(VI)-bearing experiments during the 18 month experiment (Fig. 4.3d)). Interestingly this downward trend was mirrored by the solution blank although the U(VI) concentration in the reacted solution was consistently approximately 1 mg l^{-1} lower in the experimental solution (Table A4). However, the majority of U(VI) remained in solution throughout the experiment contradicting thermodynamic modelling which predicted that at all sample points the YCL was oversaturated with respect to clarkeite, soddyite, calcium uranate ($CaUO_4$) and $Na_2U_2O_7$; and also synthetic becquerelite and compreignacite at most time points (Table A5).

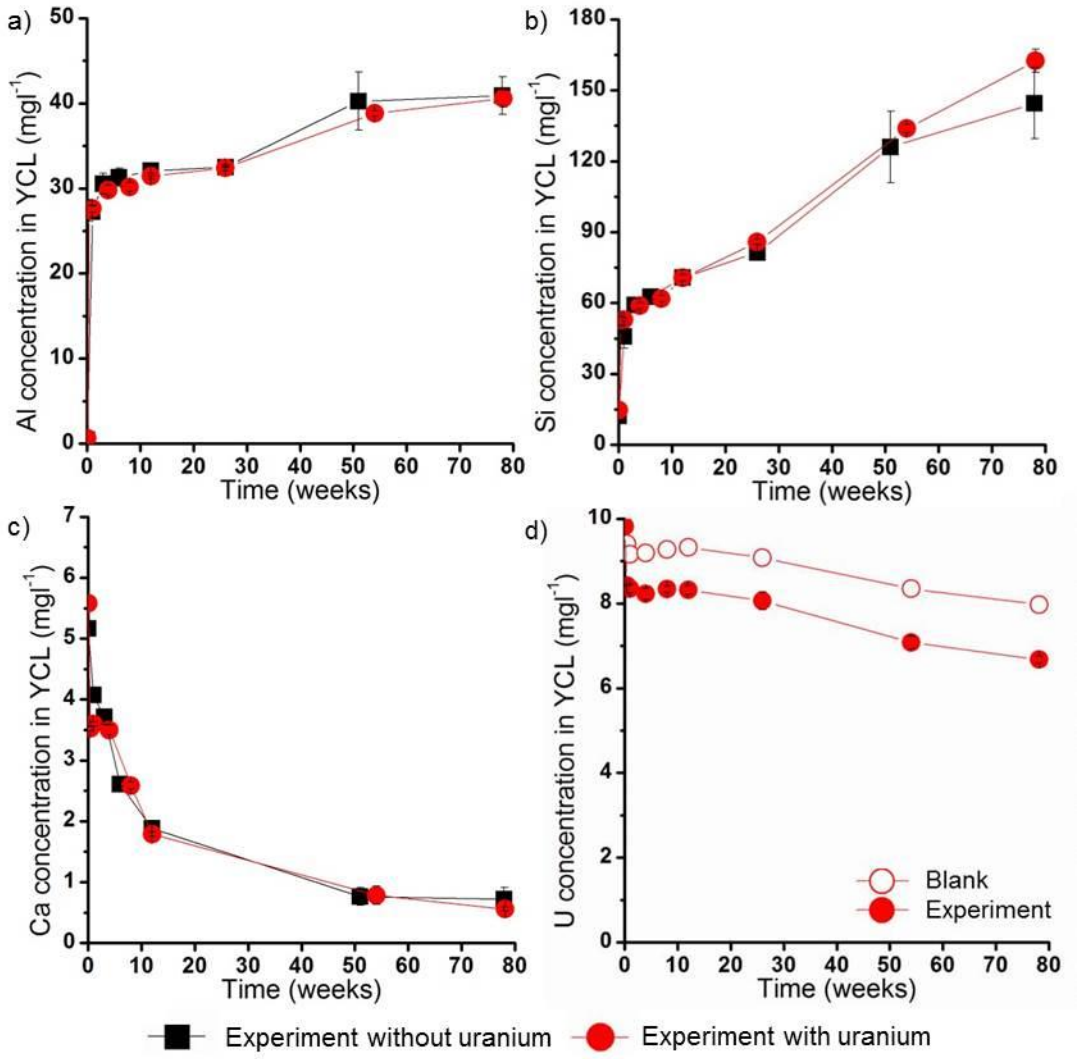

Figure 4.3: Cation concentration data for 0-18 months in the YCL batch experiments a) Al, b) Si, c) Ca and d) U

Scanning electron microscopy of the solid material extracted from the U(VI)-free and U(VI)-bearing experiments showed no evidence for mineral alteration during the initial 6 weeks of the experiment. However, after 12 weeks minor occurrences of a 'sheet-like' phase, with a particle size of 5-15 µm in size formed on the surface of the primary mineral particles was noted (Fig. 3a). The composition of these particles could not be ascertained via EDX analysis due to their limited size and thickness. After 26 weeks of reaction these particles were more abundant, though still minor in occurrence, and EDX analysis indicated they contained variable amounts of Ca, Al, K and Si (Figs 4.4b and A2). Based on chemistry and morphology the phase was identified as secondary C-(A)-(K)-S-H gel, which is consistent with other studies of high pH rock alteration (e.g. Gaucher and Blanc, 2006; Savage and Rochelle,

1993; Hodgkinson and Hughes, 1999; Braney et al., 1993; Savage et al., 1992). These C-(A)-(K)-S-H phases persisted throughout the experiment and were more abundant at each sample point though still limited in occurrence (Fig. 4.4c). This supports the evidence of the solution chemistry that primary alumino-silicate phases have dissolved throughout the experiment and a secondary Ca-bearing phase formed. The similarity in secondary phase formation between the U(VI)-free and U(VI)-bearing systems indicates that the presence of U(VI) had little / no effect on the rock alteration processes occurring. In addition, SEM did not detect any U(VI) associated with the solid phase either as a precipitate or dispersed on grain surfaces.

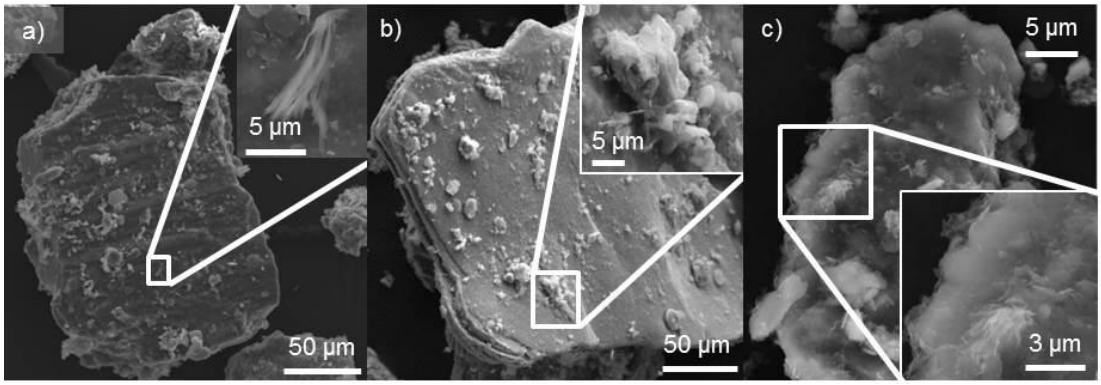

Figure 4.4: a) alteration at 12 weeks of reaction, 'sheet-like' secondary phase highlighted, b) C-(A)-(K)-S-H surface phase at 26 weeks of reaction, c) C-(A)-(K)-S-H surface phase after 52 weeks reaction.

The behaviour of U(VI) in YCL in the absence of sandstone or other reactive surfaces has been investigated by Bots et al. (2014) who identified the formation of a nano-particulate (1-2 nm) and colloidal alkaline-uranate phase ((Ca, Na, K) UO_4) in suspension. To verify whether this process occurred in the system studied here, the solid fraction from the 52 weeks sample which had passed through a 0.45 µm filter suspended in solution was isolated and analysed using TEM. This method allowed identification of particles of a crumpled 'sheet-like' phase up to 1 µm in size (Fig. 4.5). EDX analysis of these particles indicated that the phase contained Na, Ca, Al, K, Si and U (Fig. 4.5). The phase was also damaged by the electron beam during analysis indicating that it was hydrated and SAED of the phase did not produce a diffraction pattern, indicative of an amorphous structure. This solid phase was identified as a U(VI) and Na bearing silicate phase.

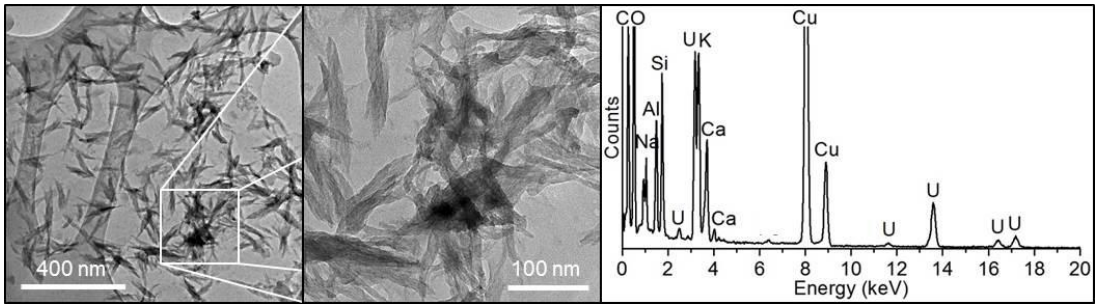

Figure 4.5: Electron micrographs and EDX spectrum of the U(VI)-bearing silicate phase isolated from solution in the 52 week sample after it had passed through a 0.45 µm syringe filter

Interestingly, relative to the solution blank, the uranium concentration in the reacted solution was consistently ~1 ppm lower throughout the experiment. This may indicate that ~ 10% of the U(VI) is associated with the sandstone, either through direct U(VI) sorption to mineral surfaces, the association of some U(VI) and Na bearing colloidal silicate phase with larger particles or a minor amount of incorporation into secondary phases precipitated on mineral surfaces. The reacted sandstone was analysed using SEM with EDX analysis, and XAS in an attempt to verify whether the ~10% U(VI) had become associated with the solid and characterise this behaviour. However, no uranium was detected in association with the solid phase via either method, though the U(VI) may have been below the detection limit of the techniques.

4.3.2 Intermediate cement leachate experiment

In the ICL system the concentration of Al in both the U(VI)-free and U(VI)-bearing systems increased rapidly in the first days of reaction from 0.15 mg l^{-1} to 3.68 ± 0.21 mg l^{-1} and 0.07 mg l^{-1} to 0.81 ± 0.03 mg l^{-1} respectively (Fig. 4.6a). In the U(VI)-free system the concentration then fell to ~2 mg l^{-1} during the rest of the experiment while in the U(VI)-bearing experiment the concentration remained relatively steady at ~0.8 mg l^{-1}. Interestingly the concentration of Al in solution was lower at all sample points in the U(VI)-bearing system relative to the U(VI)-free system, attributed to the lower solid to solution ratio in the U(VI)-bearing system limiting the availability of Al-bearing phases for dissolution. The concentration of Si in solution remained relatively constant at 5-8 mg l^{-1} during reaction in both the U(VI)-free and U(VI)-bearing systems (Fig. 4.6b). Interestingly the Al and Si concentrations

in solution were an order of magnitude lower in the ICL system than the YCL system. As in the YCL leachate, Ca concentration in ICL fell throughout the experiment in both the U(VI)-free and U(VI)-bearing systems from 800 mg l^{-1} to 445 ± 14.3 mg l^{-1} and 829 mg l^{-1} to 714 ± 11.2 mg l^{-1} respectively. The concentrations of phosphate, sulfate and nitrate were < 1 mg l^{-1} (generally below detection limits) throughout the experiment and chloride concentration was largely < 160 mg l^{-1}, approximately that added to the initial ICL (Tables A2 and A3).

In the U(VI)-bearing experiments, the concentration of uranium in solution fell rapidly to < 0.2 mg l^{-1} but this trend was also observed in the solution blank (Fig. 4.6d). Therefore it is thought likely that a U(VI)-bearing precipitate formed in these ICL systems. Thermodynamic modelling of this fluid system predicts that at each sample point the ICL was oversaturated with respect to synthetic becquerelite, clarkeite, compreignacite, soddyite and calcium uranate and with respect to sodium-compreignacite and $NaUO_4$ at most sample points (Table A6).

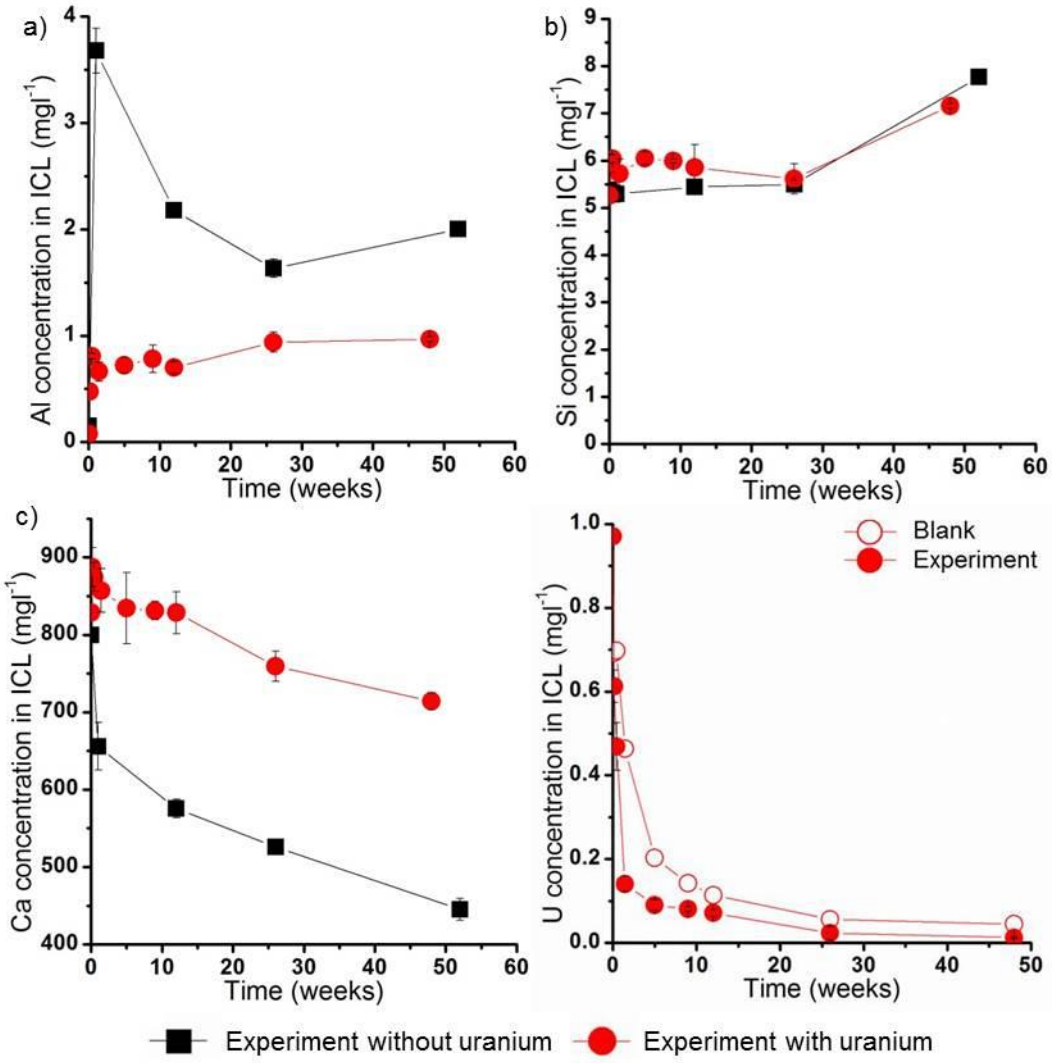

Figure 4.6: Cation concentration data for 0-12 months in the ICL a) Al, b) Si, c) Ca and d) U

Examination of the sandstone from the ICL U(VI)-free and U(VI)-bearing systems revealed that by 1 week of reaction the feldspar grains were coated in a 'sheet-like' secondary phase which persisted throughout the experiment (Fig. 4.7b and d). On grain surfaces where it formed, the coating was found to be 2-3 µm thick from 26 weeks of reaction (Fig. 4.7e). However, the quartz grains remaining uncoated and exhibited no dissolution features even after 1 year of reaction. EDX analysis indicated that the secondary phase contained variable amounts of Ca, Al, K and Si.. Based on chemistry and morphology the phase was identified as C-(A)-(K)-S-H gel.

In addition to the secondary 'sheet-like' phase, another secondary phase was identified which exhibited hexagonal morphology and occurred as particles up to 150 µm in size (Fig. 4.7a & c). This phase was present embedded in the

sheet-like phase on grain surfaces and free as separate crystals. EDX analysis indicated it contained Ca and Al. Based on chemistry and morphology is identified as the layered double hydroxide hydrocalumite ($Ca_2Al(OH)_6[Cl_{1-x}(OH)_x]\bullet 3H_2O$). Hydrocalumite is an important component of Portland cements (Taylor, 1990; Matschei et al., 2007) known to precipitate in the Si-Al-Ca systems at pH 12-13. The hydrocalumite consistently exhibited surface defects / dissolution pits and transformation to C-(A)-(K)-S-H (Fig. 4.7a and c). This transformation was found to be more extensive with time, exhibited in the difference in the extent of the 'sheet-like' C-(A)-(K)-S-H phases in Figure 4.7a and c.

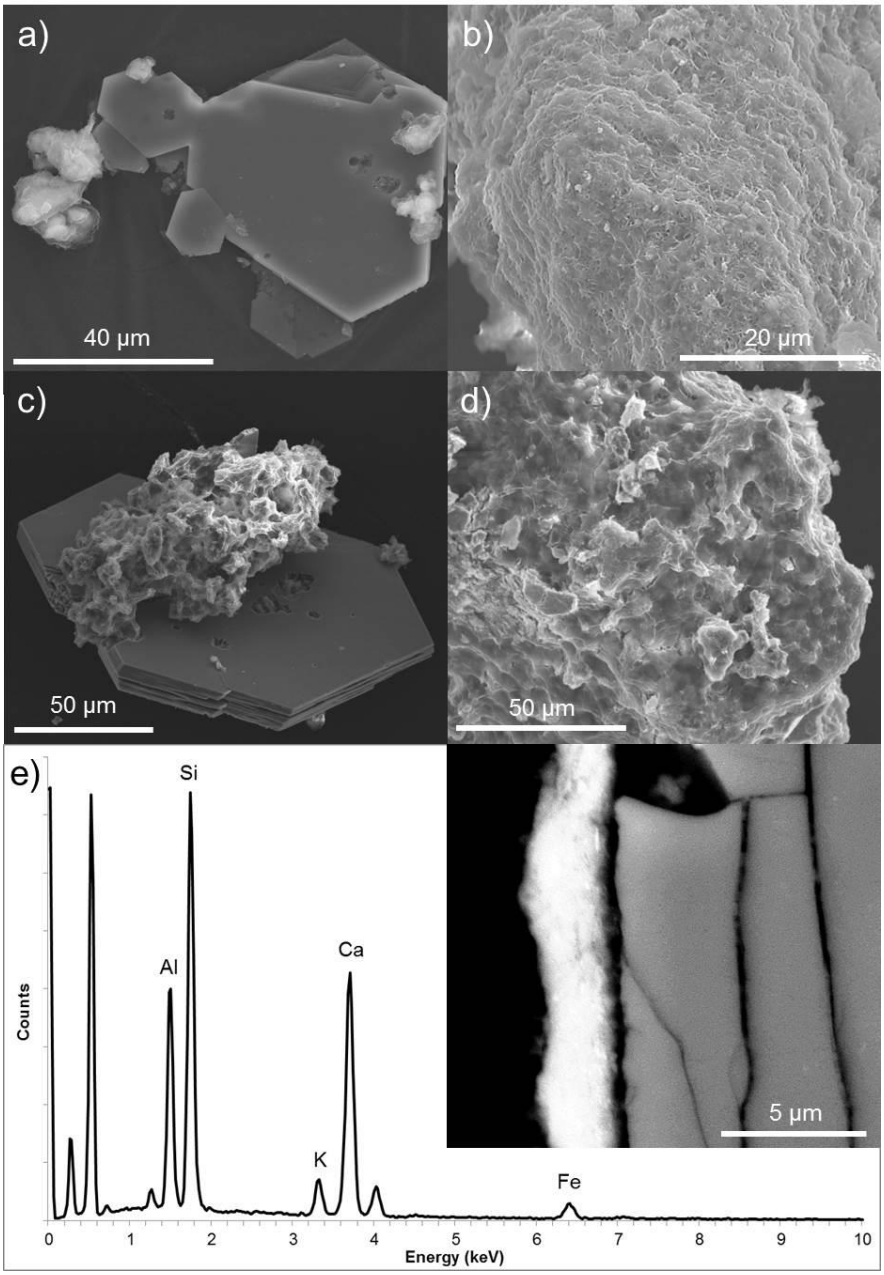

Figure 4.7: Material reacted in ICL for 12 weeks exhibiting a) C-S-H overgrowth on hydrocalumite, b) C-S-H coating silicate grain surface, and material altered for 26 weeks exhibiting c) C-(A)-(K)-S-H overgrowth on hydrocalumite, d) C-(A)-(K)-S-H coating silicate grain surface and e) section across C-(A)-(K)-S-H coating quartz grain.

Examination of the sandstone altered in the presence of U(VI) revealed the same pattern of alteration as identified in the inactive samples, but in addition, EDX analysis shows the presence of uranium at grain surfaces (Fig. 4.8). The uranium was localised in occurrence within certain areas of the 'sheet-like' C-(A)-(K)-S-H grain coatings and was not identified associated with the hydrocalumite or the uncoated quartz grains. This suggests that U(VI) preferentially associated with the C-(A)-(K)-S-H. However, it does not prohibit

association with other phases at a level below the detection limit of the EDX analysis.

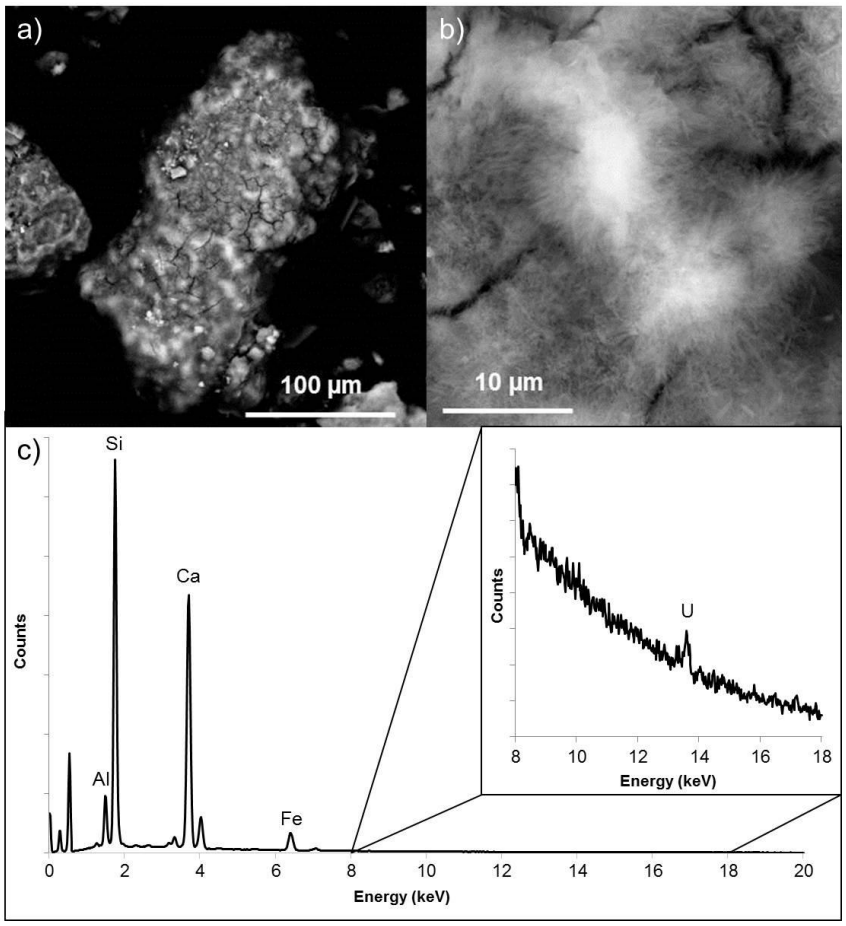

Figure 4.8: a) SEM of k-feldspar grain altered in ICL in the presence of U(VI) for 48 weeks, b) higher magnification of uranium-rich area of secondary C-(A)-(K)-S-H coating, c) EDX spectrum of the bright uranium-rich area in b.

To examine the distribution of U(VI) in the secondary material in more detail a section was taken through a U(VI) rich area of the grain coating, identified via EDX analysis, using FIB milling. TEM imaging of this section showed that the coating of secondary material was ~ 3 µm thick and comprised of three discrete phases (Fig. 4.9). These included a phase that occurred as sub-rounded particles up to 200 nm in size and a 'sheet-like' phase which extended throughout the grain coating but did not form discrete particles. EDX analysis could not resolve a difference in composition between the two phases but did indicate that they contained Ca, Al, K, Si and U (Fig. 4.9d). They are therefore identified as the C-(A)-(K)-S-H phases observed on grain surfaces via SEM with sorbed U(VI). A less abundant phase occurred as rod-shaped particles up to 200 nm in length was observed and identified as iron oxide.

Again it was not possible to resolve the composition of this individual phase. These three phases were distributed throughout the depth of the secondary material. It was also noted that the secondary material had significant porosity.

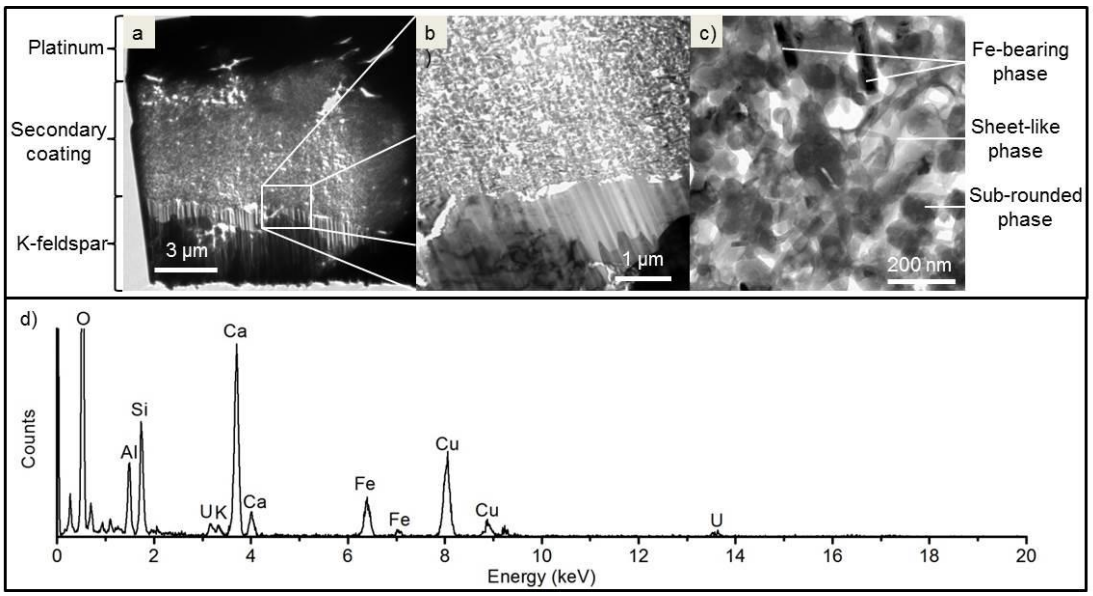

Figure 4.9: a) electron micrograph of a section through C-(A)-(K)-S-H secondary coating on a k-feldspar grain after 48 weeks of reaction in ICL, b) higher magnification of the area highlighted in a) showing the interface between the secondary phase and primary k-feldspar, c) detailed electron micrograph of the secondary surface coating.

Elemental mapping of the section using TEM and EDX analysis showed uranium to be distributed throughout the grain coating as are Al, Ca, K, Si and Fe (Fig. 4.10 and A3). The uranium could not be correlated with a discrete phase, but its distribution does suggest an association with the C-(A)-(K)-S-H phases.

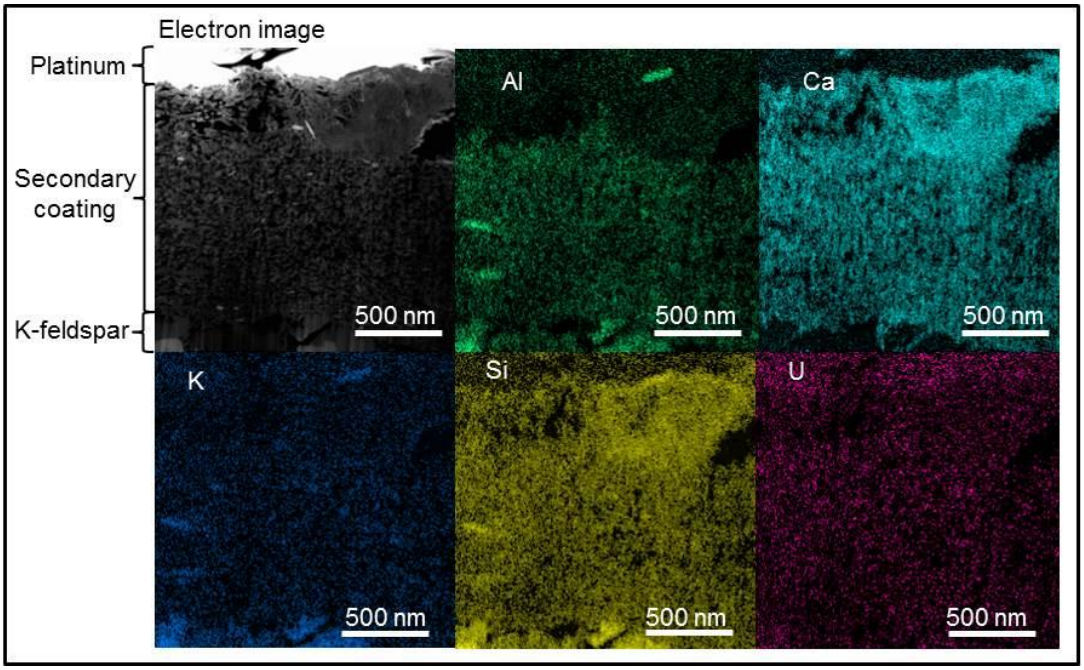

Figure 4.10: TEM electron micrograph and elemental maps (Al, Ca, K, Si and U) from a section through the coating of secondary material on a k-feldspar grain after 48 weeks of reaction in ICL

Uranium L_{III} XANES data from the samples from the U(VI)-bearing ICL leachate experiment taken at 10 days, 12 weeks and 11 months are shown in Fig. 4.11. Comparison of the XANES data highlights two significant points. Firstly, the U(VI) XANES spectra are similar throughout the experiment indicating that U(VI) coordination does not change during the experiment. Secondly, by comparison to schoepite ($(UO_2)_8O_2(OH)_{12}$•$12(H_2O)$) and Ca-uranate ($CaUO_4$) standards, it can be seen that the XANES spectra closely resemble the XANES for the Ca-uranate standard. This is indicative that the U(VI) in the ICL system is present within a uranate-like local structural environment.

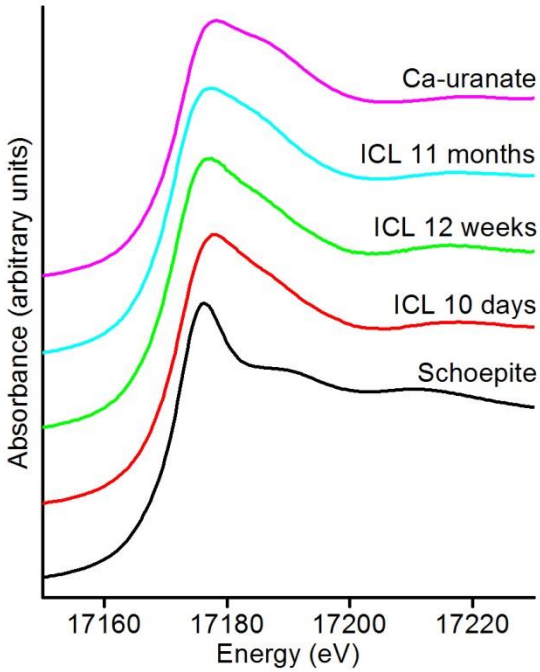

Figure 4.11: Uranium L_{III} edge XANES for the samples taken from the U(VI)-bearing ICL experiments at 10 days, 12 weeks and 11 months of reaction shown with Ca-uranate and schoepite standards

Analysis of the EXAFS spectra for each sample was conducted to gain further information on the average U(VI) bonding environment. The best fit to the EXAFS data for each sample was achieved with 2 axial O atoms at 1.88 Å, 6 equatorial O atoms at 2.24-2.31 Å and 6 Ca atoms at 3.50-3.64 Å (Fig. 4.12, Table 4.2). This arrangement of shells is similar to the experimentally derived structure of Ca-uranate ($CaUO_4$) in which the central U(VI) atom is surrounded by 2 axial oxygens at 1.91 Å, 6 equatorial oxygens at 2.31 Å and 6 calciums at 3.70 Å (Zachariasen, 1948) and supports the interpretation of a uranate type environment inferred from the XANES data. $CaUO_4$ precipitates have been previously identified in high pH solutions (pH 12.1) during U(VI) sorption to C-(A)-(K)-S-H and hardened cement paste at high U(VI) concentrations (i.e. 1 mol kg^{-1}; Tits et al., 2011; Mace et al., 2013). Splitting the equatorial oxygen shell did not provide a reasonable fit to the experimental data indicating the U(VI) was not present as the clarkeite-like precipitate identified in other CDZ-type high pH experiments (Bots et al., 2014).

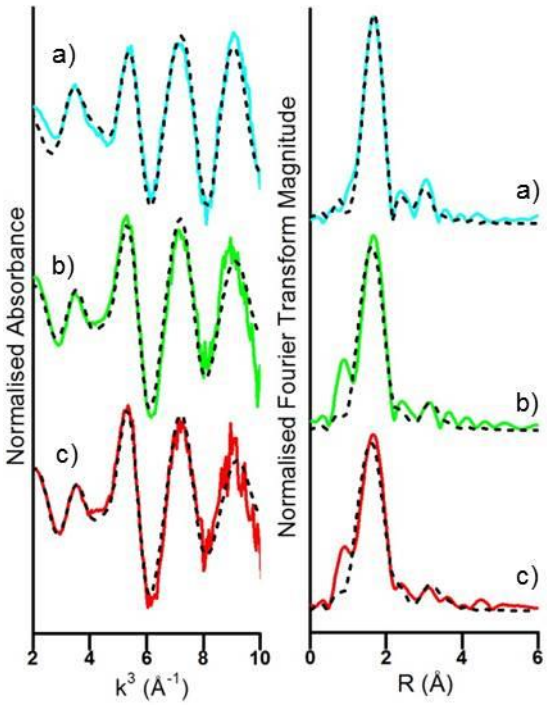

Figure 4.12: EXAFS data and modelled fit in k-space and R-space for U(VI) associated with sandstone altered in ICL for a) 11 months, b) 12 weeks and c) 10 days based on a $CaUO_4$ structure.

Table 4.2: Fit parameters for ICL EXAFS data to calcium-uranate with N fixed for each shell for each time point. N is the number of atoms, R is the interatomic distance (±1% for axial oxygens, ± 2% for equatorial oxygens, ± 2% for Ca), σ is the Debye-Waller factor and ΔE0 is the energy shift.

Sample	Shell	N	R(Å)	σ^2(Å^2)		Reduced chi-square	R-factor	ΔE0
10 days	O_{ax}	2	1.88	0.0068+/-	0.0036	80.11	0.024	5.96 +/- 4.32
	O_{eq}	6	2.31	0.0176+/-	0.0042			
	Ca	6	3.64	0.0300+/-	0.0087			
12 weeks	O_{ax}	2	1.88	0.0045+/-	0.0045	213.61	0.037	5.05+/- 5.17
	O_{eq}	6	2.30	0.0131+/-	0.0055			
	Ca	6	3.62	0.0270+/-	0.0110			
11 months	O_{ax}	2	1.88	0.0048+/-	0.0007	29.91	0.005	-2.80+/- 1.25
	O_{eq}	6	2.24	0.0083+/-	0.0014			
	Ca	6	3.50	0.0228+/-	0.0025			
$CaUO_4$*	O_{ax}	2	1.91					
	O_{eq}	6	2.31					
	Ca	6	3.70					

* CaUO4 structure taken from Zachariasen (1948)

4.3.3 Old cement leachate experiment

In the OCL U(VI)-free and U(VI)-bearing systems, Al solution concentration rose rapidly in the first 3 weeks of reaction from 0 mg l^{-1} to 4.42 ± 0.21 mg l^{-1} and 0.31 mg l^{-1} to 2.24 ± 0.06 mg l^{-1} respectively (Fig. 4.13a). The concentrations then fell gradually to 2.59 ± 0.54 mg l^{-1} and 1.36 ± 0.09 mg l^{-1} in the U(VI)-free and U(VI)-bearing systems respectively. The concentration of Si in solution in both the U(VI)-free and U(VI)-bearing systems also increased during the experiment from 0.03 mg l^{-1} to 12.63 ± 0.45 mg l^{-1} and 7.21 mg l^{-1} to 14.83 ± 0.52 mg l^{-1} respectively over the course of the experiment (Fig. 4.13b). Ca concentration in the U(VI)-free system decreased rapidly in the first week of reaction from 6.54 mg l^{-1} to 1.23 ± 0.28 mg l^{-1} and remained approximately constant during the rest of the reaction (Fig. 4.13c). In the U(VI)-bearing system Ca concentration initially increased from 6.73 mg l^{-1} to 8.48 ± 0.15 mg l^{-1} in the first 3 weeks of reaction and then remained approximately constant (Fig. 4.13c). However, in the U(VI)-bearing system Ca concentration approximated that of the blank, but was generally ~1 ppm lower. These trends indicate that, as in the YCL and ICL systems, primary alumino-silicate minerals dissolved releasing Al and Si to solution and a secondary Ca-bearing phase formed. The concentrations of phosphate, sulfate and nitrate were < 1 mg l^{-1} and generally below detection limits throughout the experiment and chloride concentration was predominantly < 6 mg l^{-1} in both U(VI)-free and U(VI)-bearing experiments throughout (Tables A2 and A3).

In the U(VI)-bearing OCL system, uranium concentration in solution fell dramatically during the first 3 weeks of the experiment from 0.97 mg l^{-1} to 0.08 ± 0.001 mg l^{-1} (Fig. 4.13d). The concentration then remained at ~ 0.1 ppm until 21 weeks into the experiment, after which it increased to 0.29 ± 0.01 mg l^{-1} after 1 year of reaction and 0.49 ± 0.02 mg l^{-1} after 18 months of reaction (Fig. 4.13). However, the solution blank for this experiment mirrors that in the reacted solution exactly. Therefore it is likely that the uranium concentration is falling due to the precipitation of a U(VI)-bearing phase which partially re-dissolves during the latter stages of the experiment.

This was supported by thermodynamic modelling of the system which predicted that the experimental solution and blank would be oversaturated with respect to becquerelite, calcium uranate ($CaUO_4$), uranophane, clarkeite, compreignacite and sodium-compreignacite throughout the experiment (Table A7).

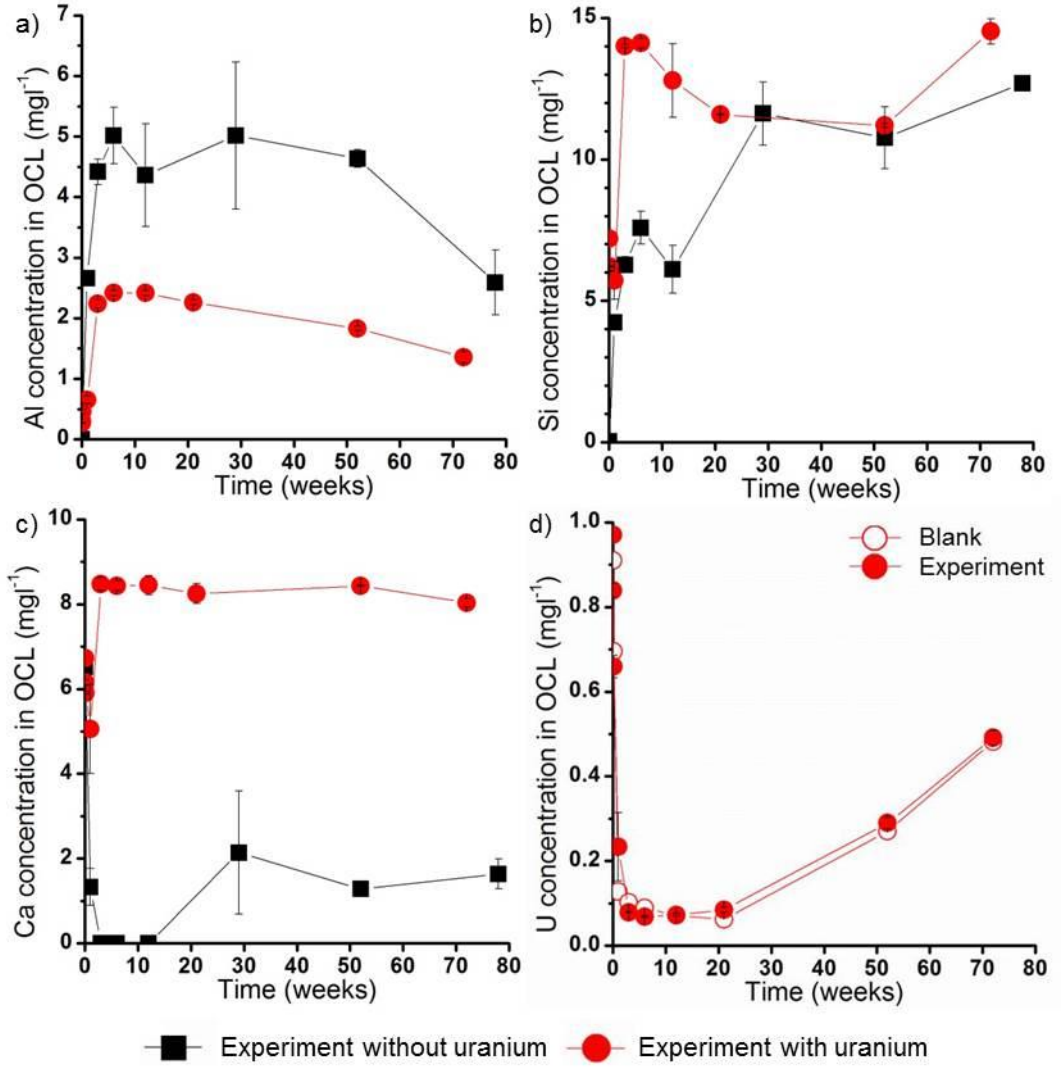

Figure 4.13: Cation concentration data for 0-18 months in the OCL experiments a) Al, b) Si, c) Ca and d) U

Through SEM imaging of the sandstone altered in both the OCL U(VI)-free and U(VI)-bearing systems 'sheet-like' particles were identified on K-feldspar grain surfaces 1-5 µm in size after 12 weeks of reaction (Fig. 4.14a and b). EDX analysis showed these phases to be Ca-rich and potentially contain Al, K and Si though the exact composition could not be resolved due to the interference of underlying primary alumino-silicate grains. However, based

on morphology and Ca content these particles were identified as a C-(A)-(K)-S-H phase. This phase persisted from 12 weeks of reaction throughout the rest of the experiment but did not significantly increase in abundance or extent during this time. By 12 weeks of reaction, some K-feldspar grain edges were also coated in a rind of secondary material that appeared blocky and was continuous for up to 50 µm (Fig. 4.14a). This phase persisted from 12 weeks of reaction throughout the experiment without significantly increasing in abundance or extent and a section through the rind showed it was 2-3 µm thick after 52 weeks of reaction (Fig. 4.14c). It is estimated qualitatively that the total volume of C-(A)-(K)-S-H formed in this leachate system was greater than that in the YCL but significantly less than that in the ICL system. EDX analysis indicated the rinds were also Ca-rich but again Al, K and Si content could not be resolved. This phase was also identified as a C-(A)-(K)-S-H phase.

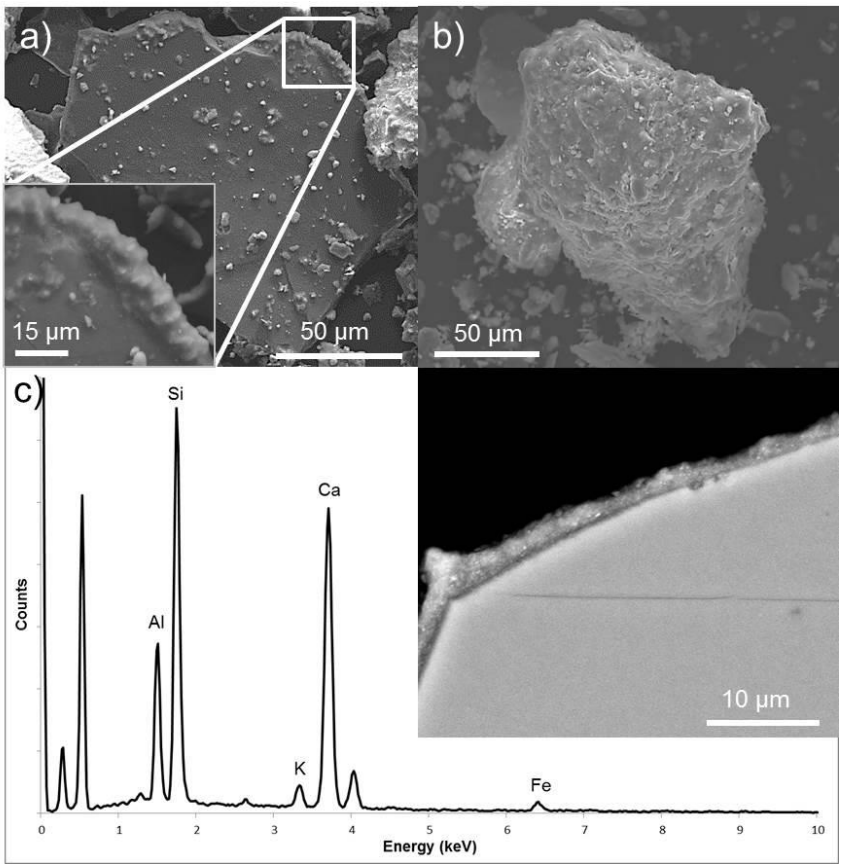

Figure 4.14: a) Image of a secondary rind formed on a feldspar grain in sandstone altered in OCL for 12 weeks b) altered sandstone grain after 26 weeks of reaction and c) section through C-(A)-(K)-S-H surface coating on k-feldspar grain after 52 weeks of reaction

Analysis of the altered sandstone from the U(VI)-bearing experiment shows the same pattern of C-(A)-(K)-S-H development as seen in the inactive experiment. Extensive EDX analysis detected no uranium associated with either these phases or primary mineral surfaces. However, a uranium L_{III} edge signal was detected via XAS analysis of the altered sandstone from all sample points, indicating that U(VI) did become associated with the sandstone during the experiment

Analysis of selected XANES spectra (some samples had U(VI) loadings too low for analysis) indicated that, as in the ICL system, during the course of the experiment the coordination environment of the uranium remained unchanged (Fig. 4.15). However, two prominent resonance features are visible in each sample, one at approximately 17190 eV and a second at approximately 17210 eV. This is similar to the reference XANES spectrum for schoepite (Fig. 4.15) and indicates that in the OCL system the U(VI) is present in uranyl coordination.

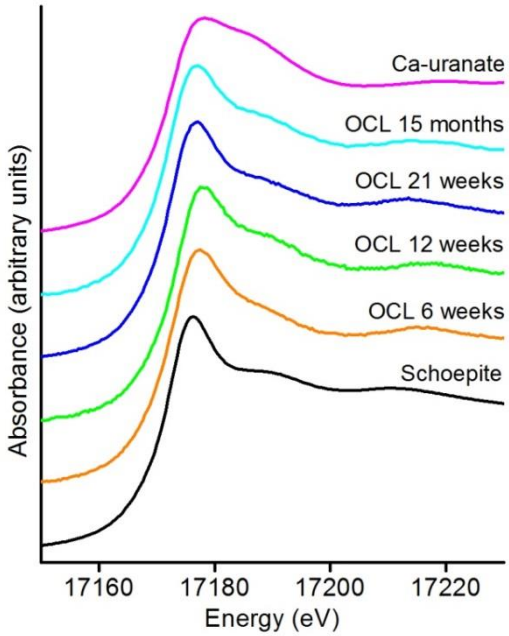

Figure 4.15: Uranium L_{III} edge XANES for the samples taken from the U(VI)-bearing OCL experiments at 6, 12, 21 weeks and 15 months of reaction shown with Ca-uranate and schoepite standards

Analysis of the EXAFS data showed that the Fourier transform of the data for all samples were dominated by a main peak at ~ 1.5 Å known to arise from backscattering from axial oxygen atoms (Fig. 4.16; Harfouche et al., 2006). However, a shoulder on this peak is clear in the data for each sample at ~ 2

Å. The EXAFS data were fit based on a uranophane structure (Ginderow, 1988) using Artemis and provides a reasonable fit at all sample points with 2 axial oxygen atoms at 1.81-1.85 Å (i.e. the uranyl moiety) and 4-6 equatorial oxygen atoms at 2.37-2.43 Å (Table 4.3). This supports the findings of the XANES analysis which indicated a uranyl-like coordination of the U(VI). In the 6 week, 21 week and 15 month samples the addition of further shells were found to improve the fit (Table A9 and A10, Figures A4-A7). The fits for all three samples were improved by the addition of two silicon shells with 1 atom at 3.15-3.21 Å, and 1-3 atoms at 3.55-3.76 Å. The addition of a 2 atom uranium shell at 3.91 Å further significantly improved the fit of the 6 week sample. In addition, the fits for the samples from 21 weeks and 15 months of reaction were significantly improved by splitting the equatorial oxygen shell with the first shell of oxygens at 2.18-2.22 Å and the second at 2.39-2.43 Å (Table 4.3). These calculated U(VI) coordination environments are similar to those identified in EXAFS studies of U(VI) adsorption / incorporation to hardened cement paste and C-S-H (Harfouche et al., 2006; Mace et al., 2013).

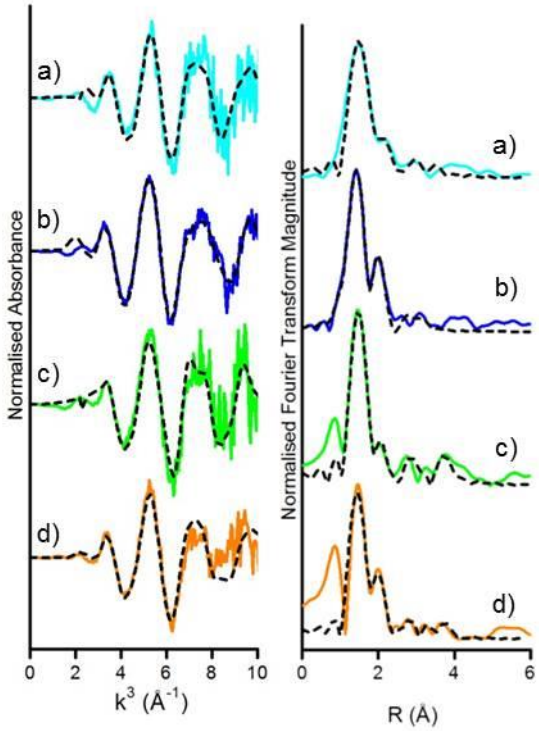

Figure 4.16: Uranium L3 edge EXAFS spectra for uranium reacted in OCL in the presence of sandstone (left) and the corresponding Fourier transformations (right) collected at a) 15 months, b) 21 weeks, c) 12 weeks and d) 6 weeks of reaction. Dashed lines represent model fits to these data produced using Artemis with the parameters given in Table 4.3)

Table 4.3: Fit parameters for OCL EXAFS data to an uranophane structure with N fixed for each shell for each time point. N is the number of atoms, R is the interatomic distance (±1% for axial oxygens, ± 2% for equatorial oxygens, ± 2% for Ca), σ is the Debye-Waller factor and ΔE0 is the energy shift.

Sample	Shell	N	R(Å)	σ^2(Å^2)	Reduced chi-square	R-factor	ΔE0
6 weeks	O_{ax}	2	1.83	0.0007+/-0.0015	28.45	0.012	12.20+/-1.44
	O_{eq}	5	2.39	0.0094+/-0.0028			
	Si_1	1	3.21	0.0076+/-0.0075			
	Si_2	1	3.76	0.0065+/-0.0115			
	U	2	3.91	0.012+/-0.0084			
12 weeks	O_{ax}	2	1.84	0.0029+/-0.0030	26.04	0.046	12.89+/-4.06
	O_{eq}	4	2.39	0.0180+/-0.0097			
21 weeks	O_{ax}	2	1.82	0.0077+/-0.0024	18.56	0.010	7.08+/-2.44
	O_{eq1}	3	2.22	0.0148+/-0.0048			
	O_{eq2}	3	2.43	0.0084+/-0.0022			
	Si_1	1	3.16	0.0155+/-0.0071			
	Si_2	1	3.69	0.0112+/-0.0061			
15 months	O_{ax}	2	1.84	0.0152+/-0.0062	12.19	0.009	-1.23+/-9.71
	O_{eq1}	4	2.18	0.0149+/-0.0071			
	O_{eq2}	2	2.39	0.0116+/-0.0097			
	Si_1	1	3.15	0.0159+/-0.0095			
	Si_2	3	3.55	0.0355+/-0.0188			
Uranophane*	O_{ax}	2	1.80				
	O_{eq1}	2	2.30				
	O_{eq2}	2	2.45				
	Si_1	1	3.14				
	Si_2	1	3.75				
	U	2	3.92				
	Ca	1	4.07				

* Uranophane structure taken from Ginderow (1988)

4.4 Discussion

In all cement leachates, in both the U(VI)-free and U(VI)-bearing systems, the concentrations of Al and Si generally increased over time, indicating the dissolution of alumino-silicate minerals. The concentration of Ca in solution generally decreased in each system, indicating the formation of a secondary Ca-bearing phase. In all the leachates, both the U(VI)-free and U(VI)-bearing

experiments, the concentrations of phosphate, sulfate and nitrate were < 1 mg l^{-1} (generally below detection limits) and chloride concentration was low / unaffected by reaction throughout the experiment (Tables S2 and S3). This provided confidence that the formation of U(VI) complexes with these species was not likely to be significant. Electron microscopy of the solids from each experiment allowed the identification of secondary C-(A)-(K)-S-H phases in all the cement leachates, in both the U(VI)-free and U(VI)-bearing systems to greater or lesser extents. This confirms the findings of other investigations of rock alteration in high pH solutions which have identified a two stage alteration process of alumina-silicate mineral dissolution followed by C-(A)-(K)-S-H precipitation (e.g. Gaucher and Blanc, 2006; Savage and Rochelle, 1993; Hodgkinson and Hughes, 1999; Braney et al., 1993; Savage et al., 1992). In addition, secondary hydrocalumite was identified in the ICL reacted material. Hydrocalumite is an important component of Portland cements (Taylor, 1990; Matschei et al., 2007) known to precipitate in the Si-Al-Ca systems at pH 12-13 where it had been shown to have a high retention capacity for anionic species (Liu et al., 2013; Grover et al., 2010; Zhang and Reardon, 2003) and has been found to remove Zn^{2+} from solution (Liu et al., 2011). It has also been identified at the Scawt Hill site in Northern Ireland which has been used as an analogue site for the hyperalkaline conditions likely to occur at a GDF site (Mills et al, 2012). However, as the hydrocalumite was progressively overeaten by C-S-H over time is it interpreted as a metastable mineral.

Despite the parity of secondary phases formed, distinct differences in the rate and extent of C-(A)-(K)-S-H formation were apparent in each of the three leachate systems. In YCL no C-(A)-(K)-S-H was observed before 12 weeks of reaction despite increased solution concentrations of Si and Al. The abundance of C-(A)-(K)-S-H then increased with time throughout the experiment but only minor amounts of the secondary phase formed by the end of the experiment. This is attributed to the low concentration of Ca in solution limiting the formation of the secondary solid phase, despite significant alumina-silicate mineral dissolution in the aggressive pH 13 solution. In ICL, the solution concentrations of Al and Si were approximately constant and an order of magnitude below those in the YCL system, indicating minimal

alumino-silicate mineral dissolution. However, significant quantities of secondary C-(A)-(K)-S-H phases were observed on reacted grain surfaces by 1 week of reaction which persisted throughout the experiment. This clearly showed alumino-silicate mineral dissolution provided a source of Al and Si, therefore the relatively constant, low concentrations of these species in solution were attributed to their equilibrium with the C-(A)-(K)-S-H phases. The extensive and rapid formation of C-(A)-(K)-S-H in this system was attributed to the high concentration of Ca in ICL in combination with significant alumino-silicate mineral dissolution. Interestingly, in this leachate the decrease in Ca solution concentration was faster in the absence of U(VI). This is likely due to the different solid to solution ratio of the two experiments as the greater surface area of rock available for reaction in the U(VI)-free system would have released more Si and Al to solution, allowing increased C-(A)-(K)-S-H precipitation. In the OCL system, as in the YCL system, no C-(A)-(K)-S-H was observed before 12 weeks of reaction. However, the material reacted for 12 weeks exhibited C-(A)-(K)-S-H formed on k-feldspar grains which persisted throughout the experiment. It was estimated that the volume of C-(A)-(K)-S-H formed in the OCL reacted material was greater than that formed in the YCL reacted material but significantly less than that in the ICL system.

The presence of U(VI) in solution was found to have no impact on the sandstone alteration processes occurring in the high pH leachates. However, the behaviour of U(VI) in each of the different leachates varied significantly. In YCL the majority of U(VI) appeared to remain in solution throughout the experiment, reminiscent of the study of Tits et al. (2011) who found U(VI) remained in solution as $UO_2(OH)_4^{2-}$ at pH 13.1. However, thermodynamic modelling predicted that at all sample points the YCL was oversaturated with respect to U(VI) minerals and detailed investigation of the 0.45 µm filterable solids identified U(VI) associated with colloidal silicate particles. The precise mineralogy of these particles could not be identified, but qualitative chemical analysis suggested they may be C-(A)-(K)-S-H with U(VI) adsorbed / structurally incorporated. However, it is possible that U(VI) may have initially precipitated as $CaUO_4$, predicted to be oversaturated during thermodynamic

modelling and found to precipitate in previous studies of U(VI) behaviour at hyperalkaline pH (Tits et al, 2011; Harfouche et al., 2006). The $CaUO_4$ may have then reacted with the aqueous Si released during alumino-silicate mineral dissolution to form a uranyl-alkali-silicate such as uranophane. This could occur in the same way as the transformation of uranyl-oxyhydroxide phases to uranyl silicate phases in studies of U(VI) behaviour in the presence of dissolved silica (Finch et al., 1992; Wellman et al., 2007; Golovich et al., 2011). Interestingly, the concentration of 0.45 µm filterable U(VI) in this system remained relatively stable during throughout the experiment, assumed to indicate colloid stability (Bots et al., 2014; Smith et al., in press). However, the gradual decrease in U(VI) solution concentration was attributed to the aggregation of the U(VI)-bearing colloids resulting in their removal during filtration or to the sorption of the colloidal particles to mineral surfaces at extended timescales as hypothesised by Smith et al. (in press).

In ICL, U(VI) concentration in solution fell rapidly in the first weeks of reaction and microscopy identified that it has preferentially associated with the secondary C-(A)-(K)-S-H, and was distributed throughout the thickness of the C-(A)-(K)-S-H grain coatings. XANES data indicated that U(VI) in this system occurred in uranate-like coordination, and fitting of the EXAFS data to a $CaUO_4$ structure was successful. As $CaUO_4$ was also one of the phases predicted to be oversaturated in the thermodynamic model of this leachate system, it is suggested that $CaUO_4$ precipitated in this system and became dispersed in the C-(A)-(K)-S-H grain coatings due to their concurrent formation from solution. $CaUO_4$ precipitates have been previously identified in high pH solutions (pH 12.1) during U(VI) sorption to C-(A)-(K)-S-H and hardened cement paste at high U(VI) concentrations (i.e. 1 mol kg^{-1}; Tits et al., 2011; Mace et al., 2013; Harfouche et al., 2006).

The concentration of U(VI) fell rapidly in OCL during the first weeks of reaction, though no U(VI)-bearing phases were identified through electron microscopy. XAS analysis of the reacted material did however detect U(VI) associated with the experimental solids. XANES data indicated that the U(VI) was present in uranyl coordination and this was supported by analysis of the EXAFS data.

Fitting of the EXAFS data also showed that, up to 12 weeks of reaction, U(VI) was coordinated with a single equatorial oxygen shell. In previous studies of U(VI) interactions with C-S-H, this was suggested to be indicative of U(VI) adsorption to C-S-H (Macé et al., 2013; Harfouche et al., 2006). However, in this study there is no clear evidence that the U(VI) is preferentially associated with C-(A)-(K)-S-H. After 21 weeks of reaction the EXAFS data indicate the presence of a split equatorial oxygen shell around the U(VI). This may suggest the transformation of U(VI) to uranophane over time (Ginderow, 1988; Macé et al., 2013), a phase predicted to be oversaturated in OCL during thermodynamic modelling. However, a split equatorial oxygen shell has also been proposed to be indicative of U(VI) adsorption into the interlayer of C-S-H or polynuclear surface complexation with silicate minerals (Harfouche et al., 2006; Sylwester et al., 2000; Walter et al., 2005; Reich et al., 1998) and the thermodynamic model could not account for this behaviour. Therefore it is possible to say that U(VI) became preferentially associated with the solid phase in the OCL system but this may have been through adsorption of the surface mediated formation of a uranyl silicate mineral such as uranophane. In the OCL experiment the concentration of U(VI) in solution also increased markedly after 21 weeks of reaction. This may indicate that U(VI) de-sorbed from mineral surfaces / uranophane dissolved due to chemical / mineralogical changes in the system. This is in contrast to the behaviour of U(VI) during the course of the YCL and ICL experiments which did not significantly alter during the reaction, indicating that the evolution of the system had little impact on U(VI).

The differences in U(VI) speciation in the different leachates potentially have significant implications for U(VI) migration from a GDF. Despite the limited solubility of U(VI) at high pH (Chapman and Flowers, 1986; Glasser, 1997; Sugiyama et al., 2007) the formation of U(VI)-bearing colloids and their persistence in the pH 13 YCL system may cause increased U(VI) mobility as the colloids could be transported away from the repository with groundwater flow (Bots et al., 2014). This contrasts with the behaviour of U(VI) in ICL as the precipitation of $CaUO_4$ and its association with secondary C-(A)-(K)-S-H phases would likely result in the retardation of U(VI) migration. The behaviour

of U(VI) in OCL is more complex. The initial U(VI) adsorption to mineral surfaces in this leachate would limit U(VI). However, the change in U(VI) coordination environment and increase in U(VI) solution concentration observed from 21 weeks of reaction is noteworthy and warrants further investigation.

4.5 Summary and conclusions

Batch experiments were performed to investigate the alteration of a model mineral assemblage and the behaviour of U(VI) during the alteration of sandstone at high pH in three cement leachates of different composition and pH. Over 12-18 months the reaction of each of the leachates with the sandstone resulted in the dissolution of primary alumino-silicate minerals and formation of predominantly C-(A)-(K)-S-H phases. This variation is predominantly associated with differences in Ca concentration in the different leachates and the extent of C-(A)-(K)-S-H phase development varied between the different leachate systems with C-(A)-(K)-S-H abundance in ICL > OCL > YCL. In the ICL system an additional secondary Ca-silicate phase, hydrocalumite, also formed but was gradually replaced by C-(A)-(K)-S-H phases. This indicates that solution composition and pH affect the extent of reaction but not which alteration processes which occur. This supports the findings of previous studies of high pH rock alteration.

The behaviour of U(VI) varied significantly in each leachate system. In the YCL system the rapid formation of stable U(VI)-bearing colloidal particles was observed. In the ICL, EXAFS analysis indicated the precipitation of U(VI) as a $CaUO_4$ phase observed within the secondary C-(A)-(K)-S-H phase grain coatings. Interestingly, in both the YCL and ICL systems the behaviour of U(VI) was not significantly affected by the progression of the sandstone alteration over 18 and 12 months respectively. In the OCL system U(VI) was associated with the solid phase through either adsorption to mineral surfaces or the surface mediated precipitation of a uranyl silicate mineral. However, in this system the increase in U(VI) solution concentration over time indicated a change in U(VI) behaviour as the system evolved.

The observed variation in U(VI) behaviour in the different cement leachates has implications for U(VI) mobility in the geosphere surrounding a cementitious repository. In YCL (representative of a KOH and NaOH dominated leachate) the U(VI)-bearing colloidal particles, potentially a $CaUO_4$ / U(VI)-beraing silicate phase, would be highly mobile in the CDZ despite the availability of mineral surfaces for sorption. Conversely in ICL and OCL ($Ca(OH)_2$ dominated leachates), U(VI) mobility would be strongly retarded due to precipitation / adsorption. As the $CaUO_4$ precipitate was apparently co-located with the secondary C-(A)-(K)-S-H phases in the ICL system, it is clear that high pH rock alteration is integral to the behaviour of U(VI) observed. In OCL, U(VI) adsorption occurred without apparent preference for primary or secondary mineral phases and so appeared initially unaffected by high pH rock alteration. However, this study has also shown that, despite initial U(VI) sorption, in OCL U(VI) remobilises to solution as the system evolves. This highlights the necessity of understanding U(VI) behaviour in high pH systems over extended timescales.

This study has highlights the potential complexity of U(VI) behaviour in the CDZ during the high pH alteration of rock. It has also indicats that the composition and pH of the leachate responsible for rock alteration may affect U(VI) behaviour and consequently may have significant implications for U(VI) mobility and the safety case of any cementitious GDF.

References

ANDRA. 2012. Low and intermediate level short-lived waste [online]. Available at: <www.andra.fr/international/pages/en/menu21/waste-management/waste-classification/short-lived-low--and-intermediate-level-waste-1609.html> [accessed 19/01/2014].

ATKINS, M. & GLASSER, F. P. 1992. Application of Portland cement-based materials to radioactive waste immobilization. *Waste Management*. 12. 105-131.

ATKINSON, A. 1985. The Time Dependence of pH Within a Repository for Radioactive Waste Disposal. *UKAEA,* AERE-R 11777.

AUROY, M., POYET, S., LE BESCOP, P. & TORRENTI, J-M. 2013.Impact of carbonation on the durability of cementitious materials: water transport properties characterization. *EPJ Web of Conferences*. 56. 01008.

BASTON, G. M. N., BROWNSWORD, M., CROSS, J. E., HOBLEY, J., MORETON, A. D., SMITH-BRIGGS, J. L. &THOMASON, H. P. 1993. The Solubility of Uranium in Cementitious Near-Field Conditions, Nirex Report. NSS/R222, Nirex, Didcot, Oxfordshire, UK.

BERNER, U. R. 1992. Evolution of Pore Water Chemistry During Degradation of Cement in a Radioactive Waste Repository Environment. *Waste Management,* 12**,** 201-219.

BOTS, P., MORRIS, K., HIBBERD, R., LAW, G. T. W., MOSSELMANS, J. F. W., BROWN, A. P., DOUTCH, J., SMITH, A. J. & SHAW, S. 2014. Formation of stable uranium(VI) colloidal nanoparticles in conditions relevant to radioactive waste disposal. Langmuir. *American Chemical Society*.

BOURDON, B., TURNER, S., HENDERSON, G. M. & LUNDSTROM, C. C. 2003. Introduction to U-series geochemistry. *In:* Bourdon, B., Henderson, G. M., Lundstrom, C. C. & Turner, S. eds. 2003. Uranium-

series geochemistry. Reviews in mineralogy and geochemistry vol. 52. Mineralogical Society of America, Washington DC, USA.

BRANEY, M. C., HAWORTH, A., JEFFERIES, N. L. & SMITH, A. C. 1993. A study of the Effects of an Alkaline Plume From a Cementitious Repository on Geological Materials. *Journal of Contaminant Hydrology,* 13**,** 379-402.

BROWNSWORD, M., BUCHAN, A. B., EWART, F. T., MCCROHON, R., ORMEROD, G. J., SMITH-BRIGGS J. L. & THOMASON, H. P. 1990. The solubility and sorption of uranium(VI) in a cementitious repository. *In*: Oversby, V. M. & Brown, P. W. eds. 1990. Scientific Basis for Nuclear Waste Management, XIII International Symposium. Materials Research Society, Virginia, USA. 176. 557.

BUTCHER, E. J., BORWICK, J., COLLIER, N. & WILLIAMS, S. J. 2012. Long term leachate evolution during flow-through leaching of a vault backfill (NRVB). *Mineralogical Magazine*. 76. 3023-3031.

CHAPMAN, N. A. & FLOWERS, R. H. 1986. Near-field solubility constraints on radionuclide mobilisation and their influence on waste package design. *Philosophical Transactions of the Royal Society of London*. A319. 83–95.

DEFRA. 2008. Managing radioactive waste safely: A framework for implementing geological disposal. Department of the environment, food and rural affairs. UK.

DENT, A. J., CIBIN, G., RAMOS, S., SMITH, A. D., SCOTT, S. M., VARANDAS, L., PEARSON. M. R., KRUMPA, N. A., JONES, C. P. & ROBBINS, P. E. 2009. B18 A core XAS spectroscopy beamline for Diamond. Journal of Physics. 190(1), 012039.

DONG, W., BALL, W. P., LIU, C, WANG, Z, STONE, A. T., BAI, J. & ZACHARA, J. M. 2005. Influence of calcite and dissolved calcium on

uranium(VI) sorption to a Hanford subsurface sediment. *Environmental Science and Technology*. 39. 7949-7955.

EVANS, N. D. M. 2008. Binding mechanisms of radionuclides to cement. *Cement and Concrete Research.* 38. 543–553.

FINCH, R. J., MILLER, M. I. & EWING, R. C. 1992. Weathering of natural uranyl oxide hydrates: schoepite polytypes and dehydration effects. *Radiochimica Acta.* 58/59. 2. 433-443.

GAONA, X., KULIK, D. A., MACÉ, N & WIELAND, E. 2012. Aqueous-solid solution thermodynamic model of U(VI) uptake in C-S-H phases. *Applied Geochemistry*. 27. 81-95.

GAUCHER, E. & BLANC, P. 2006. Cement/clay interactions – A review: Experiments, natural analogues, and modeling. *Waste Management,* 26**,** 776-788.

GIANNUZZI, L. A. & STEVIE, F. A. 1999. A review of focused ion beam milling techniques for TEM specimen preparation. Micron. 30, 197-204.

GINDEROW, D. 1988. Structure de l'uranophane alpha, Ca(UO2)2(SiO3OH)2·5H 2O. *Acta Crystallographica.* 44. 421.

GLASSER, F. P. 1997. Fundamental aspects of cement solidification and stabilisation. *Journal of Hazardous Materials*. 52. 151-170.

GLASSER, F. P. 2001. Cement in radioactive waste disposal. *Mineralogical Magazine.* 65. 621.633.

GOLOVICH, E. C., WELLMAN, D. M., SERE, R. J. & BOVAIRD, C. C. 2011. Summary of uranium solubility studies in concrete waste forms and vadose zone environments. *U.S. Department of Energy*. PNNL-20726.

GOUGAR, M. L. D., SCHEETZ, B. E. & ROY, D. M. 1996. Ettringite and C-S-H Portland cement phases for waste ion immobilization: a review. *Waste Management*. 16. 295-303.

GREATHOUSE, J. A., O'BRIEN, R. J., BEMIS, G. & PABALAN, R. T. 2002. Molecular dynamics study of aqueous uranyl interactions with quartz (010). *Journal of Physical Chemistry*. 106. 1646–1655.

GROVER, K., KOMARNENI, S. & KATSUKI, H. 2010. Synthetic hydrotalcite-type and hydrocalumite-type layered double hydroxide arsenate uptake. *Applied Clay Science*. 48. 631-637.

HARFOUCHE, M., WIELAND, E., DÄHN, R., FUJITA, T., TITS, J., KUNZ, D. AND TSUKAMOTO. 2006. EXAFS study of U(VI) uptake by calcium silicate hydrates. *Journal of Colloid and Interface Science*. 303. 195-204.

HARTMANN, E., GECKEIS, H., RABUNG, T., LUTZENKIRCHEN, J. & FANGHANEL, T. 2008 Sorption of radionuclides onto natural clay rocks. *Radhiochimica Acta*. 96. 699-707.

HEANEY, P. J., VICENZI, E. P., GIANNUZZI, L. A. & LIVI, K. J. T. 2001. Focused ion beam milling: a method of site-specific sample extraction for microanalysis of Earth and planetary metrials. American Mineralogist. 86(9), 1094-1099.

HODGKINSON, E. S. & HUGHES, C. R. 1999. The mineralogy and geochemistry of cement/rock reactions: high-resolution studies of experimental and analogue materials. *Geological Society, London, Special Publications,* 157**,** 195-211.

JOHNSON, C. A. 2004. Cement stabilization of heavy-metal-containing wastes. Geological Society, London, Special Publications. 236. 595-606.

LANGFORD, R. M. & PETFORD-LONG, A. K. 2001. Preparation of transmission electron microscopy cross-section specimens using focused ion beam milling. Journal of Vacuum Science and Technology. 19(5), 2186-2193.

LANGMUIR, D. 1997. Aqueous environmental geochemistry. Prentice Hall, New Jersey.

LINKLATER, C. M., ALBINSSON, Y., ALEXANDER, W. R., CASES, I., MCKINLEY, I. G. & SELLIN, P. 1996. A natural analogue of high-pH cement pore waters from the Maqarin area of northern Jordan: Comparison of predicted and observed trace-element chemistry of uranium and selenium. *Journal of Contaminant Hydrology*. 21. 59-69.

LIU, Q., LI, Y., ZHANG, J., CHI, Y, RUAN, X., LIU, J AND QIAN, G. 2011. Effective removal of zinc from aqueous solution by hydrocalumite. *Chemical Engineering Journal*. 175. 33-38.

LIU, X., ASAI, A., SATO, T., OPISO, E., OTAKE, T. & YONEDA, T. 2013. Mineral synthesis in Si-A;-Ca systems and their iodide sorption capacity under alkaline conditions. *Water, Air, & Soil Pollution.* 224. 1442.

MACE, N., WIELAND, E., DÄHN, R., TITS, J. & SCHEINOST, A. C. 2013. EXAFS investigation on U(VI) immobilization in hardened cement paste: influence of experimental conditions on speciation. *Radiochimica Acta.* 101. 379-389.

MAHER, K, BARGAR, J. R. & BROWN, G. E. 2013. Environmental Speciation of Actinides. *Inorganic Chemistry*. 52. 3510-3532.

MATSCHEI, T., LOTHENBACH, B. & GLASSER, F. P. 2007. The AFm phase in Portland cement. *Cement and Concrete Research*. 37. 118-130.

MILLER, W., ALEXANDER, R., CHAPMAN, N., MCKINLEY, I. & SMELLIE, J. 2000. Geological disposal of radioactive wastes and natural analogues. Waste Management series vol. 2. Elsevier Science Ltd. Kidlington, Oxford.

MILLS, S. J., CHRISTY, A. G., GÉNIN J.-M. R., KAMEDA, T. & COLOMBO, F. 2012. Nomenclature of the hydrotalcite supergroup: natural layered double hydroxides. *Mineralogical Magazine.* 76. 1289-1336.

MORONI, L. P. & GLASSER, F. P. 1995. Reactions between cement components and U(VI) oxide. *Waste Management*. 15. 243-254.

MOYCE, E. B. A., ROCHELLE, C., MORRIS, K., MILODOWSKI, A. E., CHEN, X., THORNTON, S., SMALL, J. S. & SHAW, S. 2014. Rock alteration in alkaline cement waters over 15 years and its relevance to the geological disposal of nuclear waste. Applied Geochemistry. 50. 91-105.

MOYES, L. N., PARKMAN, R. H., CHARNOCK, J. M., VAUGHAN, D. J., LIVENS, F. R., HUGHES, C. R. & BRAITHWAITE, A. 2000. Uranium uptake from aqueous solution by interaction with goethite, lepidocrocite, muscovite, and maskinawite: an X-ray absorption spectroscopy study. *Environmental Science and Technology.* 34. 1062–1068

NAGRA. 2014. Geological repository for low- and intermediate-level waste [online]. Available at: <www.nagra.ch/en/tlsmae.htm> [accessed 19/01/2014].

NDA. 2010a. Geological Disposal: Generic disposal system technical specification. NDA report NDA/RWMD/044. NDA, Harwell.

NDA. 2010b. Geological disposal radionuclide behaviour status report. NDA report NDA/RWMD/034. NDA, Harwell.

NUCLEAR WASTE MANAGEMENT ORGANISATION. 2010. DGR key features [online]. Available at: < www.nwmo.ca/dgr_keyfeatures> [accessed 19/01/2014].

OECD-NEA. 2008. Moving forward with geological disposal of radioactive waste: a collective statement by the NEA radioactive waste management committee (RWMC). NEA no. 6433.

PARKHURST, D. L. & APPELO, C. A. J. 2013. Description of input and examples for PHREEQC version 3—A computer program for speciation, batch-reaction, one-dimensional transport, and inverse geochemical calculations. In: U.S. Geological Survey Techniques and Methods, book 6, chap. A43. U.S. Geological Survey, Colorado.

POINTEAU, I., LANDESMAN, C., GIFFAUT, E. & REILLER, P. 2004. Reproducibility of the uptake of U(VI) onto degraded cement pastes and calcium silicate hydrate phases. *Radiochimica Acta*. 92. 645-650.

POINTEAU, I., REILLER, P., MACÉ, N., LANDESMAN, C. & COREAU, N. 2006. Measurement and modelling of the surface potential evolution of hydrated cement pastes as a function of degradation. *Journal of Colloid and Interface Science*. 300. 33-44.

PRIKRYL, J. D., JAIN, A., TURNER, D. R. & PABALAN, R. T. 2001. Uranium (VI) sorption behavior on silicate mineral mixtures. *Journal of Contaminant Hydrology*. 47. 241–253.

QAFOKU, N. P. & ICENHOWER, J. P. 2008. Interactions of aqueous U(VI) with soil minerals in slightly alkaline natural systems. *Reviews in Environmental Science and Biotechnology*. 7. 355-380.

RAMIREZ, S. 2005. Alteration of the Callovo-Oxfordian clay from Meuse-Haute Marne underground laboratory (France) by alkaline solution. I. A XRD and CEC study. *Applied Geochemistry,* 20**,** 89-99.

RAVEL, B. & NEWVILLE, M., 2005. ATHENA, ARTEMIS, HEPHAESTUS: data analysis for Xray absorption spectroscopy using IFEFFIT. J. Synchrotron Radiat. 12, 537–541.

REICH, T., MOLL, H., ARNOLD, T., DENECKE, M. A., HENNIG, C., GEIPEL, G., BERNHARD, G., NITSCHE, H., ALLEN, P. G., BUCHER, J. J.,

EDELSTEIN, N. M. & SHUH, D. K. 1998. An EXAFS study of uranium(VI) sorption onto silica gel and ferrihydrite. *Journal of Electron Spectroscopy and Related Phenomena.* 96. 237-243.

ROCHELLE, C., PEARCE, J., BATEMAN, K., COOMBS, P. & WETTON, P. 1997. The evaluation of chemical mass transfer in the disturbed zone of a deep geological disposal facility for radioactive waste: X. Interaction between synthetic cement porefluids and BVG: Observations from experiments of 4, 9 and 15 months duration. BGS technical report WE/97/16 Article permalink: <http://nerc.worldcat.org/oclc/703969750>.

SAVAGE, D., BATEMAN, K., HILL, P., HUGHES, C., MILODOWSKI, A. E., PEARCE, J., RAE, E. & ROCHELLE, C. 1992. Rate and mechanism of the reaction of silicates with cement pore fluids. *Applied Clay Science*. 7. 33-45.

SAVAGE, D. & ROCHELLE, C. 1993. Modelling Reactions Between Cement Pore Fluids and Rock: Implications for Porosity Change. *Journal of Contaminant Hydrology,* 13**,** 365-378.

SAVAGE, D. 2011. A review of analogues of alkaline alteration with regard to long-term barrier performance. *Mineralogical Magazine*, 75, 2401-2418.

SMITH, K. F., BRYAN, N. D., SWINBURNE, A. N., BOTS, P., SHAW, S., NATRAJAN, L. S., MOSSELMANS, J. F. W., LIVENS, F. R. & MORRIS, K. In press. U(VI) behaviour in hyperalkaline calctie systems. *Geochimica et Cosmochimica Acta.*

SUGIYAMA, D., FUJITA, T., CHIDA, T. & TSUKAMOT, M. 2007. Alteration of fractured cementitious materials. *Cement and Concrete Research*. 37. 1257–1264.

SYLWESTER, E. R., HUDSON, E. A. & ALLEN, P. G. 2000. The structure of uranium(VI) sorption complexes on silica, alumina, and montmorillonite. *Geochimica et Cosmochimica Acta*. 64. 2431-2438

SZECSODY, J. E., TRUEX, M. J., QAFOKU, N. P, WELLMAN, D. W. RESCH, T. & ZHONG, L. 2013. Influence of acidic and alkaline waste solution properties on uranium migration in subsurface sediments. *Journal of Contaminant Hydrology*. 151. 155-175.

TAYLOR, H.F.W. 1990. Cement Chemistry. *Academic Press*, London.

TITS, J., FUJITA, T., TSUKAMOTO, M. & WIELAND, E. 2008. Uranium(VI) uptake by synthetic calcium silicate hydrates. *Materials Research Society Proceedings*. 1107. 467.

TITS, J., GEIPEL, G., MACÉ, N. EILZER, M. & WIELAND, E. 2011. Determination of uranium(VI) sorbed species in calcium silicate hydrate phases: A laser-induced luminescence spectroscopy and batch sorption study. *Journal of Colloid and Interface Science*. 359. 248-256.

VINES, S. & LEVER, D. 2013. An integrated approach to geological disposal of UK wastes containing carbon-14. *ASME*, 15th international conference on environmental remediation and radioactive waste management, vol 1: low/intermediate-level radioactive waste management; spent fuel, fissile material, transuranic and high-level radioactive waste management.

WALTER, M., ARNOLD, T., GEIPEL, G., SCHEINOST, A. & BERNHARD, G. 2005. An EXAFS and TRLFS investigation on uranium(VI) sorption to pristine and leached albite surfaces. *Journal of Colloid and Interface Science.* 282. 2. 293-305.

WELLMAN, D. M., MATTIGOD, S. V., AREY, B. W., WOOD, M. I. & FORRESTER, S. W. 2007. Experimental limitations regarding the formation and characterization of uranium-mineral phases in concrete waste forms. *Cement and Concrete Research*. 37. 2. 151-160.

ZACHARIASEN, W. H. 1948. Crystal chemical studies of the 5f-series of elements. Iv. The crystal structure of $Ca(UO_2)O_2$ and $Sr(UO_2)O_2$. *Acta Crystallographica*. 1. 281-285.

ZANONATO, P. L., DI BERNARDO, P. & GRENTHE, I. 2014. A calorimetric study of the hydrolysis and peroxide complex formation of the uranyl(VI) ion. Dalton Transactions. 43. 6. 2378-2383.

ZHANG, M. & REARDON, E. J. 2003. Removal of B, Cr, Mo and Se from wastewater by incorporation into hydrocalumite and ettringite. *Environmental Science and Technology.* 37. 2947-2952.

5 Rock alteration in alkaline cement waters over 15 years and its relevance to the geological disposal of nuclear waste

5.1 Abstract

The interaction of groundwater with cement in a geological disposal facility (GDF) for intermediate level radioactive waste will produce a high pH leachate plume. Such a plume may alter the physical and chemical properties of the GDF host rock. However, the geochemical and mineralogical processes which may occur in such systems over timescales relevant for geological disposal remain unclear. This study has extended the timescale for laboratory experiments and shown that, after 15 years two distinct phases of reaction may occur during alteration of a dolomite-rich rock at high pH. In these experiments the dissolution of primary silicate minerals and the formation of secondary calcium silicate hydrate (C-S-H) phases containing varying amounts of aluminium and potassium (C-(A)-(K)-S-H) during the early stages of reaction (up to 15 months) have been superseded as the systems have evolved. After 15 years significant dedolomitisation ($MgCa(CO_3)_2 + 2OH^- \rightarrow Mg(OH)_2 + CaCO_3 + CO_3^{2-}{}_{(aq)}$) has led to the formation of magnesium silicates, such as saponite and talc, containing variable amounts of aluminium and potassium (Mg-(Al)-(K)-silicates) and calcite at the expense of the early-formed C-(A)-(K)-S-H phases. This occured in high pH solutions representative of two different periods of cement leachate evolution with little difference in the alteration processes in either a KOH and NaOH or a $Ca(OH)_2$ dominated solution but a greater extent of alteration in the higher pH leachate. The high pH alteration of the rock over 15 years also increased the rock's sorption capacity for U(VI). The results of this study provide a detailed insight into the longer term reactions occurring during the interaction of cement leachate and dolomite-rich rock in the geosphere. These processes have the potential to impact on radionuclide transport from a geodisposal facility and are therefore important in underpinning any safety case for geological disposal.

5.2 Introduction

A widely recognised concept for the disposal of radioactive waste, which will remain hazardous for hundreds of thousands of years, is emplacement in a GDF. Many proposed GDF concepts for Intermediate Level Waste (ILW), such as those in the UK, France, Canada and Switzerland (NDA, 2010a; Andra, 2012; Nuclear Waste Management Organisation, 2010; Nagra, 2014), involve cement e.g. as a wasteform, backfill and construction material. Post-closure, groundwater will saturate facilities and cement dissolution will produce a high pH leachate which will evolve in composition and pH over the lifetime of the GDF (Atkinson, 1985, Berner, 1992). Initially, dissolution of KOH and NaOH within the cement will form a leachate of pH ~ 13. The leachate pH will then decrease to ~ 12.5 where it will be buffered by equilibration with portlandite ($Ca(OH)_2$). The leachate will remain at this pH until all the $Ca(OH)_2$ has dissolved, after which, pH will be controlled by equilibrium with calcium silicate hydrate (C-S-H) gel and will decrease to ~ 10.5. The leachate will form a chemically disturbed zone (CDZ) in the geosphere surrounding the GDF, also known as an alkaline disturbed zone (ADZ; NDA 2010b). Previous studies have shown that in the CDZ high pH leachates could cause the dissolution of aluminosilicate minerals and formation of secondary mineral phases (e.g. C-S-H phases, chapter 4 of this thesis, Gaucher and Blanc, 2006 and references therein)). This could change the physical (e.g. porosity and permeability) and chemical (e.g. reactive surface area and sorption capacity) properties of the host rock thereby affecting radionuclide transport. For example, mineral dissolution could increase rock permeability and promote radionuclide transport, or the formation of secondary solid phases could block flow paths and have the opposite effect. The formation of secondary phases will also change the nature of the surfaces with which radionuclides could interact e.g. any increased sorption capacity of secondary phases could retard contaminant transport. The potential for cement leachates to alter host rock properties shows that understanding the chemical and mineralogical changes which occur will be key to developing a long term safety case for any cementitious

GDF. However, there is a lack of long-term (>10 years) experimental studies which investigate these processes.

Overall, is has been suggested that CDZ alteration can be divided into two regions (Savage, 2011). Firstly, a zone closest to the cement/rock interface (zone 1) where extensive mineral alteration occurs, including dissolution of primary silicate minerals and precipitation of secondary solid phases. Secondly, a zone further from the interface (zone 2) where fluid chemistry is perturbed and ion exchange reactions are important, but rock alteration is significantly diminished. Many short term laboratory and underground rock laboratory experimental studies have investigated rock and mineral alteration in high pH cement leachates (zone 1; e.g. Gaucher and Blanc, 2006; Bateman et al., 1999; and references therein; Braney et al., 1993; Cuevas, 2004; Mäder et al., 2006). Generally, these studies have found that reaction in high pH, Ca-bearing cement-type leachates results in the dissolution of silicate minerals (Eq. 5.1) followed predominantly by the precipitation of secondary C-S-H phases (Eq. 5.2) of varying Ca:Si ratio (e.g. 0.5-1.5 (Gaucher and Blanc, 2006)), morphology and crystallinity e.g. C-S-H gel (Savage and Rochelle, 1993; Hodgkinson and Hughes, 1999).

$$KAlSi_3O_8 + 3OH^- + 2H_2O \rightarrow Al(OH)_4^- + 3HSiO_{3\,(aq)}^- + K^+_{(aq)} \qquad \text{Eq. 5.1}$$

$$HSiO_{3\,(aq)}^- + Ca^{2+}_{(aq)} + H_2O \rightarrow C\text{-}S\text{-}H_{gel} \qquad \text{Eq. 5.2}$$

Where aluminium (e.g., from primary mineral dissolution) and potassium (e.g. dissolved in cement leachate) are present, secondary aluminium and potassium bearing C-S-H (C-(A)-(K)-S-H) phases have also been identified (e.g. Braney et al., 1993; Savage et al., 1992). Studies of clay alteration (e.g. bentonite) at high pH found the formation of a number of Na/K/Ca bearing silicate phases including zeolites (e.g. phillipsite $(K,Na,Ca)_{1\text{-}2}(Si,Al)_8O_{16}\cdot 6H_2O$, analcime $NaAlSi_2O_6\cdot H_2O$) and apophyllite ($KCa_4Si_8O_{20}(OH).8H_2O$) (Gaucher and Blanc, 2006; Ramirez, 2005). Carbonate may also be released into solution during high pH rock alteration. For example, cement pore water can promote the breakdown of dolomite ($CaMg(CO_3)_2$) according to the reaction shown in Eq. 5.3 (Poole and Sotiropoulos, 1980; Bérubé et al., 1990; Braithwaite and Heath, 2013 and

references therein) releasing carbonate to solution leading to the formation of calcium carbonate minerals e.g. calcite. However, these processes have not been studied in the context of the CDZ.

$$MgCa(CO_3)_2 + 2OH^- \rightarrow Mg(OH)_2 + CaCO_3 + CO_3^{2-}{}_{(aq)} \qquad \text{Eq. 5.3}$$

Generally, experimental studies have limited timescales, with few longer than 1-2 years (e.g. a 540 day experiment is the longest study reviewed by Gaucher and Blanc, 2006) and no longer-term experimental studies examine the stability of the secondary phases formed. However, GDFs will evolve over tens to hundreds of thousands of years. To investigate the effect of high pH alteration at timescales more comparable to GDF scenarios, natural and anthropogenic analogue sites have been studied. At natural analogue sites such as Maqarin, Jordan (Milodowski et al., 1998; Alexander, 1992; Alexander et al., 2012; Linklater, 1998; Savage, 2011) and Troodos, Cyprus (Alexander et al., 2011), alkaline groundwaters have interacted with rock at timescales extending beyond 1 million years. Whereas anthropogenic analogue sites (e.g. the Tournemire Tunnel; Tinseau, 2006; Techer et al., 2012) bridge the gap between laboratory experiments and natural analogues. A review of many such sites representing timescales of alteration from ~ 30 years to > 1 million years is provided by Savage (2011). Overall, these studies indicate that over time a variety of secondary phases can form, predominantly alkali-silica gels (e.g. C-S-H gel), which can crystallise with time to zeolites, C-S-H minerals e.g. okenite ($Ca_5Si_9O_{23}{\cdot}9H_2O$)), and feldspars. The key factors controlling which phases form are primarily solution composition (e.g. pH) and reaction time. Modelling has also been used to predict the chemical and physical evolution within the CDZ (e.g. Savage et al., 1992; Savage and Rochelle, 1993; Braney et al., 1993; Bateman et al., 1999; Pfingsten et al., 2006; Soler and Mäder, 2007; Fernandez et al., 2010; Alexander et al., 1992). These studies generally support the experimental findings that silicate mineral dissolution is followed by secondary solid phase (e.g. C-S-H) formation, with subsequent transformation of C-S-H to feldspar and zeolite over time, as found at analogue sites. However, modelling predictions are limited by the

ability to constrain which solids will form due to slow reaction rates, and a lack of reliable thermodynamic data for some phases (e.g. C-S-H gel).

The secondary solid phases produced during high pH rock alteration may affect radionuclide migration through the CDZ by changing the sorption properties of the material. A key radionuclide of concern is U(VI) which is highly mobile and hazardous over the long timescales relevant to geological disposal (NDA, 2010c). As C-S-H has been found to be the predominant secondary phase produced by high pH rock alteration and is also the most abundant phase in hardened cement paste (Taylor, 1990), which is used as an ILW wasteform, the interaction of U(VI) with these phases has been studied in some detail (Harfouche et al., 2006; Tits et al., 2011; Gaona et al., 2012; Atkins and Glasser, 1992). However, few experimental studies have looked at the interaction of U(VI) with secondary phases in-situ following high pH mineral / rock alteration and these have generally been limited to investigation after only several months of high pH reaction (e.g. Berry et al., 1999). Continued evolution of altered material over decades may further change surface properties and so affect U(VI) interactions. Therefore experimental investigation of these interactions with rock after extended periods of alteration could help fill this knowledge gap.

In this study rock alteration by high pH cement waters has been characterised in unique experiments lasting over 15 years, providing new insight into longer-term rock alteration. These experiments were originally part of the Nirex Safety Assessment Research Programme (NSARP) run by the British Geological Survey (BGS). The experiments were started in 1995 and the rock type and solution compositions used reflect the focus of NSARP at that time (Rochelle et al., 1997; details of how to access this report are provided in Supporting Information). However, as the rock contains many common rock-forming minerals the long-term alteration processes which have occurred will be representative of many rock types. The experiments investigate reaction of disaggregated dolomite-rich fracture fill rock (Borrowdale Volcanic Group (BVG), UK) with fluids representative of young (pH 13, Young Near Field Pore-water (YNFP) and intermediate (pH 12, Evolved Near Field Groundwater

(ENFG)) cement leachates. The products of these experiments (fluid and solid phases) were initially investigated up to 15 months of reaction, and a full description of the results up to that point is presented elsewhere (Rochelle et al., 1997). However, a brief summary of the results is given here. Characterisation of the rock surfaces indicated intensive dissolution of primary silicate minerals (e.g. feldspar), and the formation of poorly crystalline alkali silicate gels (i.e. C-(Al)-(K)-S-H phases), and less abundant crystalline apophyllite-KOH. Although the solid secondary phases produced in both leachates were similar, alteration was more extensive in the pH 13 YNFP system. Analysis of the pore fluids showed that the pH of the YNFP and ENFG reduced to 11.8 and 9.7 respectively. During this time the concentration of dissolved Si and Al increased significantly, due to the dissolution of the silicate minerals, and the Ca concentration decreased due to the precipitation of Ca-rich secondary phases. Overall, the reaction followed the 2-stage dissolution and precipitation process observed in other studies. However, the data indicated that the system was not at equilibrium (i.e. the concentration of ions in solution was not stable) and that further evolution of the system may occur over a longer timescale. For example, the dolomite in the rock may undergo dedolomitisation (Eq. 5.3) as observed by (Bérubé et al., 1990), leading to the release of significant amounts of carbonate and magnesium.

The aim of this study was to characterise the evolution of the BVG alteration experiments after 15 years of reaction and determine the influence of rock alteration on its reaction with U(VI). This was achieved through (1) characterisation of the changes in fluid composition and solid phase stability, crystallinity and composition between 15 months and 15 years of reaction; (2) assessment of any difference in reactions due to leachate composition; (3) comparison of U(VI) interactions with unaltered rock and rock altered at high pH for 15 years. This work will aid understanding of the longer term effects of the cement leachate on rock alteration and radionuclide transport in the CDZ.

5.3 Materials and Methodology

A full description of the experimental method is provided by Rochelle et al. (1997). A summary is given here. The rock used in the experiments was altered wallrock and dolomite-mineralised fracture fill from a hydrogeologically conductive fracture zone in the BVG, Ordovician basement volcanic rocks, UK (Milodowski et al., 1998). It was collected from the United Kingdom Nirex borehole BH14A in Cumbria, UK at 859 m depth (UK grid reference NY 0248 0569) (Rochelle et al., 1997, see Supporting Information for access details). A large (1-2 kg) sample of the rock was disaggregated and sieved. A sub-sample of the 125-250 µm size fraction was then reacted with two synthetic cement leachates. The leachates were designed (see Table 5.1) to represent a young near field pore water (YNFP; pH 13.0 at 25°C) and an evolved near field groundwater (ENFG; pH 12.2 at 25°C). The YNFP was dominated by dissolved KOH and NaOH, and saturated with respect to $Ca(OH)_2$, and the ENFG represented a synthetic deep groundwater (i.e. high salinity, Na/CaCl and $NaSO_4$ rich), saturated with respect to $Ca(OH)_2$. Each solution was prepared under a nitrogen atmosphere to minimise interactions with CO_2. For further details see Rochelle et al. 1997 in Supporting Information)

The experiments were conducted as sacrificial batch experiments in stainless steel pressure vessels lined with Teflon® (Rochelle et al., 1997). Each 150 ml vessel was loaded under a nitrogen atmosphere with 35 g of rock and 140 g of fluid. Non-reacting 'blank' experiments for both leachates were also run containing approximately 100 g of fluid in 100 ml vessels. The cells were held in an oven at 70ºC ± 0.5 ºC and shaken regularly by hand to achieve mixing.

Table 5.1: Chemical composition and pH of recipes for initial young near-field porewater (YNFP) and evolved near-field groundwater (ENFG) data to 3 significant figures (Rochelle et al., 1997). Charge is balanced by OH^-.

Chemical component	YNFP (mgl^{-1})	ENFG (mgl^{-1})
Na	1640	7730
K	3630	174
Ca	67.1	1980
Sr	-	174
Cl	-	11400
Br	-	25.2
CO_3	8.14	1.00
SO_4	-	1120
SiO_2	7.60	-
pH (at 70°C)	11.8	10.9

The experiments reported here were sampled after 15 years and 4 months in a CO_2 controlled anaerobic chamber, with a hydrogen-nitrogen atmosphere. Solution samples were filtered to < 0.2 µm with a nylon filter. A sub-sample of the solution was then immediately acidified (with 2% HNO_3) for cation analysis and another frozen (-20°C) for anion analysis. Suspended fines were collected by preserving the 0.2 µm filter papers inside a CO_2 free desiccator. The pH and Eh of the filtrates were measured at the point of sampling at room temperature within the anaerobic chamber.

Cation concentrations in the solutions were analysed by Inductively Coupled Plasma Atomic Emission Spectroscopy (ICP-AES) using a Perkin-Elmer Optima 5300 dual view system. Ion Chromatography (IC) was carried out to quantify anion concentrations using a Dionex DX120 ion exclusion system with a Dionex ICE AS1 column for carbonate analysis and a Dionex AS9-HC column for all other anions. During the 15 years of reaction some experimental fluid evaporated and the extent of this has been estimated using

the change in Cl^- concentration over time. Cl is widely used as a conservative tracer in experimental studies as it is highly soluble, generally exists in solution as a non-sorbing anion and does not readily volatilise (Nimz, 1998, Fabryka-Martin et al., 1987; Feth, 1981; Hendry et al., 2000). However, it should be noted that Cl is predominantly used as a tracer in natural waters and any potential for high pH to affect its behaviour as a conservative tracer is not fully understood. In the ENFG Cl^- concentration increased at the same rate in both the reacted and blank solutions (Table S1) and indicated approximately 34 % fluid loss. In the YNFP system it was not possible to use Cl^- due to its very low concentration. However, a similar level of evaporation was observed in all the experiments, therefore it was assumed that 34 % of the fluid was lost from every experiment and the data are corrected for this (Table S2). BET surface area analyses of the reacted rock and a sample of unaltered rock were performed using a Micromeritics Gemini V Surface Area Analyser. Quantitative analysis of the bulk mineralogy and the < 2 µm size fraction of the altered and unaltered samples were determined by powder X-ray Diffraction (XRD) using a PANalytical X'Pert Pro series diffractometer, in conjunction with Rietveld refinement (for sample preparation and data analysis details see Supporting Information).

The rock samples were imaged using an FEI QUANTA 600 environmental scanning electron microscope (ESEM) and an FEI QUANTA 650 field emission gun ESEM (FEG-ESEM) both equipped with Oxford Instruments INCA 450 energy dispersive X-ray (EDX) microanalysis systems with a 50 mm X-Max silicon drift detector (SDD). The reacted solids and the particles retained on the 0.2 µm filter papers were imaged uncoated under low vacuum. Sections through the solids were created by embedding samples in resin and polishing under ethane-2-diol. These were then viewed uncoated under low vacuum and coated with 2.5 nm of carbon under high-vacuum. Transmission electron microscopy (TEM) with EDX and selected area electron diffraction (SAED) was conducted using an FEI Tecnai TF20 FEGTEM with an Oxford Instruments INCA 350 EDX system with 80 mm X-Max SDD detector and a Gatan Orius SC600A CCD camera. Samples were prepared for TEM by

ultrasonication in ethanol to create a suspension which was then deposition onto copper TEM grids with holey carbon films.

U(VI) reaction with unaltered rock, and 15 year reacted samples from the YNFP and ENFG systems was also examined. 0.1 g of the unaltered and reacted solids were each reacted in 35 ml of a 0.1M NaCl solution (pH 7.0; representative of a simplified saline groundwater) with UO_2^{2+} spiked to a concentration of 3 mgl^{-1} under N_2. The suspensions were then agitated for 24 hours prior to sampling. The solutions were filtered to ≤ 0.45 µm (nylon filter) and acidified (1% HNO_3), while the solids were frozen moist at -80°C. The solutions were analysed by inductively coupled plasma mass spectroscopy (ICP-MS) for uranium concentration. From these data, distribution coefficient (K_d) values for U(VI) sorption (assuming no U(VI) phase precipitation) were calculated according to Eq. 5.4 (Fetter, 1999), where C* is the mass of solute sorbed per dry unit weight of solid (mg kg^{-1}) and C is the concentration of solute in solution in equilibrium with the solid (mg l^{-1})

$$C^* = K_d C \qquad \text{Eq. 5.4}$$

The speciation of U associated with the rock samples was analysed using X-ray absorption spectroscopy (XAS). For this, the moist solid samples (~ 50 % moisture) were mounted in double contained cells. Uranium L_{III}-edge XAS spectra were collected at beamline B18 of the Diamond Light Source. The data were collected in fluorescence mode using a 9 element Ge solid state detector at room temperature. Standards were collected in transmission mode for schoepite (U(VI)) and uraninite (U(IV)). The software package Athena (Ravel and Newville, 2005) was used to average multiple scans for each sample to improve the signal to noise ratio of the data and for background subtraction.

5.4 Results

5.4.1 Solution Chemistry

After 15 years, the pH values of the reacted YNFP and ENFG solutions were 9.9 and 8.8, respectively, while those of the corresponding ‘blank’ solutions

remained at 13.3 and 12.2 respectively. The Eh of the reacted YNFP and ENFG solutions were + 112 mV and + 258 mV respectively, and those of the corresponding 'blank' solutions were + 28 mV and + 90 mV respectively, indicating the experimental solutions remained oxic throughout the experiment.

The Na, K, Ca, Mg, Si, CO_3, Sr and SO_4 concentrations of all the solutions at 15 years (corrected for evaporation) are shown in Fig. 1 along with the data for 0, 4, 9 and 15 months of reaction (Rochelle et al., 1997). Al concentration was < 0.5 mgl^{-1} after 15 years of reaction and in all but the starting solutions (Rochelle et al., 1997). The concentrations of K and Na did not change between 15 months and 15 years of reaction (see Fig. 5.1 a and b). Ca, Si, Sr and SO_4 concentrations decreased in both leachates over the same period (see Fig. 5.1 c – f). However, differences in the Mg and CO_3 concentrations existed between the two leachates. After 15 years Mg concentration was elevated in the ENFG, and CO_3 concentration was elevated in the YNFP (see Fig. 1 g and h). It is highlighted that the solution concentration of Mg in the YNFP and ENFG is very low (<0.01 mgl^{-1}) up to 15 months, with the exception of the concentration in the YNFP at t=0. It should also be noted that at 9 and 15 months of reaction, an elevated concentration (approx. 40 mgl^{-1}) of CO_3 was measured in the ENFG solution blank. However, as these levels were not observed throughout the experiment, it was attributed to the ingress of atmospheric CO_2(g) during analysis.

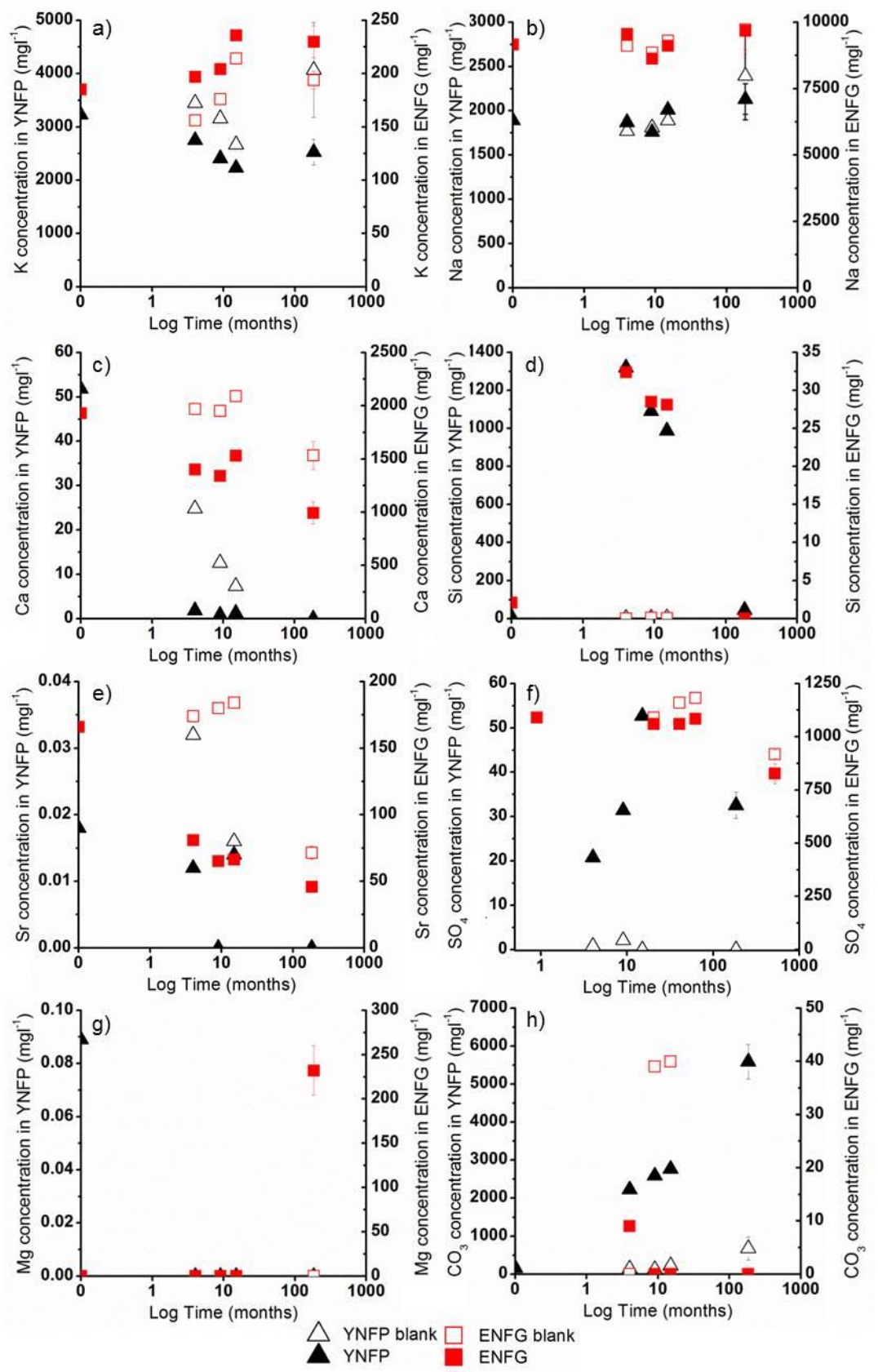

Figure 5.1: Concentrations of a) K, b) Na, c) Ca, d) Si, e) Sr, f) SO_4, g) Mg and h) CO_3 in solution in the starting solution and after 4, 9, 15 months and 15 years of reaction in YNFP and ENFG (solid triangle and square markers respectively) and in corresponding 'blank' experiments (corresponding unfilled markers).

5.4.2 Mineral Alteration

Quantitative XRD analysis of the unaltered rock showed it comprised of quartz, dolomite, mica, orthoclase feldspar, calcite, hematite and anatase (Table 5.2). Note that it was not possible to distinguish between different mica/clay phases (e.g. muscovite, biotite and illite) and they are grouped into 'mica'. XRD characterisation of the 15 year altered fracture fill identified the same bulk solids, with the addition of halite in the ENFG system, which is an artefact of sample drying. The XRD data further indicate that relative to the unaltered material, the YNFP altered rock is enriched in calcite, from 2.6 % to 6.4 %, and depleted in dolomite from 29.5 % to 23.7 % (see Table 5.2). Data for the ENFG altered rock suggest a similar but less definitive trend in this system with an increase in calcite from 2.6 % to 4.5 %, and a decrease in dolomite from 29.5 % to 28.5 %. The proportions of the other minerals remain unchanged with the exception of an increase in 'mica' in the YNFP altered material. However, it should be noted that the error on these analyses are up to ± 2.5 %, therefore some of these changes may be within analytical error.

Table 5.2: Quantitative XRD analyses of the bulk mineralogy of the rock altered in YNFP and ENFG for 15 years and a sample of unreacted rock ('mica' represents undifferentiated mica/clay species and may include muscovite, biotite, illite etc.).

Mineral	Unreacted material (weight %)	YNFP altered sample (weight %)	ENFG altered sample (weight %)
Quartz	41.3	39.1	39.3
'Mica' (muscovite/biotite /illite etc.)	12.8	15.9	13.0
Dolomite	29.5	23.7	28.5
Calcite	2.6	6.4	4.5
Orthoclase	11.9	12.9	11.9
Hematite	1.7	1.7	1.6
Anatase	< 0.5%	< 0.5%	< 0.5%
Halite	nd	nd	1.0

Further XRD characterisation of the fraction identified as 'mica' was undertaken by isolating the <2 μm size fraction from the samples. In the

unaltered rock, the clay minerals were identified as predominantly illite, with a trace amount of chlorite (Table 5.3) which confirms the findings of Rochelle et al. (1997). In the reacted YNFP and ENFG samples, XRD indicated that the predominant clay mineral was still illite and that trace amounts of chlorite were present. However, in the reacted samples, the patterns were characterised by broad, low intensity peaks centred on ~12.2 Å in the XRD pattern from the YNFP altered material and between 12.5 and 15 Å from the ENFG altered material. Following ethylene glycol-solvation a peak centred on ~17 Å appeared in the XRD patterns for both samples (Fig. B1 and B2). This suggests the presence of swelling clay, not present in the unreacted material, which is more abundant in the YNFP altered material than the ENFG material (Table 5.3). NEWMOD-modelling of the XRD data (Reynolds and Reynolds, 1996) from the YNFP altered material suggested that this interstratified illite / smectite consisted of 80% smectite, 20% illite phase. The absence of a peak at ~ 14 Å also suggests that there is no significant chlorite present in the altered samples.

Table 5.3: Summary of the clay minerals identified through XRD analysis in the <2 µm size fraction of unaltered and YNFP and ENFG altered rock after 15 years of reaction.

	% of <2 µm fraction mineral assemblage		
	Unreacted material	YNFP altered sample	ENFG altered sample
Illite	99	76	96
Chlorite	1	<1	1
Interstratified illite / smectite	nd	24	3

Characterisation of the minerals using SEM revealed that the rock grains reacted for 15 years in both the YNFP and ENFG retained their angular shape and 125-250 µm size distribution indicating that no large scale dissolution or precipitation has occurred (Fig. B3).Dolomite reacted in YNFP for 15 years showed extensive pitting, indicating dissolution of the mineral surface (Fig. 5.2a and Fig. B4). However, examination of the material in section indicated the dissolution was limited to grain surfaces. Some dissolution of dolomite

had been observed after 15 months of reaction, but to a much lesser extent than observed after 15 years (Rochelle et al., 1997). Euhedral, rhombohedral crystals of calcite, 5-10 μm in length, (Fig. 5.2b) were observed on silicate grain surfaces. This is thought to be secondary as calcite is not observed with this euhedral morphology in the early stages of the experiment (Rochelle et al., 1997).

After reaction in ENFG, grains of dolomite also exhibit surface pitting indicative of dissolution although to a much lesser extent than in the YNFP altered material (Fig. 5.2c and d). As in the YNFP system $CaCO_3$ crystals with rhombohedral morphology were observed on silicate mineral surfaces and are also identified as secondary calcite. However, in the ENFG system $CaCO_3$, identified as calcite, was also observed as poorly developed crystal coatings on dolomite grains (Fig. 5.2d). These coatings were not present on the unaltered dolomite or the material reacted for up to 15 months (Rochelle et al., 1997).

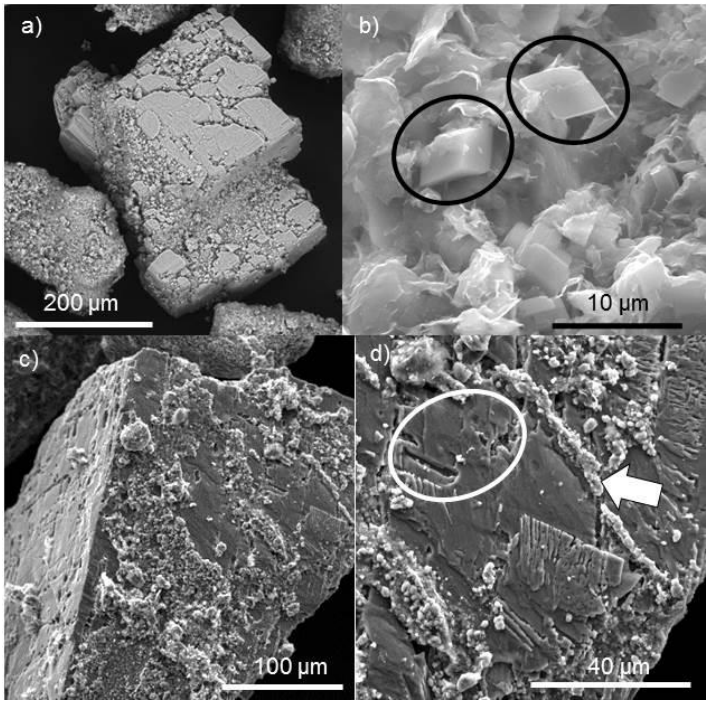

Figure 5.2: SEM images of dolomite altered for 15 years: After reaction with YNFP a) dolomite grain surface pitting, b) calcite rhombs (highlighted in black ovals) on silicate grain surface. After reaction with ENFG c) dolomite grain exhibiting minor pitting and a $CaCO_3$ coating of limited extent, d) detail of pitting on dolomite grain surface (highlighted in the white circle) with $CaCO_3$ on surface indicated by the white arrow.

The surfaces of the quartz and feldspar altered in YNFP were completely coated with secondary phases with 'sheet-like' and acicular morphologies (Fig. 5.3a). The sheets were typically several micrometers in size (see Fig. 5.3b) and the needles several micrometers in length and < 0.5 µm in width. EDX showed these particles contained Mg, Al, K and Si and, coupled with their morphology, indicated they were aluminosilicate clays, potentially the interstratified illite / smectite clay phases identified via XRD.

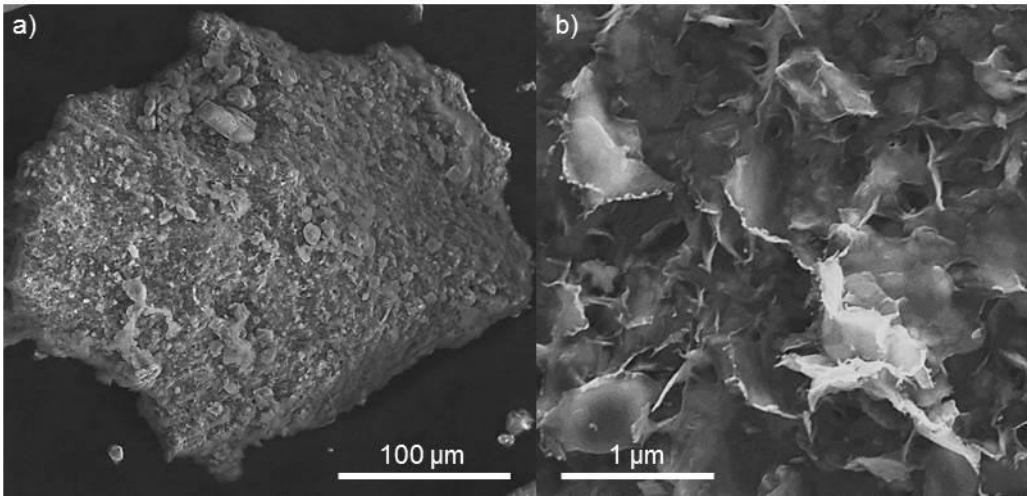

Figure 5.3: SEM images from YNFP altered material of a) a silicate mineral grain fully coated secondary phases, b) detail of silicate grain surface coating showing 'sheet-like' phase

The aluminosilicate surface coatings on the YNFP altered rock were further examined using TEM to eliminate interferences from the underlying primary mineral grains. The most abundant phase exhibited a 'sheet-like' morphology with particles ranging from 100's of nm to a few µm in size (Fig. 5.4a). Typically, this was identified via EDX as an Mg-silicate, though low levels of additional K and Fe were noted in a few examples of this phase. SAED patterns for these particles show the typical hexagonal pattern indicative of sheet silicate structured phases (Fig. 5.4a), and together with the EDX identify this phase as talc ($Mg_3Si_4O_{10}(OH)_2$). Two acicular morphology phases were also identified; (i) elongate rods approximately 100 nm in width and several µm in length, identified as a Mg-Al-silicate based on EDX analysis and exhibiting the typical hexagonal SAED pattern indicative of aluminosilicate clays (Fig. 5.4b), and; (ii) shorter rods approximately 100 nm in width and < 1 µm in length, identified by EDX as a Mg-Al-K-silicate (Fig. 5.4c). There was also a phase which consistently occurred as groups of radiating acicular

needles forming a ‘sheet-like’ morphology up to 2 µm in size (Fig. 5.4d). EDX indicated this phase was an Mg-Al-K-silicate with low and variable Fe content.

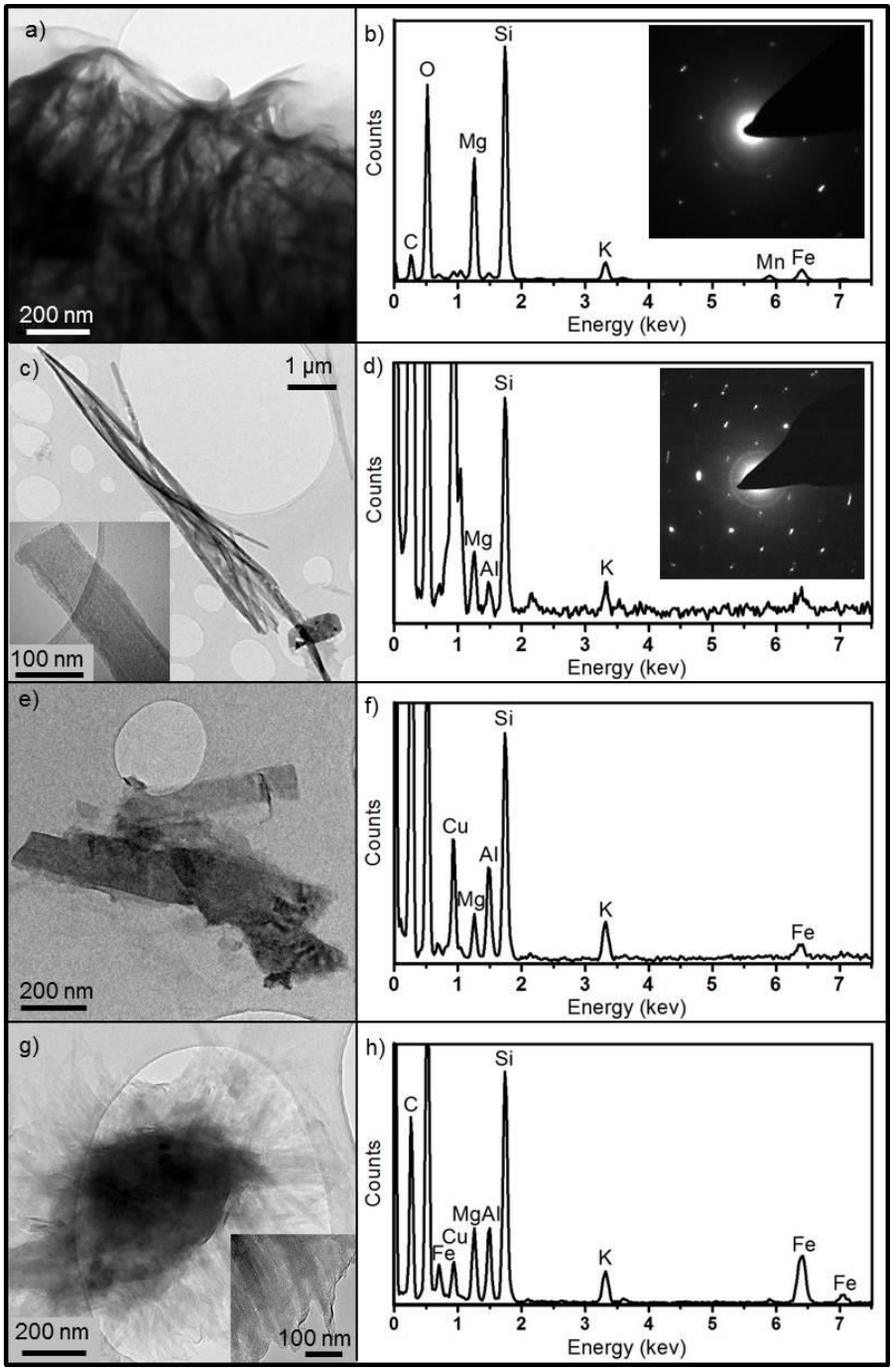

Figure 5.4: Surface phases from rock altered in YNFP for 15 years a) Mg-silicate ‘sheet-like’ phase: TEM image and b) corresponding EDX spectrum and SAED pattern; c) Mg-Al-silicate elongate rods: TEM image with inset higher resolution of rod end, d) corresponding EDX spectrum and SAED pattern; e) Mg-Al-K-silicate short rods TEM image and f) corresponding EDX spectrum; g) group of radiating rods of Mg-A-K-silicate composition TEM image with inset showing the ‘sheet-like’ nature of the group of radiating acicular needles and h) corresponding EDX spectrum.

SEM analysis of the ENFG altered rock also revealed surface coatings of aluminosilicate clay particles on the primary silicate grains, similar to those

observed in the YNFP altered system (Fig. 5.5a). These coatings comprised of particles with either 'sheet-like' or elongate needle morphologies (Fig. 5.5b) and EDX showed they contained Mg, Al, K and Si. Detailed characterisation of individual particles using TEM discriminated several different phases. The predominant phase exhibited a 'sheet-like' morphology with particles ranging from 0.1 – 1 µm in size, composed of pure Mg-silicate which were identified as talc. The elongate particles had two distinct morphologies, elongate rods (approximately 100 nm in width and several µm in length, e.g. Fig 5.5c), and short rods (approximately 100 nm in width and < 1µm in length, e.g. Fig. 5.5d) which were both identified as Mg-Al-K-silicates using EDX. The Mg, Al and K content of all the particles varied significantly, though all three elements were always present with minor Fe also present in some examples (Fig. 5.5c and d). It is believed that these Mg-(Al)-(K)-silicate phases, identified in both the YNFP and ENFG altered rock, correspond to the interstratified illite/smectite clay phase indicated in the XRD analyses, most likely a mixture of Mg-rich smectite (e.g. Mg-rich saponite-K) and interstratified illite/smectite.

Analysis of the particles suspended in the both the reacted YNFP and ENFG solutions via SEM showed that they include fragments of primary orthoclase feldspar and quartz but were predominantly made up of a phase with 'sheet-like' morphology, 10-40µm in size and of pure Mg-silicate composition (Fig. B5). This phase was identified as talc and was similar to the talc found as grain coatings in the material altered in both fluids.

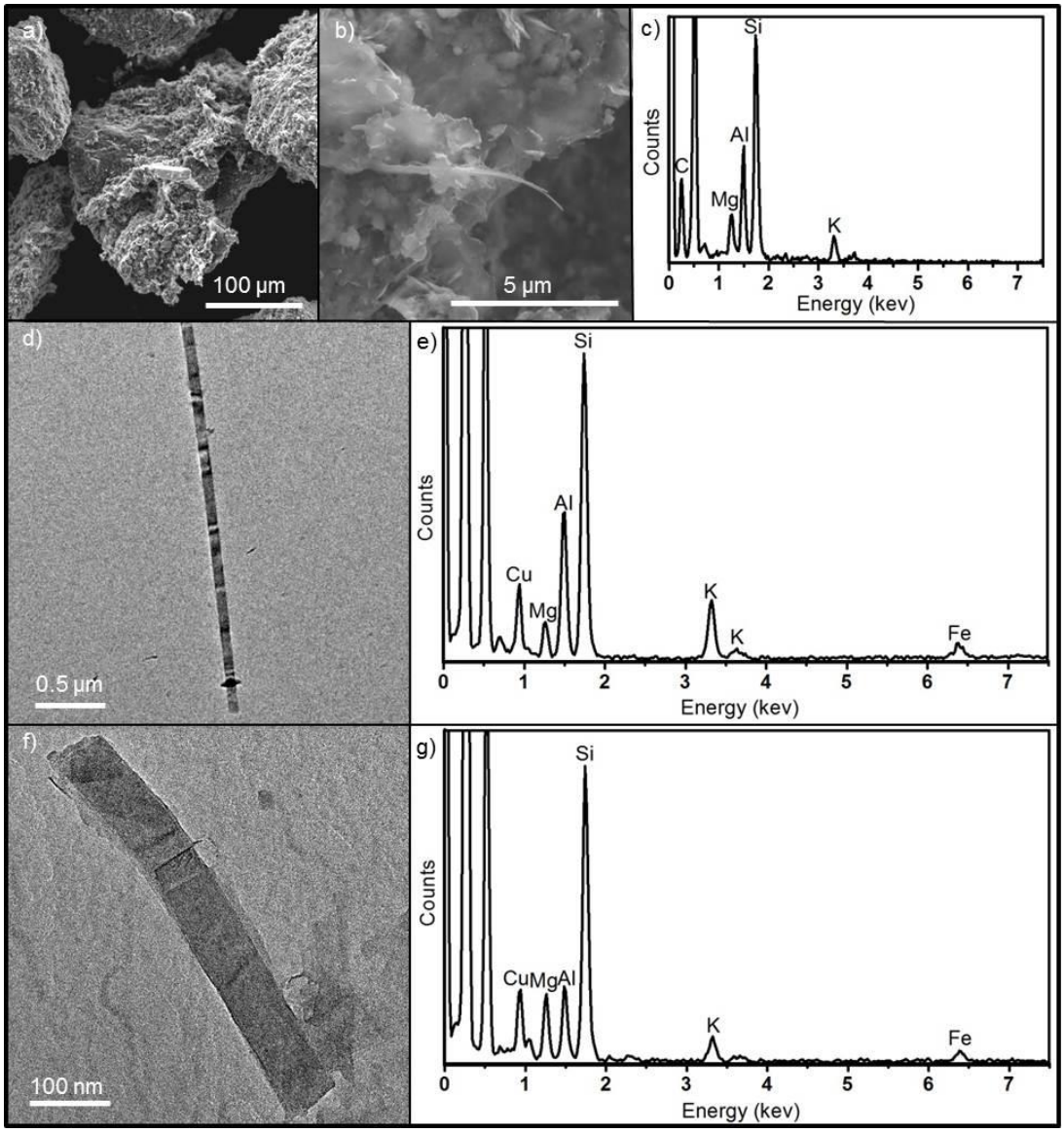

Figure 5.5: Surface phases from rock altered in ENFG: a) Silicate grain coated with secondary Mg-(Al)-(K)-silicates, b) detail of the silicate grain coating exhibiting 'sheet-like' and elongate needle morphologies c) EDX spectrum collected via SEM of coating in b, d) Mg-Al-K-silicate elongate rod, e) EDX spectrum collected via TEM correlating to phase shown in e, f) Mg-Al-K-silicate short rod and g) EDX spectrum collected via TEM correlating to phase shown in f.

In the ENFG altered rock, two additional minor secondary minerals were identified. The first occurred as groups of interlocking plates, up to 2 µm in size, containing predominantly Fe and Si hosted on silicate mineral surfaces (Fig. 5.6a). More detailed investigation of this phase using TEM confirmed this morphology and chemistry (Fig. 5.6a and b) which are indicative of the smectite mineral nontronite ($(Ca_{0.5},Na)_{0.3}Fe^{3+}{}_2\ (Si,Al)_4O_{10}(OH)_2 \cdot nH_2O$). The second phase occurred as euhedral, tabular, lath shaped crystals, 50-100 µms in size, with pitted surfaces (Fig. 5.6c). Chemically this phase was found

to contain Sr and S (Fig. 5.6d) and based on chemistry and morphology is identified as celestite ($SrSO_4$). Neither of these phases was identified in the unreacted material and nontronite was not found up to 15 months of reaction (Rochelle et al., 1997). It is believed that the strontianite observed in the ENFG reacted material up to 15 months of reaction (Rochelle et al., 1997) was in fact the celestite the identified in this study as the crystals were the same size, exhibited the same morphology and were Sr-rich. However, up to 15 months of reaction the crystals were not pitted (Rochelle et al., 1997).

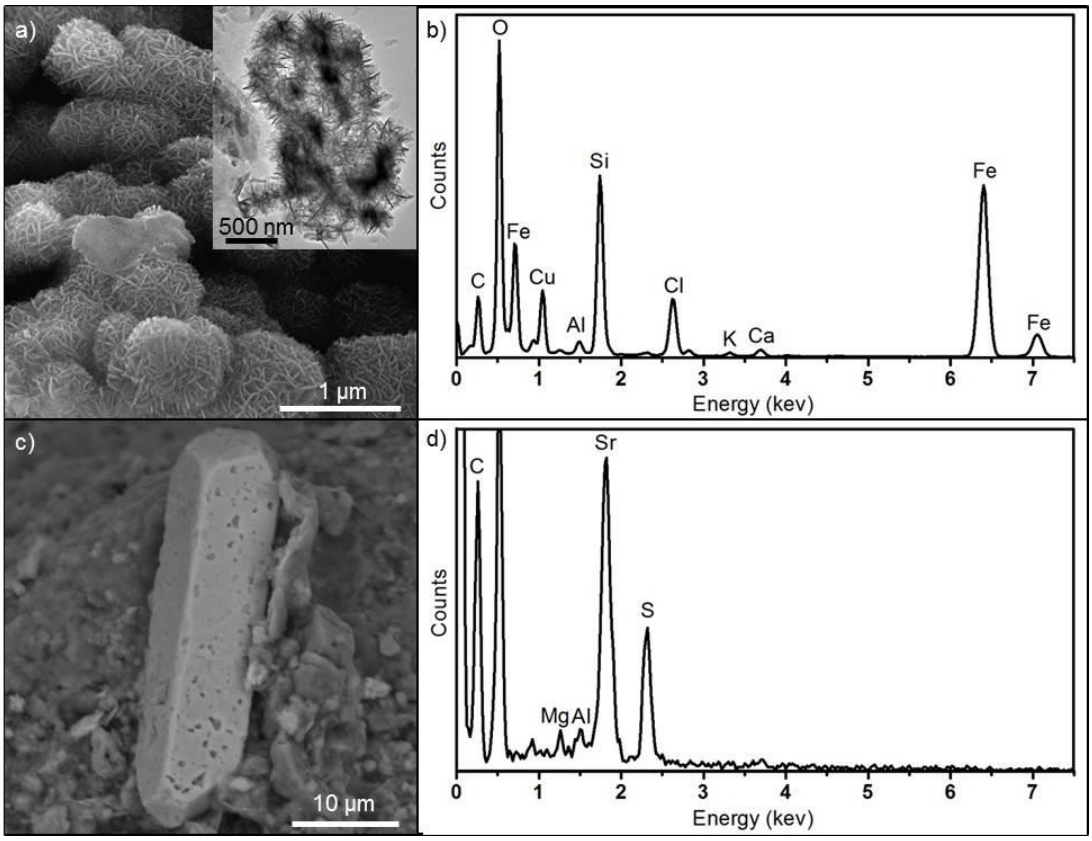

Figure 5.6: a) scanning electron micrograph of nontronite on a silicate grain surface with inset TEM image, b) EDX spectrum taken via TEM, c) scanning electron micrograph and of pitted celestite d) EDX spectrum corresponding to phase shown in c.

In summary, the altered solids from both leachate systems were found to be similar. In both systems evidence for dolomite dissolution and secondary calcite formation was observed. However, the predominant secondary phases formed in both systems were an assemblage of Mg-(Al)-(K)-silicates of varying chemical composition and morphology. These phases were identified as talc, Mg-rich smectite (e.g. Mg-rich saponite-K) and Mg-rich interlayered illite / smectite phases. As expected, the magnitude of these alteration features

were less extensive in the less aggressive ENFG system and additional minor secondary phases of nontronite and celestite were observed in this more chemically complex system. Interestingly, SEM and TEM analyses did not identify C-S-H phases or appophyllite-KOH in the materials reacted for 15 years in the YNFP or ENFG experiments although these were pervasive in the altered BVG up to 15 months of reaction (Rochelle et al., 1997).

5.4.3 U(VI) sorption

To assess whether alteration affected the absorption properties of the rock, the reaction of U(VI) with unaltered, and 15 year altered rock samples was studied. The surface areas of the unaltered and YFNP and ENFG 15 year altered rock were determined to be 5.31, 6.04 and 4.93 m^2g^{-1} (±3%), respectively, and indicated that any differences in sorption capacity between the samples was unrelated to surface area.

The concentrations of U(VI) in solution following the adsorption experiments (see Table 5.4) indicate that less than 6 % of the U(VI) was taken up by the unaltered BVG and 30 % and 40 % was taken up by ENFG and YNFP altered material, respectively.

Table 5.4: Concentration of U(VI) (to 2 s.f.) remaining in solution after 24 hours equilibration with BVG in a 0.1 M NaCl solution spiked with 3 ppm U(VI), the percentage of U(VI) adsorbed (to 2 significant figures) and the corresponding distribution coefficient (Kd) values.

	Unaltered	Altered in YNFP	Altered in ENFG
U(VI) in solution (mgl^{-1})	2.8 ± 0.06[a]	1.8 ± 0.04[a]	2.1 ± 0.06[a]
% U(VI) adsorbed	6.7	40	30
Kd (lkg^{-1})	714	6670	4290

[a] Error is 1 standard deviation from the mean (triplicate analyses).

The calculated *Kd* values for both 15 years reacted rock samples are an order of magnitude greater than the unaltered material (Table 5.4). Assuming no U(VI) phases have precipitated (no evidence for discrete U(VI) minerals was observed), this indicated that the secondary phases or altered primary mineral surfaces have a higher sorption capacity for U(VI) than the unaltered rock. Interestingly, the *Kd* of the YNFP altered system was modestly elevated compared to that of the ENFG altered system, suggesting greater U(VI)

retention on this sample. This indicates that the secondary phases / altered surfaces created during alteration are key to U(VI) adsorption and that the extent of alteration directly correlates with U(VI) uptake.

Comparison of the size, shape and positions of the peaks in the uranium X-ray absorption near edge spectroscopy (XANES) spectra from the sample with those from the standards indicated that the U(VI) sorbed to the rock samples has the same local bonding environment as U(VI) in schoepite (Fig. 7). This indicates that the uranium is present as U(VI) coordinated by six oxygen atoms, two axial oxygen atoms at ~ 1.8 Å and four equatorial oxygen atoms at ~ 2.4 Å, in a standard uranyl geometry (Grenthe et al., 2008; Burns et al., 1997). These XANES spectra and U speciation are consistent with other studies of U(VI) adsorption at neutral pH to a range of mineral phases e.g. clay (Schlegel & Descostes, 2009) and goethite (Sherman et al., 2008) which support the conclusion that uranium was adsorbed to the surface of the rock fragments. Due to the low concentration of U(VI) associated with the samples, it was not possible to collect extended x-ray absorption fine structure (EXAFS) data of sufficent quality in the time available required for further interpretation of the U(VI) coordination environment.

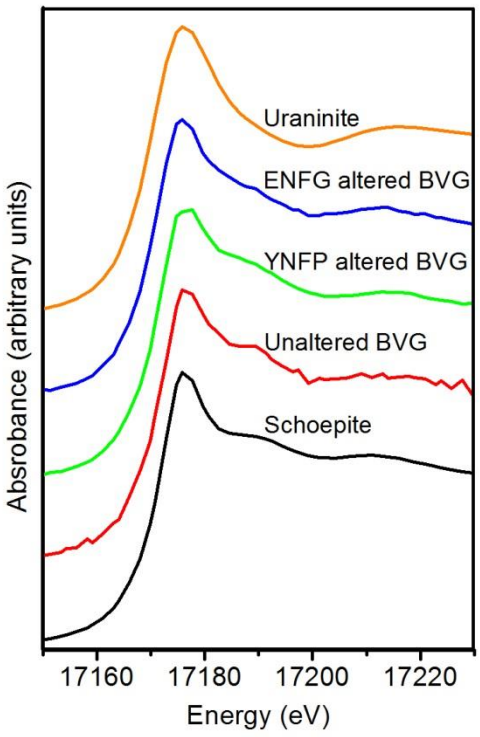

Figure 5.7: Uranium L_{III} XANES spectra of schoepite (U(VI) reference), uranium sorbed to unaltered BVG, uranium sorbed to BVG altered in YNFP, uranium sorbed to BVG altered in ENFG and uraninite (U(IV) reference)

5.5 Discussion

This investigation identified significant changes in both the mineralogy of the BVG rock and cement leachates after 15 years of reaction and demonstrated that this had an impact on radionuclide retention. However, in order to understand the evolution of these systems, it is necessary to discuss the results of this study in with those from the first 15 months of the reaction as reported by Rochelle et al. (1997). In summary, during the first 15 months of reaction poorly-ordered C-(A)-(K)-S-H phases and minor secondary appophyllite-KOH formed in both the YNFP and ENFG. However, between 15 months and 15 years of reaction the solution composition of both the YNFP and ENFG changed significantly and a different secondary mineral assemblage stabilised. This demonstrated that continued chemical and mineralogical evolution occurred and indicated a change in the reaction processes in the system. Importantly, between 15 months and 15 years, two interconnected reactions occurred: firstly, dedolomitisation; and secondly, the transformation of C-(A)-(K)-S-H and illite to Mg-bearing aluminosilicate clays. These processes are discussed in detail below.

5.5.1 Dedolomitisation

Electron microscopy and quantitative XRD show the dissolution of dolomite and formation of secondary calcite, providing evidence that dedolomitisation occurred (Eq 3). In addition, changes in solution compositions were indicative of dedolomitisation. In the YNFP carbonate concentration increased from 166 mgl^{-1} in the original solution to 5070 mgl^{-1} after 15 years of reaction (Fig. 5.1h). The gradual increase in CO_3 concentration throughout the experiment (Fig. 5.1h) is attributed to dedolomitisation, and may correlate with the minor amount of dolomite dissolution observed at the beginning of the experiment (Rochelle et al., 1997). The same increase in carbonate concentration was not observed in the ENFG system (Fig. 5.1f). However, as the concentration of Ca^{2+} in the ENFG is high, any CO_3 released through dedolomitisation would

rapidly form $CaCO_3$. Dedolomitisation would also release significant amounts of Mg^{2+}. Evidence for this is observed in the ENFG system ($[Mg^{2+}] > 200$ ppm at 15 years), but the concentration of Mg^{2+} in the YNFP remains low, < 1 mgl^{-1} throughout the experiment. This is attributed to either the low solubility of Mg^{2+} in highly alkaline solutions (Baes and Mesmer, 1976) and / or the rapid uptake of Mg^{2+} into secondary clay phase formation (see section 5.2).

The dedolomitisation reaction consumes hydroxyl ions (Eq. 5.3) and is therefore favoured at high pH (Min and Mingshu, 1993). However, as only minor dedolomitisation was observed at high pH up to 15 months we can say that the rate of this reaction was restricted in the systems studied. This highlights the importance of longer term (> 10 years) experimental studies to fully resolve the chemical and mineralogical reactions occurring in the CDZ. Thermodynamic predictions suggest that dedolomitisation would not occur below pH 11 (Min and Mingshu, 1993). As pH had decreased below 10 in the ENFG by 15 months of reaction (Rochelle et al., 1997) dedolomitisation would likely be restricted during the latter stage of the experiment. However, a high Ca^{2+} concentration, as found in both leachates, has been shown to promote dedolomitisation at lower pH, for example at cement-dolomite aggregate interfaces in concrete (Min and Mingshu, 1993). The enhancement of dedolomitisation occurs as Ca^{2+} reacts with aqueous CO_3^{2-} released in dedolomitisation to form $CaCO_3$ effectively removing CO_3^{2-} from solution and so driving the dedolomitisation reaction. Accordingly, the occurrence of dedolomitisation in the latter stage of this experiment is attributed to the presence of aqueous Ca^{2+} in the cement leachates. This suggests that this reaction will always be favoured in the CDZ.

5.5.2 Mg-silicate formation

Examination of the reacted fracture fill showed that after 15 years, in both leachate systems, grains were coated with secondary Mg-(Al)-(K)-silicate minerals, most likely a mixture of talc, smectite (Mg-rich saponite-K) and interstratified illite / smectite. Similar Mg-rich solid phases have been observed previously as minor components in high pH clay alteration experiments / analogues. For example, saponite was recognised as an

alteration product of bentonite by Cuevas (2004), secondary Mg-enriched mineral phases have been observed at the Tournemire analogue site (Tinseau et al., 2006; Techer et al., 2012) and palygorskite was identified as an Mg-rich alteration product of bentonite by high pH groundwaters in the Troodos natural analogue site (Alexander et al, 2012). The formation of these phases in these high pH conditions is not unexpected as they are commonly associated with alkaline, saline lake environments (Yeniyol, 2007; Yeniyol, 2012; Hojati et al., 2010; Akbulut and Kadir, 2003) where they form from post-sedimentary alteration of soils and rocks in high pH fluids in the presence of dolomitic material (Derkowski et al., 2013; Xie et al., 2013; Schwarzenbach et al., 2013; Birsoy, 2002). Their formation has also been identified in cement-aggregate systems where dedolomitisation in the presence of $Ca(OH)_2$ and amorphous silica resulted in the formation of a mixed calcium-magnesium silica gel (Galí et al., 2001).

The presence of secondary Mg-bearing phases provides further evidence of dedolomitisation as dolomite is the major source of Mg^{2+} in the rock. However, dedolomitisation generally results in the production of brucite ($Mg(OH_2)$ (see Eq. 5.3), which was initially found as a minor reaction product up to 15 months of reaction, but was not identified after 15 years. We suggest that this is due to the preferential reaction of the released Mg^{2+} to form the secondary Mg-(Al)-(K)-silicates. This has been observed in high pH cement systems where the presence of aqueous Mg and Si results in the formation of hydrated magnesium silicates such as talc-serpentine group minerals (Glasser, 2001; Eglinton, 2006). We propose that two independent reaction pathways result in the assemblage of secondary solid phases observed. Firstly, the reaction of Mg^{2+} released by dedolomitisation with aqueous silica to form the pure Mg-silicate, talc, by direct precipitation, as shown in Eq. 5.5.

$$3Mg^{2+} + 4H_3SiO_4^- + 2OH^- \Rightarrow Mg_3Si_4O_{10}(OH)_2 + 6H_2O \qquad \text{Eq. 5.5}$$

This is evidenced by the decrease in aqueous Si concentration in solution between 15 months and 15 years of reaction in both the YNFP and ENFG fluids (see Fig. 5.1d), and the occurrence of talc in suspension which is indicative of formation through direct precipitation from solution. Secondly, the

reaction of Mg^{2+} with primary illite and early formed C-(A)-(K)-S-H leading to transformation to Mg-(Al)-(K)-silicates. The transformation of illite to smectite (i.e. Mg-rich saponite-K) is likely to occur via an interstratified illite/smectite clay. Such interstratified clays are known to form as intermediate phases during the transformation of clay minerals (Cuadros et al., 2010). In this study the high pH and Mg^{2+} concentrations may have led to the transformation of illite either via cation exchange reactions and/or dissolution and precipitation. In addition, the absence of any C-(A)-(K)-S-H after 15 months of reaction shows that these phases have also either dissolved or transformed during the latter stages of the experiment. The transformation of C-S-H as a result of dedolomitisation has been suggested in numerical simulations of cement-aggregate systems; the release of CO_3^{2-} from dolomite results in calcite precipitation at the expense of the Ca content of C-S-H, and Mg^{2+} substitutes into the C-S-H structure eventually forming Mg-silicates (Galí et al., 2001). We proposed that this process is responsible for the destabilisation of the C-(A)-(K)-S-H formed in the early months of this experiment, and further promoted the dedolomitisation reaction by removing CO_3^{2-} from solution.

5.5.3 YNFP and ENFG comparison

Qualitatively, the degree of primary mineral dissolution and secondary phase formation appears greater in the YNFP. This would be expected due to the YNFP's more aggressive, higher pH. However, despite the difference in solution composition, no significant difference was found in the assemblage of alteration phases produced in the two cement waters or in the surface area of the two samples. This indicates that broadly similar reaction processes have occurred in both systems, with the extent of alteration directly related to solution pH. In a real repository environment i.e. an open system, there would be a constant replenishment of cement pore water into the geosphere, therefore the observed decreases in pH and changes in solution composition would not occur to the same extent within the CDZ. This would increase the overall rate of the alkaline alteration reactions, but would be unlikely to significantly change which reactions occur or the products formed. Two minor additional secondary phases, celestite and nontronite, were however

identified in the ENFG system. Celestite precipitated from solution during the first 15 months of reaction (Rochelle et al., 1997) but surface pitting after 15 years indicated re-dissolution of this phase. As Sr^{2+} is known to substitute into calcite (Tesoriero and Pankow, 1996; Lorens, 1981; Pingitore and Eastman, 1986), and as calcite formed between 15 months and 15 years of reaction, it is proposed that Sr^{2+} substitution into calcite has driven celestite dissolution. Nontronite was not identified up to 15 months of reaction and Fe concentration in solution was generally below detection limits throughout the experiment as would be expected at highly alkaline pH. However, a significant proportion of the primary dolomite in the fracture fill is known to be ferroan (Rochelle et al., 1997). Therefore the occurrence of nontronite after 15 years of reaction is attributed to the reaction of Fe released from ferroan dolomite with dissolved silica via a similar mechanism to that which formed the secondary Mg-bearing aluminosilicate phases.

5.5.4 Geochemical modelling

Geochemical speciation and reaction-path modelling (PHREEQC, Parkhurst and Appelo, 2010) has been used to investigate the potential for dedolomitisation to produce the observed formation of Mg-(Al)-(K)-silicate phases in the experiments observed between 15 months and 15 years of reaction. Firstly, saturation indices (SI) of mineral phases were calculated for the YNFP and ENFG aqueous compositions at 70°C at 15 years using the Lawrence Livermore National Laboratory (LLNL) database, see Table B2 for aqueous composition considered and Table B3 for calculated saturation indices of oversaturated silicate and carbonate phases. In both YNFP and ENFG disordered dolomite is undersaturated, consistent with the observed dolomite dissolution. More crystalline forms of dolomite are oversaturated in both solutions. Calcite is oversaturated in YNFP consistent with its precipitation, but it is undersaturated in ENFG. It should be noted that measured carbonate concentrations considered in these calculations and hence calculated SI could be higher (more positive) than in the unopened experiment as CO_2 might have dissolved in the solutions on sampling. The

model results confirm undersaturation of dolomite and oversaturation or equilibrium with calcite in YNFP consistent with dedolomitisation.

Considering silicates, for YNFP saponite phases with exchangeable K, Na, Ca and Mg, talc, phlogopite and chrysotile are the only silicate phases in the database that are oversaturated. Reaction-path calculations showed that phlogopite followed by chrysotile were the most stable phases. However, these phases are only likely to able to crystallise at high temperatures, e.g. above 100°C. The oversaturation of saponite and talc is consistent with their observed formation in YNFP. Reaction-path calculation where talc and the saponite phases are allowed to precipitate predicted the precipitation of 2.1e-07 moles/kg water of saponite-K would form.

In the case of ENFG Al concentrations were below the detection limit (0.01 mg l^{-1}) in this speciation calculation this limiting concentration was assumed in order to consider Al containing phases. A larger number of phases are oversaturated than for YNFP, which may be a consequence of the assumed Al concentration, although several high temperature pyroxene and olivine pure Mg silicate phases are thermodynamically stable at the lower pH of ENFG. Saponite and talc phases are again oversaturated, but the SI are higher than for YNFG. Interestingly brucite ($Mg(OH)_2$) is very close to saturation in ENFG (SI -0.04). Reaction path calculations that allow saponite and talc to precipitate resulted in the formation 1.1e-06 moles/kg water of Saponite-Mg and 1.4e-05 moles/kg water of talc. These speciation and reaction-path calculations on the YNFP and ENFG solution compositions confirm the dedolomitisation reaction and the associated precipitation of the Mg silicate phases saponite and talc, which drive the reaction (Eq 5).

To further examine the controls on talc or saponite precipitation in the experiments the dedolomitisation reaction was simulated as a Reaction with PHREEQC. In this reaction dolomite was reacted with C-S-H in both YNFP and ENFG fluid compositions reported at 15 months of reaction (Rochelle et al., 1997). C-S-H is represented in the reaction model as C-S-H-gel (Reardon, 1990; Reardon, 1992) for which the thermodynamic data was added to the LLNL database (the thermodynamic data for all phases are given in

Supplementary Information). Saponite and talc phases were allowed to precipitate during the reaction. For each solution two scenarios were examined (i) where the reaction occurred in solutions with no additional source of Al and (ii) where an additional source of Al was provided by muscovite representing the 'mica' phase identified in the BVG.

In these models the extent of reaction is defined by the assumption that the reaction is driven by the rate and extent of dolomite dissolution. The difference in the weight % of dolomite in the unaltered and altered rock samples, identified by quantitative XRD (Table 2), indicates that over 15 years of reaction ~ 0.019 and ~ 0.001 moles of dolomite have dissolved in the YNFP and ENFG systems respectively. A constant rate of dedolomitisation was assumed; therefore the amount of dolomite dissolved between 15 months and 15 years can be calculated as 1.7×10^{-2} moles in the YNFP and 9.2×10^{-4} moles in the ENFG. The reaction was modelled at 70°C and in order to examine the sequence of mineral precipitation products, it was divided into 18 equal reaction-steps. At each step the system was equilibrated with all components. As C-S-H was observed up to 15 months of reaction but not after 15 years, for the purpose of the model it is necessary to assume C-S-H dissolves during this time. Since there is no quantitative data for the amount of C-S-H formed in the experiment, the quantity of C-S-H dissolving in each leachate was estimated and refined using trial and error to get good agreement between the modelling results and experimental data for pH and Ca^{2+} concentration at 15 years of reaction. As a result it is assumed 2.1×10^{-4} moles and 1.1×10^{-5} moles C-S-H dissolve in the YNFP and ENFG, respectively. The solution chemistry and mineral SI evolution over time predicted by the model are summarised in tables B4 and B5. Broadly, the modelled solution chemistry at 15 years of reaction is similar to the observed solution chemistry (same order of magnitude). However, modelled Si concentrations are higher and Mg concentrations are lower.

Throughout the modelled reaction the SI of dolomite and C-S-H are negative in both the YNFP and ENFG, in the presence and absence of a dissolving Al-bearing solid, indicating that these phases were undersaturated (the predicted

SI of all phases over time in both leachates are provided in Supplementary Information). The amount of the solid reactants and precipitated secondary solid phases predicted to form in YNFP is shown in Figure 5.8. Results for ENFG are provided in Supplementary Information.

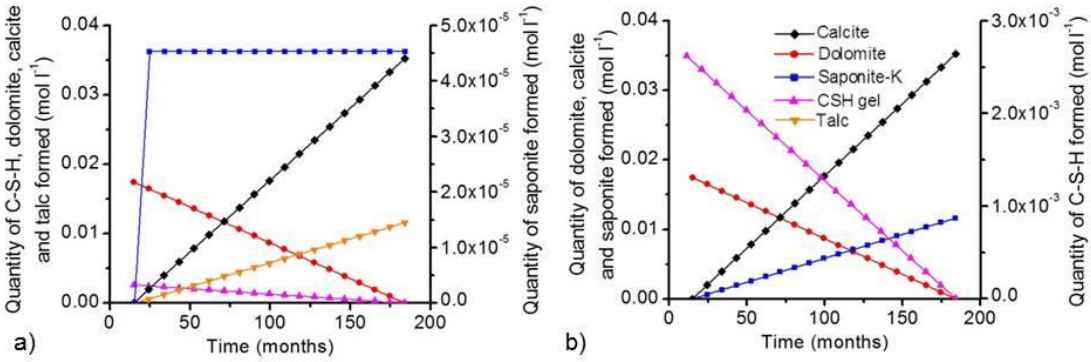

Fig 5.8: Moles of a) saponite-K, calcite, dolomite, C-S-H gel and talc in YNFP and b) saponite-K, calcite, dolomite, C-S-H gel and talc in YNFP in the presence of muscovite, predicted to form between 15 months and 15 years of reaction using computer modelling

In both leachates in the absence of a dissolving Al-bearing phase, (Fig. 8a) a very small amount of saponite forms initially, but talc is the main alteration product formed. In the case where muscovite is included in the model (Fig. 8b), saponite forms in preference to talc. The formation of talc where Al is limited is consistent with the observed occurrence of talc present as suspended particles in the experiment fluids. The formation of saponite associated with the presence of muscovite is consistent with the association of saponite and mixed layered illite-smectite with the BVG rock which provides a source of Al to stabilise saponite in preference to talc.

Approximately the same quantity of saponite is predicted to form in both YNFP and ENFG in the absence of muscovite and results also confirm the experimental observations that calcite and talc can form in both leachate systems (Fig. 5.8a and B6). In YNFP talc is the main secondary phase predicted to form in association with a minor amount of secondary saponite (Fig. 8a) while in ENFG saponite initially precipitates followed by talc (Fig. B6). The relative amounts of saponite-K and talc that form is related to the amount of K available for saponite-K formation. Interestingly, in ENFG saponite-Ca is predicted to form rather than saponite-K attributed to the significantly higher concentration of Ca in this fluid (Table B4). The model also reproduced the

drop in pH observed in both leachate systems (Table B5). The model also allowed calculation of the stability of the various secondary phases in both leachates (phase diagrams included in Fig. B7), though it should be noted that phase stability is likely to be affected by a range of species in these complex, multicomponent systems. Overall, thermodynamic considerations show that dedolomitisation can lead to the transformation of silicate phases (i.e. C-S-H), leading to the formation of talc and saponite-K, which is in agreement with experimental observations.

5.5.5 Uranium sorption

The investigation of U(VI) sorption to the materials altered in this study indicated that, despite no significant detectable change in surface area, uranyl sorption to the BVG reacted at high pH for 15 years was greater than to unreacted BVG. This suggests alteration of the rock and the formation of secondary phases, including Mg-silicates, may increase the rock's sorption capacity for U(VI). Results also show that sorption is modestly greater to the material reacted in YNFP than to that reacted in ENFG. This supports the hypothesis that the presence of secondary phases increases the sorption capacity of the rock as secondary phases are more abundant in the YNFP system. This indicates that long term, high pH mineral reactions could be beneficial for the geosphere as a barrier to radionuclide migration and highlights the need for further study of the secondary minerals formed in this study in relation to radionuclide transport.

5.6 Summary and Conclusions

This study investigated the reaction of a fracture fill material with high pH cement leachates within 15 year laboratory experiments. As a result of the extended timescale of these experiments, two different phases of the alkaline rock alteration reaction were identified. In phase 1, a Ca-silicate dominated secondary mineral assemblage (i.e. containing C-S-H and apophyllite-KOH) stabilised as reported by Rochelle et al. (1997) (Fig. 9). Subsequently these initial phases destabilised and Mg-(Al)-(K)-silicates and calcite formed under the reaction conditions of this study (Phase 2 – Fig. 10). The evolution of the

secondary mineral assemblage is attributed to a change in the dominant reactions between the early and late stages of the experiment. Initially, the high pH of the leachates caused the dissolution of primary silicate minerals and formation of C-(A)-(K)-S-H in the Ca^{2+} rich solutions (Rochelle et al., 1997). Between 15 months and 15 years of reaction (Phase 2) significant dedolomitisation occurred and the early formed C-(A)-(K)-S-H destabilised (Fig. 5.9) which led to the formation of secondary $CaCO_3$ and Mg-(Al)-(K)-silicates.

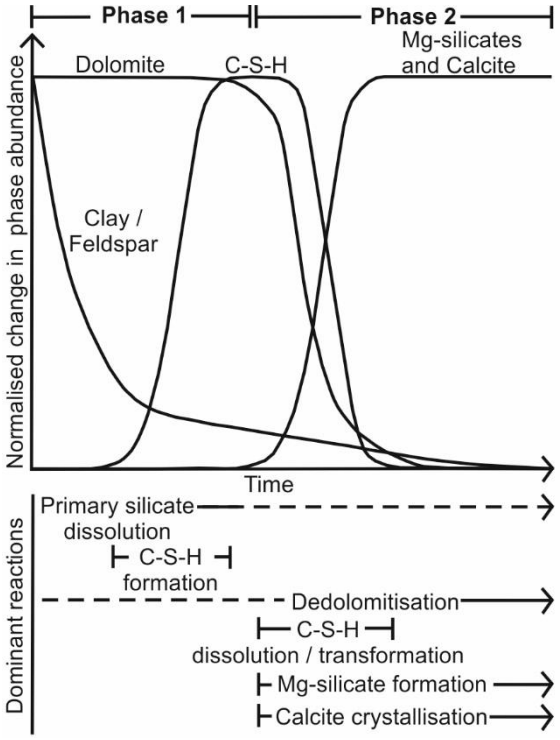

Figure 5.9: Schematic diagram describing the general evolution of reaction proposed for this experiment

Previous studies of high pH-rock alteration have identified C-(A)-(K)-S-H, feldspars and zeolites as the dominant secondary phases likely to form in a GDF environment over time (e.g. Gaucher and Blanc, 2006; Savage, 2011). The formation of Mg-(Al)-(K)-silicates has only been suggested in a few studies of CDZ-type alteration as a minor product (Cuevas, 2004; Techer, 2012) and has not been widely considered. This study has shown that, in the presence of the common rock forming mineral dolomite, these phases may form and become the dominant secondary phases in a GDF scenario. An additional implication of this finding is that other sources of Mg^{2+} may exist at a GDF site (e.g. magnox fuel cladding within the waste) which could potentially

contribute to the formation of secondary Mg-(Al)-(K)-silicates. This study also found that the secondary mineral phases resulting from high pH rock alteration may increase the rock's sorption capacity for U(VI).

At a broader level, the findings of this study illustrate that, in the CDZ around a GDF, there is potential for different mineral alteration reactions to occur over time. This may result in several different, transient mineral assemblages forming. The similar characteristics of the secondary phases produced in the two leachate systems studied here suggests that the alteration processes and resulting secondary mineral assemblages may not be significantly affected by the evolutionary stage of the cement leachate. However, the greater extent of alteration observed in the YNFP system, and the resulting increase in uranium sorption to the YNFP altered material observed, indicate that the composition of the leachate could impact radionuclide transport. Indeed, even at the relatively short timescale investigated here, the potential for significant mineralogical evolution has been demonstrated. It is also important to note that the Mg-clay mineral assemblage identified in this study cannot be shown to be a stable equilibrium assemblage, but may also be a metastable assemblage such as the C-S-H phases identified initially. The question is therefore raised as to whether further reaction may be anticipated. This work has important implications for any GDF safety case and highlights the need for longer-term experimental programmes to be considered during the implementation of geological disposal, and the need to develop the experimental-modelling interface so that predictions of CDZ evolution are robust.

References

AKBULUT, A. & KADIR, S. 2003. The geology and origin of sepiolite, palygorskite and saponite in Neogene lacustrine sediments of the Serinhisar-Acipayam Basin, Denzili, SW Turkey. *Clays and Clay Minerals.* 51. 279-292.

ALEXANDER, R. (Ed). 1992. A natural analogue study of the Maqarin hyperalkaline groundwaters. I: Source term description and

thermodynamic database testing. *Nagra Technical Report* NTB 91-10, Nagra, Wettingen, Switzerland.

ALEXANDER, W.R., DAYAL, R., EAGLESON, K., EIKENBERG, J., HAMILTON, E., LINKLATER, C.M, MCKINLEY, I.G. AND TWEED, C.J. 1992. A natural analogue of high pH cement pore waters from the Maqarin area of northern Jordan II: results of predictive geochemical calculations. *Journal of Geochemical Exploration,* 46, pp l33-146.

ALEXANDER, W.R., MILODOWSKI, A.E. & PITTY A. F. 2011. Cyprus Natural Analogue Project (CNAP) phase III final report. Posiva Working Report WR 2011-77, Posiva, Eurajoki, Finland.

ALEXANDER, W.R., MILODOWSKI, A.E., PITTY, A.F., HARDIE, S., KEMP, S. J., KORKEAKOSKI, P., RIGAS, M., RUSHTON, J. C. SELLIN, P. & TWEED, C. J. (2012). Reaction of bentonite in low-alkali cement leachates: an overview of the Cyprus Natural Analogue Project (CNAP). *Mineralogical Magazine*, 76, pp 3019-3022.

ANDRA. 2012. Low and intermediate level short-lived waste [online]. Available at: <www.andra.fr/international/pages/en/menu21/waste-management/waste-classification/short-lived-low--and-intermediate-level-waste-1609.html> [accessed 19/01/2014].

ATKINS, M. & GLASSER, F. P. 1992. Application of Portland cement-based materials to radioactive waste immobilization. *Waste Management*. 12. 105-131.

ATKINSON, A. 1985. The time dependence of pH within a repository for radioactive waste disposal. *UKAEA,* AERE-R 11777.

BAES, C. F. & MESMER, R. S. 1976. The hydrolysis of cations. John Wiley & Sons, London.

BATEMAN, K., COOMBS, P., NOY, D. J., PEARCE, J. M., WETTON, P., HAWORTH, A. & LINKLATER, C. 1999. Experimental simulation of the alkaline disturbed zone around a cementitious radioactive waste repository: numerical modelling and column experiments. *Geological Society, London, Special Publications,* 157, 183-194.

BERNER, U. R. 1992. Evolution of pore water chemistry during degradation of cement in a radioactive waste repository environment. *Waste Management,* 12, 201-219.

BERRY, J. A., BAKER, A. J., BOND K. A., COWPER, M. M., JEFFRIES, N. L. & LINKLATER, C. M. 1999. The role of sorption onto rocks of the Borrowdale Volcanic Group in providing chemical containment for a potential repository at Sellafield. In: METCALFE, R. & ROCHELLE, C. eds. 1999. Chemical Containment of Waste in the Geosphere. *Geological Society of London, Special Publication*. 157. 101-116.

BÉRUBÉ, M.-A., CHOQUETTE, M & LOCAT, J. 1990. Effects of lime on common soil and rock forming minerals. *Applied Clay Science*, 5, 145-163.

BIRSOY, R. 2002. Formation of sepiolite-palygorskite and related minerals from solution. *Clays and Clay Minerals*. 50. 736-734.

BRAITHWAITE, C. J. R. & HEATH, R. A. 2013. Alkali-carbonate reactions and 'dedolomitization' in concrete: silica, the elephant in the corner. *Quarterly Journal of Engineering Geology and Hydrogeology.* 46, p351-360.

BRANEY, M. C., HAWORTH, A., JEFFERIES, N. L. & SMITH, A. C. 1993. A study of the effects of an alkaline plume from a cementitious repository on geological materials. *Journal of Contaminant Hydrology,* 13, 379-402.

BURNS, P. C., EWING, R. C. & HAWTHORNE, F. C. 1997. The crystal chemistry of hexavalent uraniu: polyhedron geometries, bond-valence parameters, and polymerization of polyhedra. *The Canadian Mineralogist*. 35. 1551-1570.

CUADROS, J., FIORE, S. & HUERTAS, F. J. 2010. Introduction to mixed-layer clay minerals. In: FIORE, S., CUADROS, J. & HUERTAS, F. J. eds. 2010. Interstratified clay minerals: origin, characterization and geochemical significance. AIPEA Education Series, Pub no.1. Digilabs, Bari, Italy.

CUEVAS, J., 2004. Geochemical reactions in FEBEX bentonite. In: MICHAU, N. Ed. Ecoclay II: Effect of cement on clay barrier performance phase II. final report. European Commission. European contract FIKW-CT-2000-00018.

DERKOWSKI, A., BRISTOW, T. F., WAMPLER, J. M., ŚRODOŃ, J., MARYNOWSKI, L., ELLIOTT, W. C. & CHAMBERLAIN, C. P. 2013. Hydrothermal alteration of the Ediacaran Doushantuo Formation in the Yangtze Gorges area (South China). *Geochimica et Cosmochimica Acta*. 107, 279-298.

EGLINTON, M., 2006. Resistance of concrete to destructive agencies. In Hewlet, P. C. Ed. Lea's Chemistry of Cement and Concrete. 4th ed. Elsevier. 843-863.

FERNANDEZ, R., RODRÍGUEZ, M., VIGIL DE LA VILLA, R. & CUEVAS, J. 2010. Geochemical constraints on the stability of zeolites and C-S-H in the high pH reaction of bentonite. *Geochimica et Cosmochimica Acta,* 74, 890-906.

FABRYKA-MARTIN, J., DAVIS, S. N. & ELMORE, D. 1987. Applications of ^{129}I and ^{36}Cl to hydrology. Nucl. Instrum. Met. Phys. Res. B29, 361-371.

FETTER, C. W. 1999. Contaminant hydrogeology. Second edition. Prentice Hall. New Jersey, USA

FETH, J. H. 1981. Chloride in natural continental water: a review. US Geological Survey Water Supply Paper 2176. 30.

GALI, S., AYORA, C., ALFONSO, P., TAULER, E. & LABRADOR, M. 2001. Kinetics of dolomite–portlandite reaction: Application to Portland cement concrete. *Cement and Concrete Research*, 31, 933–939.

GAONA, X., KULIK, D. A., MACÉ, N & WIELAND, E. 2012. Aqueous-solid solution thermodynamic model of U(VI) uptake in C-S-H phases. *Applied Geochemistry*. 27. 81-95.

GAUCHER, E. & BLANC, P. 2006. Cement/clay interactions – A review: experiments, natural analogues, and modeling. *Waste Management,* 26, 776-788.

GLASSER, F. P. 2001. Cement in radioactive waste disposal. *Mineralogical Magazine.* 65. 621.633.

GRENTHE, I., DROŻDŻYŃSKI, J., FUJINO, K., BUCK, E. C., ALBRECHT-SCHMIDTT, T. E. & WOLF, S. F. 2008. Uranium. In: MORSS, L. R., EDELSTEIN, N. M., & FUGER, J. eds. 2008. The chemistry of the actinide and transactinide elements. 3rd Edition. Springer, Dordrecht, Netherlands.

HARFOUCHE, M., WIELAND, E., DÄHN, R., FUJITA, T., TITS, J., KUNZ, D. AND TSUKAMOTO. 2006. EXAFS study of U(VI) uptake by calcium silicate hydrates. *Journal of Colloid and Interface Science*. 303. 195-204.

HENDRY, M. J., WASSENAAR, L. I. & KOTZER, T. 2000. Chloride and chlorine isotopes (36Cl and σ37Cl) as tracers of solute migration in a thick, clay-rich aquitard system. Water Resources Research. 36. 1. 285-296.

HODGKINSON, E. S. & HUGHES, C. R. 1999. The mineralogy and geochemistry of cement/rock reactions: high-resolution studies of experimental and analogue materials. *Geological Society, London, Special Publications,* 157, 195-211.

HOJATI, S., KHADEMI, H. & CANO, A. F. 2010. Palygorskite formation under the influence of saline and alkaline groundwater in central Iranian soils. *Soil Science*. 175. 303-312.

LINKLATER, C.M. (ed). 1998. A natural analogue study of cement-buffered hyperalkaline groundwaters and their interaction with a repository host rock: Phase II. *Nirex Science Report*, S/98/003, UK Nirex Ltd., Harwell, UK.

LORENS, R. B. 1981. Sr, Cd, Mn and Co distribution coefficients in calcite as a function of calcite precipitation rate. *Geochimica et Cosmochimica Acta*. 45. 553-561.

MÄDER, U., FIERZ, T., FRIEG, B., EIKENBERG, J., RUTHI, M., ALBINSSON, Y., MORI, A., EKBERG, S. & STILLE, P. 2006. Interaction of hyperalkaline fluid with fractured rock: Field and laboratory experiments of the HPF project (Grimsel Test Site, Switzerland). *Journal of Geochemical Exploration,* 90, 68-94.

MILODOWSKI, A. E., HYSLOP, E. K., PEARCE, J. M., WETTON P. D., KEMP, S. J., LONGWORTH, G., HODGKINSON, E. & HUGHES, C. R. 1998. Mineralogy, petrology and geochemistry. In: SMELLIE, J.A.T., ed. 1998. Maqarin Natural Analogue Study: Phase III. SKB Technical Report. (TR 98-04, Vols I and II). SKB, Stockholm, Sweden.

MIN, D. & MINGSHU, T. 1993. Mechanism of dedolomitisation and expansion of dolomitic rocks. *Cement and Concrete Research*. 23. 1397-1408.

NAGRA. 2014. GEOLOGICAL REPOSITORY FOR LOW- AND INTERMEDIATE-LEVEL WASTE [ONLINE]. AVAILABLE AT: <WWW.NAGRA.CH/EN/TLSMAE.HTM> [ACCESSED 19/01/2014].

NDA. 2010a. Geological disposal steps towards implementation. NDA report NDA/RWMD/013. NDA, Harwell.

NDA. 2010b. Geological disposal: near-field evolution status report. NDA/RWMD/033.

NDA. 2010c. Geological disposal radionuclide behaviour status report. NDA report NDA/RWMD/034. NDA, Harwell.

NIMZ, G. J. 1998. Lithogenic and cosmogenic tracers in catchment hydrology. In: Kendall, C. & McDonnell. 1998. Isotope tracers in catchment hydrology. Elsevier, Oxford.

NUCLEAR WASTE MANAGEMENT ORGANISATION. 2010. DGR key features [online]. Available at: < www.nwmo.ca/dgr_keyfeatures> [accessed 19/01/2014].

PARKHURST, D.L. & APPELO, C.A.J. 2010. User's Guide to PHREEQC (Version 2)-A Computer Program for Speciation, Batch-Reaction, One-Dimensional Transport, and Inverse Geochemical Calculations, http://web.inter.nl.net/users/pyriet/bijlage%206.pdf

PFINGSTEN, W., PARIS, B., SOLER, J. & MADER, U. 2006. Tracer and reactive transport modelling of the interaction between high-pH fluid and fractured rock: Field and laboratory experiments. *Journal of Geochemical Exploration,* 90, 95-113.

PINGITORE, N. E. & EASTMAN, M. P. 1986. The coprecipitation of Sr^{2+} with calcite at 25°C and 1 atm. *Geochimica et Cosmochimica Acta.* 50, 2195-2203

POOLE, A.B. AND SOTIROPOULOS, P. 1980. Reactions between dolomitic aggregate and alkali pore fluids in concrete. Qyarterly Journal of Engineeering Geology and Hydrogeology, 13, 281-287.

RAMIREZ, S. 2005. Alteration of the Callovo-Oxfordian clay from Meuse-Haute Marne underground laboratory (France) by alkaline solution. I. A XRD and CEC study. *Applied Geochemistry,* 20, 89-99.

RAVEL, B. & NEWVILLE, M., 2005. ATHENA, ARTEMIS, HEPHAESTUS: data analysis for Xray absorption spectroscopy using IFEFFIT. J. Synchrotron Radiat. 12, 537–541.

REARDON, E.J. 1990. An ion interaction model for the determination of chemical equilibria in cement/water systems. *Cement and Concrete Research.* 20. 175-192.

REARDON, E.J. 1992. Problems and approaches to the prediction of the chemical composition in cement/water systems. *Waste Management.* 12. 221-239.

REYNOLDS, R C and REYNOLDS, R C. 1996. Description of Newmod-for-Windows™. The calculation of one-dimensional X-ray diffraction patterns of mixed layered clay minerals. R C Reynolds Jr., 8 Brook Road, Hanover, NH.

ROCHELLE, C., PEARCE, J., BATEMAN, K., COOMBS, P. & WETTON, P. 1997. The evaluation of chemical mass transfer in the disturbed zone of a deep geological disposal facility for radioactive waste: X. Interaction between synthetic cement porefluids and BVG: Observations from experiments of 4, 9 and 15 months duration. *BGS technical report* WE/97/16 Article permalink: http://nerc.worldcat.org/oclc/703969750

SAVAGE, D., BATEMAN, K., HILL, P., HUGHES, C., MILOWDOWSKI, A., PEARCE, J., RAE, M. & ROCHELLE, C. 1992. Rate and mechanism of the reaction of silicates with cement pore fluids. *Applied Clay Science,* 7, 33-45.

SAVAGE, D. & ROCHELLE, C. 1993. Modelling reactions between cement pore fluids and rock: Implications for porosity change. *Journal of Contaminant Hydrology,* 13, 365-378.

SAVAGE, D. 2011. A review of analogues of alkaline alteration with regard to long-term barrier performance. *Mineralogical Magazine*, 75, 2401-2418

SCHLEGEL, M. L. & DESCOSTES, M. 2009. Uranium uptake by hectorite and montmorillonite: a solution chemistry and polarized EXAFS study. Environmental Science and Technology. 43. 8593-8598.

SCHWARZENBACH, E. M., LANG, S. Q., FRÜH-GREEN, G. L., LILLEY, M. D., BERNASCONI, S. M. & MÉHAY, S. 2013. Sources and cycling of carbon in continental, serpentinite-hosted alkaline springs in the Voltri Massif, Italy. *Lithos.* 177. 226-244.

SHERMAN, D. M., PEACOCK, C. L. & HUBBARD, C. G. 2008. Surface complexation of U(VI) on goethite (α-FeOOH). *Geochimica et Cosmochimica Acta*. 72(2), 298-310.

SOLER, J. M. & MÄDER, U. K. 2007. Mineralogical alteration and associated permeability changes induced by a high-pH plume: Modeling of a granite core infiltration experiment. *Applied Geochemistry,* 22, 17-29.

TAYLOR, H.F.W. 1990. Cement chemistry. *Academic Press*, London.

TECHER, I., BARTIER, D., BOULVAIS, PH., TINSEAU, E., SUCHORSKI, K., CABRERA, J. & DAUZÈRES, A. 2012. Tracing interaction between natural argillites and hyper-alkaline fluids from engineered cement paste and concrete: Chemical and isotopic monitoring of a 15-years old deep-disposal analogue. *Applied Geochemistry*, 27, 1384-1402.

TESORIERO, A. J. & PANKOW, J. F. 1996. Solid solution partitioning of Sr^{2+}, Ba^{2+}, and Cd^{2+} to calcite. *Geochimica et Cosmochimica Acta.* 60, 1053-1063.

TINSEAU, E., BARTIER, D., HASSOUTA, L., DEVOL-BROWN, I. & STAMMOSE, D. 2006. Mineralogical characterization of the Tournemire Argillite after in situ interaction with concretes. *Waste Management,* 26, 789-800.

TITS, J., GEIPEL, G., MACÉ, N. EILZER, M. & WIELAND, E. 2011. Determination of uranium(VI) sorbed species in calcium silicate hydrate phases: A laser-induced luminescence spectroscopy and batch sorption study. *Journal of Colloid and Interface Science*. 359. 248-256.

XIE, Q., CHEN, T., ZHOU, H., XU, X., XU, H., JI, J., LU, H. & BALSAM, W. 2013. Mechanism of palygorskite formation in the Red Clay Formation on the Chinese Loess Plateau, Northwest China. *Geoderma*. 192. 39-49.

YENIYOL, M. 2007. Characterization of a Mg-rich and low-charge saponite from the Neogene lacustrine basin of Eskişehir, Turkey. *Clay Minerals.* 42. 541-548.

YENIYOL, M. 2012. Geology and mineralogy of a sepiolite-palygorskite occurrence from SW Eskişehir (Turkey). *Clay Minerals.* 47. 93-104.

6 Herbert's Quarry, South Wales – an anthropogenic analogue for host rock alteration at a cementitious radioactive waste repository?

6.1 Abstract

The use of cement in repositories for radioactive waste will give rise to leachates of pH > 10. As these leachates migrate into the surrounding geosphere they may alter the host rock, affecting its ability to act as a barrier to radionuclide migration. To complement the many laboratory and modelling studies of rock alteration in such fluids, natural and anthropogenic analogues have been investigated to increase understanding at timescales relevant to geodisposal, ranging up to millions of years. However, analogue systems may be affected by site specific factors and as the site histories may be poorly constrained. Therefore increasing the number of analogue sites studied is important in order to minimise uncertainty in the applicability of any results. Herbert's Quarry has been characterised and assessed in this study as a potential anthropogenic analogue. Solution sampling of streams at the site identified Ca-rich fluids, up to pH 12.0 analogous to cement leachates. However, analysis of rock and sediment samples showed extensive $CaCO_3$ precipitation in the streams and no reaction of silicate rock was found. The streamwaters were also found to be oxidising, unlike the reducing conditions expected at a repository, and maximum streamwater temperatures were 15-25°C below predicted repository temperatures. Therefore, the Herbert's Quarry site is believed to have limited applicability as an analogue in this context.

6.2 Introduction

The internationally accepted method for the disposal of higher level radioactive wastes is burial within a Geological Disposal Facility (GDF) (OECD-NEA, 2008). The use of cementitious materials is proposed in generic designs for a UK GDF for Intermediate Level Waste (ILW) as a wasteform, backfill and construction material (DEFRA, 2008; NDA, 2010b). Cement is also a proposed component in the GDF designs of other countries including

Switzerland, France and Canada (NAGRA, 2014; Andra, 2012; Nuclear Waste Management Organisation, 2010). In cementitious facilities, after groundwater resaturation, components of the cement will dissolve and form a high pH leachate. Initially the leachate will be KOH and NaOH dominated (pH ~ 13) but will evolve to a $Ca(OH)_2$ dominated composition which will fall in pH over time from ~ pH 12.5 to 10.5 (Atkinson, 1985 and Berner, 1992). However, elevated pH is expected persist in the CDZ for millions of years (Atkinson, 1985). The leachate will migrate into the geosphere in the direction of groundwater flow forming a Chemically Disturbed Zone (CDZ) in the GDF host rock where elevated pH may alter the rock and affect its ability to act as a barrier to radionuclide migration.

Many laboratory studies have been conducted to understand the rock alteration which may occur due to elevated pH and chemical perturbation in the CDZ (e.g. Gaucher and Blanc, 2006; Mäder et al., 2006; Savage and Rochelle, 1993; Hodgkinson and Hughes, 1999; Braney et al., 1993; Savage et al., 1992; Ramirez, 2005). Generally these have found that CDZ conditions would cause the dissolution of silicate minerals and precipitation of C-S-H phases. However, these studies are limited in timscale with few lasting longer than 1-2 years (e.g. 540 or 600 days (Gaucher and Blanc, 2006; Fernandez et al., 2010)) while geochemical perturbation may persist for millions of years (Atkinson, 1985) and waste may remain hazardous for 100,000 to 100,000,000 years (NDA, 2010a). To increase understanding of the potential mineral alteration processes at longer timescales, natural and anthropogenic high pH systems in which alteration analogous to that expected in the CDZ has occurred have also been studied (IAEA, 1989; Miller et al., 2000). A review of many such systems is provided by Savage (2011). These include natural analogues such as Maqarin, Jordan (Milodowski et al., 1998) where groundwater natural cements have given rise to alkaline groundwaters analogous to cement pore fluids which have interacted with surrounding rocks for over 1 million years (Savage, 2010). Studies of cements in historic structures have also allowed the interaction of cement leachates with rock to be studied over shorter timescales. For example the Tournemire tunnel, France (Tinseau, 2006; Techer et al., 2012) provides evidence of high pH

mineral alteration over ~ 15-125 years of reaction and at Hadrian's Wall, UK cement pastes exist over 1700 years old have been studied (Hodgkinson and Hughes (1999). Saline lakes, for example Searles Lake, California, are also studied as analogues for high pH (pH 7.5 – 10.5) mineral alteration representative of the later stages of cement leachate evolution (Surdam, 1977; Taylor and Surdam, 1981 in Savage 2010; Chermak 1992; Chermak 1993). In general, studies of these sites have found that high pH causes silicate mineral dissolution and the formation of secondary phases. These phases are predominantly C-S-H phases with minor occurrences of zeolites as observed in experimental studies, and have suggested that over 10s to millions of years these secondary phases may persist or evolve to K-feldspars (Savage, 2011). The findings of these studies have then been used with data from laboratory experiments to model the evolution of rock in the CDZ over timescales relevant to geological disposal and improve fundamental understanding of the processes which may occur (e.g. De Windt et al., 2004; De Windt et al., 2008; Watson et al., 2013; Savage et al., 1992; Savage and Rochelle, 1993; Braney et al., 1993; Bateman et al., 1999; Pfingsten et al., 2006; Soler and Mäder, 2007; Fernandez et al., 2010; Alexander et al., 1992; Steefel and Lichtner, 1994). However, the history of analogue systems are generally poorly constrained and they may be affected by site specific factors such as rock type and groundwater composition. Therefore increasing the number of analogue sites studied is important in order to minimise uncertainty about the alteration processes which occur at longer timescales and gain confidence in the applicability of data to CDZ scenarios (McKinley and Alexander, 1992).

To provide a good analogue of high pH mineral alteration processes, site conditions should be representative of those expected to exist at a cementitious GDF. Therefore factors that should be considered include:

- Cement leachate chemistry and pH which will be dependent on both the degradation state of the cement in the facility as highlighted above, and on local groundwater chemistry. However, cement degradation will significantly influence the pH of the leachate and whether it is

controlled by KOH and NaOH or $Ca(OH)_2$ (Atkinson, 1985 and Berner, 1992).

- Groundwater chemistry which will depend on site specific conditions. However, at the anticipated depths of GDFs, 200-1000m (NDA, 2010b), it is predicted that groundwater will be saline with 1000s mgl^{-1} Na and Cl in solution (Lagerblad and Trägårdh, 1994) and that most geological materials and groundwaters will be under reducing conditions (NDA, 2010c).
- Elevated geosphere temperature relative to ground surface which will be affected by the depth of a GDF and the local geothermal gradient. For example, for a UK facility geosphere temperatures between 40-50°C are expected (NDA, 2010b and NDA, 2010c). Temperature would also be raised by any heat generated by HLW in the case of a co-located waste facility.
- The timescale of mineral alteration at a site must also be considered when assessing its applicability as an analogue. Good analogue sites extend the timescales of laboratory experiments with reactions occurring over 10s to millions of years (Savage, 2011).
- The rock type present at a site will also affect its applicability as an analogue. Different countries are currently investigating different rock types as potential host rocks (e.g. clay in France, granite in Sweden and Finland) and many countries have yet to select any site. Generally the three generic rock types considered suitable as GDF host rocks are high strength (e.g. granite), lower strength sedimentary (e.g. clay) and evaporite rock (NDA, 2010c).

The aim of this study is to characterise a possible anthropogenic analogue site at Herbert's Quarry, South Wales, and assess its potential as an analogue for high pH rock alteration at a cementitious GDF. The Quarry is comprised of several areas of limestone working and lime kilns dated to different periods over the past 200 years. The now disused kilns were used to burn limestone to form calcium oxide (CaO). High pH streamwaters (> pH 11) have been previously identified at the site (Andrews et al., 1997) attributed to the

percolation of water through residual CaO left in the kilns following their closure and through CaO-rich spoil heaps. These streamwaters may be analogous to the cement leachates predicted form in the CDZ during the equilibration of groundwater with $Ca(OH)_2$. Therefore any alteration of the local rock caused by these fluids may by analogous to the rock alteration at a GDF.

6.3 Herbert's Quarry background

Herbert's (Foel Fawr) quarry is located on the Black Mountain, Nr Brynamman, Carmarthenshire, approximately 10 km ESE of Llandeilo (51.854915, -3.837756; Fig. 6.1). The site is within the Brecon Beacons National Park and the Fforest Fawr Geopark. It is also part of the Mynydd Du site of special scientific interest (SSSI) and the Black Mountain and Mynydd Myddfai Registered Landscape of Outstanding Historic Interest in Wales.

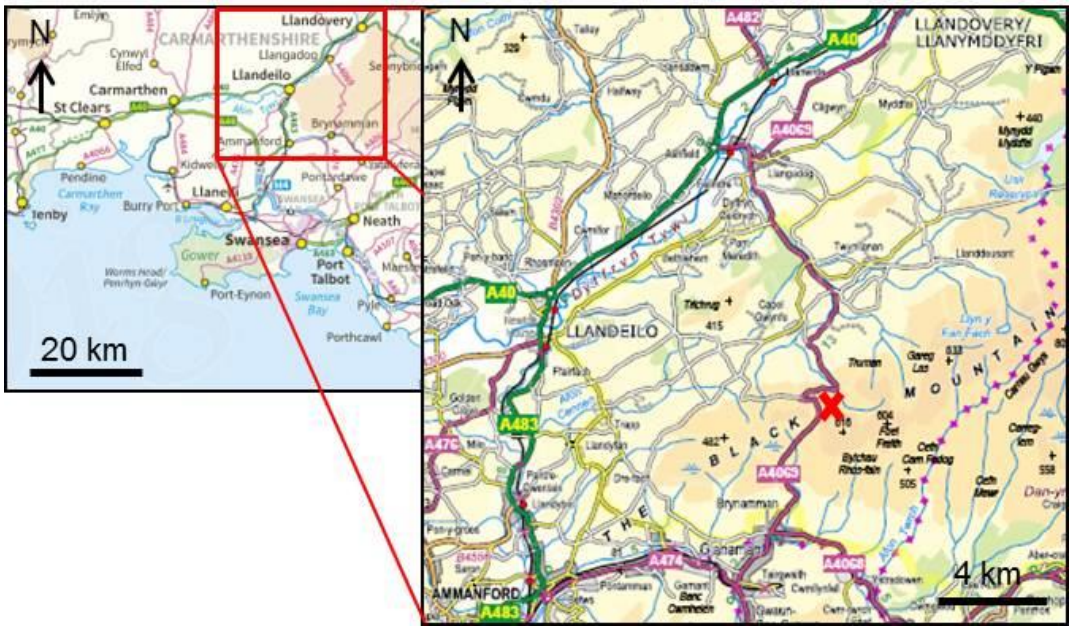

Figure 6.1: Map of the area of South Wales around Swansea indicating the location of the Herbert's Quarry Site with a red cross ©Crown Copyright/database right 2014. An Ordnance Survey/(Datacentre) supplied service.

The Herbert's quarry site is underlain by the Dowlais Limestone Formation, a member of the Pembroke Limestone Group and Carboniferous Limestone Supergroup (See Fig. 6.2). This formation is comprised of tabular, thick-bedded limestones that are mid- to dark grey in colour, with shale interbeds and some local basal sandstones (British Geological Survey, 2014). The

Dowlais Limestone Formation in underlain by the Avon Group, a limestone shale which crops out to the north of the study site (British Geological Survey, 2014). The overlying Honeycombed Sandstone Member crops out at Foel Fawr at the south of the site and, due to a N-S trending fault to the west of the site, also crops out to the west of Herbert's Quarry (British Geological Survey, 2014; See Fig. 6.2).

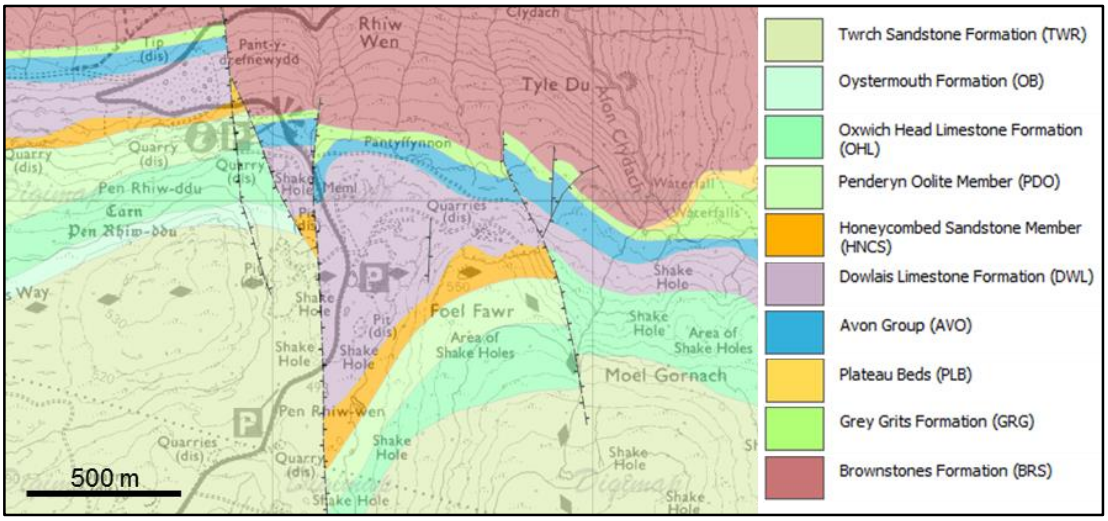

Figure 6.2: BGS 1: 50,000 geological bedrock map of the area surrounding the Herbert's Quarry site (Geological Map Data © NERC 2014)

Herbert's Quarry is an ex-limestone quarry where limestone was worked and processed to produce quicklime (calcium oxide, CaO) for over 200 years (Calch, 2014). Quicklime is an important component of cement and has also been used in the manufacture of glass and steel and a variety of other industries (Oates, 1998). The extent of the workings is approximately 0.14 km^2 in area and is comprised of several areas of lime working including areas of historic limestone quarrying, several periods of limestone kilns and areas of spoil (Fig. 3). The remains of at least 36 limekilns with associated spoil have been identified at different levels on the hillside (Calch, 2014). There are also at least five streams flowing northwards from the Herbert's Quarry site (Fig. 3).

Figure 6.3: Satellite image of the Herbert's Quarry site, Carmarthenshire (© Google Maps) with disused quarry workings and kilns highlighted by white dashed lines and high pH stream origins highlighted by white solid lines.

To produce quicklime, $CaCO_3$ is heated to the point of decomposition at which CO_2 is released and CaO remains (Eq. 6.1; Oates, 1998). It is residual CaO in the lime kilns and spoil heaps which gives rise to the high pH streamwaters found at the site as the CaO forms $Ca(OH)_2$ in aqueous solution (Eq. 6.2; Andrews et al., 1997). However, $Ca(OH)_2$ reacts with CO_2 under ambient conditions and reverts to $CaCO_3$, resulting in reduced solution pH (Eq. 6.3; Oates, 1998). Herbert's Quarry has been studied previously to examine the speleothem-like calcareous deposits which occur at the site (Andrews et al., 1997) indicating that some reversion to $CaCO_3$ has occurred, potentially minimising the extent of the high pH zone at the site. However, the same study identified streamwaters of pH >11 therefore the available CaO supply at the site must maintain high pH.

$$CaCO_3 \rightarrow CaO + CO_2 \qquad \text{Eq. 6.1}$$

$$H_2O + CaO \rightarrow Ca(OH)_2 \qquad \text{Eq. 6.2}$$

$$Ca(OH)_2 + CO_2 \rightarrow CaCO_3 + H_2O \qquad \text{Eq. 6.3}$$

Interestingly, Andrews et al. (1997) also found that the calcite deposits at the site had unusually negative isotopic compositions. This highlighted that hyperalkaline conditions in could significantly impact the isotopic composition of calcite and affect calculated palaeotemperatures. Andrews et al. (1997)

recommended that such conditions should be avoided for Holocene palaeoclimate reconstructions.

6.4 Methodology

Surveys of two streams emanating from different areas of lime working were undertaken. Sampling was conducted in summer 2013 and it was noted that the streams were at low flow. Several dry stream beds were also apparent indicating that a number of smaller ephemeral streams exist during wetter periods. Stream 1 originated at (approx. grid reference 273829,218971) the base of a spoil heap in an area known as the 'Pantyffynon limekilns' depicted as disused on the 1887 OS map (Schlee, personal communication 2014) predominantly composed of angular fragments of limestone of varying size up to ~ 20 cm (Fig. 6.4a and b). Over the course of the stream three minor streams, also originating in spoil heaps, joined the main stream. Stream 2 originated in a tailings pile overgrown with vegetation to the west of the site (approx. 273459, 219133) in an area of lime working marked as in use as the Craig y nos and blaen y gawr limekilns on the 1887 OS map (Fig. 6.4c and d).

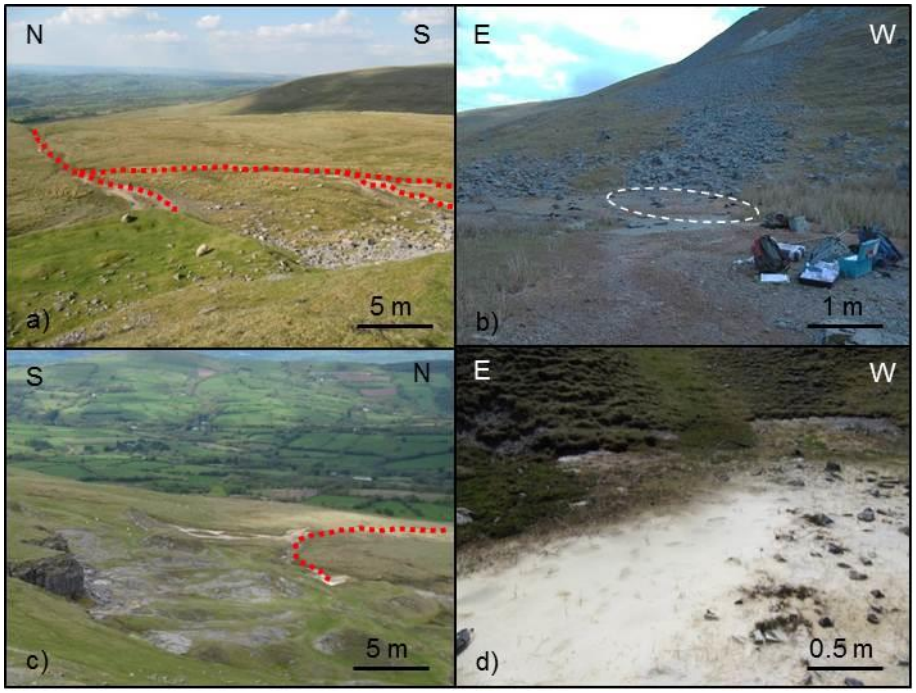

Figure 6.4: a) stream 1 with course highlighted in red, b) origin of stream 1, c) stream 2 with course highlighted in red and d) origin of steam 2.

Along each stream measurements of pH, Eh, temperature, total dissolved solids (TDS), and conductivity were taken using a MyronL Ultrameter 6PIIfc multimeter and a Hanna Multiparameter meter, the results of which have been averaged. Salinity and dissolved oxygen were also measured in-situ using the Hanna Multiparameter meter and the GPS coordinates of each site recorded using a Garmin, hand-held GPS unit.

At selected locations solution samples were also taken. At each location, a 2 ml sample was taken for analysis by Ion Chromatography (IC) in cryo-tubes with no headspace to minimise CO_2 ingress. On return to the laboratory, they were then filtered through 0.45 µm syringe filters inside a H_2/N_2 anaerobic chamber with CO_2 concentration minimised and re-sealed in fresh cryo-tubes. These samples were analysed using a Dionex DX120 ion exclusion system with a Dionex ICE AS1 column for carbonate analysis and a Dionex AS9-HC column for all other anions (Cl^-, NO_3^-, SO_4^{2-} and PO_4^{3-}). An additional 10 ml sample was taken at each location for analysis by ICP-AES and ICP-MS to quantify cation concentrations in solution. These samples were filtered through 0.45 µm syringe filters and 1 ml of 4 N nitric acid added in the field. All fluid samples were transported back to the laboratory on ice where they were diluted to a 1 in 10 dilution in 2% nitric acid. ICP-AES was then used to determine cation concentrations in the solutions (Ca, Fe, Mn, Mg, S, Al, Si, Mg, K, Na, Sr, Ba, Ti, Zn, Co, Cr, Cu, P, Li, Mo, Ni and Pb) using a Perkin-Elmer Optima 5300 dual view ICP-AES. Due to the relatively low concentrations of all cations except Ca, further analysis of cation concentrations was conducted by ICP-MS using an Agilent 7500cx with samples diluted in 2% nitric acid to a 1 in 100 dilution.

Up to 10 rock samples were taken from the stream beds at each solution sampling point where rock was present. These were transported to the laboratory in air tight polythene bags and subsequently dried in an anaerobic chamber under a N_2 atmosphere to minimise CO_2 interaction. Sediment cores approx. 5 cm in diameter by 30 cm in length were collected at stream 1 site 1 and stream 2 site 2 using a hand auger. These were also transported to the laboratory in air tight polythene bags but were then frozen at -20 °C to

minimise CO_2 interaction. In addition to the rock samples from the stream beds, blocks of siliceous rocks were identified cemented into tufa deposits formed at the base of an ephemeral stream, though at the time (height of summer) this stream was not at surface. This stream bed originated approximately 60 m west (approx. 273396, 219185) of stream 2 in workings dated to the same period. The rock samples were sectioned, resin embedded and examined under a Scanning Electron Microscope (SEM) using an FEI QUANTA 650 field emission gun ESEM (FEG-ESEM).

6.5 Results and discussion

6.5.1 Fluid Chemistry

Stream temperature varied between 15°C and 24°C during sampling due to the changing air temperature as each day progressed (Fig. 6.5 and Table 6.1). Sample Eh was consistently positive, varying between 9 and 286 mV, indicating oxic conditions at all points in both streams (Fig. 6.5 and Table 6.1). pH measurements show that the streams investigated were of alkaline pH at source with values up to pH 11.96 (Fig. 6.5 and Table 6.1). These findings are in agreement with those of Andrews et al. (1997) who showed that streamwaters of pH > 11 exist at the site. However, in this study high pH (> pH 11) streamwaters have been identified in areas of lime working dated to different periods. Variation of pH has also been more finely characterised showing that pH remained elevated in stream 2 for only approx. 20-80 m (to site 3) and that in stream 1, although pH varied significantly as minor high pH tributaries joined the main stream, pH remained elevated for approx. 180-240 m (to site 14). At the head of stream 2 it was also noted that a freshwater source (stream 2, site 1; pH 7.94) joined and mixed with the high pH stream (stream 2, site 2; pH 10.95). The difference in pH was indicated visually by the presence of white/grey suspended particles in the high pH waters (discussed further in section 6.5.2). At stream 2, site 2a pH was elevated above source pH to 11.96. This was attributed to concentration of the streamwaters by evaporation in an area of low flow.

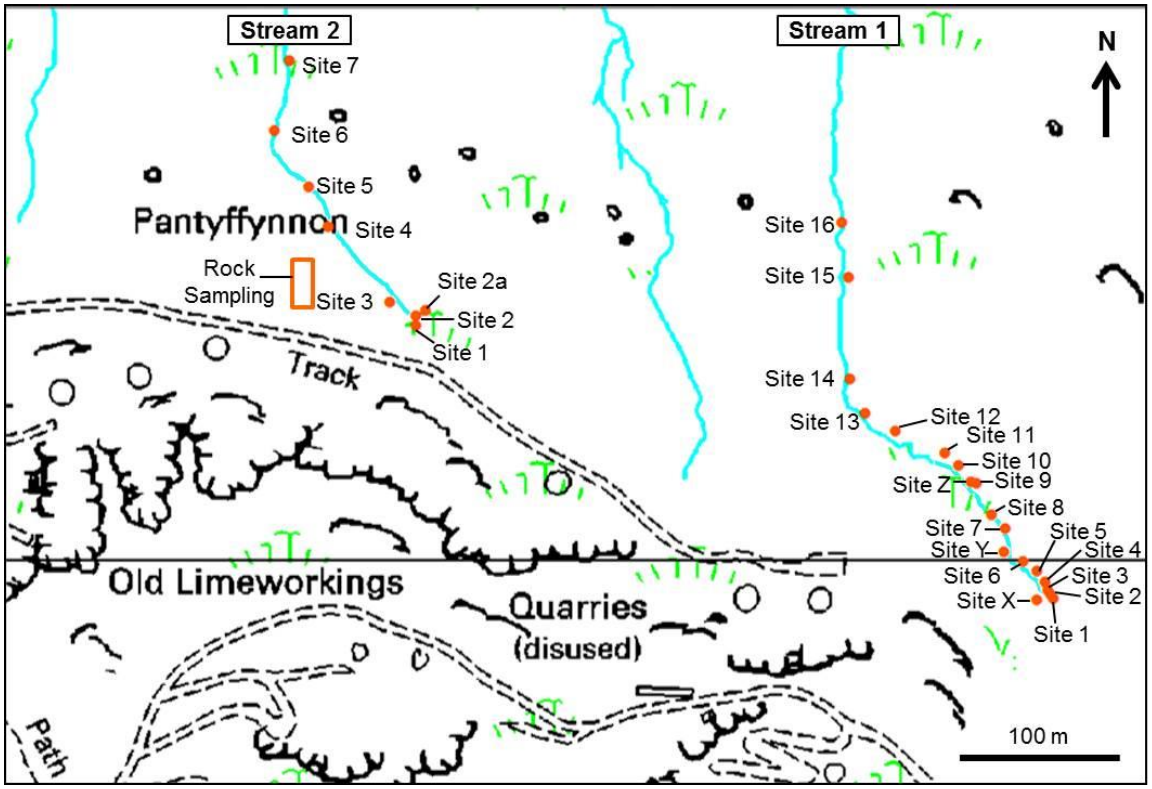

Figure 6.5: Ordnance Survey map of Herbert's Quarry with sample site locations overlain ©Crown Copyright/database right 2014. An Ordnance Survey/(Datacentre) supplied service. Stream 1 is to the east of the site, stream 2 is to the west and the rock sampling area highlighted is the area where rock that was cemented in the dry, tufa cemented stream bed.

Table 6.1: Stream 1 and 2 chemistry, pH, redox, TDS and temperature measurements (to 3 significant figures; 2 standard deviations error shown).

Sample site	pH	ORP (mv)	temp (°C)	Conductivity (µs/cm)	TDS (ppm)	Ca mgl^{-1}	Si mgl^{-1}	Na mgl^{-1}	K mgl^{-1}	Mg $µgl^{-1}$	Al $µgl^{-1}$	Fe $µgl^{-1}$	Sr $µgl^{-1}$	sulphate mgl^{-1}	nitrate mgl^{-1}	chloride mgl^{-1}	carbonate mgl^{-1}
Stream 1 - Site 1	11.8	9	15.6	1540	1078	147±3.16	4.84±2.58	4.49±0.02	7.93±0.09	36.7±3.90	664±11.84	19.3±2/09	176±0.73	13.3	2.97	30.1	n.a.
Stream 1 - Site 2	11.8	107	16.8	1590	1461.5	152±0.67	4.13±0.08	4.03±0.03	3.50±0.01	35.5±0.25	655±7.36	9.00±0.38	172±1.58	12.1	2.53	7.66	2.51
Stream 1 - Site 3	11.7	65	22.2	1300	770.75	132	4.43	3.69	2.03	37.4	699	19.3	169	12.6	2.15	5.37	26.9
Stream 1 - Site 4	8.51	208	21.9	115	28.855												
Stream 1 - Site X	8.40	193	15.5	211	133.15	47.3	3.08	3.04	0.59	941	308	7.86	84.4	4.93	1.82	4.99	134
Stream 1 - Site 5	10.7	227	15.8	344	199.4	21.4±0.68	5.16±2.82	3.81±0.08	1.59±0.01	538±2.25	390±4.37	11.5±0.38	104±0.61	9.53	2.29	5.34	31.4
Stream 1 - Site 6	8.72	209	18.9	198	120.2												
Stream 1 - Site Y	11.3	95	17.6	724	432.25												
Stream 1 - Site 7	9.68	138	16.3	173	99.2	38.7	7.84	3.92	1.60	566	209	11.4	86.6	7.99	1.66	4.87	95.0
Stream 1 - Site 8	11.2	103	19.9	439	259.65												
Stream 1 - Site 9	9.19	133	20.4	189	106.8												
Stream 1 - Site Z	11.7	63	16.0	1220	741.8												
Stream 1 - Site 10	11.4	63	19.7	579	339.15	69.5±4.67	8.66±0.77	3.47±0.14	1.11±0.01	174±7.55	348±7.43	41.2±1.37	106±2.93	11.2	2.28	5.02	71.2
Stream 1 - Site 11	10.7	83	20.7	223	127.1												
Stream 1 - Site 12	9.99	105	20.5	151	85.345												
Stream 1 - Site 13	9.56	111	19.3	157	89.35												
Stream 1 - Site 14	9.31	114	20.3	162	92												
Stream 1 - Site 15	8.29	129	18.0	199	113.4	42.2	6.59	3.85	1.41	606	169	28.2	81.2	7.10	0.65	4.86	123
Stream 1 - Site 16	8.21	134	16.4	196	112.55												
Stream 2 - Site 1	7.94	286	20.0	198	108.75	32.3±0.57	6.28±0.09	3.76±0.04	3.87±0.12	1120±23.67	204±6.89	34.7±18.67	73.9±0.57	9.26	0.10	8.63	116
Stream 2 - Site 2	11.0	160	23.2	391	238.7	206±2.77	6.23±0.02	3.84±0.04	2.03±0.00	51.0±1.53	462±7.34	13.9±0.24	151±2.23	13.5	0.76	5.25	26.0
Stream 2 - Site 2a	12.0	85	23.9	2210	81.105	268	5.79	3.61±0.05	1.75±0.01	49.6±1.53	181±6.35	12.3±1.07	148±3.17	20.8	1.03	5.02	22.0
Stream 2 - Site 3	9.61	163	23.0	143	1401.5	21.9	5.82	5.49	3.80	960	228	11.1	62.0	9.49	0.51	5.72	61.0
Stream 2 - Site 4	8.39	154	19.8	196	112.8	42.0	5.68	3.44	0.86	1135	124	9.38	63.5	4.46	0.72	5.58	122
Stream 2 - Site 5	8.15	274	20.4	188	108.05												
Stream 2 - Site 6	8.45	260	20.9	175	100												
Stream 2 - Site 7	8.49	211	20.3	181	103.55												

In all samples: phosphate was below detection limits, dissolved oxygen concentrations were measured at between 5 and 18 ppm, Cr, Cu, Ni, Pb and Mo below 10 ppb and Zn and Ba below 75 ppb

In-situ measurements of TDS at each sample point were found to vary with pH with values an order of magnitude greater in the highest pH areas compared to those below pH 10.5 (Fig. 6.5, Table 6.1). This mirrors a similar trend in conductivity (Fig. 6.5, Table 6.1).

The fluid chemistry of the streamwater samples show that in the highest pH samples Ca concentration was elevated up to 268.18 mgl^{-1} (Table 6.1). Concentrations of 800 mgl^{-1} are analogous to cement leachates in equilibrium with $Ca(OH)_2$ and concentrations of 80 mgl^{-1} are analogous to leachates in equilibrium with C-S-H phases (Atkinson, 1985). It was also noted that Ca concentration fell markedly from hundreds of mgl^{-1} to <50 mgl^{-1} in both streams as pH fell downstream (Fig. 6.6a). Conversely, the concentration of CO_3 in solution rose in both streams as pH fell from tens to hundreds of mgl^{-1} attributed to streamwater equilibration with atmospheric CO_2 (Fig. 6.6b). Similar trends were observed in Al and Mg concentrations. Al concentration fell with pH from several hundred of μgl^{-1} to 100-200 μgl^{-1} (Fig. 6.6c) while Mg concentration rose with falling pH from <50 μgl^{-1} to hundreds of μgl^{-1} (Fig. 6.6d). It was also noted that Si concentration was <9 mgl^{-1} in all samples with no discernible trend in concentration relative to pH.

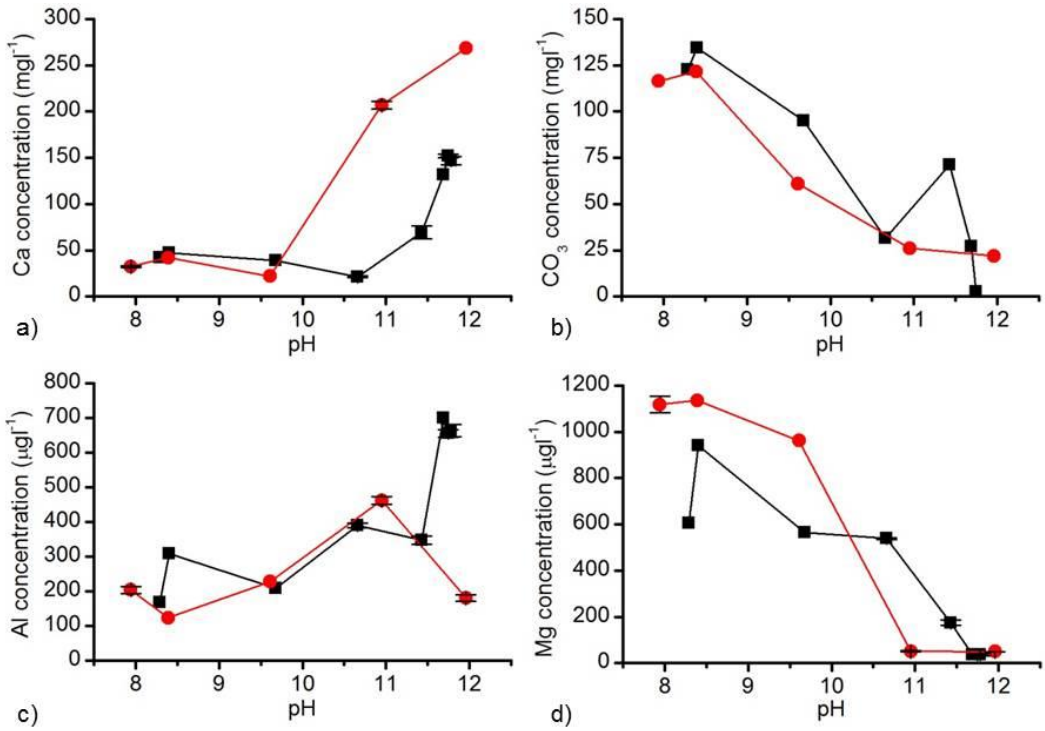

Figure 6.6: concentration of a) Ca, b) CO_3, c) Al and d) Mg in solution versus pH in stream 1 (black) and stream 2 (red).

6.5.2 Solid phase characterisation

6.5.2.1 Stream 1

For approximately the first 100 m of stream 1 the stream the bed comprised of 1-3 cm round to sub-angular cream / grey / brown ‘pebbles’ with friable surfaces (Fig. 6.7a and b). Examination of the ‘pebbles’ in section via SEM showed them to be comprised of high purity $CaCO_3$ around fossil rich limestone fragments up to 20 mm in size (Fig. 6.7c-e). The limestone fragments had jagged edges and no alteration zone was apparent indicating no significant dissolution of the primary rock surfaces. Interestingly, the $CaCO_3$ coatings appeared highly porous (Fig. 6.7c) with distinct growth layers up to 10s µms in thickness visible in many samples parallel to the underlying limestone fragment edges (Fig. 6.7e). These coatings have been interpreted as $CaCO_3$ precipitates formed directly from solution due to the equilibration of atmospheric CO_2 with Ca^{2+} in solution (Eq. 6.3) and mediated by the presence of limestone fragment surfaces. There were also minor examples of quartz particles up to 200 µms in size entrained in the $CaCO_3$ coatings (Fig. 6.7f). The surfaces of these entrained particles were also coated in $CaCO_3$ (Fig. 6.7f), again indicating the preferential precipitation of $CaCO_3$ at pre-existing mineral surfaces.

Solid samples were not taken in the lower pH region of the stream, where the stream bed was comprised of alluvial deposits, as non-hyperalkaline conditions are not analogous to the scenario considered in this study.

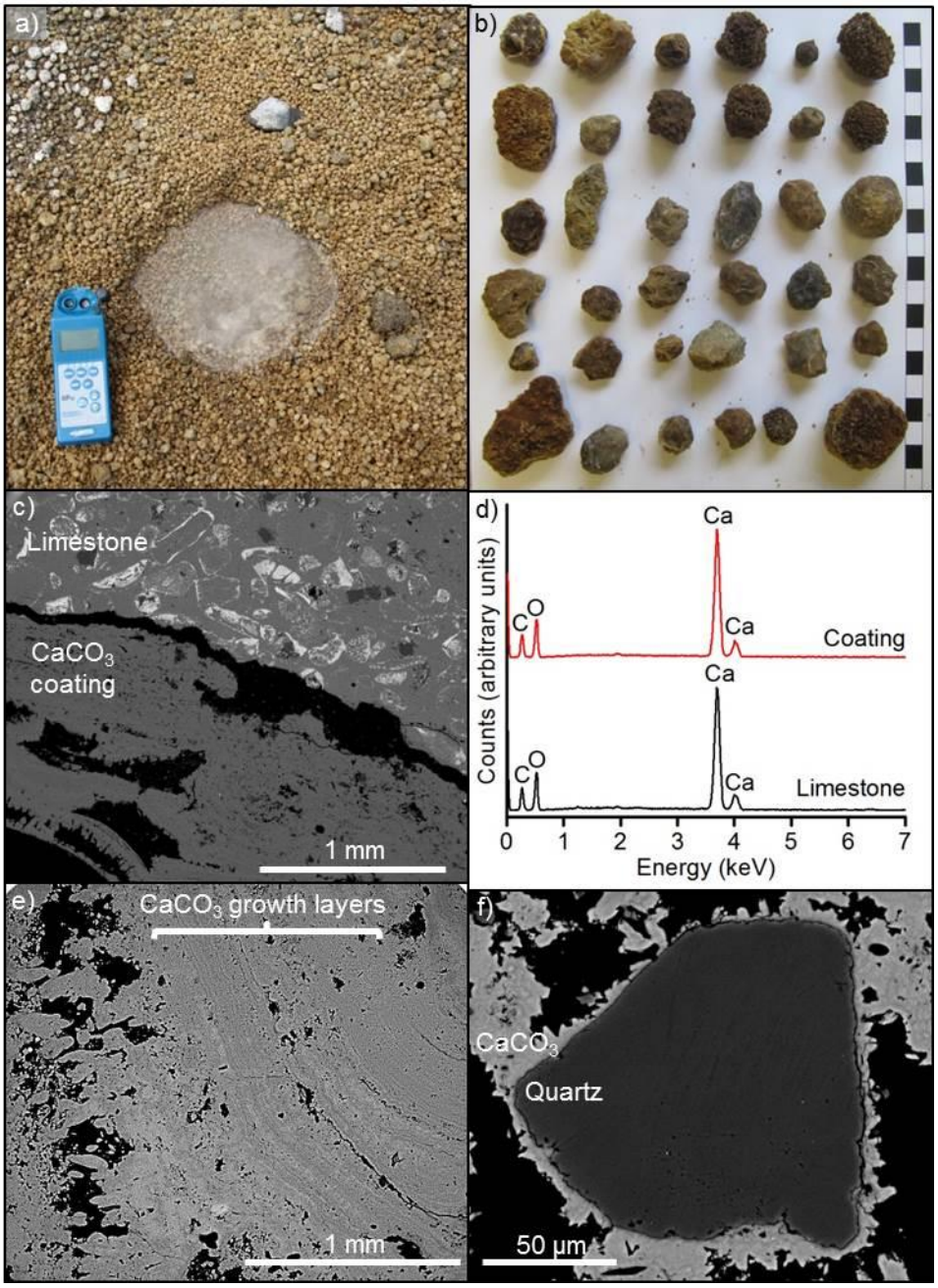

Figure 6.7: a) area of dry stream bed at stream 1, site 1 comprised of $CaCO_3$ 'pebbles', b) $CaCO_3$ 'pebbles' in hand specimen (scale shown in cm), c) electron micrograph of section through a $CaCO_3$ 'pebble', d) EDX spectra of the limestone fragment and $CaCO_3$ coating shown in c, e) electron micrograph of section through a $CaCO_3$ 'pebble' highlighting growth layers in the $CaCO_3$ outer coating and e) section through quartz fragment entrained in $CaCO_3$ outer coating of $CaCO_3$ 'pebble'

6.5.2.2 Stream 2

At the head of stream 2, clear non-hyperalkaline water occurred for approximately 30cm (stream 2 – site 1) before mixing with cloudy high pH water containing fine grained white/grey suspended particles (stream 2 – sites 2 and 2a; see Table 2 and Fig. 6.8a). The cloudiness at sites 2 and 2a

occurred across a 3m x 4m pool and the stream bed in this high pH zone was comprised of friable 'pebbles' (Fig. 6.8a). Though downstream, where pH remained > pH 8.5, the stream bed was cemented with a layer of $CaCO_3$ tufa (Fig. 6.8b). The 'pebbles' at sites 2 and 2a were shown via SEM to be identical to the $CaCO_3$ 'pebbles' in stream 1. However, at stream 2 these were coated in a fine grained, white material similar to the suspended particles in the waters in this area. The fine grained coating and suspended material were isolated, analysed by SEM and found to be sub-rounded / angular, 50-100µm, $CaCO_3$ particles (Fig. 6.8c and d). This indicates that CaCO3 formation is rapid in the zone where high pH, Ca rich water mixes with CO_3 rich freshwater.

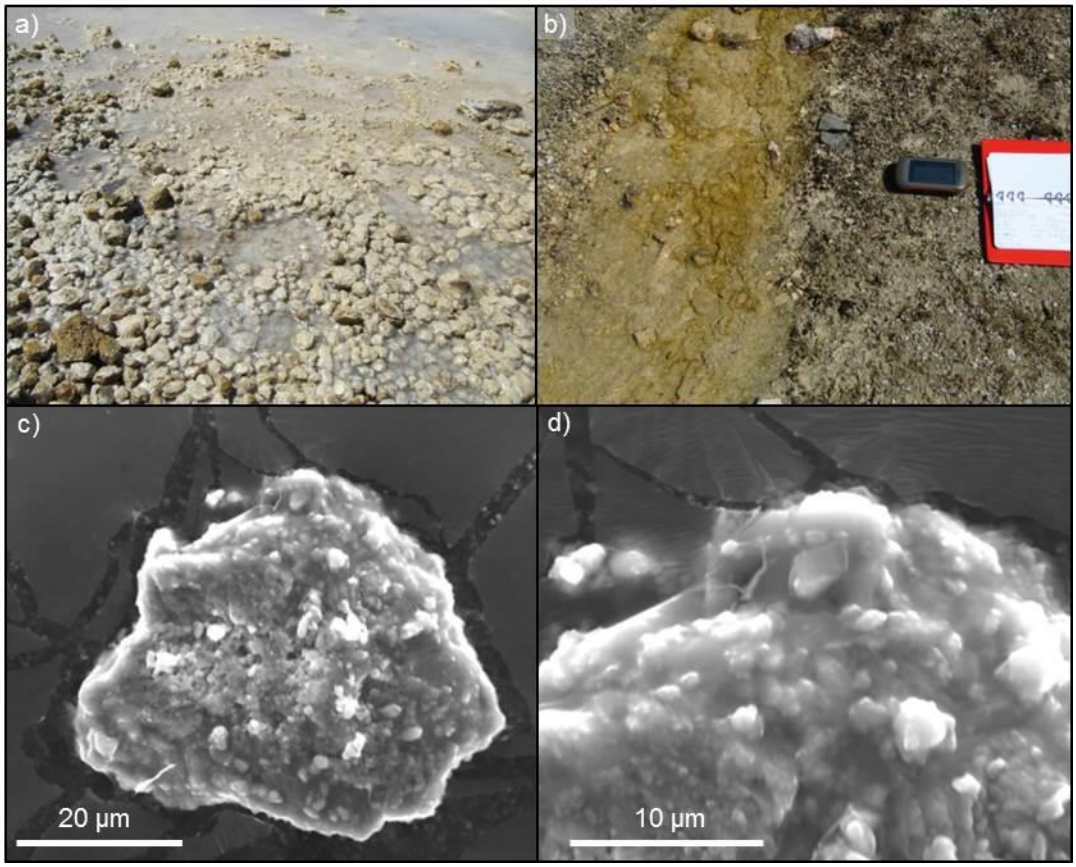

Figure 6.8: stream 2 a) site 2 comprised of $CaCO_3$ 'pebbles' coated in fine grained white material, b) bed of site 3 cemented by tufa deposit, c) electron micrograph of $CaCO_3$ particle from streamwater suspension site 2, d) higher magnification electron micrograph of c.

6.5.2.3 Rock Samples

To assess the alteration of silicate minerals by high pH at the Herbert's Quarry site additional rock samples were extracted from a dry stream bed approx. 60 m west of the head of stream 2, as no silicate rock was identified in stream 1 or 2. This stream bed was comprised of blocks of rock cemented within a

layer of $CaCO_3$ tufa. Therefore, due to the presence of tufa, it was inferred that at periods of high flow, high pH waters would have affected these samples. It was also noted that when the rock samples were removed from the tufa the ground was wet beneath them indicating sub-surface flow even at low stream flow.

Two silicate rock samples were taken from this site, though it was noted that silicate rocks were minor in occurrence. The first was a block of conglomerate containing quartz pebbles and was approximately 15 cm in all dimensions (Fig. 6.9a). This block is thought to have originated from the Honeycombed Sandstone Member or the Twrch Sandstone Formation (British Geological Survey, 2014). A white / grey coating was noted on the block though this was limited in extent. A section was taken through the sample including an area where the coating occurred. SEM analysis of the section showed that the white / grey coating was up to 1 mm thick and porous, and EDX analysis showed it to be pure $CaCO_3$. It was not possible to identify any dissolution features attributable to high pH alteration as the conglomerate would have been pre-weathered before entering the stream.

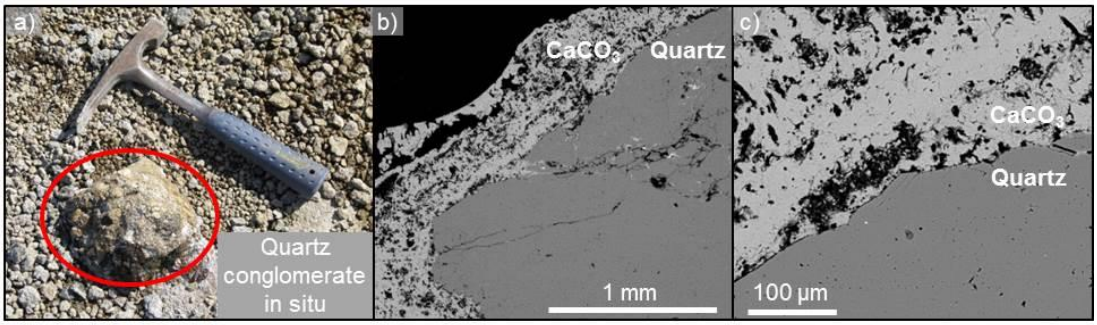

Figure 6.9: a) Quartz conglomerate cemented in tufa in dry stream bed in situ, b) electron micrograph of $CaCO_3$ formed around quartz in conglomerate, c) higher magnification electron micrograph of $CaCO_3$ formed around quartz in conglomerate.

The second rock sample collected was a sample of slate approx. 5 cm x 5 cm x 1 cm (Fig 6.10a). The sample was friable, indicative of weathering, but as with the conglomerate it is likely that the rock would have undergone weathering prior to entering the stream. White material occurred on the surface of the slate that had been below the surface of the tufa. A section was taken through the slate and analysed via SEM (Fig 6.10b-d). This showed a layer of increased porosity (approximately 30% porosity) in the outer 100-250

μm of slate on its sub-tufa surface with pores up to 20 μm in size (Fig. 6.10b and c). A distinct boundary between this layer and the lower porosity body of material was visible (Fig. 6.10b and c). The increased porosity is indicative of dissolution and, as it was limited to the side of the sample in contact with the river bed, is suggestive of silicate mineral dissolution by the high pH streamwater as found in CDZ-type systems previously studied (e.g. Gaucher and Blanc, 2006; Mäder et al., 2006; Savage and Rochelle, 1993; Hodgkinson and Hughes, 1999; Braney et al., 1993; Savage et al., 1992; Ramirez, 2005). However, dissolution due to weathering prior to the slate entering the stream cannot be precluded. It was noted that locally the outer edge of the higher porosity layer was coated with a blocky material up to 30 μm thick and there was also material locally infilling pores (Fig 6.10b and c). In both instances this was identified via EDX as $CaCO_3$. Material was also identified formed within cleavage planes both as layers up to 20 μm thick along slate surfaces and as sub-rounded particles up to 100 μm (Fig. 6.10d). This was also identified as $CaCO_3$ via EDX analysis (Fig. 6.10e and f). The widespread occurrence of $CaCO_3$ precipitates in streams 1 and 2 is attributed to precipitation from solution from high pH, high Ca streamwaters promoted by slate surfaces / voids / pores.

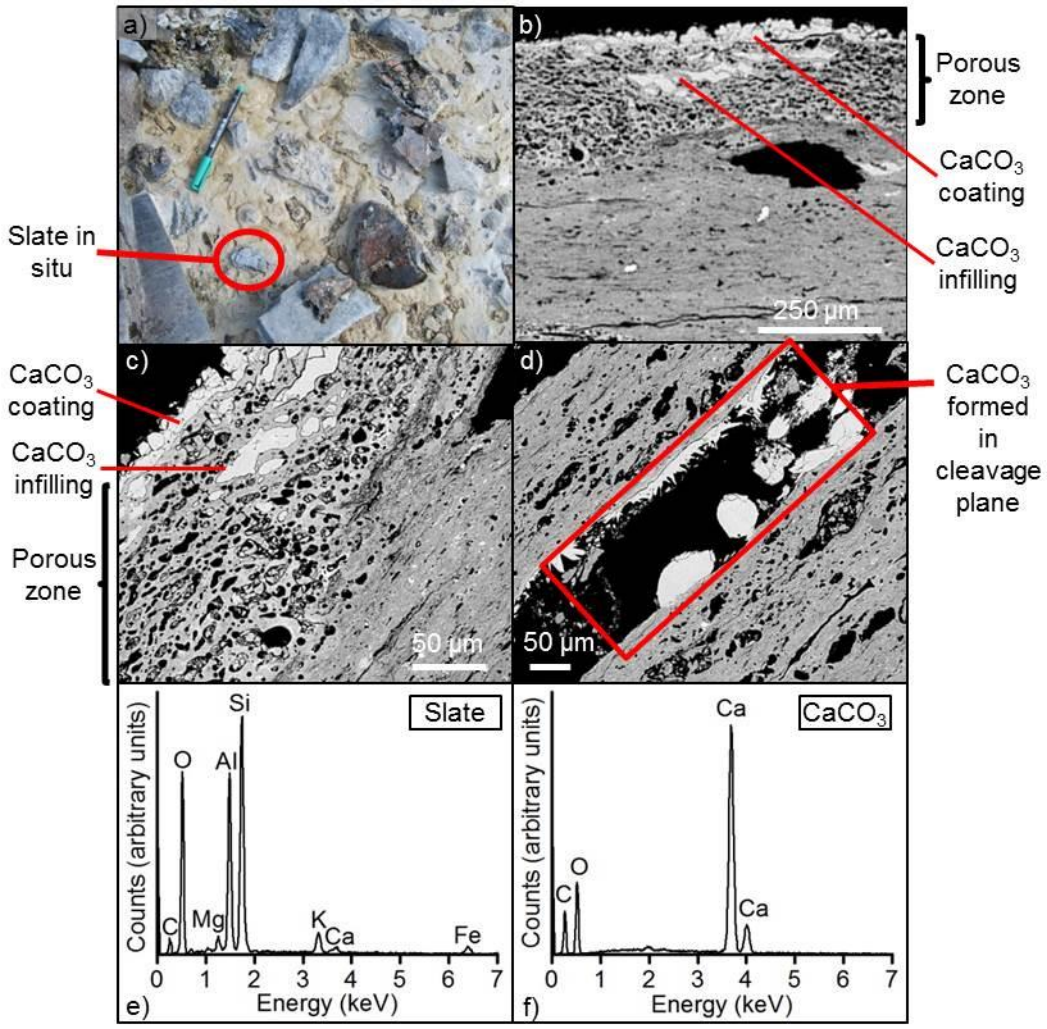

Figure 6.10: Slate cemented in tufa in dry stream bed a) in situ, b) in section via SEM exhibiting increased porosity at surface with infilling by $CaCO_3$, c) higher magnification electron micrograph of areas of increased porosity with $CaCO_3$ infilling, d) electron micrograph of slate cleavage plane with $CaCO_3$ formed on slate surfaces and within the cleavage plane, e) EDX spectrum of slate and f) EDX spectrum of $CaCO_3$.

6.6 Discussion

Zones of hyperalkaline pH, up to pH 11.96, were found in two streams at the Herbert's Quarry site. However, pH and Ca concentration fell rapidly downstream of each stream source, attributed to the precipitation of $CaCO_3$ (Eq. 6.3) which would remove Ca from solution and consume OH^- thereby lowering pH. This is demonstrated by the presence of the $CaCO_3$ 'pebbles' and tufa in the high pH zones of both streams. The reaction also sequesters CO_3 in $CaCO_3$, but in both streams CO_3 concentration increased with decreasing pH. This is attributed to the equilibration of the streamwaters with atmospheric CO_2 in zones of lower pH where lower Ca concentration prevents

extensive $CaCO_3$ precipitation. As pH decreased the concentration of Mg in solution increased while that of Al decreased. These trends are attributed to the change in solubility of these species with pH. For example, the precipitation of brucite ($MgOH_2$) above pH 10 (Pokrovsky and Schott, 2004) would limit the concentration of Mg in the highest pH zones at the site whereas gibbsite ($Al(OH)_3$) solubility increases with increasing pH above pH 6 (May et al., 1979).

At Herbert's Quarry silicate rocks do not crop out in the vicinity of the streams and the low streamwater Si concentration indicated the absence of a significant Si source. Investigation of detrital silicate rocks cemented within stream bed tufa deposits indicated little dissolution directly attributable to reaction in high pH fluid and no precipitation of secondary C-S-H phases as found in other studies of rock reaction in high pH solutions ((e.g. Gaucher and Blanc, 2006; Mäder et al., 2006; Savage and Rochelle, 1993; Hodgkinson and Hughes, 1999; Braney et al., 1993; Savage et al., 1992; Ramirez, 2005) but provided further evidence of $CaCO_3$ precipitation.

Ca concentrations of 80-800 mgl^{-1} and pH of 10.5-12.2 are representative of cement leachates in equilibrium with $Ca(OH)_2$ / C-S-H phases (Atkinson, 1985). Therefore the Herbert's Quarry streamwaters of pH > 10.5 and Ca concentration up to 268 mgl^{-1} may be analogous to cement leachates predicted to form at a GDF (Atkinson, 1985). Also, as the high pH streamwaters are likely to have existed at Herbert's Quarry for ~ 200 years (Calch, 2014) the site could extend laboratory studies. However, the prevalence of limestone and only minor occurrence of silicate rocks limits the applicability of the site for currently considered GDF host rocks. The restricted the extent of high pH solutions and resultant extensive precipitation of $CaCO_3$, also limit the potential for high pH reactions relevant to geodisposal as do the oxidising streamwater conditions (GDF conditions are expected to be reducing) and temperatures 15-25°C below those anticipated at a GDF (NDA, 2010b and NDA, 2010c). Therefore the usefulness of this site as an analogue for mineral alteration in the high pH leachates formed at cementitious waste facilities is thought to be limited.

6.7 Summary and Conclusions

In summary, high pH, Ca rich streamwaters were identified at Herbert's Quarry, analogous to high pH leachates predicted to form at a GDF. Analysis of sediment and rock samples indicated extensive $CaCO_3$ mineralisation due to reaction of Ca^{2+} with dissolved CO_2. This precipitation of $CaCO_3$ reduces the extent of high pH streamwaters and so limits the potential for rock alteration at high pH. The occurrence of silicate rocks was rare at the site. No formation of secondary silicate phases was observed in contrast to previous silicate rock alteration studies. Dissolution of silicate minerals was observed at the margins of a slate sample in contact with high pH leachate streams. This resulted in enhanced porosity within the slate matrix. Some of this alteration may be partly caused by weathering of these rocks prior to high-pH reaction. However, this alteration may be analogous to that expected from high-pH rock-water interaction in fractured silicate rocks, leading to enhanced matrix porosity in the fracture wallrock. This type of alteration may be important in regard to understanding rock-matrix diffusion processes influencing radionuclide migration within the CDZ.

Thus the presence of Ca-rich, high pH streamwaters at Herbert's Quarry is balanced by the widespread $CaCO_3$ mineralisation, paucity of silicate rock, oxic conditions and low water temperature to limit the applicability of the site as an analogue for geological disposal. However, the site may hold interest for microbial studies at high pH as alkaliphilic bacteria may be present which are starting to be recognised as important components for deep disposal (Rizoulis et al., 2012; Bassil et al., 2014; Williamson et al., 2013) and further, targeted studies may be warranted. The extensive formation of $CaCO_3$ in various forms at this site may also provide an analogue for the predicted $CaCO_3$ precipitation within a GDF (NDA, 2010d).

References

ALEXANDER, W.R., DAYAL, R., EAGLESON, K., EIKENBERG, J., HAMILTON, E., LINKLATER, C.M, MCKINLEY, I.G. AND TWEED, C.J. 1992. A natural analogue of high pH cement pore waters from the

Maqarin area of northern Jordan II: results of predictive geochemical calculations. *Journal of Geochemical Exploration,* 46, pp l33-146.

ANDRA. 2012. Low and intermediate level short-lived waste [online]. Available at: <www.andra.fr/international/pages/en/menu21/waste-management/waste-classification/short-lived-low--and-intermediate-level-waste-1609.html> [accessed 19/01/2014].

ANDREWS, J. E., GARE, S. G. AND DENNIS, P. F. 1997. Unusual isotopic phenomena in Welsh quarry water and carbonate crusts. Terra Nova, Vol. 9, No. 2, pp. 67-70.

ATKINSON, A. 1985. The Time Dependence of pH Within a Repository for Radioactive Waste Disposal. *UKAEA,* AERE-R 11777.

BASSIL, N. M., BRYAN, N. & LLOYD, J. R. 2014. Microbial degradation of isosaccharinic acid at high pH. The ISME Journal. 1751-7362/14. 1-11.

BATEMAN, K., COOMBS, P., NOY, D. J., PEARCE, J. M., WETTON, P., HAWORTH, A. & LINKLATER, C. 1999. Experimental simulation of the alkaline disturbed zone around a cementitious radioactive waste repository: numerical modelling and column experiments. *Geological Society, London,Special Publications,* 157**,** 183-194.

BERNER, U. R. 1992. Evolution of Pore Water Chemistry During Degradation of Cement in a Radioactive Waste Repository Environment. *Waste Management,* 12**,** 201-219.

BRANEY, M. C., HAWORTH, A., JEFFERIES, N. L. & SMITH, A. C. 1993. A study of the effects of an alkaline plume from a cementitious repository on geological materials. *Journal of Contaminant Hydrology,* 13**,** 379-402.

BRITISH GEOLOGICAL SURVEY. 2014. BGS lexicon – named rock unit: Dowlais Limestone Formation [online]. Available at http://data.bgs.ac.uk/doc/Lexicon/NamedRockUnit/DWL.html [accessed 07/6/2014]

CALCH. 2014. Discover the lime industry of the Black Mountains [online]. Available at: http://www.calch.org.uk/ [accessed 20/04/2014]

CHERMAK. J. A. 1992. Low temperature experimental investigation of the effect of high pH NaOH solutions on the Opalinus shale, Switzerland. *Clays and Clay Minerals*. 40. 6. 650-658.

CHERMAK. J. A. 1993. Low temperature experimental investigation of the effect of high pH KOH solutions on the Opalinus shale, Switzerland. *Clays and Clay Minerals*. 41. 3. 365-372.

DEFRA. 2008. Managing radioactive waste safely: A framework for implementing geological disposal. Department of the environment, food and rural affairs. UK.

DE WINDT, L., MARSAL, F., TINSEAU, E. & PELLEGRINI, D. 2008. Reactive transport modelling of geochemical interactions at a concrete/argillite interface, Tournemire site (France). *Physics and Chemistry of the Earth.* 33. S295-S305.

DE WINDT, L., PELLEGRINI, D. & VAN DER LEE, J. 2004. Coupled modelling of cement/claystone interactions and radionuclide migration. *Journal of Contaminant Hydrology*. 68. 165-182.

FERNANDEZ, R., RODRÍGUEZ, M., VIGIL DE LA VILLA, R. & CUEVAS, J. 2010. Geochemical constraints on the stability of zeolites and C-S-H in the high pH reaction of bentonite. *Geochimica et Cosmochimica Acta,* 74**,** 890-906.

GAUCHER, E. & BLANC, P. 2006. Cement/clay interactions – A review: experiments, natural analogues, and modeling. *Waste Management,* 26**,** 776-788.

HODGKINSON, E. S. & HUGHES, C. R. 1999. The mineralogy and geochemistry of cement/rock reactions: high-resolution studies of experimental and analogue materials. *Geological Society, London, Special Publications,* 157**,** 195-211.

IAEA. 1989. Natural analogues in performance assessments for the disposal of long lived radioactive wastes. Technical Report Seiries 304.

LAGERBLAD, B. & TRÄGÅRDH, J. 1994. Conceptual model for concrete long time degradation in a deep nuclear waste repository. SKB Technical Report 95-21.

MÄDER, U., FIERZ, T., FRIEG, B., EIKENBERG, J., RUTHI, M., ALBINSSON, Y., MORI, A., EKBERG, S. & STILLE, P. 2006. Interaction of hyperalkaline fluid with fractured rock: Field and laboratory experiments of the HPF project (Grimsel Test Site, Switzerland). *Journal of Geochemical Exploration,* 90**,** 68-94.

MAY, H. M., HELMKE, P. A. & JACKSON, M. L. 1979. Gibbsite solubility and thermodynamic properties of hydroxy-aluminium ions in aqueous solution at 25°C. *Geochimica et Cosmochimica Acta*. 43. 861-868.

MCKINLEY, I. G. & ALEXANDER, W. R. 1992. A review of the use of natural analogues to test performance assessment models of a cementitious near field. *Waste Management*, 12, 253-259.

MILLER, W., ALEXANDER, R., CHAPMAN, N., MCKINLEY, I. & SMELLIE, J. 2000. Geological disposal of radioactive wastes & natural analogues. Elsevier Science Ltd. Oxford.

MILODOWSKI, A. E., HYSSLOP, E. K., PEARCE, J. M., WETTON, P. D., KEMP, S. J., LONGWORTH, G., HODGKINSON, E. S. & HUGHES, C. R. 1998. Mineralogy, Petrology and Geochemistry. *In:* SMELLIE, J. (ed.) *Maqarin Natural Analogue Study: Phase III.* Stockholm: Swedish Nuclear Fuel and Waste Management Company.

NAGRA. 2014. Geological repository for low- and intermediate-level waste [online]. Available at: <www.nagra.ch/en/tlsmae.htm> [accessed 19/01/2014].

NDA. 2010a. Geological Disposal: Radionuclide behaviour status report. NDA/RWMD/034

NDA. 2010b. Geological Disposal: Generic disposal system technical specification. NDA/RWMD/044.

NDA. 2010c. Geological Disposal: Geosphere status report. NDA/RWMD/035.

NDA. 2010d. Geological Disposal: Near-field status report. NDA/RWMD/033.

NUCLEAR WASTE MANAGEMENT ORGANISATION. 2010. DGR key features [online]. Available at: < www.nwmo.ca/dgr_keyfeatures> [accessed 19/01/2014].

OATES, J. A. H. 1998. Lime and limestone: chemistry and technology, production and uses. Wiley-VCH, Weinham, Germany.

OECD-NEA. 2008. Moving forward with geological disposal of radioactive waste: a collective statement by the NEA radioactive waste management committee (RWMC). NEA no. 6433.

PFINGSTEN, W., PARIS, B., SOLER, J. & MADER, U. 2006. Tracer and reactive transport modelling of the interaction between high-pH fluid and fractured rock: Field and laboratory experiments. *Journal of Geochemical Exploration.* 90. 95-113.

POKROVSKY, O. S. & SCHOTT, J. 2004. Experimental study of brucite and precipitation in aqueous solutions: surface speciation and chemical affinity control. *Geochimica et cosmochimica acta.* 68. 1, 31-45.

RAMIREZ, S. 2005. Alteration of the Callovo-Oxfordian clay from Meuse-Haute Marne underground laboratory (France) by alkaline solution. I. A XRD and CEC study. *Applied Geochemistry,* 20**,** 89-99.

RIZOULIS, A.; STEELE, H.; MORRIS, K.; LLOYD, J. 2012. The potential impact of anaerobic microbial metabolism during the geological disposal of intermediate-level waste. *Mineralogical Magazine.* 76(8). 3261-3270

SAVAGE, D. 2010. A review of PA-relevant data from analogues of alkaline alteration. Wettingen: NAGRA.

SAVAGE, D. 2011. A review of analogues of alkaline alteration with regard to long-term barrier performance. *Mineralogical Magazine*, 75, 2401-2418

SAVAGE, D., BATEMAN, K., HILL, P., HUGHES, C., MILOWDOWSKI, A., PEARCE, J., RAE, M. & ROCHELLE, C. 1992. Rate and mechanism of the reaction of silicates with cement pore fluids. *Applied Clay Science,* 7**,** 33-45.

SAVAGE, D. & ROCHELLE, C. 1993. Modelling reactions between cement pore fluids and rock: Implications for porosity change. *Journal of Contaminant Hydrology,* 13**,** 365-378.

SOLER, J. M. & MÄDER, U. K. 2007. Mineralogical alteration and associated permeability changes induced by a high-pH plume: Modeling of a granite core infiltration experiment. *Applied Geochemistry,* 22**,** 17-29.

STEEFEL, C. I. & LICHTNER, P. C. 1994. Diffusion and reaction in rock matrix bordering a hyperalkaline fluid-filled fracture. Geochimica et Cosmochimica Acta. 58. 17. 3595-3612.

TECHER, I., BARTIER, D., BOULVAIS, PH., TINSEAU, E., SUCHORSKI, K., CABRERA, J. & DAUZÈRES, A. 2012. Tracing interaction between natural argillites and hyper-alkaline fluids from engineered cement paste and concrete: Chemical and isotopic monitoring of a 15-years old deep-disposal analogue. *Applied Geochemistry*. 27, 1384-1402.

TINSEAU, E., BARTIER, D., HASSOUTA, L., DEVOL-BROWN, I. & STAMMOSE, D. 2006. Mineralogical characterization of the Tournemire Argillite after in situ interaction with concretes. *Waste Management,* 26**,** 789-800.

WATSON, C., SAVAGE, D., WILSON, J., BENBOW, S., WALKER, C. & NORRIS, S. 2013. The Tournemire industrial analogue: reactive-transport modelling of a cement-clay interface. *Clay Minerals*. 48. 167-184.

WILLIAMSON, A.J., MORRIS, K., SHAW, S., BYRNE, J.M., BOOTHMAN, C. & LLOYD, J.R. 2013. Microbial reduction of Fe(III) under alkaline conditions relevant to geological disposal. *Applied and Environmental Microbiology*. 79(11). 3320-3326.

7 Summary, future work and implications

The dissolution of the cement used in a geological disposal facility (GDF) will perturb groundwater chemistry elevate pH (10.5-13.1) in the surrounding geosphere. This may cause mineral alteration and affect the rock's ability to act as a barrier to radionuclide migration. The research presented in this thesis investigated how mineral alteration in the CDZ could change the chemical and physical properties of rock over time and the potential impact of this on U(VI) mobility.

The study presented in chapter 4 investigated mineral alteration over 1-1.5 years of sandstone reaction in three synthetic high pH solutions and the effect of alteration on U(VI) speciation. In these batch experiments all three synthetic cement leachates (YCL – KOH and NaOH dominated, pH 13.1; ICL – $Ca(OH)_2$ dominated, pH 12.4; OCL - $Ca(OH)_2$ dominated, pH 10.5) caused the dissolution of primary alumino-silicate minerals in a sandstone and the formation of varying amounts of secondary C-(A)-(K)-S-H phases, as found in previous studies of high pH mineral / rock alteration (e.g. Gaucher and Blanc, 2006; Bateman et al., 1999; Braney et al., 1993; Cuevas, 2004; Mäder et al., 2006; Savage et al., 1992). However, despite the similarity in alteration processes, U(VI) behaviour varied between the three fluid systems. In YCL the U(VI) formed colloidal particles which were suspended in solution throughout the experiment. In ICL, the radionuclide became associated with secondary C-(A)-(K)-S-H coatings on primary mineral grains but this is thought to have been as a discrete $CaUO_4$ phase. U(VI) in the OCL system also became associated with the bulk solid phase, though this was through either through adsorption or the surface mediated precipitation of a uranyl silicate mineral. This characterisation of different U(VI) behaviour between the three leachates investigated has potential implications for U(VI) migration from a cementitious GDF. The formation of a colloidal phase in the YCL system indicates that although U(VI) solubility may be limited at high pH (Chapman and Flowers, 1986; Glasser, 1997; Sugiyama et al., 2007), U(VI)-bearing particles could remain highly mobile and be transported in suspension. The formation of such U(VI) colloids at pH 13 has also been recently identified by

Bots et al. (2014), and Smith et al. (in press). However, in the ICL and OCL systems the association of U(VI) with the bulk solid phase may limit its mobility. However, the increase in U(VI) solution concentration after 21 weeks of reaction in OCL does indicate that the behaviour of (UVI) may change as the system evolves. Therefore further experimental investigation at extended timescales may be required to aid understanding of U(VI) behaviour in these high pH systems. The work presented in chapter 4 could be extended by investigating rock reaction and U(VI) behaviour at high pH in the different leachates successively, analogous to the evolution of the leachate migrating from the GDF. A comparative assessment of the sorption of U(VI) to unaltered rock and the altered rock could also yield useful information on the impact mineral alteration would have on U(VI) behaviour if it occurred prior to U(VI) entering the system. In addition, the study could be extended by the investigation of the behaviour of different radionuclides during high pH rock alteration.

In chapter 5 rock alteration at high pH was investigated after 15 years of reaction in batch experiments. This significantly extended the usual timescales of laboratory alteration to increase knowledge of the evolution in mineral alteration processes as the reaction progressed over time. The initial investigation up to 15 months of reaction identified silicate mineral dissolution and secondary C-(A)-(K)-S-H formation as the predominant mineral alteration processes in two different synthetic cement leachates (Rochelle et al., 1997). This was in agreement with the findings of many other studies, including chapter 4 of this thesis. However, after 15 years of reaction, in both leachates the early-formed C-(A)-(K)-S-H phases destabilised and extensive dedolomitisation occurred. Over the same period a suite of secondary Mg-silicate minerals of varying chemical composition and morphology formed. The formation of different successive stable mineral assemblages over time demonstrated the potential for the evolution of mineral alteration processes in the CDZ. In addition, this work identified the potential for the formation of secondary Mg-silicate phases, not generally considered in relation to geological disposal previously. This has highlighted the need to study such phases as potential alteration products in the CDZ. As previously the

transformation of C-S-H phases to feldspars and zeolites were the most widely predicted evolutionary processes in the CDZ (Savage, 2011). It has also emphasised more broadly the potential need to consider a wider range of reaction processes and alteration products during the extended timescales of CDZ evolution. Chapter 5 also drew attention to the potential impact of alteration on radionuclide transport. Comparison of U(VI) adsorption to the 15 year altered rock against adsorption to a sample of unaltered rock found increased retention of U(VI) on the altered rock. This indicates that rock alteration in high pH leachates, and the formation of Mg-silicates, may increase U(VI) adsorption in the geosphere and improve the rock's ability to act as a barrier to radionuclide migration.

As mentioned in chapter 5 it is unclear whether the Mg-silicate phase identified in this study is the final stable mineral assemblage for these systems and it would be useful to investigate whether further evolution of the system would occur over time by running longer experiments. Further detail could also be provided by rerunning the experiments to better constrain and understand the transformation of C-S-H to Mg-silicate phases which could only be inferred in this study. This would improve understanding of the transformation process and could provide data to allow such evolution to be accurately modelled. In addition, the effect of the presence of free Mg^{2+} ions, i.e. investigate Mg^{2+} sources other than dolomite, during the experiment could be investigated. This would provide information on whether other potential Mg sources, such as Magnox fuel cladding, could impact the mineral alteration reactions. Another opportunity to further the work could be to assess the fate of U(VI) and / or other radionuclides when present in the system throughout alteration, as in the study presented in Chapter 4. Such an investigation would allow radionuclide behaviour to be assessed not only during C-S-H formation, but also through Mg-silicate transformation and potentially additional mineral reactions. This would allow characterisation of the impact of the system's evolution on radionuclide transport.

Chapter 6 focused on the characterisation of the Herbert's Quarry site in South Wales to assess its potential as an anthropogenic analogue of high pH

alteration in the CDZ. Stream waters from two streams at the site were analysed and found to be comparable in pH and Ca concentration to the $Ca(OH)_2$ dominated cement leachates predicted to form in the CDZ. However, as the surface waters were in equilibrium with the atmosphere, the reaction of dissolved $Ca(OH)_2$ in the streams with atmospheric CO_2 resulted in the extensive precipitation of $CaCO_3$ at the site. The $CaCO_3$ was identified both as porous coatings on rock fragments and as particles suspended in the streamwaters. This process also reduced the pH of the stream waters and limited the extent of the high pH leachate comparable zones to 10s of metres from the stream sources. Investigation of silicate rock samples from the high pH streamwater zones showed that reaction was predominantly restricted to $CaCO_3$ formation on sample surfaces and, in the case of slate, within porosity / cleavage planes. Also, though no secondary silicate minerals were identified in any solid phase samples from the site, some silicate mineral dissolution which had increased the rock's porosity and was attributed to reaction in high pH streamwater, identified in a sample of slate. This may be analogous to the high-pH rock-water interaction expected to occur in a fractured silicate host rocks and would lead to enhanced matrix porosity. This type of alteration may be important for understanding the diffusive transport properties that could influence radionuclide migration within the CDZ. However, the widespread $CaCO_3$ mineralisation, paucity of silicate rock, oxic conditions and low water temperature at the site were found to limit the applicability of Herbert's Quarry as an analogue for geological disposal.

Despite this, the site may hold interest for microbial studies at high pH as alkaliphilic bacteria may be present which are starting to be recognised as important components for deep disposal (Rizoulis et al., 2012; Bassil et al., 2014; Williamson et al., 2013). Therefore, further studies targeted at microbial characterisation may be warranted. The extensive formation of $CaCO_3$ in various forms at this site may also provide a useful analogue for the predicted $CaCO_3$ precipitation within a GDF (NDA, 2010) and further investigation of the site could be considered for this purpose.

The research presented in this thesis has provided insight and highlighted several key points with regard to the high pH rock alteration predicted to occur at a cementitious GDF. Firstly, the findings of previous investigations which identified silicate mineral dissolution and C-S-H precipitation as the dominant short term alteration processes have been confirmed. This provided additional confidence in the relevance of these processes to the CDZ. However, this study has also shown that, in the presence of dolomite, continued reaction can lead to the formation of Mg-silicates at the expense of early formed C-S-H phases. This evolutionary trend has not been widely considered in the context of high pH alteration in the CDZ, where predictive modelling and analogue studies have previously suggested that C-S-H evolution to feldspars and zeolites would be the most important evolutionary trends. This has important implications for any cementitious GDF safety case as not only does it demonstrate that a host rock assessed prior to GDF emplacement may change significantly during the evolution of the system, but it also highlights that the variety of alteration processes considered in modelling and analogue studies may be limited by their basis on the results of short term experimental studies. The assessment of the Herbert's Quarry site also emphasised that the geochemical complexity of the CDZ may limit the applicability of many sites where high pH fluids exist as analogues for mineral alteration at longer (10^2 – 10^6 years) timescales. This may significantly limit the availability of useful analogue sites and potentially constrain understanding of mineral alteration processes on GDF relevant timescales.

The effect of rock alteration on a rock's ability to act as a barrier to U(VI) transport was also investigated through the work presented in this thesis. Two key points were highlighted. Firstly, it was demonstrated that the chemistry and pH of the leachate causing rock alteration may significantly influence the behaviour of U(VI) behaviour. This may have an impact of U(VI) transport as it could exist either as a mobile colloidal phase or bound to mineral surfaces. Secondly, it was found that high pH alteration over 15 years increased a rock's sorption capacity for U(VI), indicating rock alteration could be beneficial as a barrier to U(VI) migration. These points highlight that mineral alteration in the CDZ could either enhance or retard U(VI) migration and therefore a more

detailed understanding of the processes involved may be required for any cementitious GDF safety case.

References

BASSIL, N. M., BRYAN, N. & LLOYD, J. R. 2014. Microbial degradation of isosaccharinic acid at high pH. The ISME Journal. 1751-7362/14. 1-11.

BATEMAN, K., COOMBS, P., NOY, D. J., PEARCE, J. M., WETTON, P., HAWORTH, A. & LINKLATER, C. 1999. Experimental simulation of the alkaline disturbed zone around a cementitious radioactive waste repository: numerical modelling and column experiments. *Geological Society, London, Special Publications,* 157, 183-194.

BRANEY, M. C., HAWORTH, A., JEFFERIES, N. L. & SMITH, A. C. 1993. A study of the effects of an alkaline plume from a cementitious repository on geological materials. *Journal of Contaminant Hydrology,* 13, 379-402.

BOTS, P., MORRIS, K., HIBBERD, R., LAW, G. T. W., MOSSELMANS, J. F. W., BROWN, A. P., DOUTCH, J., SMITH, A. J. & SHAW, S. 2014. Formation of stable uranium(VI) colloidal nanoparticles in conditions relevant to radioactive waste disposal. Langmuir. *American Chemical Society*.

CHAPMAN, N. A. & FLOWERS, R. H. 1986. Near-field solubility constraints on radionuclide mobilisation and their influence on waste package design. *Philosophical Transactions of the Royal Society of London*. A319. 83–95.

CUEVAS, J., 2004. Geochemical reactions in FEBEX bentonite. In: MICHAU, N. Ed. Ecoclay II: Effect of cement on clay barrier performance phase II. final report. European Commission. European contract FIKW-CT-2000-00018.

GLASSER, F. P. 2001. Cement in radioactive waste disposal. *Mineralogical Magazine.* 65. 621.633.

MÄDER, U., FIERZ, T., FRIEG, B., EIKENBERG, J., RUTHI, M., ALBINSSON, Y., MORI, A., EKBERG, S. & STILLE, P. 2006. Interaction of hyperalkaline fluid with fractured rock: Field and laboratory experiments of the HPF project (Grimsel Test Site, Switzerland). *Journal of Geochemical Exploration,* 90, 68-94.

NDA. 2010. Geological Disposal: Near-field status report. NDA/RWMD/033.

RIZOULIS, A.; STEELE, H.; MORRIS, K.; LLOYD, J. 2012. The potential impact of anaerobic microbial metabolism during the geological disposal of intermediate-level waste. *Mineralogical Magazine.* 76(8). 3261-3270

ROCHELLE, C., PEARCE, J., BATEMAN, K., COOMBS, P. & WETTON, P. 1997. The evaluation of chemical mass transfer in the disturbed zone of a deep geological disposal facility for radioactive waste: X. Interaction between synthetic cement porefluids and BVG: Observations from experiments of 4, 9 and 15 months duration. *BGS technical report* WE/97/16 Article permalink: http://nerc.worldcat.org/oclc/703969750

SAVAGE, D., BATEMAN, K., HILL, P., HUGHES, C., MILOWDOWSKI, A., PEARCE, J., RAE, M. & ROCHELLE, C. 1992. Rate and mechanism of the reaction of silicates with cement pore fluids. *Applied Clay Science,* 7, 33-45.

SAVAGE, D. 2011. A review of analogues of alkaline alteration with regard to long-term barrier performance. *Mineralogical Magazine*, 75, 2401-2418

SMITH, K. F., BRYAN, N. D., SWINBURNE, A. N., BOTS, P., SHAW, S., NATRAJAN, L. S., MOSSELMANS, J. F. W., LIVENS, F. R. & MORRIS, K. In press. U(VI) behaviour in hyperalkaline calctie systems. *Geochimica et Cosmochimica Acta.*

SUGIYAMA, D., FUJITA, T., CHIDA, T. & TSUKAMOT, M. 2007. Alteration of fractured cementitious materials. *Cement and Concrete Research*. 37. 1257–1264.

WILLIAMSON, A.J., MORRIS, K., SHAW, S., BYRNE, J.M., BOOTHMAN, C. & LLOYD, J.R. 2013. Microbial reduction of Fe(III) under alkaline conditions relevant to geological disposal. *Applied and Environmental Microbiology*. 79(11). 3320-3326.

.

Appendix A
Supplementary information to chapter 4

Table A1: Modal mineralogical analysis of the Hollington Red Sandstone as determined by WD-XRFS

	Modal mineralogical analysis (%)
Quartz	75.5
K-feldspar	16
Albite	0
Illite/Chlorite/Smectite	3.7
Kaolinite	3.5
Dolomite	0
Calcite	0
Muscovite	0.7
Biotite	0
Phlogopite	0.2
Zircon	0
Apatite	0.2
TiO2	0.3
Ilmenite	0
Magnetite	0
Fe Oxide/Oxyhdroxide	0

Table A2: Chemical compositions of minerals used in PHREEQC modelling (taken from the LLNL thermodynamic database)

Mineral	**Chemical composition**	**Weight % in sandstone**	**Molar weight**	**No. moles in YCL experiment**
Quartz	SiO_2	76	60	0.253
Orthoclase feldspar (K-Feldspar)	$KAlSi_3O_8$	16	278	0.0115
Illite	$K_{0.6}Mg_{0.25}Al_{1.8}Al_{0.5}Si_{3.5}O_{10}(OH)_2$	4	383.25	0.00209
Kaolinite	$Al_2Si_2O_5(OH)_4$	4	258	0.00310

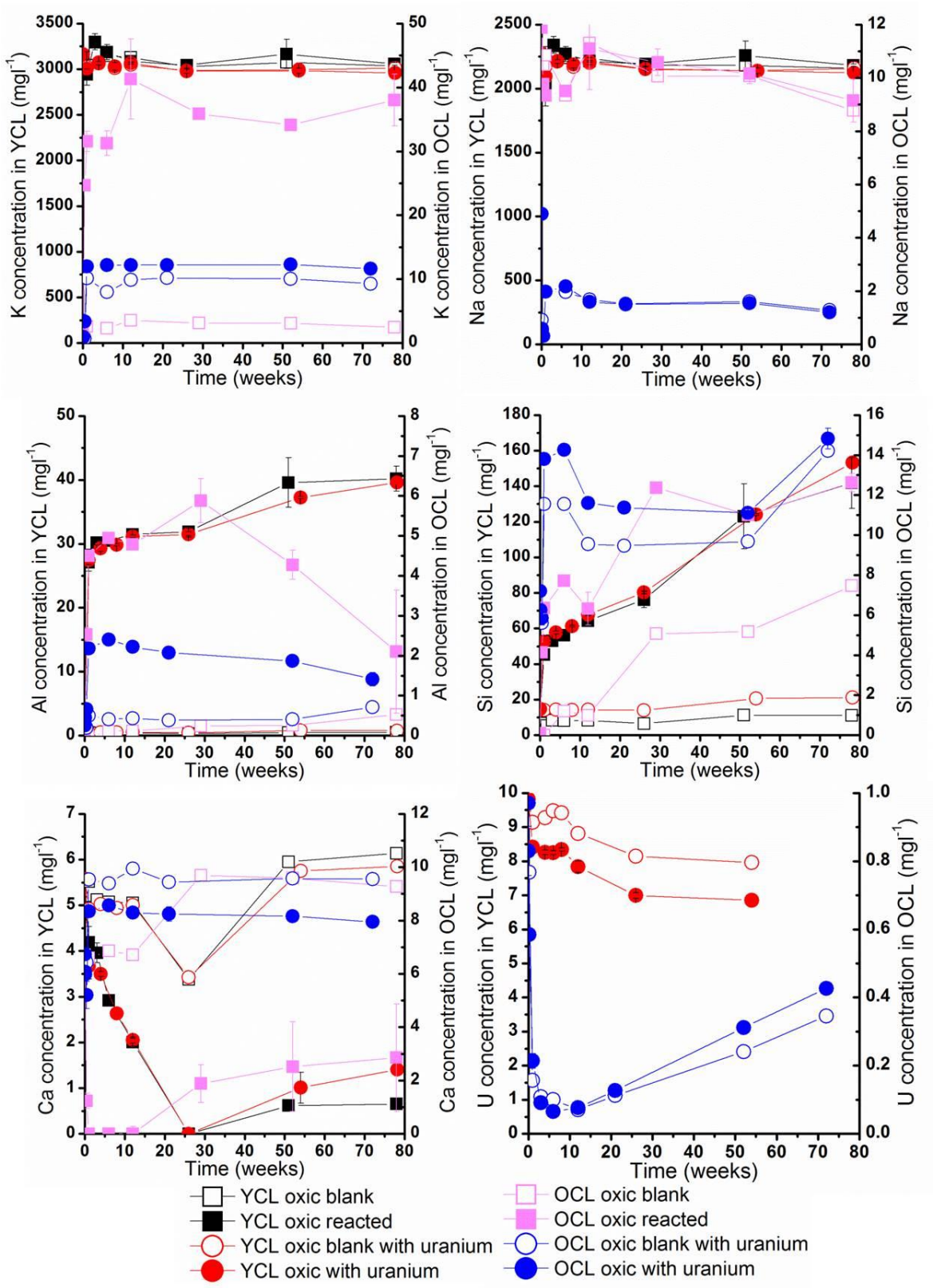

Figure A1: *Concentrations of the major cations in solution in the oxic YCL and OCL experiments*

Table A3: *Anion concentrations in non-uranium experiments*

Time	Sample	Chloride (mgl^{-1})	Sulphate (mgl^{-1})	Nitrate (mgl^{-1})	Phosphate (mgl^{-1})	Carbonate (mgl^{-1})
0	YCL anoxic	4.41	0.22	0.04	n.a.	248.03
	YCL oxic	6.63	0.26	0.05	n.a.	51.26
7 days	YCL anoxic blank	5.00	0.30	0.06	n.a.	70.31
	YCL anoxic	5.58	0.24	n.a.	n.a.	101.25
	YCL anoxic blank	4.64	0.29	n.a.	n.a.	40.40
	YCL oxic	5.07	0.24	n.a.	n.a.	268.93
3 weeks	YCL anoxic blank	5.66	0.21	n.a.	n.a.	131.41
	YCL anoxic average	4.75	0.27	0.08	n.a.	30.74
	YCL anoxic standard deviation	0.28	0.01	n.a.	n.a.	1.06
	YCL anoxic blank	6.35	0.27	n.a.	n.a.	27.66
	YCL oxic average	4.30	0.27	0.08	n.a.	29.34
	YCL oxic standard deviation	0.92	0.00	n.a.	n.a.	5.41
6 weeks	YCL anoxic blank	4.30	0.19	n.a.	n.a.	38.57
	YCL anoxic average	4.78	0.27	0.10	n.a.	46.82
	YCL anoxic standard deviation	0.38	0.02	n.a.	n.a.	16.25
	YCL anoxic blank	7.03	0.29	n.a.	n.a.	4.26
	YCL oxic average	4.36	0.27	0.11	n.a.	44.24
	YCL oxic standard deviation	1.08	0.01	n.a.	n.a.	27.47
12 weeks	YCL anoxic blank	7.22	0.23	n.a.	n.a.	24.68
	YCL anoxic average	18.16	0.28	n.a.	n.a.	26.51
	YCL anoxic standard deviation	18.45	n.a.	n.a.	n.a.	n.a.

	YCL anoxic blank	7.63	0.26	n.a.	n.a.	46.43
	YCL oxic average	4.83	0.26	0.08	n.a.	51.35
	YCL oxic standard deviation	1.14	0.02	0.05	n.a.	23.23
26 weeks	YCL anoxic blank	8.25	0.25	n.a.	n.a.	11.51
	YCL anoxic average	5.68	0.26	0.13	n.a.	35.17
	YCL anoxic standard deviation	0.27	0.00	n.a.	n.a.	12.12
	YCL anoxic blank	9.40	0.29	n.a.	n.a.	27.63
	YCL oxic average	5.36	0.29	0.13	n.a.	42.58
	YCL oxic standard deviation	1.23	0.01	n.a.	n.a.	28.63
51 weeks	YCL anoxic blank	8.24	0.22	n.a.	n.a.	81.05
	YCL anoxic average	5.51	0.23	0.08	n.a.	85.68
	YCL anoxic standard deviation	0.58	0.02	n.a.	n.a.	8.24
	YCL anoxic blank	9.37	0.24	n.a.	n.a.	74.06
	YCL oxic average	5.23	0.26	0.08	n.a.	78.91
	YCL oxic standard deviation	0.99	0.01	n.a.	n.a.	9.96
Time	**Sample**	**Chloride (mgl^{-1})**	**Sulphate (mgl^{-1})**	**Nitrate (mgl^{-1})**	**Phosphate (mgl^{-1})**	**Carbonate (mgl^{-1})**
0	ICL	152.65	0.19	n.a.	n.a.	n.a.
2 weeks	ICL anoxic blank	142.97	0.17	n.a.	n.a.	n.a.
	ICL anoxic average	144.17	0.05	0.05	n.a.	n.a.
	ICL anoxic standard deviation	10.08	n.a.	n.a.	n.a.	n.a.
12 weeks	ICL anoxic blank	154.51	0.24	0.02	n.a.	n.a.
	ICL anoxic average	141.76	0.04	0.11	n.a.	n.a.
	ICL anoxic standard deviation	3.48	0.02	0.11	n.a.	n.a.

26 weeks	ICL anoxic blank	151.22	0.38	0.04	n.a.	n.a.
	ICL anoxic average	139.50	0.04	0.07	n.a.	n.a.
	ICL anoxic standard deviation	18.63	0.01	0.02	n.a.	n.a.
12 months	ICL anoxic blank	140.40	0.65	0.02	n.a.	n.a.
	ICL anoxic average	113.23	0.42	0.10	n.a.	n.a.
	ICL anoxic standard deviation	32.53	0.21	0.08	n.a.	n.a.
Time	**Sample**	**Chloride (mgl^{-1})**	**Sulphate (mgl^{-1})**	**Nitrate (mgl^{-1})**	**Phosphate (mgl^{-1})**	**Carbonate (mgl^{-1})**
0	OCL anoxic	5.27	n.a.	n.a.	n.a.	n.a.
	OCL oxic	5.33	n.a.	n.a.	n.a.	n.a.
1 week	OCL anoxic blank	5.40	n.a.	n.a.	n.a.	n.a.
	OCL anoxic average	5.75	0.19	0.09	n.a.	n.a.
	OCL anoxic standard deviation	0.28	0.01	n.a.	n.a.	n.a.
	OCL oxic blank	5.31	0.02	n.a.	n.a.	n.a.
	OCL oxic average	5.68	0.18	0.09	n.a.	n.a.
	OCL oxic standard deviation	0.18	0.00	n.a.	n.a.	n.a.
3 weeks	OCL anoxic blank	5.38	0.02	n.a.	n.a.	n.a.
	OCL anoxic average	6.96	0.31	0.14	n.a.	n.a.
	OCL anoxic standard deviation	1.81	0.07	n.a.	n.a.	n.a.
	OCL oxic blank	5.13	0.01	n.a.	n.a.	n.a.
	OCL oxic average	5.80	0.16	0.04	0.07	29.64
	OCL oxic standard deviation	0.46	0.01	0.03	0.00	13.79
6 weeks	OCL anoxic blank	5.35	n.a.	0.02	n.a.	24.65
	OCL anoxic average	5.53	0.16	0.05	0.07	35.99

	OCL anoxic standard deviation	0.31	0.01	0.04	0.01	0.20
	OCL oxic blank	5.63	n.a.	n.a.	n.a.	18.29
	OCL oxic average	5.99	0.19	0.05	0.07	31.63
	OCL oxic standard deviation	0.65	0.01	0.04	0.00	10.19
12 weeks	OCL anoxic blank	5.51	n.a.	n.a.	n.a.	n.a.
	OCL anoxic average	5.97	0.19	0.04	0.07	32.93
	OCL anoxic standard deviation	0.36	0.00	0.03	0.01	n.a.
	OCL oxic blank	6.00	n.a.	n.a.	n.a.	n.a.
	OCL oxic average	6.25	0.22	0.04	0.07	0.89
	OCL oxic standard deviation	0.65	0.03	0.03	0.00	n.a.
26 weeks	OCL anoxic blank	5.60	0.08	n.a.	n.a.	n.a.
	OCL anoxic average	6.14	0.26	0.07	0.07	31.82
	OCL anoxic standard deviation	0.89	0.02	n.a.	0.01	n.a.
	OCL oxic blank	6.09	0.04	n.a.	n.a.	n.a.
	OCL oxic average	6.50	0.30	0.05	0.07	10.94
	OCL oxic standard deviation	0.95	0.02	0.03	0.01	n.a.
18 months	OCL anoxic blank	12.42	0.19	0.04	n.a.	20.66
	OCL anoxic average	12.31	0.65	0.10	0.16	67.59
	OCL anoxic standard deviation	5.26	0.22	0.08	0.02	46.29
	OCL oxic blank	13.59	0.22	0.07	n.a.	21.06
	OCL oxic average	14.39	0.99	0.17	0.25	52.00
	OCL oxic standard deviation	1.93	0.05	0.16	0.00	5.50

Table A4: *Anion concentrations in uranium experiments*

Time	Sample	Chloride (mgl^{-1})	Sulphate (mgl^{-1})	Nitrate (mgl^{-1})	Phosphate (mgl^{-1})	Carbonate (mgl^{-1})
0	YCL	n.a.	0.41	0.02	n.a.	172.73
3 days	YCL anoxic blank	2.38	0.39	0.05	n.a.	77.09
	YCL anoxic average	2.51	0.40	0.06	0.20	116.79
	YCL anoxic standard deviation	0.04	0.01	0.01	0.01	4.30
1 week	YCL anoxic blank	2.34	0.38	0.05	n.a.	113.00
	YCL anoxic average	1.81	0.30	0.04	0.16	497.27
	YCL anoxic standard deviation	1.16	0.18	0.02	0.08	639.81
	YCL anoxic blank	2.41	0.41	0.04	n.a.	140.92
	YCL oxic average	2.51	0.41	0.05	0.21	158.85
	YCL oxic standard deviation	0.05	0.00	0.00	0.02	16.96
4 weeks	YCL anoxic blank	2.74	0.46	0.05	n.a.	100.14
	YCL anoxic average	2.84	0.44	0.05	0.21	111.38
	YCL anoxic standard deviation	0.38	0.03	0.01	0.02	5.16
	YCL oxic blank	2.80	0.45	0.04	n.a.	97.52
	YCL oxic average	2.29	0.34	0.05	0.17	91.41
	YCL oxic standard deviation	0.88	0.15	0.02	0.06	15.66
8 weeks	YCL anoxic blank	1.01	0.18	0.04	n.a.	756.39
	YCL anoxic average	2.97	0.44	0.06	0.19	96.63
	YCL anoxic standard deviation	0.22	0.01	0.00	0.01	11.16
	YCL oxic blank	2.77	0.45	0.05	n.a.	90.02
	YCL oxic average	2.90	0.42	0.06	0.23	93.10

	YCL oxic standard deviation	0.02	0.05	0.00	0.02	10.47
12 weeks	YCL anoxic blank	2.65	0.42	0.05	n.a.	125.50
	YCL anoxic average	4.06	0.43	0.10	0.22	118.59
	YCL anoxic standard deviation	1.99	0.01	0.03	0.03	24.36
	YCL oxic blank	2.80	0.43	0.07	n.a.	124.30
	YCL oxic average	4.06	0.57	0.07	0.26	96.40
	YCL oxic standard deviation	1.92	0.24	0.01	0.01	18.77
26 weeks	YCL anoxic average	2.97	0.45	0.08	0.33	136.41
	YCL anoxic standard deviation	0.12	0.01	0.01	0.02	5.32
51 weeks	YCL anoxic blank	0.73	0.19	0.07	n.a.	1031.09
	YCL anoxic average	4.05	0.44	0.10	0.39	219.03
	YCL anoxic standard deviation	2.21	0.06	0.00	0.04	117.87
	YCL oxic blank	0.97	0.22	0.07	n.a.	549.69
	YCL oxic average	2.89	0.44	0.11	0.67	150.73
	YCL oxic standard deviation	0.41	0.02	0.01	0.43	19.84
Time	**Sample**	**Chloride (mgl^{-1})**	**Sulphate (mgl^{-1})**	**Nitrate (mgl^{-1})**	**Phosphate (mgl^{-1})**	**Carbonate (mgl^{-1})**
0	ICL	155.75	0.10	0.02	n.a.	n.a.
1 day	ICL anoxic blank	141.21	0.18	0.15	n.a.	n.a.
	ICL anoxic average	142.70	0.14	0.21	n.a.	n.a.
	ICL anoxic standard deviation	6.66	0.02	0.10	n.a.	n.a.
3 days	ICL anoxic blank	95.95	0.16	0.14	n.a.	n.a.
	ICL anoxic average	148.19	0.12	0.14	n.a.	n.a.
	ICL anoxic standard deviation	3.87	0.02	0.01	n.a.	n.a.

10 days	ICL anoxic blank	154.31	0.16	0.19	n.a.	n.a.
	ICL anoxic average	151.35	0.10	0.08	n.a.	n.a.
	ICL anoxic standard deviation	6.47	0.06	0.05	n.a.	n.a.
5 weeks	ICL anoxic blank	154.51	0.18	0.10	n.a.	n.a.
	ICL anoxic average	153.40	0.11	0.10	n.a.	n.a.
	ICL anoxic standard deviation	0.64	0.02	0.01	n.a.	n.a.
9 weeks	ICL anoxic blank	154.06	0.20	0.12	n.a.	n.a.
	ICL anoxic average	154.21	0.06	0.22	n.a.	n.a.
	ICL anoxic standard deviation	2.26	0.06	0.24	n.a.	n.a.
12 weeks	ICL anoxic blank	159.47	0.27	0.10	n.a.	n.a.
	ICL anoxic average	152.78	0.11	0.07	n.a.	n.a.
	ICL anoxic standard deviation	11.53	0.05	0.04	n.a.	n.a.
11 months	ICL anoxic blank	161.13	0.86	0.16	n.a.	n.a.
	ICL anoxic average	161.92	0.27	0.14	n.a.	n.a.
	ICL anoxic standard deviation	2.89	0.13	0.05	n.a.	n.a.

Time	**Sample**	**Chloride (mgl^{-1})**	**Sulphate (mgl^{-1})**	**Nitrate (mgl^{-1})**	**Phosphate (mgl^{-1})**	**Carbonate (mgl^{-1})**
0	OCL	0.53	n.a.	n.a.	n.a.	12.94
1 hour	OCL anoxic blank	0.30	n.a.	n.a.	n.a.	11.30
	OCL anoxic average	0.30	n.a.	n.a.	n.a.	15.06
	OCL anoxic standard deviation	0.00	n.a.	n.a.	n.a.	n.a.
	OCL oxic blank	0.34	n.a.	n.a.	n.a.	58.55
	OCL oxic average	0.37	n.a.	n.a.	n.a.	24.69
	OCL oxic standard deviation	0.10	n.a.	n.a.	n.a.	17.01

1 day	OCL anoxic blank	0.66	n.a.	n.a.	n.a.	20.28
	OCL anoxic average	0.28	n.a.	n.a.	n.a.	15.35
	OCL anoxic standard deviation	0.01	n.a.	n.a.	n.a.	2.50
	OCL oxic blank	0.27	n.a.	n.a.	n.a.	16.01
	OCL oxic average	0.30	n.a.	n.a.	n.a.	14.70
	OCL oxic standard deviation	0.02	n.a.	n.a.	n.a.	2.96
1 week	OCL anoxic blank	0.34	n.a.	n.a.	n.a.	17.73
	OCL anoxic average	0.57	n.a.	n.a.	n.a.	22.11
	OCL anoxic standard deviation	0.03	n.a.	n.a.	n.a.	3.49
	OCL oxic blank	0.40	n.a.	n.a.	n.a.	22.10
	OCL oxic average	0.48	n.a.	n.a.	n.a.	20.79
	OCL oxic standard deviation	0.08	n.a.	n.a.	n.a.	2.74
3 weeks	OCL anoxic blank	1.30	n.a.	n.a.	n.a.	28.01
	OCL anoxic average	1.12	n.a.	n.a.	n.a.	30.62
	OCL anoxic standard deviation	0.22	n.a.	n.a.	n.a.	2.11
	OCL oxic blank	4.51	n.a.	n.a.	n.a.	24.44
	OCL oxic average	1.01	n.a.	n.a.	n.a.	30.95
	OCL oxic standard deviation	0.38	n.a.	n.a.	n.a.	1.43
6 weeks	OCL anoxic blank	1.97	n.a.	n.a.	n.a.	15.85
	OCL anoxic average	1.13	n.a.	0.04	n.a.	11.00
	OCL anoxic standard deviation	0.37	n.a.	n.a.	n.a.	8.50
	OCL oxic blank	2.59	n.a.	0.06	n.a.	10.52
	OCL oxic average	0.90	0.12	0.05	n.a.	5.41

	OCL oxic standard deviation	0.35	0.03	0.01	n.a.	4.28
12 weeks	OCL anoxic blank	2.68	0.34	0.04	n.a.	19.66
	OCL anoxic average	1.74	0.12	0.04	n.a.	11.10
	OCL anoxic standard deviation	0.51	0.00	0.01	n.a.	0.75
	OCL oxic blank	4.13	0.11	0.05	n.a.	14.99
	OCL oxic average	0.97	0.15	0.04	n.a.	12.35
	OCL oxic standard deviation	0.27	n.a.	0.01	n.a.	4.99
21 weeks	OCL anoxic blank	3.51	0.11	0.04	n.a.	22.14
	OCL anoxic average	2.21	0.14	0.04	n.a.	13.67
	OCL anoxic standard deviation	0.62	0.02	0.01	n.a.	0.63
	OCL oxic blank	4.33n.a.		0.05	n.a.	27.30
	OCL oxic average	1.15	0.14	0.04	n.a.	25.05
	OCL oxic standard deviation	0.38	0.00	0.00	n.a.	2.40
15 months	OCL anoxic blank	4.76	0.20	0.06	n.a.	14.59
	OCL anoxic average	3.93	0.23	0.06	0.04	15.75
	OCL anoxic standard deviation	0.44	0.02	0.01	n.a.	0.64
	OCL oxic blank	5.08	0.14	0.08	n.a.	18.49
	OCL oxic average	1.59	0.14	0.06	0.02	15.16
	OCL oxic standard deviation	0.58	0.06	0.02	n.a.	1.98

Table A5: Cation concentrations in the anoxic experimental blanks (mg l^{-1})

	YCL							ICL							OCL						
	Ca	Ca	Al	Al	Si	Si	U	Ca	Ca	Al	Al	Si	Si	U	Ca	Ca	Al	Al	Si	Si	U
Time (weeks)	Blank no U(VI)	U(VI) Blank	Blank no U(VI)	U(VI) Blank	Blank no U(VI)	U(VI) Blank	Blank	Blank no U(VI)	U(VI) Blank	Blank no U(VI)	U(VI) Blank	Blank no U(VI)	U(VI) Blank	Blank	Blank no U(VI)	U(VI) Blank	Blank no U(VI)	U(VI) Blank	Blank no U(VI)	U(VI) Blank	Blank
0	5.17	5.58	0.46	0.64	12.23	14.78	9.81	799.92	828.52	0.15	0.08	5.38	5.26	0.97	6.52	6.73	0.03	7.21	0.00	0.31	0.97
0.00595	-	-	-	-	-	-	-	-	-	-	-	-	-	-	-	6.53	-	6.00	-	0.24	0.91
0.14286	-	-	-	-	-	-	-	-	908.05	-	0.61	-	6.15	0.69	-	6.59	-	6.06	-	0.20	0.70
0.42857	-	4.85	-	0.48	-	14.16	9.40	-	891.88	-	0.11	-	5.61	0.70	-	-	-	-	-	-	-
1	5.54	5.06	0.29	0.56	5.95	14.32	9.16	796.84	-	0.13	-	5.23	-	-	6.42	4.46	0.01	4.44	0.03	0.14	0.13
1.42857	-	-	-	-	-	-	-	-	877.91	-	0.11	-	5.51	0.46	-	-	-	-	-	-	-
3	5.43	-	0.64	-	14.38	-	-	-	-	-	-	-	-	-	6.47	9.33	0.03	11.51	0.02	0.51	0.10
4	-	5.08	-	0.51	-	14.34	9.19	-	-	-	-	-	-	-	-	-	-	-	-	-	-
5	-	-	-	-	-	-	-	-	799.70	-	0.04	-	6.12	0.20	-	-	-	-	-	-	-
6	5.16	-	0.65	-	14.44	-	-	-	-	-	-	-	-	-	6.41	9.21	1.31	11.34	0.13	0.35	0.09
8	--	5.01	-	0.57	-	14.17	9.28	-	-	-	-	-	-	-	-	-	-	-	-	-	-
9								-	852.87	-	0.07	-	5.76	0.14	-	-	-	-	-	-	-
12	5.31	5.12	0.69	0.54	14.41	14.21	9.32	788.04	844.07	0.12	-0.04	5.45	5.68	0.11	6.60	9.33	0.53	11.73	0.08	0.50	0.07
21	-	-	-	-	-	-	-	-	-	-	-	-	-	-	-	9.21	-	9.46	-	0.31	0.06
26	-	-	0.51	0.50	12.06	13.83	9.08	799.37	816.93	0.11	0.29	5.41	5.76	0.06	-	-	-	-	-	-	-
29	-	-	-	-	-	-	-	-	-	-	-	-	-	-	9.23	-	5.17	-	0.46	-	-
48	-	-	-	-	-	-	-	-	725.45	-	0.50	-	8.00	0.04	-	-	-	-	-	-	-

	YCL							ICL							OCL							
	Ca	Ca	Al	Al	Si	Si	U	Ca	Ca	Al	Al	Si	Si	U	Ca	Ca	Al	Al	Si	Si	U	
Time (weeks)	Blank no U(VI)	U(VI) Blank	Blank no U(VI)	U(VI) Blank	Blank no U(VI)	U(VI) Blank	Blank	Blank no U(VI)	U(VI) Blank	Blank no U(VI)	U(VI) Blank	Blank no U(VI)	U(VI) Blank	Blank	Blank no U(VI)	U(VI) Blank	Blank no U(VI)	U(VI) Blank	Blank no U(VI)	U(VI) Blank	Blank	
51	6.28	-	0.68	-	17.90	-	-	-	-	-	-	-	-	-	-	-	-	-	-	-	-	-
52	-	-	-	-	-	-	-	736.56	-	0.32	-	7.68	-	-	9.44	9.64	5.32	9.78	0.29	0.34	0.27	
54	-	5.98	-	0.77	-	21.22	8.35	-	-	-	-	-	-	-	-	-	-	-	-	-	-	-
72	-	-	-	-	-	-	-	-	-	-	-	-	-	-	-	9.54	-	14.09	-	0.64	0.48	
78	6.11	-	0.66	-	17.92	-	-	-	-	-	-	-	-	-	9.10	-	7.39	-	0.53	-	-	
78.2143	-	5.93	-	0.77	-	21.23	7.97	-	-	-	-	-	-	-	-	-	-	-	-	-	-	

Table A6: Saturation indices of the U(VI)-bearing phases in YCL at each time point during reaction with sandstone predicted using thermodynamic modelling

Time (weeks)	0	0.46	1	4	8	12	26	51	78
Becquerelite(nat)	-2.52	-2.72	-2.71	-2.73	-2.86	-3.02		-3.38	-3.52
Becquerelite(syn)	-17.2	-17.39	-17.39	-17.4	-17.53	-17.69		-18.05	-18.2
CaU2O7:3H2O(cr)	-1.57	-1.77	-1.76	-1.77	-1.9	-2.06		-2.43	-2.57
Clarkeite	3.8	3.78	3.78	3.79	3.78	3.78	3.77	3.77	3.77
Compreignacite	-9.98	-10.01	-10.01	-10	-10.01	-10.01	-10.02	-10.02	-10.03
Schoepite	-5.59	-5.59	-5.59	-5.59	-5.59	-5.59	-5.59	-5.59	-5.59
Schoepite(desy)	-4.16	-4.16	-4.16	-4.16	-4.16	-4.16	-4.16	-4.16	-4.16
Soddyite(synt1)	-10.99	-10.43	-10.43	-10.39	-10.36	-10.31	-10.22	-10.03	-9.94
Soddyite(synt2)	-13.31	-12.75	-12.75	-12.7	-12.68	-12.62	-12.53	-12.34	-12.26
Sodium-compreignacite	-8.97	-9.01	-9.01	-8.99	-9	-9.01	-9.02	-9.03	-9.03
U2O7Na2(s)	3.47	3.43	3.43	3.45	3.44	3.43	3.42	3.42	3.41
UO2(OH)2(beta)	-4.08	-4.08	-4.08	-4.08	-4.08	-4.08	-4.08	-4.08	-4.08
UO3(alfa)	-8.37	-8.37	-8.37	-8.37	-8.37	-8.37	-8.37	-8.37	-8.37
UO3(beta)	-7.21	-7.21	-7.21	-7.21	-7.21	-7.21	-7.21	-7.21	-7.21
UO4Ca(cr)	6.64	6.44	6.45	6.44	6.3	6.14		5.78	5.64
UO4Na2(alfa)	-4.33	-4.36	-4.37	-4.35	-4.36	-4.36	-4.38	-4.38	-4.39
Uranophane	-3.28	-2.37	-2.35	-2.28	-2.36	-2.41		-2.21	-2.18

Table A7: Saturation indices of the U(VI)-bearing phases in ICL at each time point during reaction with sandstone predicted using thermodynamic modelling

Time (weeks)	0	0.14	0.46	1.43	5	9	12	26	48
Becquerelite(nat)	-2.61	-2.59	-2.59	-2.6	-2.61	-2.61	-2.61	-2.64	-2.65
Becquerelite(syn)	-17.28	-17.26	-17.26	-17.27	-17.28	-17.28	-17.28	-17.31	-17.33
CaU2O7:3H2O(cr)	-0.71	-0.68	-0.69	-0.7	-0.71	-0.71	-0.71	-0.74	-0.77
Clarkeite	0.41	0.45	0.43	0.43	0.65	0.66	0.65	0.63	0.37
Compreignacite	-15.18	-15.11	-15.12	-15.12	-15.12	-15.12	-15.12	-15.16	-15.16
Schoepite	-5.83	-5.83	-5.83	-5.83	-5.83	-5.83	-5.83	-5.83	-5.83
Schoepite(desy)	-4.4	-4.4	-4.4	-4.4	-4.4	-4.4	-4.4	-4.4	-4.4
Soddyite(synt1)	-10.49	-10.44	-10.43	-10.46	-10.43	-10.44	-10.45	-10.46	-10.35
Soddyite(synt2)	-12.81	-12.76	-12.75	-12.77	-12.75	-12.75	-12.76	-12.77	-12.66
Sodium-compreignacite	-16.69	-16.63	-16.65	-16.65	-16.22	-16.2	-16.21	-16.24	-16.77
U2O7Na2(s)	-3.31	-3.24	-3.27	-3.27	-2.84	-2.82	-2.83	-2.87	-3.4
UO2(OH)2(beta)	-4.32	-4.32	-4.32	-4.32	-4.32	-4.32	-4.32	-4.32	-4.32
UO3(alfa)	-8.61	-8.61	-8.61	-8.61	-8.61	-8.61	-8.61	-8.61	-8.61
UO3(beta)	-7.46	-7.46	-7.46	-7.46	-7.46	-7.46	-7.46	-7.46	-7.45
UO4Ca(cr)	7.73	7.76	7.75	7.74	7.73	7.73	7.73	7.7	7.67
UO4Na2(alfa)	-10.86	-10.8	-10.82	-10.82	-10.39	-10.37	-10.38	-10.42	-10.96
Uranophane	-0.45	-0.32	-0.31	-0.36	-0.33	-0.34	-0.36	-0.42	-0.22

Table A8: Saturation indices of the U(VI)-bearing phases in OCL at each time point during reaction with sandstone predicted using thermodynamic modelling

Time (weeks)	0	0.006	0.14	1	3	6	12	21	52	72
Becquerelite(nat)	4.03	4	3.99	3.92	4.11	4.11	4.11	4.1	4.11	4.08
Becquerelite(syn)	-10.65	-10.67	-10.69	-10.76	-10.57	-10.57	-10.57	-10.58	-10.57	-10.59
CaU2O7:3H2O(cr)	-2.02	-2.05	-2.06	-2.13	-1.93	-1.93	-1.93	-1.94	-1.93	-1.95
Clarkeite	0.42	-0.38	-0.68	-0.78	0.03	0.02	-0.05	-0.09	-0.07	-0.2
Compreignacite	-10.23	-11.28	-11.31	-9.86	-9.1	-9.1	-9.08	-9.07	-9.06	-9.19
Schoepite	-3.84	-3.84	-3.84	-3.84	-3.84	-3.84	-3.84	-3.84	-3.84	-3.84
Schoepite(desy)	-2.41	-2.41	-2.41	-2.41	-2.42	-2.42	-2.42	-2.42	-2.42	-2.42
Soddyite(synt1)	-4.23	-4.3	-4.29	-4.33	-3.95	-3.95	-3.99	-4.03	-4.05	-3.92
Soddyite(synt2)	-6.55	-6.62	-6.61	-6.64	-6.27	-6.26	-6.31	-6.35	-6.36	-6.24
Sodium-compreignacite	-8.74	-10.33	-10.92	-11.13	-9.52	-9.53	-9.68	-9.75	-9.73	-9.98
U2O7Na2(s)	-3.3	-4.9	-5.49	-5.7	-4.08	-4.09	-4.24	-4.31	-4.29	-4.54
UO2(OH)2(beta)	-2.34	-2.33	-2.33	-2.33	-2.34	-2.34	-2.34	-2.34	-2.34	-2.34
UO3(alfa)	-6.63	-6.63	-6.63	-6.63	-6.63	-6.63	-6.63	-6.63	-6.63	-6.63
UO3(beta)	-5.47	-5.47	-5.47	-5.47	-5.48	-5.48	-5.48	-5.47	-5.47	-5.47
UO4Ca(cr)	4.44	4.41	4.39	4.32	4.53	4.53	4.53	4.52	4.53	4.5
UO4Na2(alfa)	-12.84	-14.44	-15.03	-15.24	-13.61	-13.63	-13.78	-13.85	-13.82	-14.07
Uranophane	2.83	2.65	2.66	2.52	3.49	3.49	3.41	3.32	3.3	3.51

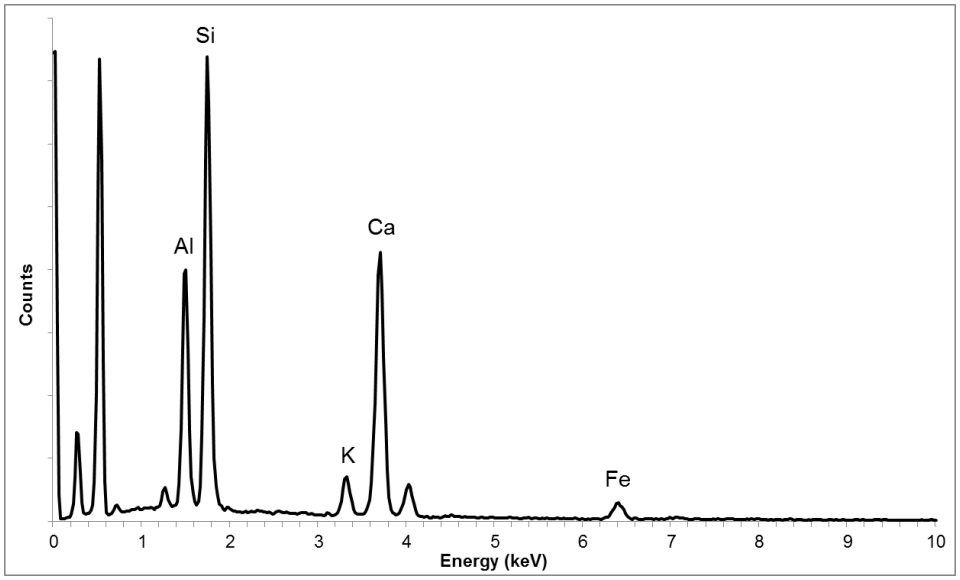

Figure A2: EDX of C-S-H formed on alumino-silicate grain surfaces after 26 weeks of reaction in YCL.

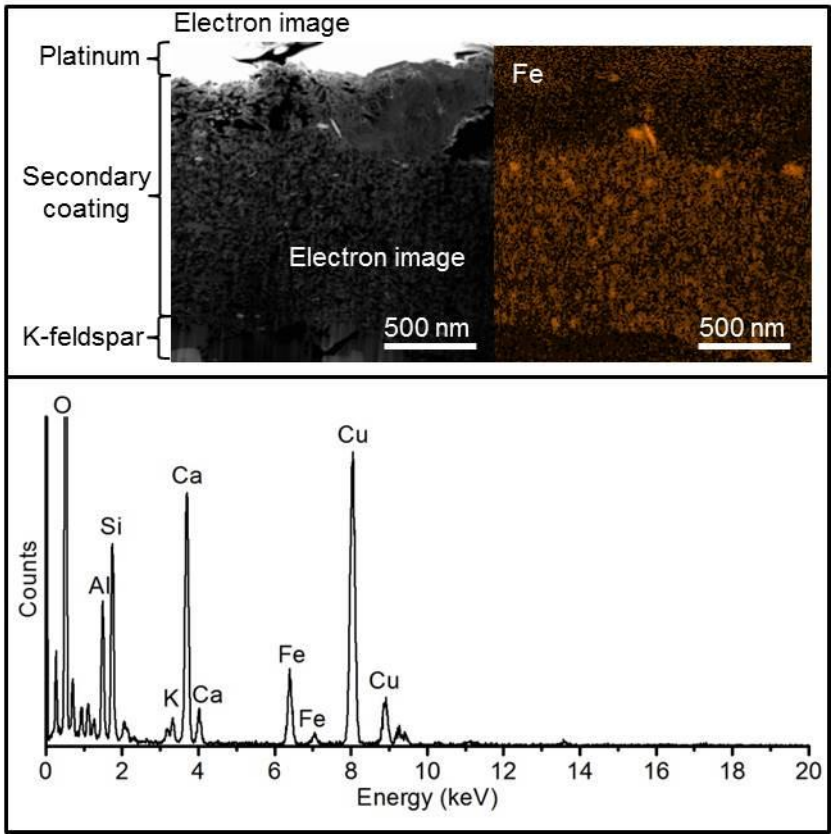

Figure A3: TEM Fe map through secondary phase section from ICL altered feldspar grain and EDX spectrum for and Fe-bearing area

Table A9: Co-ordination numbers for shells in the fitting models applied to the OCL EXAFS data

Fit	a)	b)	c)	d)	e)	f)	g)	h)	i)	j)	k)	l)	m)	n)	o)	p)	q)	r)	s)	t)	u)
	6 weeks					12 weeks				21 weeks							15 months				
Oax	2	2	2	2	2	2	2	2	2	2	2	2	2	2	2	2	2	2	2	2	2
Oeq1	5	5	5	5	5	4	4	3	3	4	4	4	3	3	3	3	4	5	4	4	4
Oeq2				1	1			3	3				3	3	3	3			2	2	2
Si1		1	1	1	1		1	1	1		1	1	1	1	1	1		1	1	1	1
Si2		1	1	1	1		2	2	2		2	2	1	1	1	1		3	3	3	3
U			2		1				2			2		2		2				3	
Ca																2	2				2

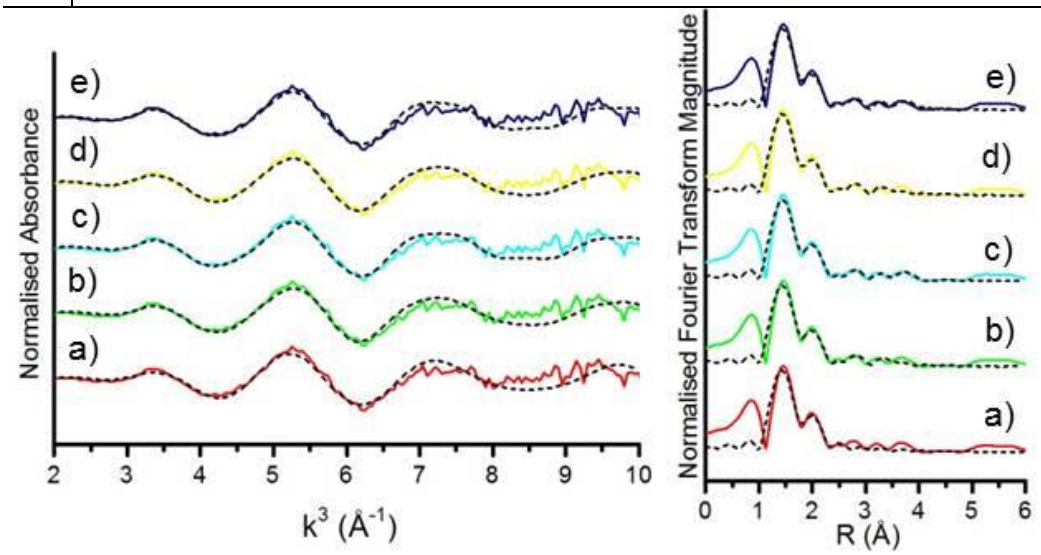

Figure A4: OCL EXAFS data and fits 6 weeks

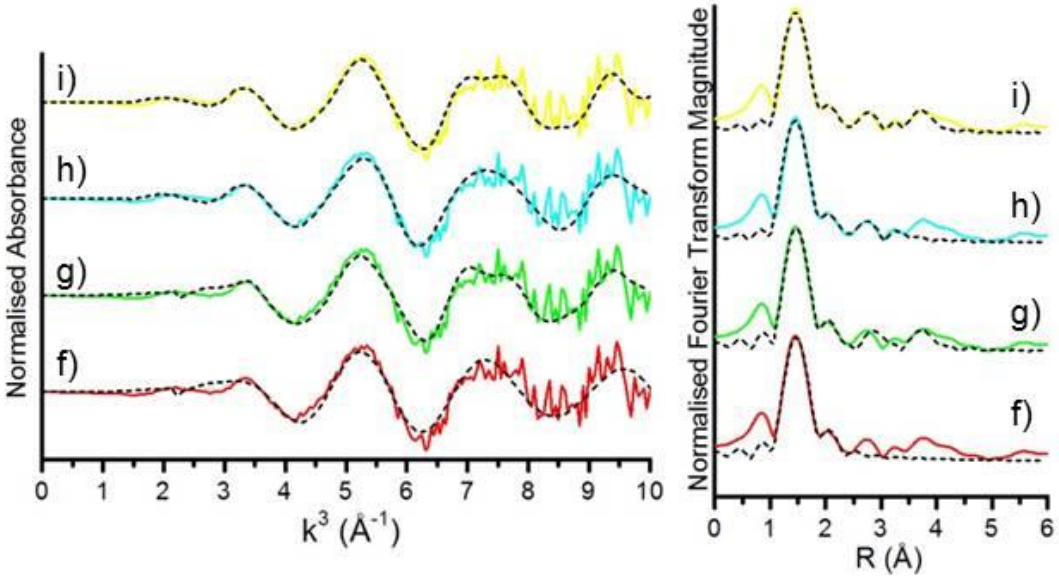

Figure A5: OCL EXAFS data and fits 12 weeks

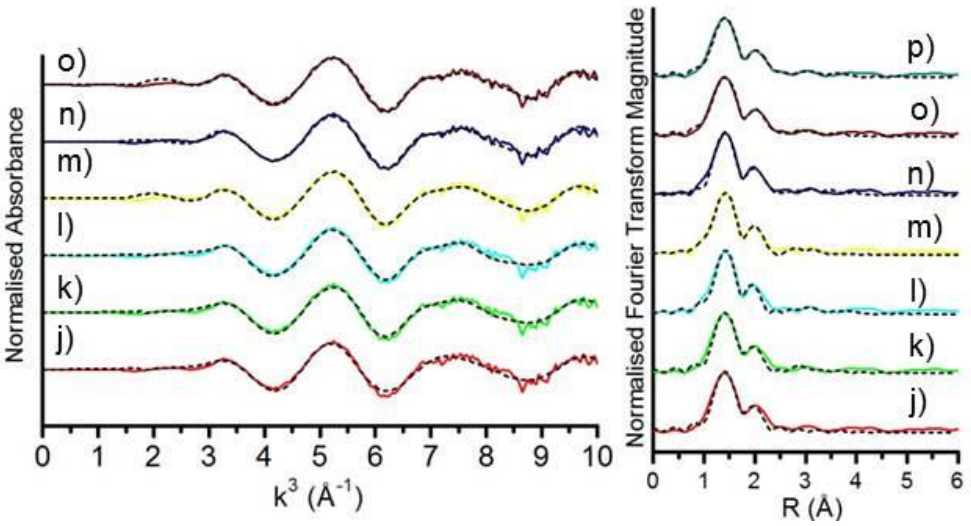

Figure A6: OCL EXAFS data and fits 21 weeks

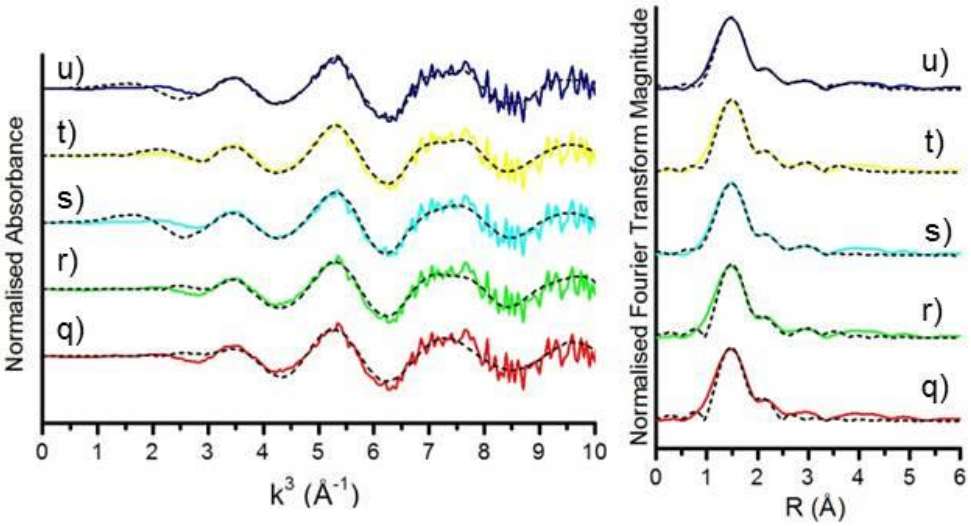

Figure A7: OCL EXAFS data and fits 15 months

Table A10: Parameters for EXAFS fits a)-u)

	Shell	N	σ^2	R	Reduced chi-square	R-factor	ΔE0 (eV)
a)	O_{ax}	2	0.00028	1.8287	80.20559	0.019036	11.509
	O_{eq}	5	0.00889	2.38308			
b)	O_{ax}	2	0.00081	1.83384	52.16941	0.017625	12.505
	O_{eq}	5	0.00969	2.39326			
	Si_1	1	0.00639	3.21378			
	Si_2	1	0.0036	3.77946			
c)	O_{ax}	2	0.00071	1.83258	28.4541	0.011801	12.198
	O_{eq}	5	0.0094	2.38875			
	Si_1	1	0.00762	3.21332			
	Si_2	1	0.00652	3.76088			

	U	2	0.01165	3.90515			
d)	O_{ax}	2	0.00001	1.83175	45.92648	0.015621	12.094
	O_{eq1}	5	0.00802	2.37616			
	O_{eq2}	1	0.00948	2.53689			
	Si_1	1	0.00553	3.21319			
	Si_2	1	0.00313	3.77514			
e)	O_{ax}	2	0.00018	1.83037	54.97827	0.011256	11.619
	O_{eq1}	5	0.00857	2.37023			
	O_{eq2}	1	0.00873	2.50579			
	Si_1	1	0.00651	3.2074			
	Si_2	1	0.0089	3.79506			
	U	1	0.0052	3.86816			
f)	O_{ax}	2	0.00294	1.83949	26.03745	0.045986	12.889
	O_{eq}	4	0.01802	2.38748			
g)	O_{ax}	2	0.00281	1.85972	14.89907	0.0152269	16.927
	O_{eq}	4	0.00214	2.42267			
	Si_1	1	0.00360	3.19698			
	Si_2	2	0.00561	4.10515			
h)	O_{ax}	2	0.00097	1.82109	28.04144	0.017341	8.696
	O_{eq1}	3	0.00324	2.27199			
	O_{eq2}	3	0.00423	2.45088			
	Si_1	1	0.0012	3.14214			
	Si_2	2	0.00986	3.73868			
i)	O_{ax}	2	0.00141	1.82317	35.2578	0.004623	8.734
	O_{eq1}	3	0.00419	2.27073			
	O_{eq2}	3	0.00537	2.45124			
	Si_1	1	0.00234	3.14467			
	Si_2	2	0.02287	3.65324			
	U	2	0.0059	3.85174			
j)	O_{ax}	2	0.00355	1.81450	66.24970	0.030830	10.373
	O_{eq}	4	0.01283	2.40243			
k)	O_{ax}	2	0.00275	1.82609	58.15099	0.016847	13.138
	O_{eq}	4	0.01076	2.43099			
	Si_1	1	0.00192	3.10080			
	Si_2	2	0.00675	3.30871			
l)	O_{ax}	2	0.00284	1.82599	71.76588	0.014687	13.135
	O_{eq}	4	0.01091	2.43235			
	Si_1	1	0.00099	3.10033			
	Si_2	2	0.00540	3.30400			

	U	2	0.03268	3.62501			
m)	O_{ax}	2	0.00766	1.81795	18.56062	0.009743	7.084
	O_{eq1}	3	0.01482	2.22356			
	O_{eq2}	3	0.00842	2.42745			
	Si_1	1	0.01554	3.16115			
	Si_2	1	0.01117	3.69297			
n)	O_{ax}	2	0.00152	1.79625	32.2688	0.009745	7.006
	O_{eq1}	3	0.00215	2.27798			
	O_{eq2}	3	0.0003	2.44903			
	Si_1	1	0.00714	3.1488			
	Si_2	1	0.0007	3.65948			
	U	2	0.01346	3.91639			
o)	O_{ax}	2	0.00936	1.82575	41.2793	0.006558	7.265
	O_{eq1}	3	0.01445	2.21108			
	O_{eq2}	3	0.00896	2.42935			
	Si_1	1	0.01621	3.13692			
	Si_2	1	0.008	3.69027			
	Ca	2	0.03084	3.81043			
p)	O_{ax}	2	0.0069	1.82854	78.93102	0.004321	10.936
	O_{eq1}	3	0.02187	2.24288			
	O_{eq2}	3	0.00995	2.45036			
	Si_1	1	0.00601	3.1056			
	Si_2	1	0.00567	3.30617			
	U	2	0.02407	3.86032			
	Ca	2	0.01769	4.01736			
q)	O_{ax}	2	0.00161	1.85307	50.3426	0.028161	18.066
	O_{eq}	4	0.01341	2.42433			
r)	O_{ax}	2	0.00151	1.85678	12.64497	0.015926	18.455
	O_{eq}	5	0.0163	2.43486			
	Si_1	1	0.00258	3.25132			
	Si_2	3	0.02146	4.05605			
s)	O_{ax}	2	0.01524	1.84241	12.19338	0.009081	-1.232
	O_{eq1}	4	0.01487	2.18411			
	O_{eq2}	2	0.01163	2.39316			
	Si_1	1	0.01588	3.14591			
	Si_2	3	0.03546	3.55245			
t)	O_{ax}	2	0.00723	1.84105	33.36225	0.006717	9.143
	O_{eq1}	4	0.01071	2.26125			
	O_{eq2}	2	0.00464	2.45684			

	Si_1	1	0.007	3.20947			
	Si_2	3	0.02885	3.61382			
	U	3	0.02359	3.8335			
u)	O_{ax}	2	0.0123	1.83217	10.06909	0.001967	-2.475
	O_{eq1}	4	0.01136	2.17484			
	O_{eq2}	2	0.00763	2.37117			
	Si_1	1	0.01051	3.13596			
	Si_2	3	0.03392	3.50315			
	Ca	2	0.01445	4.6388			

Appendix B
Supplementary information to chapter 5

Table B1: Concentration of Cl^- in solution in YNFP and ENFG reacted with BVG at 0, 4, 9 and 15 months and 15 years and solution blanks (to 3 s.f.)

YNFP			YNFP + BVG		ENFG		ENFG + BVG	
Time (months)	Concentration (mg/l)	increase factor	Concentration (mg/l)	increase factor	Concentration (mg/l)	increase factor	Concentration (mg/l)	increase factor
0	63.7	n/a	63.7	n/a	15100	n/a	15100	n/a
4	85.8	1.347	298	4.678	15100	1	16270	1.077
9	131	2.057	423	6.641	16400	1.086	16700	1.106
15	123	1.931	412	6.468	15659	1.037	15796	1.046
184	150	2.355	600	9.419	20250	1.341	20240	1.340

Table B2: Concentration of major ions in solution in YNFP and ENFG reacted with BVG for 15 years and solution blanks uncorrected and corrected for evaporation (to 3 s.f.)

	Na	K	Ca	Mg	Si	Al	CO_3
Concentration in YNFP after 15 years reaction (mgl^{-1})	2670	3070	0.450	0.0600	49.2	0.0400	6790
Corrected concentration in YNFP after 15 years reaction (mgl^{-1})	1990	2290	0.336	0.0448	36.7	0.0299	5070
Concentration in YNFP blank after 15 years (mgl^{-1})	2610	4340	0.600	0.0200	7.31	0.0300	1380
Corrected concentration in YNFP blank after 15 years (mgl^{-1})	1950	3240	0.448	0.0149	5.46	0.0224	1030
Concentration after 15 years reaction in ENFG (mgl^{-1})	11700	286	1180	268	13.3	BDL	BDL

Corrected concentration after 15 years reaction in ENFG (mgl^{-1})	8690	214	878	200	9.93	-	-
Concentration in ENFG blank after 15 years (mgl^{-1})	11900	248	1850	BDL	0.12	BDL	BDL
Corrected concentration in ENFG blank after 15 years (mgl^{-1})	8850	185	1380	-	0.0900	-	-

Details of X-ray Diffraction (XRD) sample preparation and data analysis

Prior to analysis the samples were rinsed in isopropanol, milled, and microionised under acetone with 10% corundum internal standard added (American Elements, Al_2O_3, AL-OX-03-P). The samples were then back-loaded into stainless steel sample holders and analysed using a PANalytical X'Pert Pro series diffractometer with a cobalt-target tube, X'Celerator detector operated at 45kV and 40mA. They were scanned at4.5-85°2θ at 2.76°2θ/minute. The diffraction data were analysed using PANalytical X'Pert Highscore Plus version 2.2e software coupled to the latest version of the International Centre for Diffraction Data (ICDD) database. After identification of the mineral species present, quantification was conducted using Rietveld refinement e.g.(Snyder and Bish, 1989). In order to quantify the clay phases present, an additional portion of material was ground and dispersed in deionised water using a reciprocal shaker combined with ultrasound treatment. Each suspension was then allowed to stand with a few drops of sodium hexametaphosphate to prevent the flocculation of clay crystals. After a time period determined from Stokes' Law, the <2 µm size fraction was isolated and dried at 55 °C. 15 mg of this <2 µm material was re-suspended in a minimum of deionised water, Ca-saturated with 0.1M $CaCl_2.6H_2O$ solution, washed, pipetted onto a 'zerp-background' silicon crystal substrate and air-dried overnight. The <2 µm samples were then scanned from 2-40°2θ at 1.02°2θ/minute after ethylene glycol solvation and heating at 550°C for 2 hours. Clay species were identified from their characteristic peak positions and their reaction to the diagnostic testing program. Quantification was again conducted through Rietveld refinement using PANalytical Highscore Plus software. To gain further information about the nature of the clay minerals present and assess their relative proportions, modelling of the XRD profiles was conducted using Newmod-for-Windows™ (Reynolds and Reynnolds,

1996) software. An estimate of the crystallite size distribution was also determined following the method outlined in (Moore and Reynolds, 1997).

References:

MOORE, D. M. & REYNOLDS, R. C. 1997. *X-ray diffraction anf the identification and analysis of clay minerals, second edition,* New York, Oxford University Press.

REYNOLDS, R. C. and REYNOLDS, R. C. 1996. Description of Newmod-for-Windows™. The calculation of one-dimensional X-ray diffraction patterns of mixed layered clay minerals. R C Reynolds Jr., 8 Brook Road, Hanover, NH.

SNYDER, R. L. & BISH, D. L. 1989. Quantitative analysis. *In:* L, B. D. & E, P. J. (eds.) *Modern powder diffraction, reviews in mineralogy.* USA: Mineralogical Society of America.

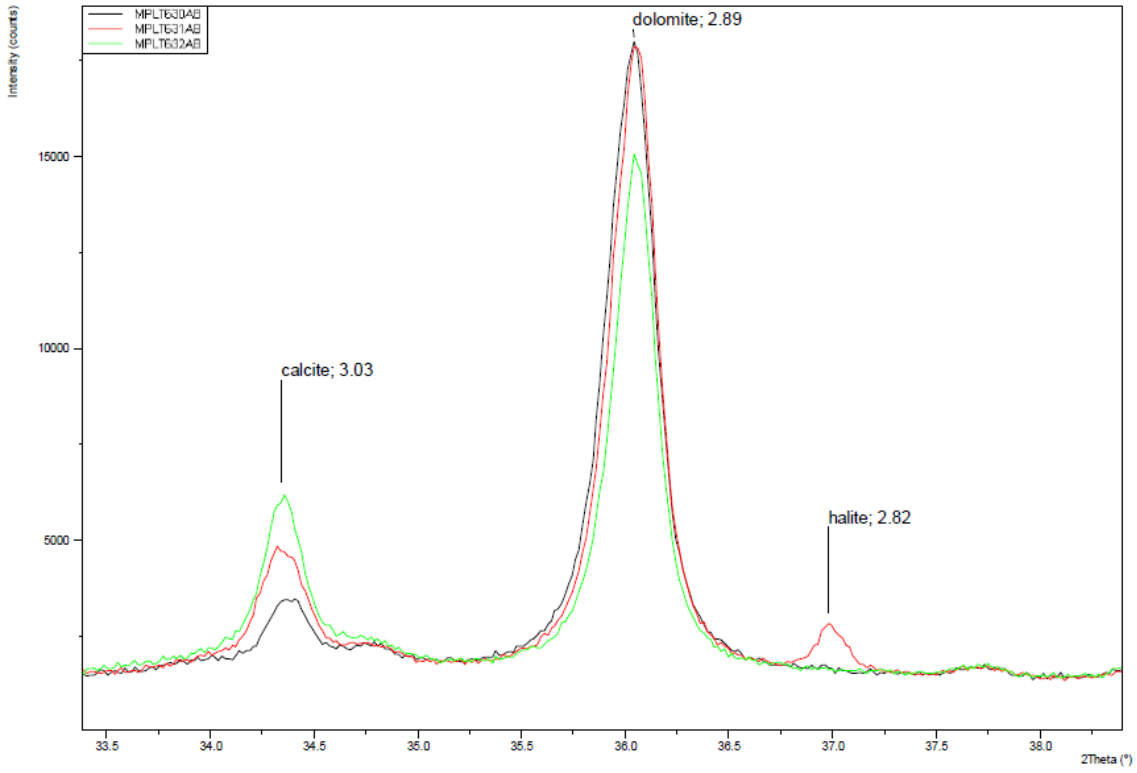

Figure B1: XRD patterns for bulk BVG rock (Unaltered - black, YNFP altered - green, ENFG altered - red)

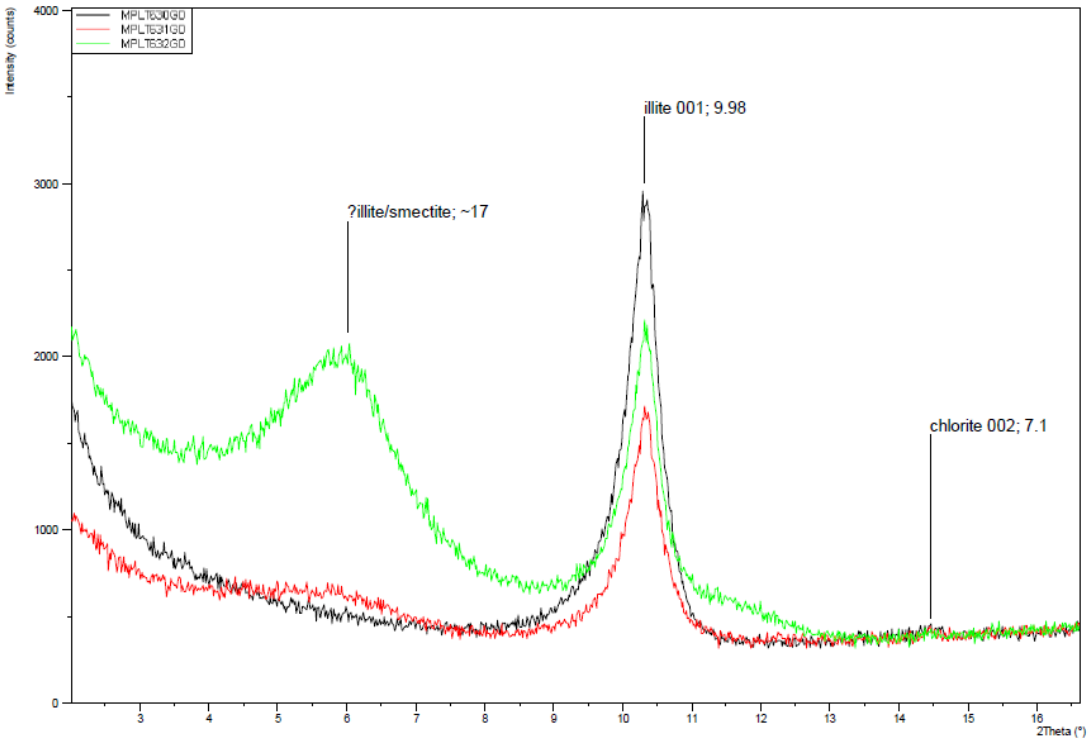

Figure B2: XRD patterns for the <2µm size fraction after Ca saturation, glycol treatment and heating at 550°C for 2 hours (Unaltered - black, YNFP altered - green, ENFG altered - red)

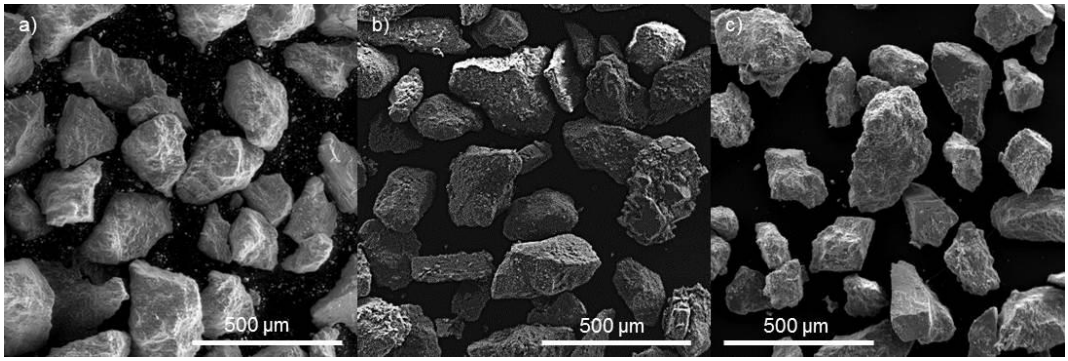

Figure B3: SEM image of a) unaltered BVG grains and grains reacted for 15 years in a) YNFP and b) ENFG.

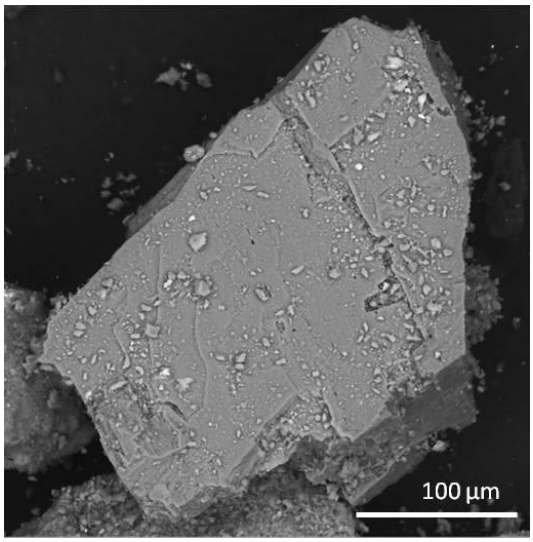

Figure B4: Unaltered dolomite from original BVG material used in this study

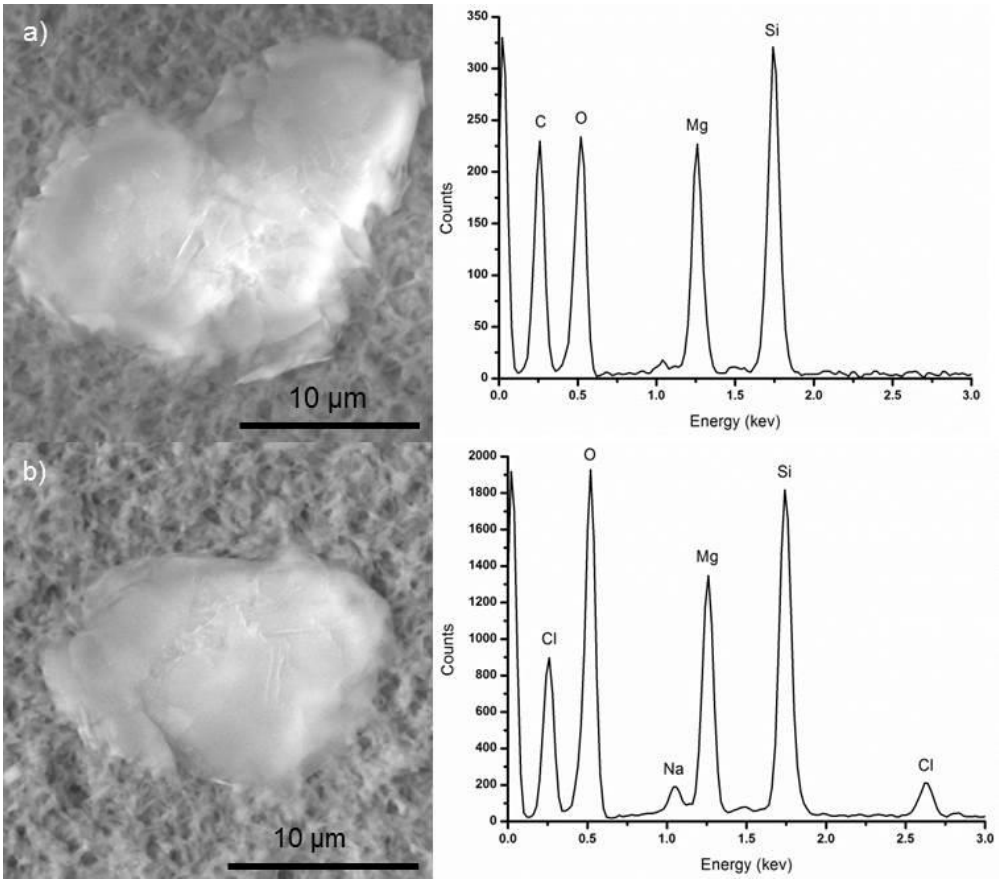

Figure B5: SEM images and EDX analyses of Mg-silicate particle filtered from a) YNFP solution reacted with disaggregated BVG for 15 years and b) ENFG solution reacted with disaggregated BVG for 15 years

Supplementary information for computer modelling

Table B3: Saturation Indices (SI) of all oversaturated silicate and all carbonate phases in YNFP and ENFG at 15 years of reaction extracted from PHREEQC output

YNFP				
Phase	SI	log IAP	log KT	Formula
Aragonite	0.07	1.4	1.33	CaCO3
Calcite	0.22	1.4	1.18	CaCO3
Chrysotile*	1.09	27.06	25.97	Mg3Si2O5(OH)4
Clinochlore-14A*	-0.09	52.82	52.91	Mg5Al2Si3O10(OH)8
Dolomite	0.9	1.92	1.01	CaMg(CO3)2
Dolomite-dis	-0.35	1.92	2.27	CaMg(CO3)2
Dolomite-ord	0.91	1.92	1	CaMg(CO3)2
Magnesite	-0.7	0.51	1.22	MgCO3
Phlogopite*	3.85	33.88	30.02	KAlMg3Si3O10(OH)2
Saponite-Ca	1.21	22.37	21.16	Ca.165Mg3Al.33Si3.67O10(OH)2
Saponite-H	-0.16	20.21	20.38	H.33Mg3Al.33Si3.67O10(OH)2
Saponite-K	1.86	23	21.14	K.33Mg3Al.33Si3.67O10(OH)2
Saponite-Mg	1.17	22.22	21.05	Mg3.165Al.33Si3.67O10(OH)2
Saponite-Na	1.64	23.01	21.37	Na.33Mg3Al.33Si3.67O10(OH)2
Talc	0.3	17.65	17.34	Mg3Si4O10(OH)2
ENFG				
Amesite-14A	5.85	62.76	56.91	Mg4Al4Si2O10(OH)8
Anthophyllite*	9.59	64.51	54.92	Mg7Si8O22(OH)2
Aragonite	-0.58	0.75	1.33	CaCO3
Brucite	-0.04	13.72	13.76	Mg(OH)2
Calcite	-0.44	0.75	1.18	CaCO3
Celadonite*	2.25	7.6	5.34	KMgAlSi4O10(OH)2
Chrysotile*	7.3	33.28	25.97	Mg3Si2O5(OH)4
Clinochlore-14A*	11.75	64.65	52.91	Mg5Al2Si3O10(OH)8
Clinochlore-7A	8.67	64.65	55.98	Mg5Al2Si3O10(OH)8
Diopside*	2.22	19.92	17.7	CaMgSi2O6
Dolomite	0.12	1.13	1.01	CaMg(CO3)2
Dolomite-dis	-1.13	1.13	2.27	CaMg(CO3)2
Dolomite-ord	0.13	1.13	1	CaMg(CO3)2
Enstatite*	0.45	9.78	9.33	MgSiO3
Forsterite*	0.45	23.51	23.05	Mg2SiO4
Mesolite	1.14	10.32	9.18	Na.676Ca.657Al1.99Si3.01O10:2.647H2O

Phlogopite*	8.97	39	30.02	KAlMg3Si3O10(OH)2
Saponite-Ca	9.16	30.32	21.16	Ca.165Mg3Al.33Si3.67O10(OH)2
Saponite-H	7.61	27.99	20.38	H.33Mg3Al.33Si3.67O10(OH)2
Saponite-K	8.74	29.88	21.14	K.33Mg3Al.33Si3.67O10(OH)2
Saponite-Mg	9.2	30.26	21.05	Mg3.165Al.33Si3.67O10(OH)2
Saponite-Na	9.12	30.49	21.37	Na.33Mg3Al.33Si3.67O10(OH)2
Sepiolite	4.84	31.19	26.35	Mg4Si6O15(OH)2:6H2O
Talc	8.05	25.39	17.34	Mg3Si4O10(OH)2
Tremolite*	14.1	65.23	51.13	Ca2Mg5Si8O22(OH)2

* indicates high temperature phase

The thermodynamic database used in this study is the Lawrence Livermore National Laboratory (LLNL) database. However, the data for C-S-H gel were added to the database from the literature sources detailed below:

Dolomite

CaMg(CO3)2 = Ca+2 + Mg+2 + 2 CO3-2

log_k -17.090

delta_h -9.436 kcal

Saponite-K

K.33Mg3Al.33Si3.67O10(OH)2 +7.3200 H+ = + 0.3300 Al+++ + 0.3300 K+ + 3.0000 Mg++ + 3.6700 SiO2 + 4.6600 H2O

log_k 26.0075

-delta_H -196.402 kJ/mol # Calculated enthalpy of reaction Saponite-K

Enthalpy of formation: -1437.74 kcal/mol

-analytic 3.2113e+001 1.8392e-002 1.7918e+004 -2.2874e+001 -1.3542e+006

-Range: 0-300

Talc

Mg3Si4O10(OH)2 +6.0000 H+ = + 3.0000 Mg++ + 4.0000 H2O + 4.0000 SiO2

log_k 21.1383

-delta_H -148.737 kJ/mol # Calculated enthalpy of reaction Talc

Enthalpy of formation: -1410.92 kcal/mol

-analytic 1.1164e+001 2.4724e-002 1.9810e+004 -1.7568e+001 -1.8241e+006

-Range: 0-300

Calcite

CaCO3 +1.0000 H+ = + 1.0000 Ca++ + 1.0000 HCO3-

log_k 1.8487

-delta_H -25.7149 kJ/mol # Calculated enthalpy of reaction Calcite

Enthalpy of formation: -288.552 kcal/mol

-analytic -1.4978e+002 -4.8370e-002 4.8974e+003 6.0458e+001 7.6464e+001

-Range: 0-300

C-S-H gel: (CaO)(SiO2)(H2O) + H2O = Ca++ + SiO(OH)3- + OH-

log K=-8.91848

References for C-S-H gel solubility:

REARDON, E.J. 1990. An ion interaction model for the determination of chemical equilibria in cement/water systems. *Cement and Concrete Research.* 20. 175-192.

REARDON, E.J. 1992. Problems and approaches to the prediction of the chemical composition in cement/water systems. *Waste Management.* 12. 221-239.

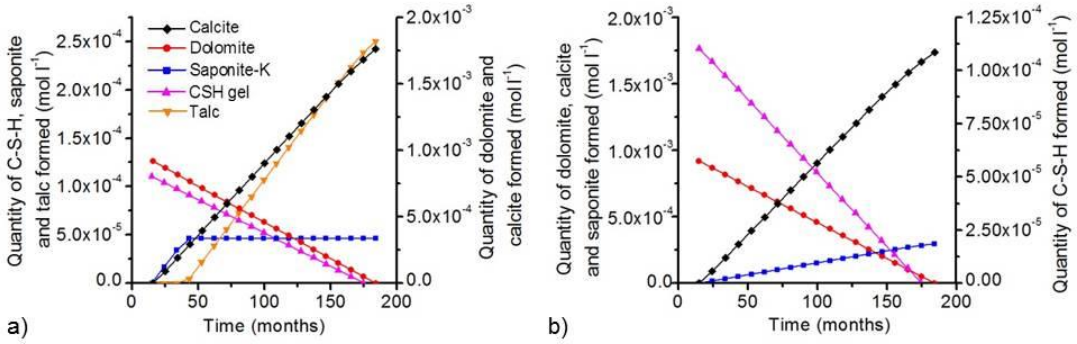

Figure B6: Moles of a) saponite-K, calcite, dolomite, C-S-H gel, saponite and talc in ENFG and b) saponite, calcite, dolomite, C-S-H gel and talc in ENFG in the presence of muscovite, predicted to form between 15 months and 15 years of reaction using computer modelling.

Table B4: Mineral saturation indices in YNFP and ENFG in the presence and absence of a dissolving Al-bearing mineral phase over time calculated using computer modelling.

YNFP with no Al-bearing phase					
Time	Saponite-K	Talc	CSHgel	Calcite	Dolomite
15	9.8439	8.0906	-5.3387	0.8792	0.4347
24.38889	0	0	-6.2073	0	-3.1816
33.77778	0	0	-6.2052	0	-3.2118
43.16667	0	0	-6.2103	0	-3.2339
52.55556	0	0	-6.2222	0	-3.2487
61.94444	0	0	-6.2408	0	-3.2567
71.33333	0	0	-6.2662	0	-3.2581
80.72222	0	0	-6.299	0	-3.2529
90.11111	0	0	-6.34	0	-3.2408

99.5	0	0	-6.3905	0	-3.2209
108.8889	0	0	-6.4521	0	-3.1925
118.2778	0	0	-6.5273	0	-3.154
127.6667	0	0	-6.6188	0	-3.1039
137.0556	0	0	-6.7284	0	-3.041
146.4444	0	0	-6.854	0	-2.9667
155.8333	0	0	-6.9856	0	-2.8875
165.2222	0	0	-7.1097	0	-2.8119
174.6111	0	0	-7.2186	0	-2.7443
184	0	0	-7.3124	0	-2.6846
ENFG with no Al-bearing phase					
Time	Saponite-K	Talc	CSHgel	Calcite	Dolomite
15	-0.191	-1.6109	-5.264	-2.728	-10.0747
24.38889	0	-0.9719	-5.5171	0	-4.5385
33.77778	0	-0.8472	-5.5711	0	-4.443
43.16667	0	0	-5.6285	0	-4.1032
52.55556	0	0	-5.6899	0	-4.0417
61.94444	0	0	-5.7559	0	-3.9758
71.33333	0	0	-5.8271	0	-3.9045
80.72222	0	0	-5.9045	0	-3.8271
90.11111	0	0	-5.9892	0	-3.7424
99.5	0	0	-6.0828	0	-3.6488
108.8889	0	0	-6.1872	0	-3.5444
118.2778	0	0	-6.3052	0	-3.4264
127.6667	0	0	-6.4407	0	-3.291
137.0556	0	0	-6.5991	0	-3.1326
146.4444	0	0	-6.7885	0	-2.9431
155.8333	0	0	-7.0201	0	-2.7115
165.2222	0	0	-7.3047	0	-2.427
174.6111	0	0	-7.6323	0	-2.0993
184	0	0	-7.9463	0	-1.7854
YNFP with Al-bearing phase					
Time	Saponite-K	Talc	CSHgel	Calcite	Dolomite
15	9.8439	8.0906	-5.3387	0.8792	0.4347
24.38889	0	-1.3824	-6.1216	0	-4.0676
33.77778	0	-1.3796	-6.1624	0	-4.0259
43.16667	0	-1.3766	-6.204	0	-3.9833
52.55556	0	-1.3733	-6.2466	0	-3.9396
61.94444	0	-1.3699	-6.2904	0	-3.8946

71.33333	0	-1.3662	-6.3355	0	-3.8483
80.72222	0	-1.3623	-6.3822	0	-3.8003
90.11111	0	-1.3581	-6.4306	0	-3.7505
99.5	0	-1.3536	-6.4808	0	-3.6987
108.8889	0	-1.3488	-6.5333	0	-3.6447
118.2778	0	-1.3436	-6.588	0	-3.5882
127.6667	0	-1.3381	-6.6453	0	-3.529
137.0556	0	-1.3322	-6.7055	0	-3.467
146.4444	0	-1.326	-6.7687	0	-3.4017
155.8333	0	-1.3193	-6.8352	0	-3.3329
165.2222	0	-1.3121	-6.9052	0	-3.2605
174.6111	0	-1.3044	-6.979	0	-3.1841
184	0	-1.2963	-7.0569	0	-3.1036

ENFG with Al-bearing phase

Time	Saponite-Ca	Talc	CSHgel	Calcite	Dolomite
15	0.2552	-1.6109	-5.264	-2.728	-10.0747
24.38889	0	-1.1343	-5.5139	0	-4.5958
33.77778	0	-1.1281	-5.57	0	-4.5377
43.16667	0	-1.1215	-5.6299	0	-4.4756
52.55556	0	-1.1144	-5.6941	0	-4.409
61.94444	0	-1.1068	-5.7632	0	-4.3373
71.33333	0	-1.0985	-5.8382	0	-4.2596
80.72222	0	-1.0894	-5.92	0	-4.1748
90.11111	0	-1.0795	-6.0101	0	-4.0814
99.5	0	-1.0684	-6.1103	0	-3.9775
108.8889	0	-1.056	-6.223	0	-3.8607
118.2778	0	-1.0418	-6.3517	0	-3.7272
127.6667	0	-1.0252	-6.5016	0	-3.5718
137.0556	0	-1.0055	-6.6801	0	-3.3867
146.4444	0	-0.9814	-6.899	0	-3.1598
155.8333	0	-0.951	-7.1751	0	-2.8735
165.2222	0	-0.9128	-7.5225	0	-2.5134
174.6111	0	-0.8703	-7.9079	0	-2.1138
184	0	-0.8342	-8.2366	0	-1.7731

Table B5: pH (at 70°C) and concentrations of major ions in solution in YNFP and ENFG in the presence and absence of a dissolving Al-bearing mineral phase over time calculated using computer modelling.

YNFP with no Al-bearing phase

Time (months)	pH	Ca mgl^{-1}	Mg mgl^{-1}	Na mgl^{-1}	K mgl^{-1}	Si mgl^{-1}	Al mgl^{-1}	C mgl^{-1}
15.00	11.60	2.35	1.01E-03	2027.21	2249.07	465.85	4.03E-01	549.88
24.39	11.57	0.31	1.84E-06	2027.17	2248.45	530.19	2.41E-06	572.37
33.78	11.54	0.31	1.71E-06	2027.12	2248.37	594.14	2.93E-06	595.47
43.17	11.50	0.31	1.62E-06	2027.10	2248.33	658.06	3.54E-06	618.57
52.56	11.46	0.31	1.56E-06	2027.05	2248.29	721.98	4.26E-06	641.68
61.94	11.42	0.31	1.52E-06	2027.01	2248.25	785.90	5.12E-06	664.77
71.33	11.37	0.31	1.52E-06	2026.98	2248.21	849.82	6.17E-06	687.87
80.72	11.32	0.31	1.53E-06	2026.94	2248.17	913.75	7.48E-06	710.97
90.11	11.26	0.31	1.57E-06	2026.91	2248.14	977.67	9.14E-06	734.08
99.50	11.20	0.31	1.64E-06	2026.89	2248.14	1041.59	1.13E-05	757.17
108.89	11.12	0.31	1.75E-06	2026.87	2248.10	1105.51	1.42E-05	780.28
118.28	11.03	0.31	1.91E-06	2026.87	2248.10	1169.43	1.84E-05	803.39
127.67	10.93	0.31	2.14E-06	2026.87	2248.10	1233.35	2.45E-05	826.50
137.06	10.81	0.31	2.47E-06	2026.89	2248.14	1297.30	3.38E-05	849.62
146.44	10.67	0.31	2.93E-06	2026.94	2248.17	1361.28	4.82E-05	872.76
155.83	10.52	0.31	3.53E-06	2027.03	2248.25	1425.26	6.92E-05	895.90
165.22	10.38	0.31	4.21E-06	2027.17	2248.41	1489.29	9.66E-05	919.07
174.61	10.26	0.31	4.94E-06	2027.33	2248.60	1553.35	1.28E-04	942.26
184.00	10.16	0.31	5.69E-06	2027.51	2248.80	1617.44	1.62E-04	965.47

ENFG with no Al-bearing phase

Time (months)	pH	Ca mgl^{-1}	Mg mgl^{-1}	Na mgl^{-1}	K mgl^{-1}	Si mgl^{-1}	Al mgl^{-1}	C mgl^{-1}
15.00	9.66	1.58E+03	1.03E-03	9.38E+03	243.00	13.53	0.41	2.03E-04
24.39	8.95	1.57E+03	1.24E-03	9.38E+03	242.78	48.35	0.26	0.15
33.78	8.93	1.57E+03	1.54E-03	9.38E+03	242.56	46.21	0.11	0.15
43.17	8.90	1.57E+03	3.36E-03	9.38E+03	242.40	44.08	2.96E-04	0.15
52.56	8.87	1.57E+03	3.87E-03	9.38E+03	242.40	41.94	2.96E-04	0.16
61.94	8.84	1.57E+03	4.50E-03	9.38E+03	242.40	39.81	2.96E-04	0.16
71.33	8.80	1.57E+03	5.30E-03	9.38E+03	242.40	37.67	2.96E-04	0.17
80.72	8.76	1.56E+03	6.33E-03	9.38E+03	242.40	35.54	2.96E-04	0.17
90.11	8.72	1.56E+03	7.68E-03	9.38E+03	242.40	33.42	2.96E-04	0.18
99.50	8.67	1.56E+03	9.52E-03	9.38E+03	242.40	31.30	2.96E-04	0.19
108.89	8.62	1.56E+03	0.01	9.38E+03	242.40	29.18	2.96E-04	0.20
118.28	8.56	1.56E+03	0.02	9.38E+03	242.40	27.07	2.96E-04	0.21

127.67	8.50	1.55E+03	0.02	9.38E+03	242.40	24.97	2.96E-04	0.23
137.06	8.42	1.55E+03	0.03	9.38E+03	242.40	22.90	2.96E-04	0.26
146.44	8.32	1.55E+03	0.05	9.38E+03	242.40	20.87	2.96E-04	0.30
155.83	8.21	1.55E+03	0.08	9.38E+03	242.40	18.92	2.96E-04	0.36
165.22	8.06	1.55E+03	0.16	9.38E+03	242.40	17.13	2.97E-04	0.47
174.61	7.90	1.55E+03	0.33	9.38E+03	242.40	15.68	2.97E-04	0.64
184.00	7.74	1.55E+03	0.69	9.38E+03	242.40	14.71	2.98E-04	0.88

YNFP with Al-bearing phase

Time (months)	pH	Ca mgl^{-1}	Mg mgl^{-1}	Na mgl^{-1}	K mgl^{-1}	Si mgl^{-1}	Al mgl^{-1}	C mgl^{-1}
15.00	11.60	2.35	1.01E-03	2027.21	2249.07	465.85	0.40	549.88
24.39	11.10	0.31	2.40E-07	2027.79	2244.15	2118.45	0.39	572.54
33.78	11.08	0.31	2.63E-07	2027.67	2238.44	2031.05	0.38	595.63
43.17	11.07	0.31	2.89E-07	2027.58	2232.77	1944.66	0.38	618.72
52.56	11.06	0.31	3.19E-07	2027.47	2227.10	1859.34	0.37	641.81
61.94	11.04	0.31	3.52E-07	2027.37	2221.43	1775.11	0.36	664.89
71.33	11.03	0.31	3.91E-07	2027.28	2215.76	1692.01	0.35	687.98
80.72	11.01	0.31	4.35E-07	2027.19	2210.09	1610.00	0.35	711.06
90.11	10.99	0.31	4.86E-07	2027.10	2204.42	1529.17	0.34	734.14
99.50	10.97	0.31	5.47E-07	2027.03	2198.79	1449.52	0.33	757.22
108.89	10.95	0.31	6.18E-07	2026.94	2193.12	1371.05	0.32	780.31
118.28	10.93	0.31	7.02E-07	2026.87	2187.49	1293.85	0.31	803.39
127.67	10.91	0.31	8.03E-07	2026.80	2181.86	1217.88	0.30	826.48
137.06	10.88	0.31	9.25E-07	2026.75	2176.23	1143.23	0.29	849.56
146.44	10.85	0.31	1.07E-06	2026.68	2170.60	1069.95	0.27	872.65
155.83	10.83	0.31	1.26E-06	2026.64	2164.97	998.06	0.26	895.73
165.22	10.79	0.31	1.48E-06	2026.59	2159.38	927.70	0.25	918.82
174.61	10.76	0.31	1.76E-06	2026.55	2153.75	858.95	0.24	941.90
184.00	10.73	0.31	2.12E-06	2026.50	2148.16	791.94	0.23	964.99

ENFG with Al-bearing phase

Time (months)	pH	Ca mgl^{-1}	Mg mgl^{-1}	Na mgl^{-1}	K mgl^{-1}	Si mgl^{-1}	Al mgl^{-1}	C mgl^{-1}
15.00	9.66	1575.39	1.03E-03	9380.15	243.00	13.53	0.41	2.03E-04
24.39	8.96	1573.94	1.08E-03	9380.15	242.89	48.48	0.04	0.15
33.78	8.93	1572.06	1.24E-03	9380.15	242.96	46.26	0.03	0.15
43.17	8.90	1570.14	1.43E-03	9380.15	243.03	44.03	0.03	0.15
52.56	8.87	1568.25	1.66E-03	9380.15	243.10	41.80	0.03	0.16
61.94	8.83	1566.37	1.96E-03	9380.15	243.18	39.58	0.03	0.16
71.33	8.80	1564.44	2.34E-03	9380.15	243.25	37.36	0.03	0.17

80.72	8.75	1562.56	2.84E-03	9380.15	243.32	35.14	0.03	0.17
90.11	8.71	1560.68	3.52E-03	9380.15	243.39	32.93	0.02	0.18
99.50	8.66	1558.79	4.46E-03	9380.15	243.47	30.72	0.02	0.19
108.89	8.60	1556.95	5.83E-03	9380.15	243.54	28.51	0.02	0.20
118.28	8.54	1555.07	7.92E-03	9380.15	243.61	26.32	0.02	0.22
127.67	8.47	1553.22	0.01	9380.15	243.68	24.13	0.02	0.24
137.06	8.38	1551.46	0.02	9380.15	243.75	21.98	0.01	0.28
146.44	8.27	1549.70	0.03	9380.15	243.82	19.87	0.01	0.33
155.83	8.13	1548.09	0.06	9380.15	243.89	17.87	0.01	0.42
165.22	7.96	1546.69	0.13	9380.15	243.96	16.10	7.75E-03	0.57
174.61	7.76	1545.69	0.32	9380.15	244.02	14.81	5.78E-03	0.84
184.00	7.60	1545.01	0.71	9380.15	244.07	14.09	4.50E-03	1.19

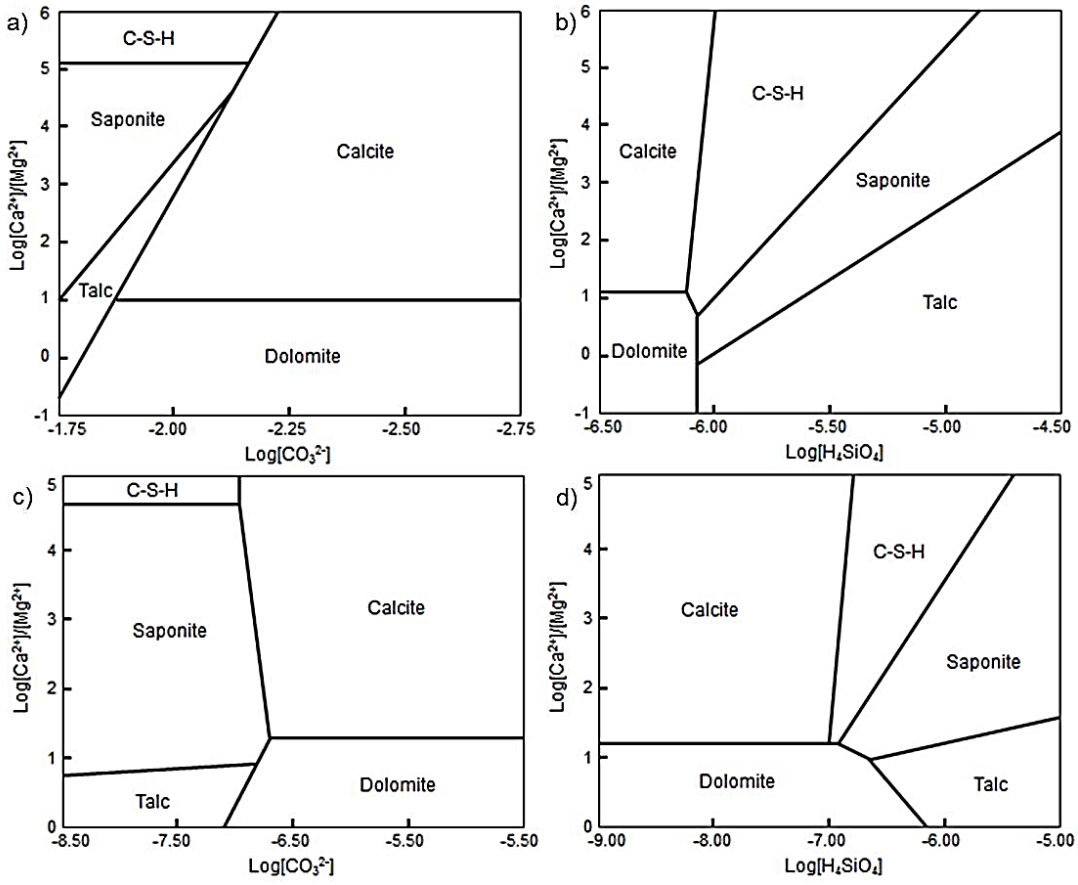

Figure B7: Stability phase diagrams showing the secondary phases predicted to form using computer modelling in the YNFP system a) relative to carbonate and b) relative to silica and the ENFG system c) relative to carbonate and d) relative to silica (70°C, based on 15 year reacted solution compositions).

Appendix C
Associated publications

C.1. Publications based on this thesis

MOYCE, E. B. A., ROCHELLE, C., MORRIS, K., MILODOWSKI, A. E., CHEN, X., THORNTON, S., SMALL, J. S. & SHAW, S. 2014. Rock alteration in alkaline cement waters over 15 years and its relevance to the geological disposal of nuclear waste. Applied Geochemistry. 50. 91-105.

MOYCE, E. B. A., MILODOWSKI, A. E., MORRIS, K., & SHAW, S. In submission. Herbert's Quarry, South Wales - an analogue for host rock alteration at a cementitious radioactive waste repository? *Mineralogical Magazine.*

C.2. Associated publications

ROCHELLE, C., MILODOWSKI, A. E., BATEMAN, K. & MOYCE, E. B. A. In submission. A long-term experimental study of the reactivity of basement rock with highly alkaline cement waters: Reactions over the first 15 months. *Mineralogical Magazine.*

C.3. Conference proceedings

MOYCE, E. B. A., MORRIS, K., MILODOWSKI, A. E., ROCHELLE, C. AND SHAW, S. (2012) Mineral reactions at high pH relevant to radwaste disposal: a 15 year experimental study. *Mineralogical Magazine*, 76, p.A2142

FIELD, L, MILODOWSKI, A., BATEMAN, K., MOYCE, E., SHAW, S. & ROCHELLE C. (2013) Petrology of Column Experiments on the Interaction of Young Cement Leachate with Silicate Host Rock in a Geological Disposal Facility. *Mineralogical Magazine*, 77, p.A1082

MOYCE, E. B. A., MORRIS, K., MARSHALL, T. A. AND SHAW, S. The BIGRAD consortium - alteration of sandstone by alkaline cement leachates and its effect on uranium speciation. Migration 2013, Brighton, England, September 2013 (*Oral*)

CHEN, X., THORNTON, S., SMALL, J., MOYCE, E. B. A., SHAW, S., MILODOWSKI, A. E. AND ROCHELLE, C. Numerical analysis of multi-

mineral transfer between the host rock and groundwater against experiment for nuclear waste disposal. Migration 2013, Brighton, England, September 2013 (*Oral*)